Universidade de Lisboa

Faculdade de Farmácia

3-Oxo-β-Sultams and 4-Oxo-β-Lactams as Chemical Tools for Activity-based Protein Profiling of Serine Hydrolases

Relatório Final De Bolsa de Doutoramento Individual
SFRH/BD/100400/2014

Luís Miguel Afonso Ramos de Carvalho

Doutoramento em Farmácia
Especialidade de Química Farmacêutica e Terapêutica

Projeto orientado pelo Professor Doutor Rui Moreira e coorientado pela Doutora Susana Lucas e pela Doutora Deborah Penque

2019

This work was developed under scientific supervision of Professor Rui Moreira and co-supervision of Dr.ª Susana Lucas, from iMed.ULisboa (Instituto de Investigação do Medicamento), Faculty of Pharmacy, University of Lisbon, and Dr.ª Deborah Penque from the Instituto Nacional de Saúde Dr. Ricardo Jorge, Portugal. The work was financially supported by Fundação para a Ciência e Tecnologia, through the doctoral grant SFRH/BD/100400/2014. The work was partially performed in The Scripps Research Institute in La Jolla, California, under the supervision of Professor Ben Cravatt.

Table of Contents

Figure Index

Figure 26 – Labeling of THP-1 and HEK293T whole cell lysates (1 mg/mL) with increasing concentrations of 3-Oxo-β-Sultam **108** in whole cell lysates of THP-1 and HEK293T cell lines. Labeling seems to be reasonably selective up to high concentrations of 50 µM.

Figure 27 – Labeling of decreasing concentrations of pure HNE by 3-Oxo-β-Sultams **92** and **108** at 50 µM. Compound **92** was clicked with Rhodamine azide after incubation with the proteome. While labeling is clearly observed with the Rhodamine probe, the alkyne probe provides a weak signal, only visible at 500 nM of HNE.

Figure 28 – HNE spiking experiments in HEK293T cells. 3-Oxo-β-Sultam-Rhodamine **108** labeling of pure HNE (first lane) and spiking of pure HNE in decreasing concentrations into HEK293T whole cell lysates (1mg/mL). Labeling of HNE is observed even in the presence of a complete proteome but not completely selective. As spiked HNE concentration decreases, labeling of some proteins clearly increases, indicating these might be HNE substrates.

Figure 29 – Testing of HNE labeling in a pure form, spiked into a complete proteome and in a cell line that expresses active HNE with compound **108**. Labeling is clearly visible in all three types of experiments, being suppressed by pre-incubation with ONO-6818. When in the presence of a complete proteome, labeling of additional proteins is visible.

Figure 30 – Competitive ABPP of 3-Oxo-β-Sultam compounds **109**, **92** and **102** against FP-Rhodamine (left) and Iodoacetamide-Rhodamine (right).

Figure 31 – ReDiMe results for 3-Oxo-β-Sultams. A ratio higher than 3 is considered a hit. The results were filtered to show only the serine hydrolase family of proteins. Each line represents one experiment.

Figure 32 – ABPP-SILAC results for 3-Oxo-β-Sultams. The results were filtered for the serine hydrolase family. Hits were considered when the protein is enriched with a ratio of at least 3 when compared with a DMSO control in at least two experiments. A.**109** [10 µM (Probe VS. DMSO)]; B.**109** [50 µM (Probe VS. DMSO)]; C. [**108** (100µM) VS. DMSO], then **109** (10 µM); D. [(**108** (100µM) VS. DMSO)], then **109** (50 µM).

Figure 33 - Example of the peptide count plotted against observed ratios for: A. **109**, 10 uM vs. DMSO experiment; B. **109**, 10 uM vs. DMSO experiment; C. Probe vs. probe

Table Index

Scheme Index

Abbreviations

2-AG – 2-arachidonoylglycerol

ABHD10 – α/β hydrolase domain fold family protein 10

ABHD12 – α/β hydrolase domain fold family protein 12

ABHD16A – α/β hydrolase domain fold family protein 16A

ABHD2 – α/β hydrolase domain fold family protein 2

ABHD3 – α/β hydrolase domain fold family protein 3

ABHD6 – α/β hydrolase domain fold family protein 6

ABP – Activity-based Probe

ABPP – Activity-based Protein Profiling

ACOT7 – Cytosolic acyl coenzyme A thioester hydrolase

APEH – Acylamino-acid-releasing enzyme

CDCA – Chenodeoxycholic acid

CES1 – Carboxylesterase 1

CES2 – Carboxylesterase 2

CES3 – Carboxylesterase 3

COPD – Chronic Obstructive Pulmonary Disease

CPVL – Carboxypeptidase

CUAAC – Copper-catalyzed azide-alkyne cyclocondensation

DCA – Deoxycholic acid

DPP4 – Dipeptidyl dipeptidase 4

DPP7 – Dipeptidyl dipeptidase 7

DPP8 – Dipeptidyl dipeptidase 8

DPP9 – Dipeptidyl dipeptidase 9

FAAH – Fatty acid amide hydrolase

FAP – Fibroblast activation protein/FAP Seprase

FASN – Fatty acid synthase

FluoPol – Fluorescence Polarization

GLP-1 - Glucagon-like peptide-1

HMGB1 – Alarmin high mobility group box 1

HNE – Human Neutrophil Elastase

HyCoSul – Hybrid combinatorial substrate library

ICAT – Isotope-coded affinity tag

LE – Ligand Efficiency

LLE – Ligand Lipophilic Efficiency

LYPLA1 – Acyl-protein thioesterase 1

LYPLA2 – Acyl-protein thioesterase 2

MAGL – Monoacylglycerol lipase

MHC – Major histocompatibility complex

MMP-2 – Matrix metalloproteinase-2

MMP-9 – Matrix metalloproteinase-9

MRSA – methicillin-Resistant S. Aureus

MudPIT – Multidimensional Protein Identification Technology

NBD – Nitrobenz-2-oxa-1,3-diazole

NET – Neutrophil extracellular trap

NSCLC – Non-small cell lung cancer

PAFAH2 - Platelet-activating factor acetylhydrolase 2

PBP – Penicillin binding proteins

PEI – Polyethyleneimine

PPE – Porcine Pancreatic Elastase

PR3 – Proteinase 3

PRCP – Lysosomal Pro-X carboxypeptidase

PREP – Prolyl endopeptidase

ReDiMe – Reductive dimethylation

ROS – Reactive oxygen species

SAR – structure-activity relationship

SCPEP1 – Retinoid-inducible serine carboxypeptidase

SDS-PAGE – Sodium Dodecyl Sulfate-polyacrylamide gel electrophoresis

SILAC – Stable isotope labeling by amino acids in cell culture

SLPI – Secretory leukocyte protease inhibitor

SUMO1 – Small ubiquitin-related modifier 1

TEV – Tobacco etch virus

TMT – Tandem mass tag

TOP – Tandem orthogonal proteolysis

TOP – Tandem orthogonal proteolysis

TUDCA – Tauroursodeoxycholic acid

UDCA – Ursodeoxycholic acid

Abstract

Activity-based protein profiling (ABPP) is a technique that analyzes the dynamics in enzymatic activity in complex proteomes by using small molecular probes, deemed activity-based probes (ABPs), containing a reactive group to covalently bind enzyme catalytic residues, a tag for detection of labeled targets and a linker as a spacer and also specificity-enhancing. Different warheads have been developed to engage a wide range of enzymatic families but there is a constant need to create new chemical tools to expand the pool of engageable targets. In this work we evaluated two 4-membered ring warheads as new warheads for ABPP of serine hydrolases. The 3-Oxo-β-Sultam warhead was revealed to be a highly reactive chemotype which labels a wide range of proteins with limited target occupancy. A crystallographic analysis of the reaction of 3-Oxo-β-Sultams with elastase enzymes revealed a previously unknown mechanism of inhibition of these enzymes by sulfonylation, suggesting 3-Oxo-β-Sultam compounds could be used to expand the pool of available sulfonylating tools in chemical biology. 4-Oxo-β-Lactams were shown to potently hit a selected group of serine hydrolase with high target occupancy, including human neutrophil elastase (HNE) and members of the ABHD and DPP families of enzymes. A competitive-ABPP approach revealed high potency of a library of 4-Oxo-β-Lactams to target these enzymes. 4-Oxo-β-Lactams were identified used as a new chemotype for DPP8 and DPP9 inhibition. Crystallography experiments revealed a new binding mode of these enzymes with 4-Oxo-β-Lactams, highlighting that these compounds could be used to pursue selective DPP8 or DPP9 inhibitors, a highly pursued field in current medicinal chemistry.

Keywords: activity-based protein profiling • activity-based probe • serine hydrolase • 4-Oxo-β-Lactam • 3-Oxo-β-Sultam

Resumo

A análise de proteínas baseada na actividade (ABPP) é uma técnica que possibilita o estudo da actividade de proteínas em proteomas complexos. A principal vantagem desta técnica em relação a outras técnicas de quantificação é que o resultado reportado corresponde somente à fracção activa da enzima em estudo, permitindo associar padrões complexos de actividade enzimática a fenótipos da amostra em estudo.

O conceito de ABPP depende das sondas baseadas na actividade (ABPs), que contém um grupo reactivo, responsável pela reacção com formação de ligação covalente com uma proteína alvo ou um grupo de proteínas, e um elemento marcador, que produz um sinal mensurável que permite reportar a actividade da proteína alvo ou facilitar a sua purificação. Estes dois elementos são normalmente separados por um elemento de espaçamento, diminuindo possíveis impedimentos estéreos e podendo contribuir para o aumento da especificidade da sonda. Uma experiência de ABPP envolve a incubação das ABPs com proteomas complexos, onde as sondas se vão ligar apenas à forma activa das suas enzimas alvo. As enzimas que reagiram com a ABP podem ser identificadas por ensaios de gel de electroforese de proteínas, caso o elemento marcador da ABP seja um fluoróforo, através da leitura directa de fluorescência no gel. Alternativamente, se o elemento sinalizador da ABP é a biotina, as proteínas alvo são enriquecidas através de incubação com streptavidina e analisadas por espectrometria de massa para identificação exacta da identidade das proteínas atingidas. A análise simultânea de várias amostras permite comparar padrões de actividade enzimática e potencialmente definir novos biomarcadores associados a um fenótipo específico.

Existe uma procura contínua de novos grupos reactivos de modo a aumentar a variabilidade de ferramentas disponíveis e conseguir cobrir o maior número possível de famílias enzimáticas. Hidrolases de serina são uma das maiores famílias de enzimas, tendo papéis relevantes em inúmeros processos biológicos e patológicos e existindo um interesse contínuo no seu estudo para desenvolvimento de inibidores e sondas. Análises ABPP de hidrolases de serina são normalmente realizadas com o grupo reactivo fluorofosfonato. Neste trabalho estudámoss dois potenciais grupos reactivos baseados em anéis de 4 membros, as 3-Oxo-β-Sultamas e as 4-Oxo-β-Lactamas para análise de hidrolases de serina.

As 3-Oxo-β-Sultamas são anéis de 4 membros que contém um grupo acil sulfonamida. Uma biblioteca de compostos baseada neste group reactivo foi sintetizada via química click. Ensaios bioqímicos de inibição enzimática utilizando a elastase neutrofílica humana como modelo revelaram valores de inibição submicromolares para os compostos com substituição 3-dietilo, com as ABPs a evidenciar que a adição de um elemento sinalizador volumoso não compromete a actividade dos compostos. A análise da reatividade destes compostos num proteoma complexo revelou que estes são dotados de alta reactividade, reagindo com uma elevada percentagem das proteinas identificadas nos ensaios de ABPP. As análises de espectrometria de massa revelaram que, apesar de identificarem várias enzimas da família das hidrolases de serina, as 3-Oxo-β-Sultamas fazem-no com baixa percetagem de ocupação de alvo, o que limita a sua aplicação como ABPs. O mecanismo de inibição de hidrolases de serina pelas 3-Oxo-β-Sultamas não se encontra bem definido. Estudos anteriores com a elastase porcina humana (PPE) levaram autores a sugerir que o mecanismo é a acilação, mas estes resultados basearam-se apenas em análise cinética da reacção e verificação da sua reversibilidade com o tempo. Utilizando técnicas de cristalografia demonstrámos, pela primeira vez, através de análise de raios X de complexos entre a PPE e a HNE, que o mecanismo de acção é a sulfonilação da serina catalítica das enzimas. Estes resultados são bastante promisores para a expansão da biblioteca de ferramentas de sulfonilação disponíveis na química biológica, um mecanismo sub-explorado de inibição enzimática.

As 4-Oxo-β-Lactamas são derivados de β-Lactamas que contém um grupo carbonilo adicional na posição 4 do anel de 4 membros. A análise ABPP revelou um perfil selectivo de inibição de enzimas num proteoma complexo, que incluem a HNE, um alvo previamente conhecido, mas também novas proteínas anteriormente não identificadas como alvos deste grupo reactivo, que incluem enzimas das famílias domínio αβ-hidrolase (ABHD) e dipeptidil peptidase (DPP). Ao contrário do que acontece com as 3-Oxo-β-Sultamas, estes alvos são inibidos com alta ocupação de alvo, o que sugere que a 4-Oxo-β-Lactama é um bom grupo reactivo para aplicações ABPP.

Uma biblioteca de inibidores baseados na 4-Oxo-β-Lactamas com substituinte N-arilo foi sintetizada de modo a estudar as características estruturais que definem a preferência de inibição para as enzimas identificadas nos ensaios ABPP. Uma análise por ABPP competitivo revelou que a posição dos substituintes no grupo N-arilo parece influenciar a especificidade dos compostos, com compostos com substuintes em para a apresentar, em geral, maior afinidade para a HNE e ABHD6, e compostos com substituintes em meta

a apresentar maior especificidade para as DPPs. Compostos com substituintes em orto não apresentaram alvos relevantes dos ensaios em gel e não foram testados em espectrometria de massa. A validação dos alvos utilizando sobreexpressão de hidrolases de serina de interesse revelou que a maioria dos compostos inibe alguns destes alvos com IC_{50} submicromolar. Estes resultados enfatizam o potencial da 4-Oxo-β-Lactamas como grupo reactivo para aplicações ABPP e para o desenvolvimento de novos inibidores de hidrolases de serina. Uma ABP com um alcino terminal foi sintetizada para aplicações bioortogonais, demostrando alta selectividade para a HNE em ensaios ABPP em gel, tendo potencial para estudos futuros da HNE na doença pulmonar obstrutiva crónica.

De entre os novos alvos identificados para as 4-Oxo-β-Lactamas são de salientar a DPP8 e a DPP9. A procura de inibidores da DPP8 e da DPP9 é uma grande área de interesse actual na química medicinal. Estas duas enzimas possuem alta similaridade estrutural entre si e não possuem inibidores específicos, sendo frequentemente inibidas em conjunto. Os inibidores que apresentaram melhores resultados para estas duas enzimas foram estudados mais aprofundadamente com as DPP8 e DPP9. Os compostos revelaram ter um efeito modesto na indução da piroptose, uma consequência da inibição destas enzimas e estudos de similaridade confirmaram que este grupo reactivo é completamente diferente dos grupos reactivos previamente utilizados para a inibição destas enzimas. Análise de complexos de raio X entre um inibidor 4-Oxo-β-Lactama e a DPP8 revelou a formação de uma ligação covalente entre o composto e a serina catalítica da DPP8. A parte distal da molécula apresenta interacções com aminoácios vizinhos ao sítio activo e um mecanismo de inibição que nunca tinham sido reportados anteriormente para os inibidores conhecidos da DPP8. Esta informação será vital para o futuro desenho de inhibidores destas enzimas e a exploração desta nova interacção poderá ser a chave para a descoberta de inibidores específicos para as mesmas.

Adicionalmente, reportamos a síntese de sondas contendo vinil sulfonas como grupo reactivo para a análise de proteases de serina, sondas sintetizadas por modificação da estrutura de ácidos biliares e a síntese de sondas e inibidores baseados em modificações da 4-Oxo-β-Lactama como actividades complementares ao projeto princial aqui descrito. Em resumo, a utilização de ABPP e técnicas cristalográficas revelou o potencial de grupos reactivos com anéis de 4-membos, com as 3-Oxo-β-Sultamas comportando uma alta reactividade associada a baixa ocupação de alvo, mas com um mecanismo de acção inesperado via sulfonilação do centro activo de enzimas como a HNE. Os resultados revelaram também o enorme potencial das 4-Oxo-β-Lactamas como ABPs e como grupo

reactivo para o desenvolvimento de inibidores, incluindo enzimas como a DPP8 e DPP9, para as quais a procura de inibidores é uma área de grande interesse actual. A descoberta de que os inibidores contendo 4-Oxo-β-Lactamas ibibem a DPP8 através de interacções previamente não conhecidas poderá resultar na descoberta dos primeiros inibidores específicos da DPP8 ou DPP9.

Palavras-chave: Análise de proteínas baseada na actividade • sondas baseadas na actividade • hidrolases de serina • 4-Oxo-β-Lactama • 3-Oxo-β-Sultama.

Chapter 1 – Introduction and General Concepts

1.1. Activity-based Protein Profiling

In the current scientific landscape, the complete genome sequences of several organisms have been determined, with the human genome project being completed in 2001.[5] With the exception of cells that demonstrate genomic mosaicism, nearly all cells contain identical DNA.[6,7] Despite this, complex organisms present vastly different cell types, mostly due to the expression of different proteins. Furthermore, through mechanisms like gene splicing and post-translational modifications, our genome, which contains around 30000-40000 genes, can generate over 100000 structurally and functionally diverse protein entities.[8] Many of these proteins remain unannotated regarding their biochemical activities.[9]

The annotation of the human proteome is a colossal task which is complicated by the complex dynamics of proteins in the cell. The large-scale approaches to characterize the myriad of proteins expressed in biological systems are collectively termed proteomics and have been greatly assisted by the development of mass-spectrometry techniques, which have supported the study of the proteome for a long time.[1,7,10] One of the goals of proteomics is to develop techniques capable of analyzing protein expression levels and assigning functional roles to proteins in normal and pathologic states.[11]

Protein dynamics in biological systems depend on a variety of factors, including the wide range of abundances, compartmentalization of proteins in cellular organelles, different temporal expression, the possibility of diverse post-translational modifications affecting protein function and the existence of amino acid side-chain reactivity, which strongly varies, depending on the local microenvironment.[10,12] Additionally, endogenous inhibitors and protein-protein interactions contribute to the modulation of protein activity, adding an additional layer of complexity to the system.[13] These factors make it so that protein abundance or expression levels are frequently not directly correlated with that protein's activity. Traditional proteomic methods, including two-dimensional electrophoresis coupled with mass spectrometry, provide data focused on protein

expression levels, with no information regarding the activity state of the proteins. These methods also struggle with low abundance proteins and proteins with particular features like transmembrane domains.[1,14,15]

The need of new platforms to analyze protein function and activity instead of abundance led to the development of ABPP, a group of chemoproteomic techniques that are able to quantify only the active fraction of total enzyme in complex proteomes and profile the functional dynamics of enzymes in complex systems (figure 1).[16-19]

The application of ABPP relies on ABPs, the molecular players that perform covalent tethering of single or multiple enzymes and provide a readable signal which can be analyzed as a measurement of protein function. The basic structure of an ABP contains a reactive warhead,[20,21] responsible for binding to the active target enzyme; a tag, which provides a readable signal or a means of purifying the probe-target complex;[11] and a linker, which separates the warhead from the tag and can also contain additional elements that contribute to increased potency and selectivity by interacting with non-catalytic residues of the target enzymes (figure 1).[8]

A typical ABPP experiment involves the treatment of a protein sample, that can be a complete proteome, with an ABP. The reaction of ABPs with their target enzymes results in the formation of a covalent bond between them. Downstream analysis protocols vary depending on the experiment. Proteomes labeled with fluorescent tags can be analyzed by SDS-PAGE techniques and are commonly used for direct visualization of labeled proteins in-gel.[8,22] Gel bands can then be excised for mass-spectrometry-based protein identification. If the probe is biotinylated, engaged targets can be directly enriched from the proteome using a streptavidin-coated solids surface and the enriched peptides can then be processed and analyzed by LC-MS/MS, resulting in a list of engaged proteins after appropriate processing.[23]

The probes can be applied in parallel to normal and diseased tissues to profile and compare enzymatic activities in both samples, resulting in a fingerprint of the key enzymes that are differently active between them and might be up or downregulated in the disease state. In an ideal situation, the readable signal is significantly and consistently different between tissues and allows the target enzyme to be classified as a potential

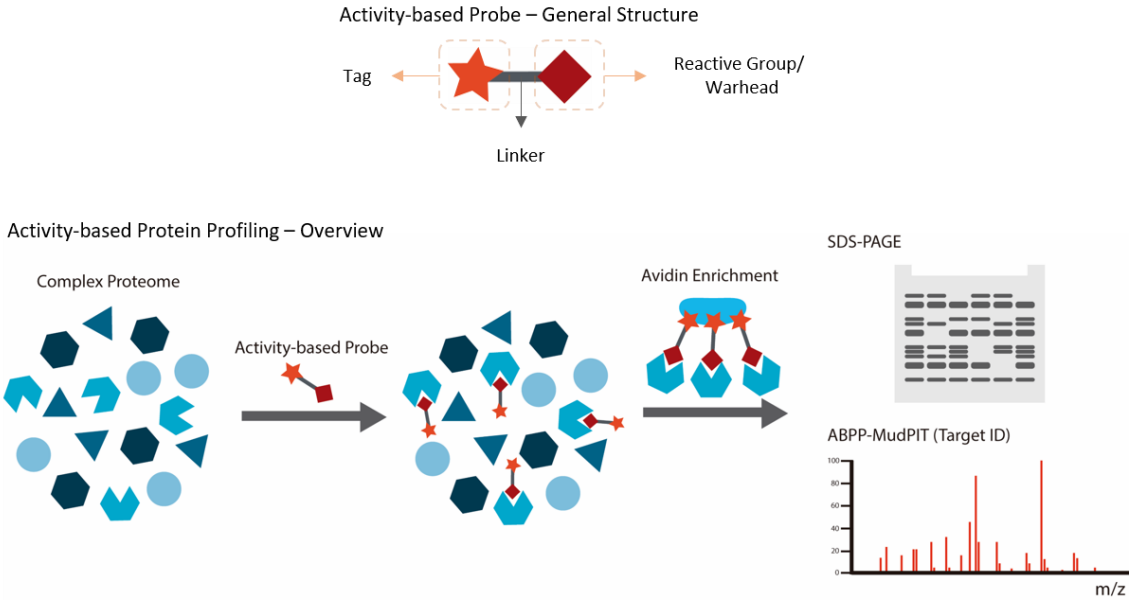

Figure 1 – General Structure of an ABP, comprising a reactive group/warhead, a linker and a tag, and general overview of an ABPP experiment, where an ABP is incubated with a complex proteome, labeling its targets that are in a catalytically active state. This is followed by analysis via gel-based methods or streptavidin enrichment of labeled proteins and analysis by mass spectrometry.

biomarker of disease (figure 2).[24] The application of ABPs in different stages of disease can also provide insight into molecular mechanisms that promote disease progression and that characterize different disease stages.[14]

ABPs can be directed to a single enzymatic target or have a broader scope of targets that share a certain substrate specificity or mechanistic machinery. Using ABPs with broad reactivity in non-directed approaches allows groups of biomarkers to be analyzed together and different patterns of expression associated with diverse disease stages.[25] These probes can also react with previously uncharacterized enzymes, allowing the study of their reactivity, the search for specific inhibitors and the allocation of these enzymes into known enzyme families.[26] Additionally, these broad reactivity probes have been successfully used in competitive ABPP, where libraries of inhibitors compete with probe labeling, allowing preliminary information on potency and selectivity to be obtained for specific targets without the need of a specific ABP (see chapter 1.1.4.). The application of on-off fluorescent ABPs can also allow provide in vivo or in situ visualization of enzymatic activity and has been used for tumor border imaging in brain tissue.[27]

ABPP probes have been successfully developed for diverse classes of enzymes, including proteases,[9,21,28-31] kinases,[32-34] phosphatases,[35,36] glycosidases,[37,38] gluthatione-S-transferases,[39] among others. Application-wise, ABPs have been successfully used in the identification of critical molecules in pathologic states[28,40], discovery of enzyme targets[41], in vivo visualization of enzymatic activity[27,42,43], inhibitor discovery[44] and biomarker discovery and validation[24], among other examples.

Ideally, multiple probes of complementary specificity could potentially be used simultaneously to provide a universal platform for comprehensive analysis of enzymatic activity dynamics across complex proteomes.[45]

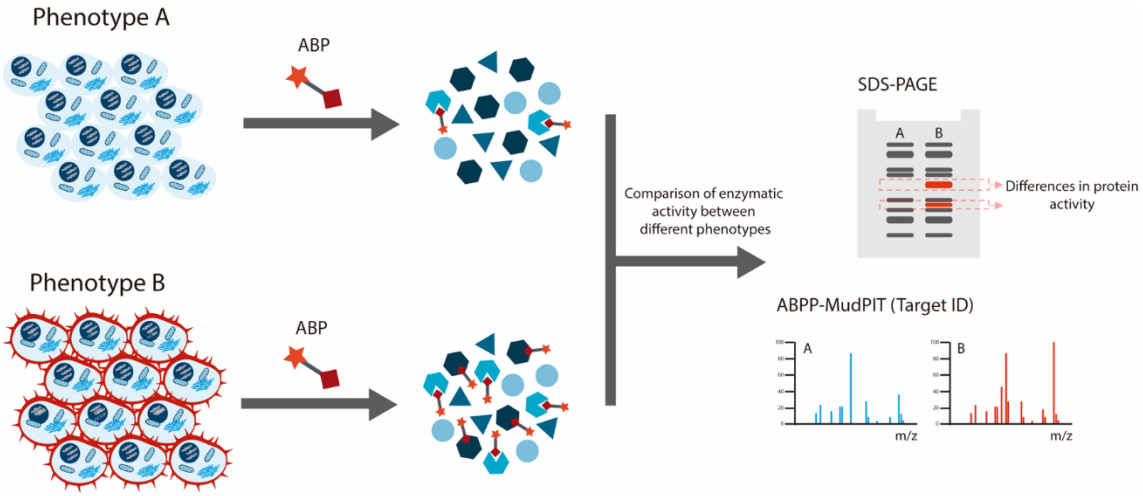

Figure 2 – Application of ABPs in the discovery of enzymatic activities potentially responsible for specific phenotypes. Different phenotypes can be incubated with the same ABP and analyzed by ABPP techniques to identify enzymatic activities that are upregulated or downregulated and can potentially be responsible for the phenotype.

1.1.1. Designing Activity-based Probes

The basic structure of an ABP contains a reactive warhead[20,21], which binds to the active target enzyme, a tag which provides a readable signal or a means of purifying the probe-target complex[11], and a linker, which separates the warhead from the tag and might

contribute to increase potency and selectivity by interaction with non-catalytic residues.[8] For specific applications additional elements can be present, including quenchers, recognition moieties, among others. In the following sections, specific details regarding these probe elements will be discussed with relevant examples. Figure 3 depicts an example of an ABP for serine hydrolases, highlighting the components of the probe.

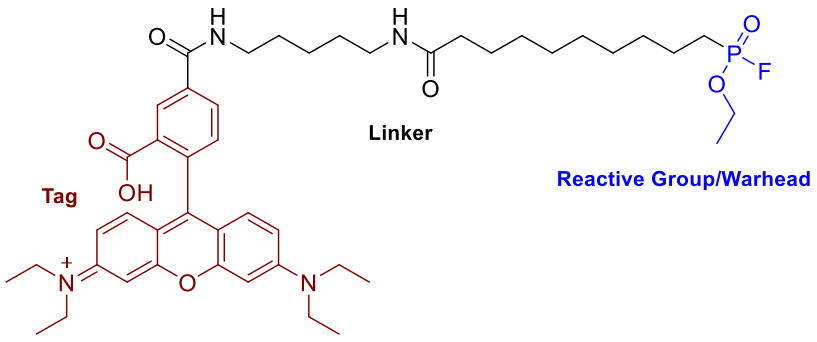

1

Figure 3 – Example of an FP ABP commonly used for ABPP of serine hydrolases. The probe uses an FP reactive group/warhead, an alkyl linker containing an amide and a rhodamine tag.

1.1.1.1. The Warhead/Reactive Group

The warhead or reactive group is the element of the ABP responsible for target engagement and covalent binding to the enzyme's active site. It is usually based on an electrophilic chemotype (figure 4). If the enzyme to be targeted has known covalent inhibitors, preliminary probe design can take advantage of adapting the inhibitor structure and modifying it to include an appropriate tag.[2]

The choice of warhead depends on the type of enzyme to be targeted, ease of synthesis and the desired selectivity/reactivity. A myriad of reactive groups is available to target diverse enzymatic families.[2] Electrophiles that target enzymes that use cysteine, serine and threonine as catalytic residues are well established.[2,20,21,46] Other enzymes like metalloproteases and aspartyl proteases don't use a catalytic aminoacid and are usually

targeted by reactive cross-linkers that activate with light exposure and establish a non-specific covalent bond with a neighboring aminoacid. This is called affinity-based protein profiling and has allowed the application of ABPP techniques for enzymes that form no direct covalent bonds.[9,47,48] Concerning selectivity and reactivity, care must be taken in choosing an adequate warhead for each specific task. Absolute specificity is not a requirement for ABPs, as long as efficient separation of the labeled proteins by SDS-PAGE or LC-MS/MS allows unequivocal detection and analysis of the target protein of interest. The simultaneous measurement of multiple enzymatic activities is often advantageous since it can provide a better understanding of proteome dynamics, where biologic or pathologic phenotypes are usually associated with multiple enzymatic activities. Additionally, broad reactivity probes are essential in competitive variants of ABPP and allow profiling of potency and selectivity of large libraries of potential inhibitors for multiple enzymes using a single broad reactivity ABP. This type of technique is called competitive ABPP will be discussed later in a later chapter.[18]

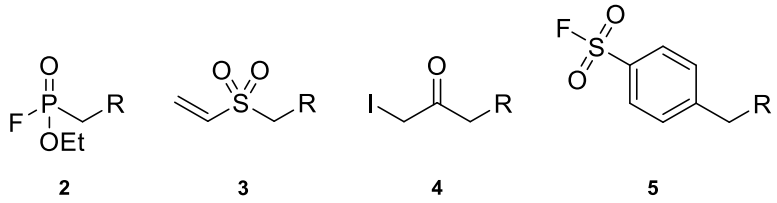

Figure 4 – Common warheads in ABPP.

1.1.1.2. The Tag

The tag is the element of the probe that provides either a readable signal or allows for affinity enrichment of labeled proteins. Choosing the tag depends on the analytical platform and the type of data desired. ABP imaging can be achieved by using fluorophores or radioactive tags, while mass-spectrometry-based identification of proteins requires biotin as the tag. Biotin makes it possible to enrich labeled proteins using avidin- or streptavidin-coated surfaces.[11] Commonly used tags in ABPP are presented in figure 5.

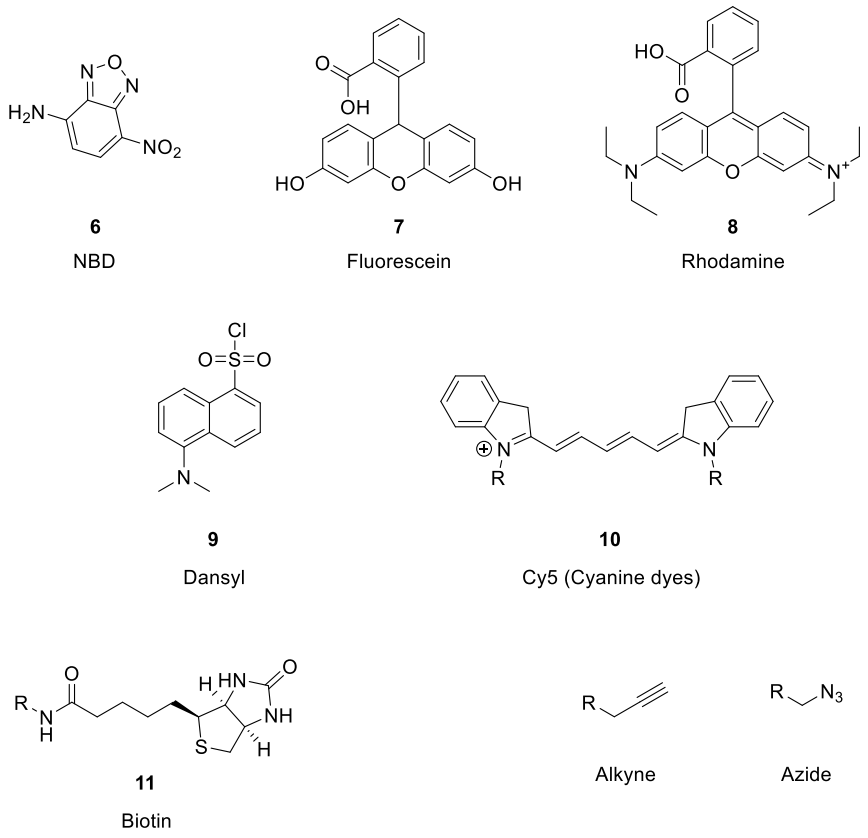

Figure 5 – Commonly tags in ABPP.

^{125}I tagging is an example of an isotopic tag. It can be easily achieved by iodination methods and has been incorporated in several ABPs. The probes provide highly sensitive signals with low background noise but require specialized equipment for manufacture and handling and have limited storage time due to the low half-life of ^{125}I. The signal can be read by SDS-PAGE and allows discrimination of singular labeled proteins in complex mixtures. These probes have been used successfully in the labeling of cysteine proteases. Bogyo and coworkers developed a highly selective probe for cathepsin B based on an epoxide warhead and containing radioactive iodine and showed that the enzyme is the only identifiable target of the compounds, also unveiling some structure-activity relationship (SAR) information vital for designing cell permeable compounds.[49] Kato and coworkers developed an optimized synthetic route for acyloxy methyl ketone probes to target cysteine proteases that included variable peptidic linkers and were labeled by ^{125}I. These probes were able to label enzyme groups like caspases, cathepsins, among others.[21] Stable isotopes are frequently used in ABPP in techniques like SILAC and have also been

incorporated into ABPs.[50] Swieten and coworkers incorporated stable deuterium isotope tags into an aminoacid spacer and derivatized the known DCG-04 cysteine protease probe into heavy and light variants which, through the presence of a biotin tag, allowed relative quantification of enzymatic activity in mass spectrometry.[51]

Fluorophores are one of the most prevalent tagging strategies in ABPP. There is a multitude of available fluorophores, covering a broad range of absorption and emission wavelengths, containing varied structural properties and being commercially available in diverse formats, including for example, alkyne and azide derivatives for click chemistry. The most used fluorophores are rhodamine, fluorescein, nitrobenz-2-oxa-1,3-diazole (NBD), BODIPY and cyanine dyes. BODIPY and Cyanine dyes are more resistant to photobleaching than more classic fluorophores like rhodamine and fluorescein and present much better cell permeation due to their lipophilicity.[11] However, most commercially available forms of these dyes are significantly more expensive than more classic options.

One of the biggest advantages of using fluorophores is the possibility of in-gel analysis of fluorescently labeled peptides, allowing for quick readout of labeled proteins immediately after running the SDS-PAGE gel and without requiring additional processing. Fluorophore-tagged ABPs can also be adapted into high-throughput screening protocols like Fluorescence Polarization (FluoPol) (see chapter 1.1.4.).[52] Applications of fluorophores in real-time analysis are usually hindered by the need to remove the excess of unlabeled probe. This can be solved by engineering a quencher into the ABP structure, which suffers an "activity-based displacement" upon engagement with the target enzyme, leading to generation of fluorescence only after reaction with a target enzyme.[53]

Biotin is the tag of choice for affinity purification of labeled peptides for mass spectrometry applications. Its use is based on taking advantage of the strong bond that forms between biotin and avidin or streptavidin, which is one of the strongest non-covalent bonds known, involving a complex network of polar and hydrophobic interactions and having an affinity constant of 10^{15} M^{-1}.[54] Binding of biotin do avidin seems to induce ordering of an avidin loop that locks biotin into its active site. Upon labeling of target proteins by a biotinylated probe, labeled proteins can be affinity-purified using biotin or streptavidin coated solid surfaces like beads.[14,16]

The use of biotin is associated with some problems, including poor cell permeability, the existence of endogenously biotinylated proteins, which are enriched together with probe-labeled proteins, and the strength of the biotin-avidin bond, which can make the elution

of labeled peptides difficult without using harsh conditions.[55,56] All these hindrances have currently been solved by simple protocol modifications and biotin remains the handle of choice for affinity purification of proteins for mass spectrometry analysis in ABPP. Alternatives to biotin usually involve the incorporation of peptide sequences that are specifically recognized by antibodies, oligonucleotide microarrays or resin-bound probes.[57-59]

Tags like biotin and some fluorophores significantly change the ABP's properties, making them unsuitable for cell permeation, which means they can't be used in assays using whole cells. The cell is a complex system that cannot be accurately replaced by whole cell lysates, which makes it important to study whole cells whenever possible. To circumvent the permeability problem, ABPs can be modified with simple handles that have little to no effect on their properties like cellular permeability and that can be modified to add a fluorophore or affinity handle after incubation with whole cells. The most common tandem labeling strategy is appending an alkyne or an azide handle to the ABP structure instead of a proper fluorophore or biotin. The ABP is then incubated with whole cells, labeling its targets, and an appropriate tag can be then attached by click chemistry after cell lysis using fluorophores or biotin with the complementary handle.[55,56,60,61]

An additional variant in tagging consists in combining more than one type of tag in the ABP, creating the so-called "trifunctional" probes. These probes usually have a fluorophore to provide an in-gel fluorescent signal and a biotin probe so that portions of the gel can be extracted, enriched and analyzed by mass spectrometry.[62]

1.1.1.3. The Linker and/or Recognition Sequence

The linker functions as a spacer between the warhead and other probe elements. It can have a simple function of removing steric hindrance between other probe elements, but can also contribute to determine target specificity, in which case it can also be called a recognition sequence. Linkers can vary from simple alkyl chains to PEG polymers of varying lengths, peptidic chains and combinations of these elements (figure 6). In some cases, the linker can be a protein domain or an entire substrate protein. However, in most cases where a peptidic sequence is used, a small peptide based on optimal protease substrate is sufficient.[18] The incorporation of ubiquitin in ABP linkers has been used as a

strategy to profile deubiquitinating enzymes, allowing isolation and identification of these enzymes, which are essential for the ubiquitin-proteasome pathway of protein turnover and other cell mechanisms.[63,64]

Focusing on the example of HNE, probe development has taken advantage of knowing the enzyme's optimal substrates contain the peptide sequence Ala-Ala-Pro-Val.[65] Target specificity can be hard to achieve even when knowing the optimal recognition sequences of specific enzymes since substrate preferences are often similar between related enzymes. The inclusion of non-natural aminoacids in peptidic linkers has proven to be efficient in achieving selectivity between related enzymes. Kasperkiewicz and coworkers have established a protocol called Hybrid Combinatorial Substrate Library (HyCoSul) to determine protease substrate specificity for HNE, including more than 100 non-natural aminoacids in their library. Optimal aminoacid recognition for each position in the peptide sequence was determined and allowed the authors to obtain a substrate that was more selective for HNE when against related serine proteases like proteinase 3 (PR3).[66]

A more functionalized strategy is the use of cleavable linkers. These linkers are stable in the conditions of proteome incubation but can be selectively cleaved by chemicals, light exposure, pH changes, enzymatic activity, among others.[67,68] In standard ABPP experiments, after trypsin digestion, filtration of the tryptic peptides leads to the loss of the sequence that was directly labeled by the ABP, since it remains bound to the streptavidin beads. Cleavable linkers can be applied after avid-enrichment of labeled proteins and trypsinization to release the ABP-modified peptides from the avidin beads. These can then be profiled to obtain direct information on the site of prove binding.[69]

A notable case is the incorporation of a tobacco etch virus (TEV) protease recognition fragment (figure 7). The incorporation of the TEV recognition sequence allows these peptides to be selectively eluted from the avidin beads and the LC-MS/MS analysis that follows provides information about the specific binding site of ABPs. Briefly, an alkynylated ABP is incubated with the proteome and then click chemistry is used to append an azide with a biotin tag and the TEV cleavage site. Labeled proteins are subjected to the usual ABPP protocol involving enrichment and on-bead trypsin digestion. After elution of tryptic peptides by filtration the labeled peptides are eluted from the beads by incubating with TEV protease. This tandem orthogonal proteolysis (TOP) approach provides the identities of all probe-labeled proteins and their modification sites in a single experiment.[1,70] Weerapana and coworkers adapted this protocol into a quantitative analysis of cysteine reactivity, labeling 1,082 reactive

cysteines, out of a total of 8,910 that existed on the 890 human proteins detected in the study.[1,12] This type of strategy is also used in isoTOP-ABPP.[12,71]

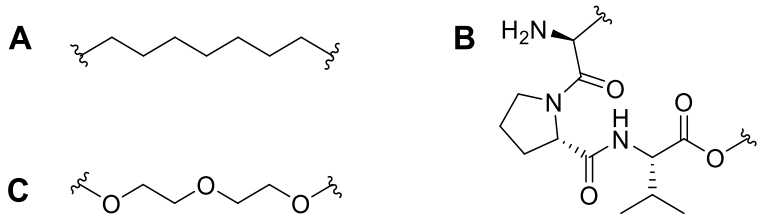

Figure 6 – Common linkers in ABPP: A. Alkyl linker; B. PEG linker; C. Peptidic linker (functions as a spacer but can also help define specificity of the probe).

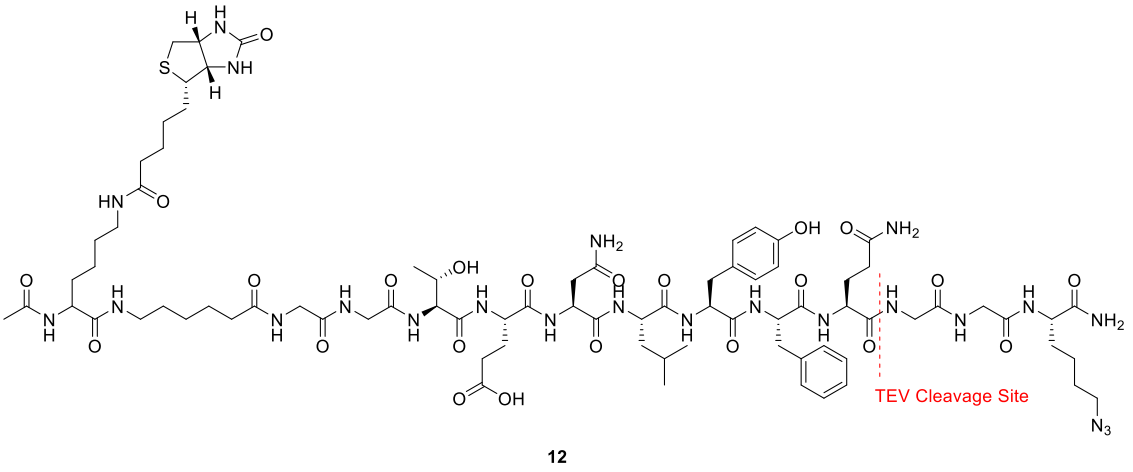

Figure 7 – TEV-biotin linker/tag. The TEV cleavage site is labeled In red.[1]

1.1.2. Gel-based ABPP

As previously noted, ABPP relies mostly on gel- and mass-spectrometry-based techniques for downstream analysis of probe-labeled proteins. Gel-based approaches are usually the first technique used to test labeling of proteins by ABPs. SDS-PAGE has been a standard technique in ABPP since its inception, allowing for rapid separation and

visualization of ABP-labeled proteins.[23,72] Application of SDS-PAGE allows up to hundreds of ABP-labeled proteomes to be quickly analyzed in a short period of time.[45] The necessary equipment to perform SDS-PAGE experiments is also more easily accessible and much less expensive than mass-spectrometry tools and equipment.

Briefly, in a gel-based ABPP experiment using SDS-PAGE, a target proteome is labeled with a pre-determined concentration of ABP. A control where the proteome is incubated with an equivalent amount of DMSO is usually performed. After a set period of time, loading buffer is added to the sample, quenching the reaction and denaturing the proteins, while SDS non-specifically covers the surface of the peptides, assuring a constant charge to weight ratio, which guarantees that the proteins will be separated by molecular weight. The samples are loaded into the gel, together with a molecular weight marker, and run at constant voltage. After separation of proteins, several techniques can be used for analysis of the results. Analysis of in-gel fluorescence allows the direct readout of protein labeling as long as an appropriate fluorescently labeled ABP was used. Other possibilities include coomassie staining and other protein staining methods, which result in total protein staining. Additionally, downstream analysis of specific proteins can be achieved by western blot, and to identify labeled proteins gel bands can be excised, enriched with streptavidin, assuming a biotinylated probe was used, and analyzed by mass spectrometry for identification. The combination of gel-based techniques with mass-spectrometry-based techniques, like in Multidimensional Protein Identification Technology (MudPIT)-ABPP, provides a very powerful platform for high-content functional proteomic analysis.[45,73]

The limitations of SDS-PAGE are mostly associated with limited resolution and sensitivity. While the technique allows for a quick glimpse into proteome reactivity of a determined probe, proteins with similar molecular weight generate superimposed signals and low abundance proteins can provide signals below the method's limit of detection or be occluded by higher abundance proteins that are also labeled.[74]

Two-dimensional polyacrylamide gel electrophoresis is also a well-established technique in proteomics and allows proteins to be separated sequentially by their isoelectric point and molecular weight.[22]

1.1.3. Mass Spectrometry-based ABPP

Mass spectrometry is an essential technique in proteomics. It is unmatched in its ability to analyze complex mixtures of peptides and provide high-content quantitative information about complex biological samples. In mass-spectrometry based ABPP, peptide mixtures are usually obtained by proteolytic digestion of a protein mixture or proteome. Sample complexity can be simplified by running an SDS-PAGE of the mixture and fractioning the sample by excising different gel bands. As per ABPP definition, the complexity of the sample is reduced in the enrichment step of the protocol. The peptide sample is then fractioned in-line with the instrument by a one- or multi-dimensional liquid chromatography separation system, commonly using a reverse-phase system that separates the peptide mixture by hydrophobicity prior to MS analysis. Introduction of the sample in the MS device is done by electrospray ionization and is concentration-dependent, meaning that peptides should be introduced in narrow peaks to improve detection limits. Application of a potential causes the sample solution to spray from the column into the mass spectrometer. Complex mixtures of peptides usually benefit from using a second dimension of separation to improve resolution. A strong cation exchange resin is a good choice to achieve this, since it can be packed together with the reverse phase matrix and allow a two-dimensional separation to be achieved in a single column by using different buffers to gradually release fractions of peptides. The mass-to-charge ratios of the peptides are measured by MS and the molecular weight is determined on a first stage. The peptide ions are directed into a collision cell and fragmentation produces a tandem mass spectrum. These data are analyzed with an appropriate software, providing the peptide sequence, which is identified by comparison with a protein database.[16,45,75]

In terms of sample preparation, a biotinylated probe is commonly used for labeling of the proteomes, but an alkynylated probe can also be used, with subsequent click reaction with biotin azide. Briefly, the technique involves the labeling of the target proteome with the probe for a predetermined time. The reactions are quenched by adding the mixture to cold methanol. The protein content of the samples is precipitated using a mixture of methanol, chloroform and PBS and the excess of probe is washed off. The proteins are denatured in the presence of urea and reduced using TCEP and alkylation of reactive side chains is achieved by incubating with iodoacetamide. Labeled proteins are enriched with streptavidin and non-enriched proteins are washed off. The enriched proteins are

trypsinized overnight. The tryptic peptides are sequenced in an LC-MS/MS equipment. A control can be prepared to be run simultaneously or separately, depending on the technique used. Processing of the data using appropriate software provides a list of engaged proteins.

Quantitative mass spectrometry methods usually take advantage of analyzing multiple samples of differently labeled peptides, which allow relative quantification of one of several samples in comparison with a control sample. This can be achieved in a single experiment by using the so-called "heavy" and "light" samples. By modifying the peptides of either the experimental/treated sample or the control sample with heavy isotope-labeled reagents, one of them will present a consistent shift in the mass of all peptides, which will allow both samples to be run and analyzed simultaneously. Peptides coming from "heavy samples" will always have a mass shift when compared with the "light sample", allowing for H/L or L/H ratios to be calculated, providing relative quantification data and eliminating the need for control probes or running the control separate to the treated sample.

Several techniques are available to achieve this, including Isotope-coded affinity tag (ICAT), reductive dimethylation (ReDiMe), stable isotope labeling by amino acids in cell culture (SILAC) and (tandem mass tag) TMT-labeling.

One of the first techniques introduced was ICAT, where identical tags with different mass are appended to peptides, allowing the differentiation of proteins from different samples at the MS^1 level. Early ICAT tags had a iodoacetamide reactive group, a linker with light or heavy isotopes, and a biotin for affinity enrichment.[76]

A different technique, ReDiMe, where labeling is performed by methylation of the N-terminal of peptides using formaldehyde, leads to irreversible dimethylation of the peptide N-terminal, resulting in a molecular weight shift of +6 to all the peptides labeled with "heavy" formaldehyde (figure 8 – A).[77]

In SILAC, the isotopic labels are introduced during cell culture. Cells are grown in either heavy or light media, resulting in either heavy or light cells. Peptides coming from the sample grown in "heavy media" will have a mass shift when compared with the ones grown in "light media" (figure 8 – B).[50] SILAC is advantageous when compared with ReDiMe since the early introduction of the labels simplifies the protocol, reduces the number of samples and minimizes variability in samples preparation.

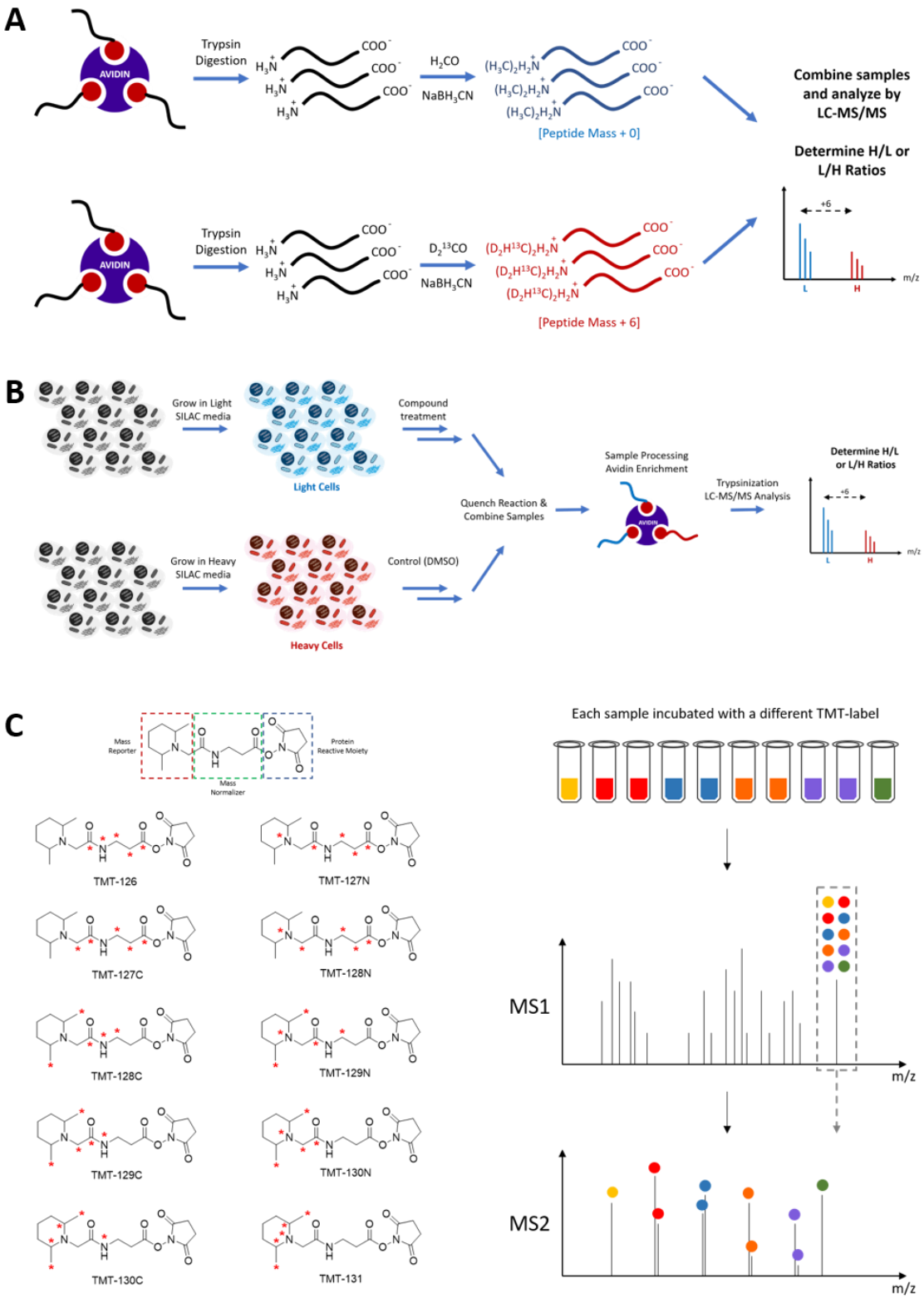

Figure 8 – A. ABPP-ReDiMe. B. ABPP-SILAC. C. TMT tags used in 10plex TMT.

A more recent iteration of quantitative relative protein quantification in proteomics is TMT-labeling. The TMT-labeling procedure makes use of isobaric tags. These reagents are composed of a mass reporter, a mass normalizer and an amine-reactive group. The mass reporter and the mass normalizer have different distributions of stable isotopes, such that the mass of each tag is the same and the signal resulting from labeling of a protein with each different tag is the same in a MS^1 spectrum, but able to be resolved in a MS^2 spectrum. Since the different tags possess the same mass and similar chemical properties ensures that peptides labeled with the same TMT tags will have similar chromatographic elution and ionization. This makes it so that multiple samples (up to 10 with 10plex TMT – figure 8 – C) can be labeled with different TMT-tags and analyzed in parallel in the same LC-MS/MS run.[78]

A detailed description of the methods of analysis of ABPP mass spectrometry data is out of the scope of this project. Nevertheless, a brief description of the process used for the processing of the proteomics data generated in this project is given here. After running the samples in the LC-MS/MS, protein identification and quantification and analysis were done with the Integrated Proteomics Pipeline-IP2. Spectrum raw files were extracted into ms1 and ms2 files from raw files and searched against a human protein database. A static modification to account for the isotopes introduced in SILAC or the dimethylation in ReDiMe were specified. Quantification of light/heavy or heavy/light ratios was performed using software developed by the Cravatt Lab which reads raw chromatographic data in the mzXML format. Ion chromatograms are analyzed to identify target peptide m/z values for which both a light and heavy modification was identified. Candidate co-eluting pairs of ms1 peaks (light and heavy) are analyzed and the ratio of integrated peak area is calculated. The combined ratios for peptides belonging to a protein are grouped and the median value found is reported as the final ratio. A more detailed description of this method has been reported by Weerapana et al.[12]

1.1.4. Competitive Activity-based Protein Profiling

In many ABPP experiments where an alkyne derivative of a covalent inhibitor is used it is common to perform a competition experiment with the original inhibitor to demonstrate the blocking of probe labeling and prove that the probe and the inhibitor have similar

reactivities. This approach has been adapted to the screening of libraries of compounds in a technique called competitive ABPP. The technique uses a broad reactivity probe for labeling of groups of enzymes, usually within the same family, and tests compounds for their ability to block labeling by the reactive probe.[69] Briefly, whole cells or cell lysates are incubated with the compound and DMSO separately. After a pre-determined incubation time both samples are labeled with fluorescent probe. The samples are run in SDS-PAGE or LC-MS/MS and the protein profiles are compared between the DMSO control and the compound-treated sample. If a target enzyme's active site is covalently inhibited by the tested compound, labeling by the probe is blocked and the specific signal for that protein will be absent when compared with the DMSO control (figure 9).[79] Alternatively, a biotinylated probe can be used and the protocol adapted for mass-spectrometry-based competitive ABPP. In this case, the labeled proteins can be directly identified and information regarding reaction stoichiometry can also be inferred.

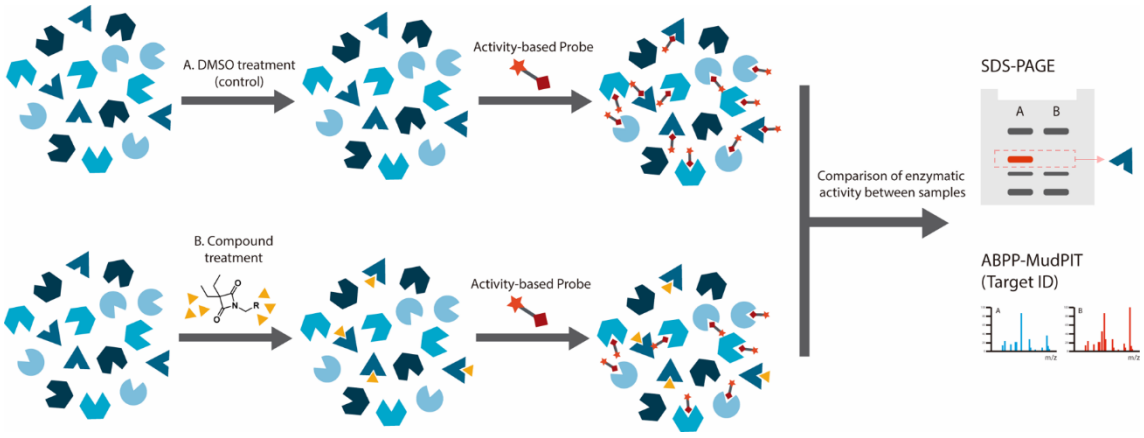

Figure 9 – Competitive ABPP Workflow. Separate samples are prepared for DMSO (control) and compound treatment. The compound will label its targets in the proteome. Both samples are then labeled with an appropriate broad reactivity ABP. The results can be read by SDS-PAGE (fluorescent ABP) or mass spectrometry (biotinylated ABP). If an enzyme is a target of the compound being tested the signal corresponding to this enzyme will be absent or attenuated when compared with the DMSO control.

This allows for the application of ABPP techniques to non-probe compounds and can be performed for preliminary screening of large libraries, generating quick data on compound reactivity, potency, selectivity and allowing the calculation of parameters like IC_{50}, even for uncharacterized enzymes. The pool of analyzable targets will, however, be

limited to the scope of targets engaged by the ABP, which means that broad reactivity probes with good coverage of high occupancy targets are required and highly valuable. Commonly used ABPs for competitive ABPP include the FP probes for serine hydrolases[20,80] and iodoacetamide probes for reactive cysteine residues.[12,81] An ideal competitive ABPP assay should use a probe or a combination of probes that covers the largest percentage of engageable targets possible.

A derivative of the competitive ABPP platforms is Fluopol-ABPP which allows an enzyme to be screened in vitro for compounds that bind to it. ABPP-Fluopol provides a signal in the form of light polarization, which can be associated with the size of the complexes formed after the reaction of a fluorescent ABP and a target enzyme. In this technique, a target enzyme is incubated with a library of inhibitors for a pre-determined period and then the fluorescent probe is added to the reaction. When excited with plane-polarized light, light emission from the fluorophore is parallel to the excitation plane, which can be altered by the rotation of the structure containing the fluorophore. A probe that reacted with an enzyme will have slower rotation and emit polarized light. On the other hand, if a library inhibitor is very potent and fully inhibits the enzyme, probe labeling will be blocked and the free probe with have faster rotation and emit depolarized light. Evaluation of light polarization can then be associated with inhibitor potency. The technique is compatible with high throughput screening and can be easily adapted to different enzyme classes, as long as the pure target enzyme is available. Bachovchin et al used ABPP-Fluopol to discover selective inhibitors for the enzymes retinoblastoma-binding protein-9 and glutathione S-transferase omega 1.[52] Knuckley and coworkers developed a high throughput screening based on Fluopol-ABPP to identify protein arginine deiminase isozyme-selective inhibitors, with 10 successful hits inhibitors, including a selective inhibitor, from a library of 2000 compounds.[82]

1.2. Activity-based Protein Profiling of the Serine Hydrolase Family of Enzymes

The serine hydrolases are one of the most well-studied classes of enzymes by ABPP, comprising over 200 enzymes and 1% of the proteome. Approximately half of these are the serine proteases, with the other half being the "metabolic serine hydrolases".[83,84] Among them we find several enzyme types, including lipases, esterases, thioesterases, amidases, peptidases and proteases.[85]

They play vital roles in numerous processes in human biology, including digestion, coagulation, inflammation, peptide processing, immunoregulation, reproduction, among others.[20,85] Disfunctions in their behavior are therefore responsible for numerous pathologies, including cancer, hemorrhagic disorders, chronic obstructive pulmonary disease (COPD) and many others, while also being involved in processes like pathogen infection and drug resistance.[83] These factors make them attractive targets for the development of inhibitors and drugs, with some serine hydrolase inhibitors being approved for the treatment of diseases like Alzheimer's (acetylcholinesterase), type 2 diabetes (DPP4), obesity (pancreatic and gastric lipases), thrombosis (thrombin and factor Xa).[85]

The defining characteristic of this enzyme family is the catalytic serine residue that is used to cleave their substrates.[83] The general mechanism involves the activation of the hydroxyl group in the serine residue, assisted by additional active site residues, typically histidine and aspartic acid, but with other possible variations. Additionally, the existence of an oxyanion hole, formed by other surrounding aminoacid side-chains, assists the nucleophilic attack by helping to stabilize the tetrahedral intermediate formed upon

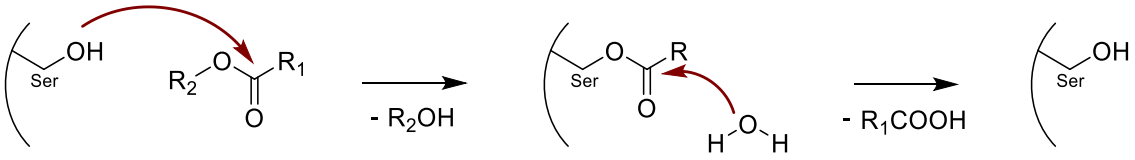

Scheme 1 – Representative mechanism of serine hydrolase catalytic activity.

hydroxyl attack on the substrate.[86] The nucleophilic hydroxyl of the catalytic serine residue attacks an electrophilic moiety of the substrate, forming an acyl-enzyme intermediate. Water-induced saponification of the product regenerates the enzyme active site for the next catalytic cycle (scheme 1).[83]

Several chemotypes have been used for serine hydrolase labeling in ABPP.[2] The shared catalytic mechanism dependent on a highly nucleophilic serine residue makes serine hydrolases susceptible to irreversible inhibition by reagents like fluorophosphonate (FP), the most common warhead for serine hydrolase ABPP.[20,84] Additional examples are presented in figure 10 and include diphenyl phosphonates,[87] diphenyl phosphoramidates,[88] β-Lactams,[89-91] β-Lactones,[92,93] sulfonyl fluorides,[94,95] coumarins and isocoumarins,[96,97] carbamates[98] and heterocyclic ureas.[99]

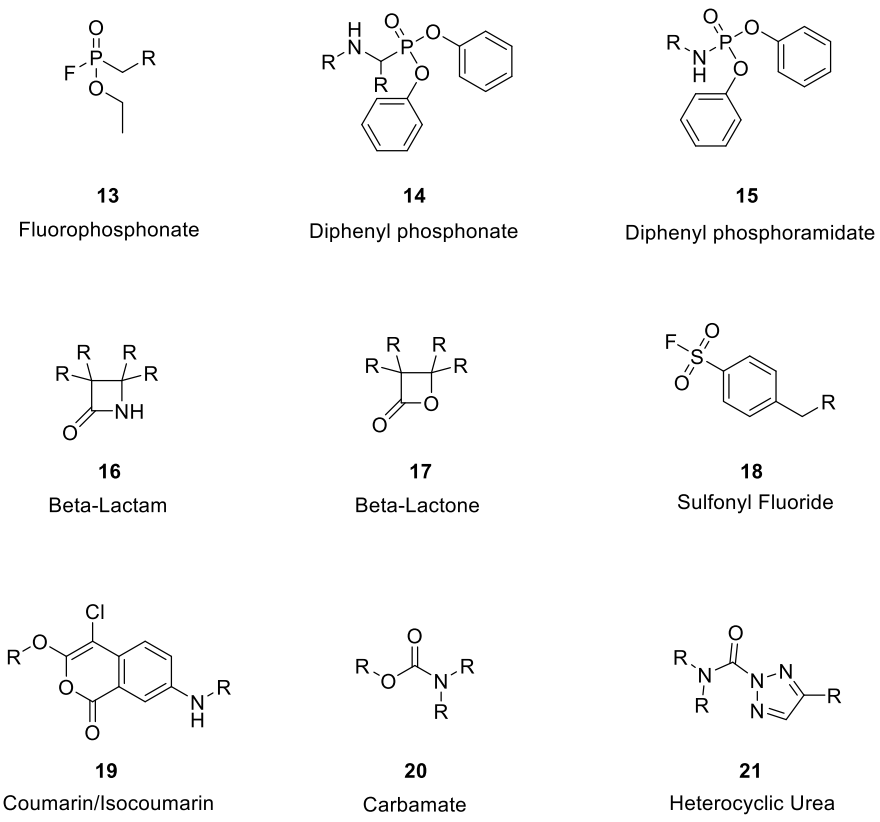

Figure 10 – Serine-reactive electrophiles. Adapted from Shannon and Weerapana.[2]

FP probes have had broad application in ABPP experiments of the serine hydrolase family of enzymes and supported most of the ABPP studies performed for this family of enzymes in complex proteomes.[100] Liu et al reported the profiling of serine hydrolases using an FP-biotin probe (figure 11). The FP-Biotin probe was first tested with fatty acid amide hydrolase (FAAH), behaving as a potent irreversible inhibitor of the enzyme and tagging only the active form of the enzyme. Overall, the FP probe was shown to efficiently label serine hydrolases in crude cell and tissue samples, allowing differences in the enzyme's functional state to be identified, even when enzyme activity varies with no correlation to its quantity or expression.[20]

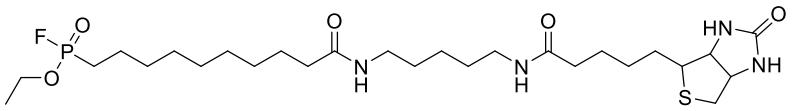

22

Figure 11 – FP-Biotin ABP.

Kidd et al showed that the nature of the linker between the FP warhead and the biotin tag had little to no influence on the reaction of FP with serine hydrolases, except for select proteins like FAAH, which reacts faster with a FP probe containing an alkyl linker. The optimal concentrations of probe to achieve the best specific to nonspecific proteome reactivity were determined to be between 4 and 8 μM and the optimal pH was determined to be around 8, with significant increase of nonspecific reactivity at pH 9. The probes were shown to efficiently label membrane proteins, which are usually harder to profile by conventional methods.[80]

Some of the first examples of the use of ABPP in the serine hydrolase superfamily were related to the study of cancer. Jessani et al used FP probes to study the serine hydrolase dynamics across human breast and melanoma cell lines with differences in hormone responsiveness, invasiveness, and metastatic potential, fractioning the proteomes into secreted, membrane and soluble protein fractions. The resulting serine hydrolase activity profiles allowed different cancer types to be clustered into subtypes according to properties like tissue of origin and invasiveness.[28] The authors also studied the enzymatic

activities of serine hydrolases in the process of breast tumor growth in vivo. The objective was to identify the differences between human breast cancer line MDA-MB-231 in vitro and in xenografts in immunodeficient mice. While several serine hydrolases were shown to be similarly expressed in both systems, several others were shown to be expressed exclusively in xenografts, potentially due to the presence of host factors, which induce alterations in the proteomic expression pattern, as confirmed by the identification of mice serine hydrolases in the samples. This work supported the fact that experiments using human cancer cell lines provide results that are not always representative of in vivo tumor properties like proliferation, invasiveness, and drug sensitivity.[101]

Nomura et al used FP to perform a functional proteomic analysis of aggressive and nonaggressive human cancer cell lines, identifying neutral cholesterol ester hydrolase (1KIAA1363) and monoacylglycerol lipase (MAGL) to be consistently elevated in aggressive cancer cell lines, suggesting a role of these enzymes in cancer aggressiveness. The work unveiled a MAGL-dependent pathway that regulates free fatty acid levels in cancer cells, which is associated with migration, survival, and in vivo tumor growth.[102]

These approaches focused mostly on gel-based assays, but ABPP truly excels at providing functional information on enzyme families when these are combined with mass-spectrometry techniques. An integrated strategy for profiling of serine hydrolase activities in cancer was described by Jessani et al. On a first phase, 33 primary breast tumor samples were characterized and split into classes based on their serine hydrolase activity profiles obtained through one-dimensional electrophoresis. A second phase using ABPP-MudPIT provided a complete in-depth analysis of the serine hydrolase activities in these samples. Over 50 serine hydrolase activities were identifies, including proteases, lipases, esterases and numerous uncharacterized enzymes. fibroblast activation protein (FAP), platelet-activating factor acetylhydrolase 2 (PAFAH2) and KIAA1363 were found among the enzymes that were elevated in ER(-)/PR(-) cancers.[45] Madsen et al determined that urokinase-type plasminogen activator is a determinant enzyme in tumor cell entry into the vasculature, one of the earliest steps in metastasis, by applying serine hydrolase targeting probes in high disseminating and a low disseminating human fibrosarcoma cell lines. The low disseminating cells were shown to contain abundant amounts of inactive enzyme, highlighting that the active enzyme state is necessary for the high disseminating characteristic.[103]

ABPP was also applied in the characterization of brain enzymes responsible for the hydrolysis of 2-arachidonoylglycerol, a ligand for cannabinoid receptors, after the

observation that upon FP probe treatment, the hydrolysis of this molecule was halted. Among the identified targets were MAGL, α/β hydrolase domain fold family protein 6 (ABHD6) and α/β hydrolase domain fold family protein 12 (ABHD12).[104] Viader and coworkers used ABPP to map serine hydrolase dynamics across different mouse brain cell types, detecting a large number of enzymatic activities that varied between cell types, including the enzymes that regulate 2-arachidonoylglycerol (2-AG) metabolism in microglia, ABHD12 and diacylglycerol lipase β.[105]

ABPP has also been used to clarify the roles of some serine hydrolases. Diphenyl phosphonate ABPs were used to clarify the roles of granzymes A and B in cytotoxic lymphocyte-mediated cell death. The results suggested that granzyme B plays a major role in lymphocyte-mediated lysis of targeted cells. This study provided information that could not be obtained from conventional genetic or biochemical experiments.[106]

In the field of infection and microbiology, ABPs based on 4-membered ring chemotypes like β-Lactams have been extensively used for the study of bacterial pathogenesis.[107,108] Even before the ABPP concept had been established, Dargis and Malouin developed the first biotinylated β-Lactams (figure 12 – A), to more easily characterize and purify penicillin binding proteins (PBPs) in bacteria.[109] PBP labeling was traditionally done with isotope-labeled penicillin. Zhao and coworkers introduced the use of Bocillin-FL (figure 12 – B), which consisted of penicillin V with an appended BODIPY tag, as a reagent for quick visualization of nanogram amounts of PBPs.[110]

Staub and Sieber developed a library of alkyne probes based on the β-Lactam structure. The β-Lactam chemotype was appended with a short alkyne handle, different side chains and modifications of the amide by sulfonylation or acylation to provide chemical variability. Well-established antibiotics were also derivatized with an alkyne handle, including aztreonam, ampicillin and cephalosporin (figure 12 – C). Labeling of *P. putida* with the antibiotic probes showed high specificity and significantly different target profiles. Target deconvolution by LC-MS revealed labeling of several PBPs by the antibiotic probes. The synthetic β-Lactam probes did not label PBPs, but instead targeted other proteins like virulence factors. Targeting these molecules was envisaged as a potential new strategy for treatment of bacterial infections.[90] In a follow-up work with *S. aureus* and methicillin-Resistant *S. Aureus* (MRSA), a subset of the best compounds identified 5 enzymatic activities unique to MRSA, suggesting they may be relevant for resistance development.[89]

β-Lactones have also been extensively studied in ABPP and found to be efficient inhibitors of crucial virulence factors. Examples of β-Lactone probes are showed in figure 12 – D. These experiments also guided the development of novel inhibitors which showed promise in the treatment of resistant strains and helped identifying enzymes that are active in dormant states of pathogens like Mycobacterium bovis.[61,92,111-113] β-sultams were also studied in ABPP (figure 12 – E), revealing the modification of internal threonine residues in azoreductases present in bacterial proteomes instead of the expected serine reactivity.[114]

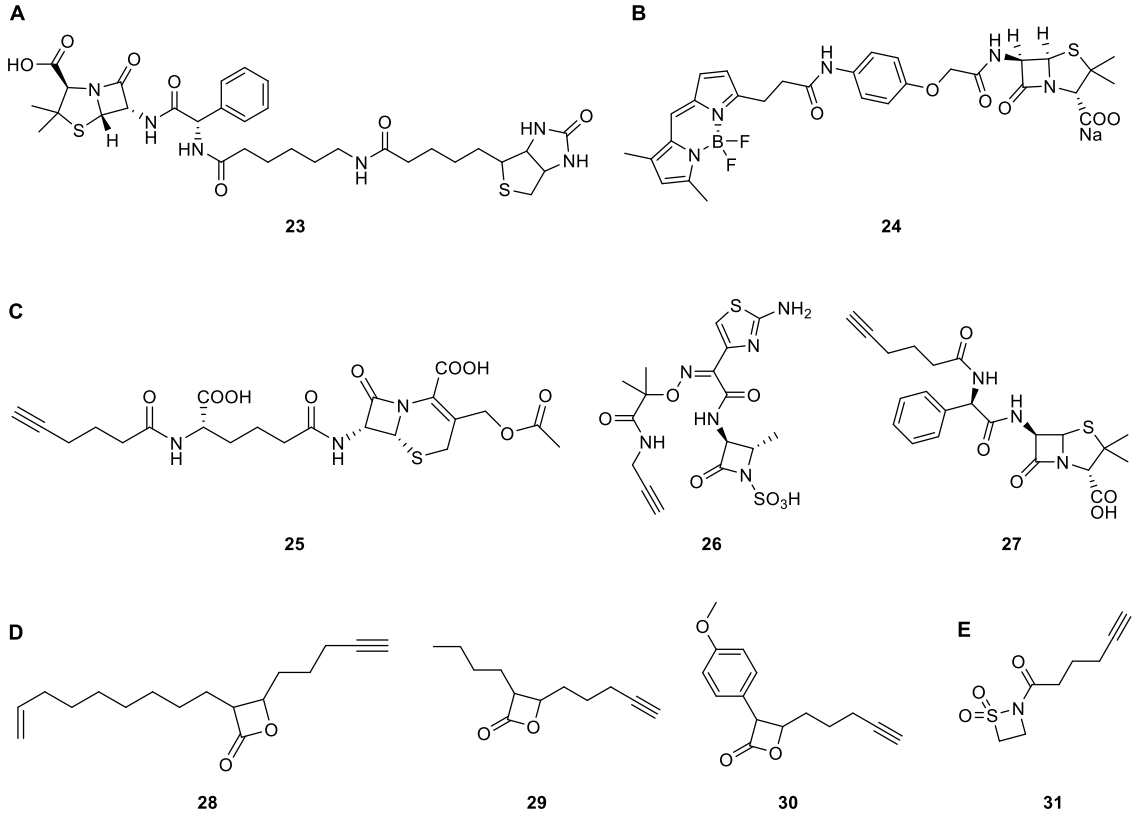

Figure 12 – ABPs based on β-Lactam, β-Lactone and β-Sultam warheads.

Another notable example was the characterization of active enzymes in both active and persistent Mycobacterium tuberculosis. The study identified enzymes that remain active in persistent states and that could potentially be therapeutically targeted to eliminate

resistant forms of the disease.[115] FP was also used in numerous other studies that helped characterize serine hydrolase dynamics in Mycobacterium tuberculosis.[116-120]

Additional examples include the use of ethyl-p-nitrophenyl phosphonates to profile lipolytic enzymes and esterases and FP probes for the study of rhomboid proteins.[96,121-125]

Competitive ABPP has also greatly contributed to the study of serine hydrolases and the discovery of new inhibitors. Li et al used a competitive ABPP platform to develop inhibitors for the enzyme ABHD6, which was uncharacterized at the time. The ABPP approach allowed a small library of carbamate inhibitors to be screened for the enzyme and also guided the optimization of the best hit into a potent and selective ABHD6 inhibitor.[126] Competitive ABPP was also used to assess the targets of a compound containing a piperidine/piperazine urea group as the electrophilic warhead, revealing that the compound is highly selective for FAAH, with no detectable activity against other serine hydrolases, a particular reactivity profile which was attributed to the high chemical stability of the urea and FAAH's ability to hydrolyze C(O)-N bonds.[127] In a follow up work a FP-based competitive ABPP screen was used to guide medicinal chemistry optimization of dual FAAH/MAGL inhibitors based on the *N*-substituted piperazine carbamate scaffold, which resulted in inhibition of the hydrolysis of the substrates of these enzymes, anandamide and 2-AG, allowing the study of the impact of elevations in these endocannabinoids.[128]

A modified approach where, instead of the blockade of probe labeling, the slowing down of the rate of probe reaction is measured at a kinetically relevant time point, has also allowed the competitive ABPP technique to be applied to reversible inhibitors and led to the discovery of inhibitors for enzymes like FAAH, triacylglycerol hydrolase and KIAA1363.[129] The uncharacterized enzyme KIAA1363's role in lipid signaling pathways was later uncovered through a multidimensional platform that included competitive ABPP.[130]

Despite being one of the most well-studied families of enzymes by ABPP, it was reported in an excellent review by Simon and Cravatt in 2010 that nearly half of the human metabolic serine hydrolases remain uncharacterized in terms of their substrates and functions.[84] Considering the importance of the currently annotated serine hydrolases and the magnitude of impactful discoveries made by ABPP of serine hydrolases that were described in this section, we can deduce that non-annotated serine hydrolase surely have

similar vital roles in human biology and can be an important source of new targets for drug design endeavors.

1.2.1. Target Enzymes for our Project

In this work we focused our attention of a small group of serine hydrolases, which included known targets of our 4-membered ring chemotypes, like HNE, and additional serine hydrolase families like α/β hydrolase domain fold (ABHD) and dipeptidyl peptidase (DPP) enzymes that were discovered as targets of 4-Oxo-β-Lactams by ABPP-MudPIT through the course of the project. Herein we describe relevant information regarding these enzymes, focusing on HNE, the model enzyme for the development of our libraries, and members of the DPP and ABHD families of serine hydrolases.

1.2.1.1. Human Neutrophil Elastase and Chronic Obstructive Pulmonary Disease

HNE is a neutrophil serine protease. Neutrophils are important effectors of the immune system and participate in the first line of host defense against invading pathogens using a combination of oxidative and non-oxidative mechanisms and mediating the link between the innate and adaptive arms of the immune response. Microorganisms are engulfed by neutrophils via phagocytosis, a process which activates the membrane-bound NADPH oxidase system. This system produces reactive oxygen species (ROS), which directly kill microorganisms, constituting the oxidative mechanism of neutrophil action. The non-oxidative pathway involves fusion of neutrophil granules with the phagolysosome, releasing antimicrobial peptides and neutrophil proteases into it.[131] The most commonly described neutrophil serine proteases are HNE, PR3 and cathepsin G. More recently, additional members like proteinase 4 have been described.[132,133]

HNE is a basic single-chain glycoprotein with 218 aminoacids and approximately 25 kDa in size. It contains four intramolecular disulfide bridges and two asparaginyl N-linked carbohydrate side chains, resulting in different isoforms. The catalytic triad is composed of serine, histidine and aspartate, which come together at the catalytic center. Like for

other serine hydrolases, catalysis involves proton transfer between the catalytic triad and allows serine to become a highly reactive nucleophile and attack an electrophilic moiety in the target.[134]

HNE's activity is tightly regulated due to its destructive potential for biological tissues. The enzyme is first regulated at the synthetic level during transcription in granulocyte development and then at a post-translational level before being stored in the azurophilic granules of neutrophils in its active form. The enzyme is synthesized as an inactive prepro-protein, which contains a signal peptide and an amino-terminal prodipeptide that must be cleaved to generate the active form.[135] HNE is stored in the azurophilic granules of neutrophils, but also associates with the nuclear envelope.

Activation of neutrophils leads to mobilization of neutrophil serine proteases and secretion into the extracellular medium. A fraction of the expelled serine proteases associates with the cellular membrane.[136,137] Neutrophil activation leads to a significant increase of membrane-bound HNE.[138] Previous studies have shown that structures of high HNE concentration upon neutrophil activation can contain HNE that is mostly in an inactive state.[66]

The S1 pocket in HNE is hemispherical and hydrophobic and its substrate preference has been well studied.[66] The pocked preferentially accommodates small hydrophobic residues, with the same happening for PR3, which has a smaller active site.[65,139-141] The preferences for the additional subsites of HNE using both natural and non-natural aminoacids have also been determined and are discussed in more detail in section 1.2.1.1.[66]

Functionally, HNE and other neutrophil serine protease are mainly involved in pathogen killing, chemotaxis and regulation of inflammation. The mechanisms involve varied methods like processing of bacterial outer membrane proteins, cleavage of virulence factors and trapping of bacteria in phagolysosomes.[131]

The proteolytic activity of HNE is tightly controlled by several endogenous inhibitors to avoid excessive destruction of connective tissue proteins like elastin, collagen and proteoglycans. The most commonly referenced inhibitor is alpha1-antitrypsin. Its primary function is to protect lung parenchyma against destruction by neutrophil serine proteases. It acts by irreversible inhibition using a suicide substrate inhibition mechanism that alters HNE's active site into a non-functional state. Other HNE endogenous inhibitors include

SerpinB1, the recombinant form of PI9, elafin and secretory leukocyte protease inhibitor (SLPI), which acts by a reversible mechanism.[135,142]

HNE-associated pathogenesis is usually related with an imbalance between protease and antiprotease activity, which is required for lung tissue homeostasis. In persistent inflammatory states, the balance is shifted towards the protease side and the inflammatory process becomes self-sustained, leading to tissue injury.

Our main interest in studying HNE is its role in the development of COPD.[4] Other HNE-related lung pathologies include cystic fibrosis, acute lung injury and acute respiratory distress syndrome which are mostly caused by trauma, sepsis and pneumonia, and are associated with massive accumulation of neutrophils in the lung.[143] HNE's role in cancer development is also well established.[144,145]

COPD describes a broad syndrome that encompasses a group of diseases, including chronic bronchitis and emphysema, that cause progressive and non-reversible limitation of lung airflow. The chronic bronchitis component is associated with persistent productive cough and obstruction of small airways, while emphysema stems from loss of lung elasticity, destruction of lung parenchyma and enlargement of air spaces.[146,147] COPD is predicted to become the 3rd leading cause of death worldwide by 2020, with COPD prevalence and mortality being still underestimated due to underdiagnosis and because comorbidities are commonly recorded as the causes of death.[148-150]

The disease is mainly caused by prolonged exposure to cigarette smoke but other factors include occupational and environmental toxins and air pollutants, recurrent bronchopulmonary infections, history of tuberculosis and asthma, airway hyper-responsiveness and genetic factors like deficiency in alpha-1-antitrypsin.[151-154]

Neutrophil migration to the site of inflammation to neutralize the external aggression and externalize serine proteases like HNE.[152,153] These enzymes are clinically relevant for disease initiation and progress.[4,155] In a synergistic pro-COPD effect, oxidized inactive alpha-1-antytrypsin has been found in the bronchoalveolar fluid of smokers, together with oxidized forms of other endogenous inhibitors of HNE like SLPI. When the external aggression is persistent the inflammatory process becomes self-sustained and an imbalance between HNE and its endogenous inhibitors may occur. The excessive activity of HNE leads to an increase in elastin degradation, which causes loss of elasticity of lung tissue and limitations in the tissue's ability to expand and contract. Furthermore, the sustained inflammation, associated with T cell release of granzyme B and perforins leads

to an increase in pneumocyte apoptosis. The replacement of these native lung tissues with fibrous tissue hinders the breathing process and eventually causes emphysema when small airway walls collapse for not being able to withstand lung expansion during inhalation. The chronic bronchitis component is associated with chronic irritation that leads to failure of the mucociliary system due to cellular atrophy and decrease in ciliated cell number and length. Furthermore, alterations in the number and function of secretory cells, including enlargement of mucous glands and hyperplasia of goblet cells in the airways lead to overproduction of mucus. The failure of clearance mechanisms leads to accumulation of the secretions, which cause airway obstruction and potentiate the development of bacteria and infection (figure 13).[156-162]

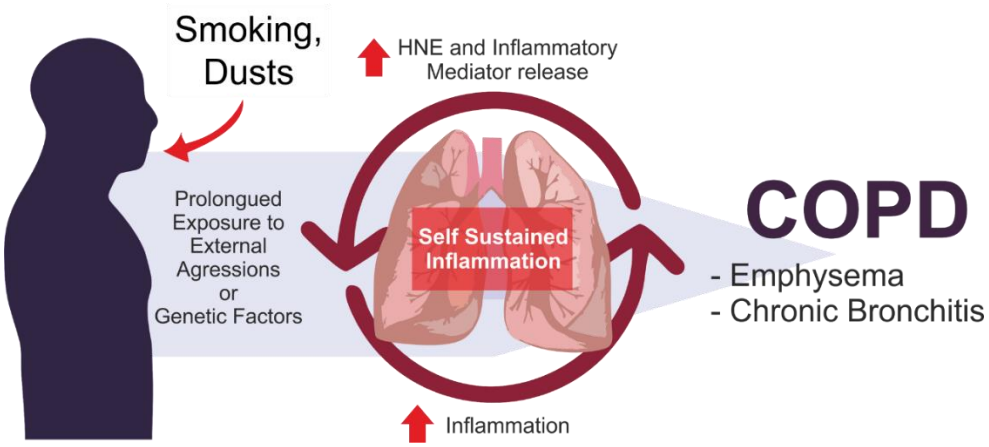

Figure 13 – COPD Ethiology.

1.2.1.1.1. Human Neutrophil Elastase Inhibitors

No current treatments show efficacy in halting or reversing COPD progression. The existing therapeutic strategies are mostly based around the control of symptoms and increase in quality of life by use of bronchodilators, anticholinergics, phosphodiesterase inhibitors, glucocorticosteroids, and supplemental oxygen.[4]

Despite the high amount of research put into developing HNE inhibitors, Sivelestat or ONO-5046 (scheme 2) is the only elastase inhibitor to ever reach the market (Ono

Pharmaceutical). It was developed in Japan, where it is approved and widely used for the treatment of acute lung injury with systemic inflammatory response syndrome.[163,164]
HNE inhibitors usually fall into 4 categories: acylating-enzyme inhibitors, mechanism-based inhibitors, transition-state analogs, and noncovalent inhibitors.[4]

The mechanism of HNE inhibitors usually involves taking advantage of the nucleophilic character of the active site serine and inducing its attack on a substrate which results in a stable adduct. The attack of the serine on a nucleophilic moiety of the inhibitor leads to the formation of a tetrahedral intermediate. This intermediate can be stabilized by hydrogen bonding with NH groups of the enzyme's oxyanion hole to promote a more stable inhibition or be hydrolyzed and regenerate the enzyme's active site. The intermediate can also collapse, displacing a leaving group and resulting in a covalently modified active site. Furthermore, bulky hydrophobic substituents can help prevent hydrolysis of the inhibitor from the active site. These factors influence the reversibility of the inhibition process and if the tetrahedral intermediate is stable enough the enzyme can be considered irreversibly inhibited.[4]

ONO-5046 is an example of an acylating agent, with an IC_{50} of 44nM and K_i of 0.2 µM. Its mechanism is reversible, which could account for its higher safety when compared to other inhibitors (scheme 2).

Among the acylating agents we find several types of inhibitors based on 4-membered rings. β-Lactams have been extensively used in Medicinal Chemistry, particularly due to their importance in antibiotic development.[107,165,166] β-Lactams were first derivatized into HNE inhibitors by Merck in 1986, with the major modification from a traditional cephalosporin antibiotic being the conversion of the ionizable carboxylate group from position 4 into an amide or ester. This preference for non-ionic moieties is consistent with the function of HNE in cleaving peptide linkages between non-ionic aminoacids.[167] Inhibition was shown to depend on the attack of the serine to the β-Lactam ring and formation of a tetrahedral intermediate. The collapse of the intermediate is facilitated by the presence of a leaving group and leads to the opening of the β-Lactam ring, potentially generating a secondary electrophilic moiety that would allow for a suicidal inhibition mechanism to take place. Some of these cephalosporin-based inhibitors were considered functionally irreversible inhibitors, since the recovery of HNE activity after inactivation is slow.[168] Additional experiments found monocyclic β-Lactams to be remarkably potent,

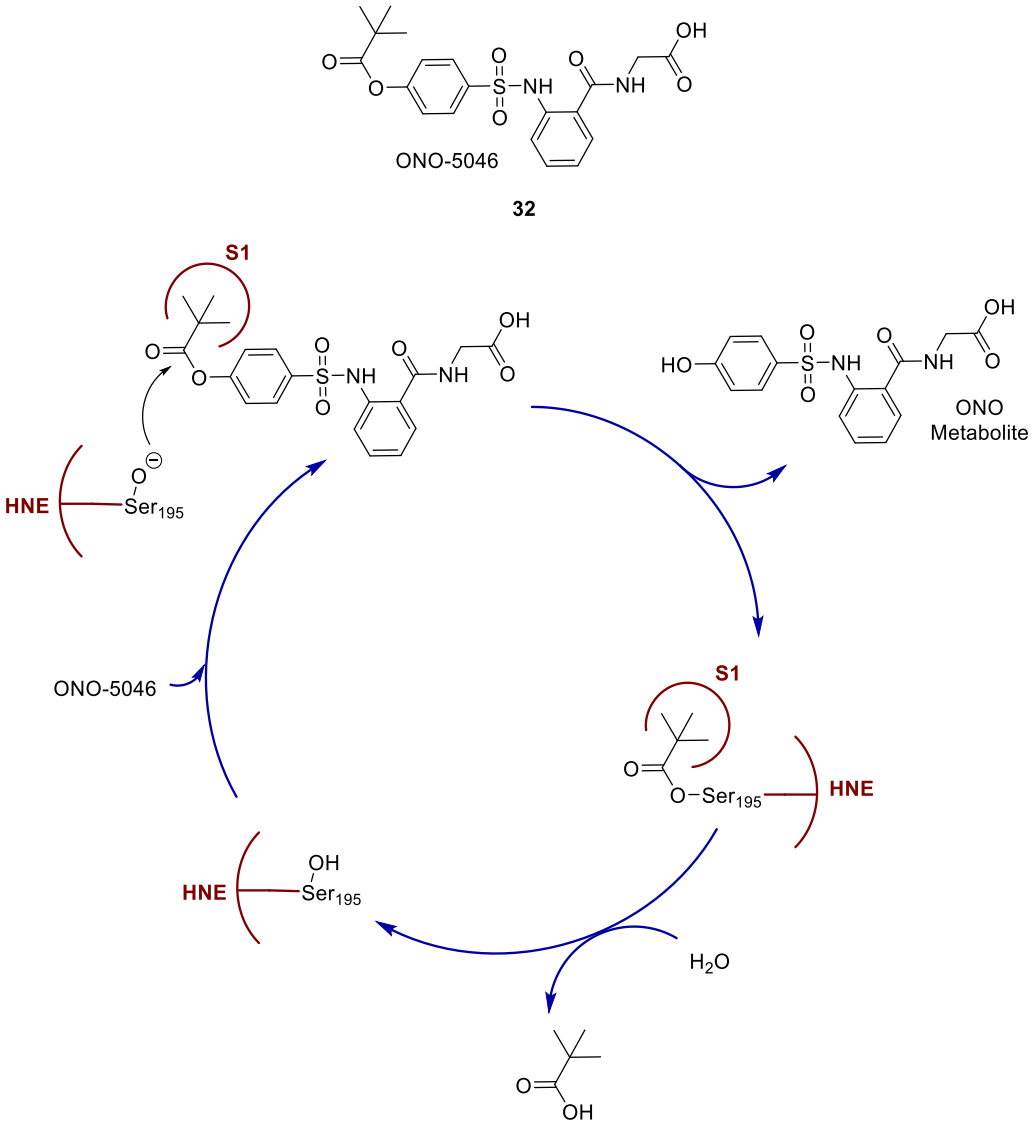

Scheme 2 – ONO-5046 (Sivelestat) and its mechanism of HNE inhibition. Adapted from Lucas et al.[4]

selective and orally active as HNE inhibitors (figure 14 – A).[169] Moreira's group also developed β-Lactams as suicide inhibitors of HNE. Clemente et al reasoned that adapting the leaving group strategy to β-Lactams could lead to development of suicide inhibitors of HNE and developed C-3 and C-4 substituted N-acyloxymethyl and Naminocarbonyloxymethyl-2-azetidinones (figure 14 – B).[170] Since β-Lactam reactivity is dependent on how good the amine leaving group formed from tetrahedral intermediate decomposition is, the group performed additional testing, obtaining good results with a

oxazolidin-2,4-dione moiety on the leaving group and with electron withdrawing substituents at position 4 (figure 14 – C).[171]

Other 4-membered rings that were developed for HNE inhibition include β-sultams. Inhibition by β-sultams is hindered by the fact that sulfonyl derivatives are less reactive than their acyl counterpart, but efficient inhibitors were developed from N-aryl β-sultams.[172] Additional 4-membered ring scaffolds include the 3-Oxo-β-Sultams, developed as HNE inhibitors by the Page Lab,[173] and 4-Oxo-β-Lactams developed by Moreira's Lab.[174,175] These scaffolds will be the basis for our project and will be discussed in detail in the following sections (see section 1.3.1. for 3-Oxo-β-Sultams and section 1.3.2. for 4-Oxo-β-Lactams).

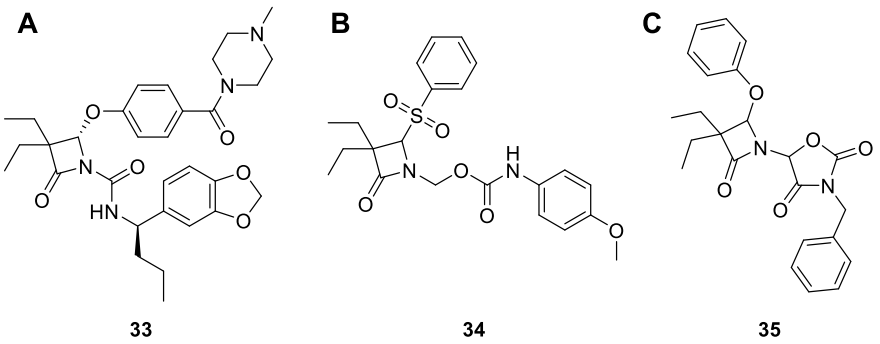

Figure 14 – Examples of HNE Inhibitors based on the β-Lactam scaffold.

Bicyclic pyrrolidine trans-lactams were also developed, with some compounds being reported to be potent, selective, and to have prolonged pharmacodynamic and acceptable clearance rates in animal models.[176]

The concept of transition-state analogs involves the replication of van der Waals interactions and molecular electrostatic potential surfaces as close as possible to those that stabilize the transition state of a given enzyme.[177] An example of these compounds is ONO-6818 (figure 15 – A), disclosed as a promising therapeutic agent to treat HNE-related inflammation. The compound was shown to react with the catalytic serine of porcine pancreatic elastase (PPE) and result in a stable, tetrahedral, hemiketal adduct, with the oxygen anion stabilized by hydrogen bonds to the backbone amide N-H of both SER-195 and GLY-193. An alternative strategy to increase inhibitor residence time in the lungs was developed by Guarnieri et al, who hypothesized that linking an HNE inhibitor

to a fragment of a lung surfactant molecule could improve the inhibitor's lung residence time when administered intratracheally. A transition state analog was appended to the N-terminal 1–25 residues of human surfactant peptide B and showed more efficient protection against HNE-related emphysema when compared with the original unlinked inhibitor. This seems to be a valuable strategy to increase inhibitor residence time in the lung since due to the high profusion of the organs, small hydrophobic molecules are usually cleared very fast.[178]

Mechanism-based inhibitors are designed to take advantage of the nucleophilic attack of the catalytic machinery of the target enzyme to induce a structural change in the inhibitor that generates a highly reactive electrophilic group, which is able to react with the enzyme a second time, rendering the enzyme irreversibly inhibited. Upon formation of the tetrahedral intermediate after attack of the catalytic serine, the intermediate can either be hydrolyzed and regenerate the active enzyme or the suicidal mechanism occurs.[179] Some mechanism-based HNE inhibitors are based on the saccharin moiety. In the example shown in scheme 3, attack of the serine to the acyl center of the saccharin core leads to formation of a tetrahedral intermediate that, upon collapsing, induces the departure of a leaving group and formation of a sulfonyl imine, which is subsequently engaged via Michael addition by an active site histidine residue. The Groutas lab has done extensive work with 1,2,5-thiadiazolidin-3-one 1,1-dioxide compounds (figure 15 – B), achieving potent and selective HNE inhibitors.[180,181]

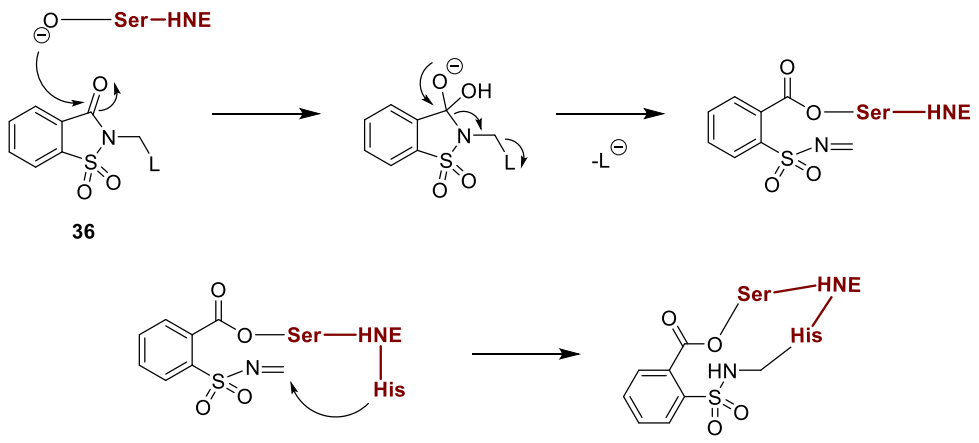

Scheme 3 – Irreversible inhibition of HNE by a saccharin-based suicide inhibitor.

Natural products are an important source for therapeutic molecules and have been explored to develop HNE inhibitors. However, most of the reported inhibitors usually don't go below micromolar potency and a better use of natural products for HNE inhibitor development will probably lie in the adaptation of natural products into semi-synthetic inhibitors. An example is the discovery of cyclic peptidic inhibitors, lyngbyastatins (figure 15 – C), isolated from marine cyanobacteria which showed low nanomolar IC_{50}s against PPE.[182]

Non-covalent inhibitors are also described for HNE, including the C-shaped aurones (figure 15 – D) developed in our lab, for which the c-shape seems to promote an induced fit towards HNE inhibition.[183]

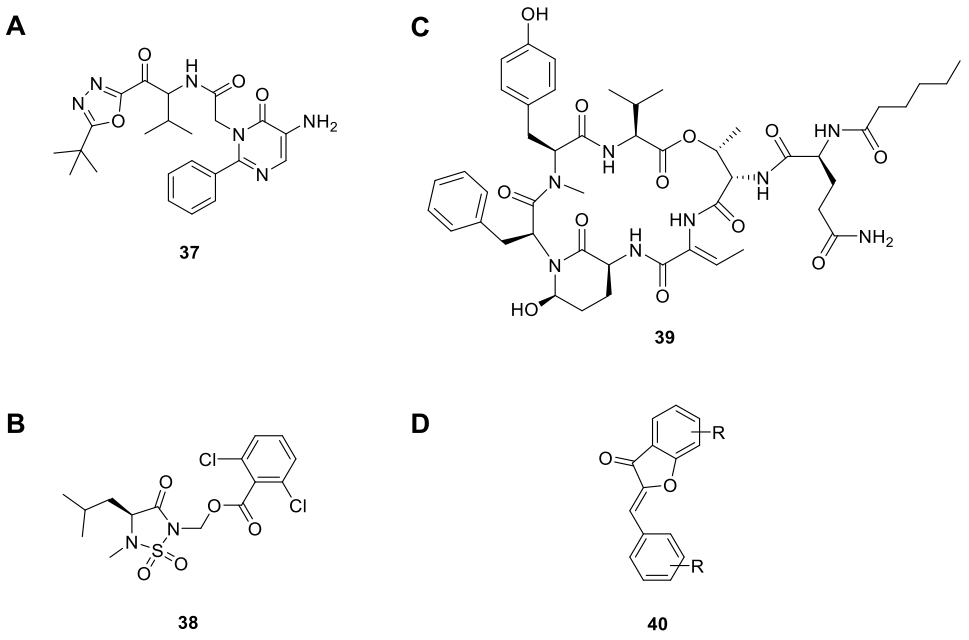

Figure 15 – HNE Inhibitors; A. ONO-6818, a transition state analog; B. 1,2,5-thiadiazolidin-3-one 1,1-dioxide compounds, mechanism-based inhibitors; C. Lyngbyastatin 7, a natural product-derived HNE inhibitor; D. "C-shaped" aurones, non-covalent inhibitor.

1.2.1.1.2. Activity-based Probes targeting Human Neutrophil Elastase

Our proposal for ABP synthesis and application is driven towards the targeting of HNE. In this section a summary of the currently existing HNE-targeting ABPs is presented, together with examples of their applications.

One of the first reports of the applications of ABPs in HNE was done by Gilmore et al, who described the solid-phase synthesis of diphosphonate probes for serine proteases, including elastase-like enzymes. The ABPs comprised a diphenyl phosphonate warhead attached to either a fluorophore or biotin via a linker like PEG (figure 16 – A). The probes detected HNE down to a 32 ng amount of enzyme. The labeling was shown to be dependent on the active state of the catalytic serine residue.[87]

One of the limits of ABP synthesis for a particular enzyme is the fact that a lot of times probe interaction with the target is limited to a strong P1 interaction, while other exosites, when existent, might be hard to reach.[184] Exploiting distant exosites in HNE could result in inhibitors with improved selectivity. Kasperkiewicz et al designed an ultrasensitive ABP for HNE based on the development of optimal and highly selective HNE substrates, which include non-natural aminoacids, by a process the authors call Hybrid Combinatorial Substrate Library (HyCoSuL). This strategy uses the tetrapeptide Ala-Ala-Pro-Val, which is routinely used for HNE, as a starting point and then the optimal aminoacids for each subsite P1-P4 are individually determined, in order to establish the best tetrapeptide for HNE inhibition. The optimal aminoacids were found to be Abu for P1, octahydro-1H-indole-2-carboxylic acid (Oic) for P2, methionine dioxide for P3 and 6-benzyloxy-L-norleucine at P4. The optimal peptide Ac-Nle(O-Bzl)-Met(O)2-Oic-Abu-ACC was determined to be more than 7000 times better hydrolyzed by HNE than the commonly used commercial peptide Ac-Ala-Ala-Pro-Val-ACC. Cleavage of the optimal tetrapeptide by HNE is also 900 times more efficient than cleavage by PR3, a closely related serine protease with similar substrate preference which is frequently also potently inhibited by HNE inhibitors. The optimal tetrapeptide was adapted with a PEG linker, a biotin tag and a phosphonate warhead to generate an ABP (figure 16 – B). The ABP labeled both HNE and PR3, with preference for HNE. The ABP was tested on induced neutrophil extracellular traps (NETs), showing that proteolytic activity was concentrated in perinuclear punctate structures and not in induced NETs. Overall, this work helped determine key features of substrate recognition by HNE that can provide selectivity

against related enzymes for which selectivity is usually hard to achieve. Furthermore, the results concerning HNE inactivity in neutrophil NETs also create new questions concerning HNE's role in the inflammatory process associated with these structures and emphasize the importance of developing new HNE ABPs.[184]

Grzywa et al also took advantage of peptidic linkers to design HNE-directed ABPs, containing aromatic esters of 1-aminophosphonic acids as warheads, which are well known potent and selective inhibitors of serine proteases. Kinetic studies showed that an ABP with the peptidyl chain Val-Pro-Ala (figure 16 – C) is selective for elastase, being inactive against PR3 and cathepsin G. When used as ABPs however, most compounds didn't show good specificity or selectivity, providing similar signals for HNE, PR3 and CatG.[185]

Preliminary work was made with 4-Oxo-β-Lactams ABPs to probe HNE related proteomes. The 4-Oxo-β-Lactam was derivatized through copper-catalyzed azide-alkyne cyclocondensation (CuAAC) (figure 16 – D) and the resulting compounds showed low nanomolar IC_{50} values. Despite the small and highly reactive warhead, the compounds showed a good biochemical selectivity profile against related proteases. An alkyne derivative presented an IC_{50} of 82 nM, which makes it potentially suitable for biorthogonal experiments. Incubation with neutrophils and fluorescence microscopy revealed probe internalization, a possible advantage over the use of some peptide-based ABPs.[186]

Edington-Mitchel and co-workers designed fluorescent diphenylphosphonate-based probes (figure 16 – E), Cy5-PK-DPhPh and Cy5-Val-DPhPh, to detect serine proteases. Cy5-V-DPhPh strongly labeled HNE and, to a lesser extent, PR3. When applied in mouse bone-marrow cells, Cy5-V-DPhPh labeled HNE at 10 μM concentration, while simultaneously binding an additional high molecular weight protein.[187] Schulz-Fincke and coworkers developed an HNE ABP using a α-aminoalkylphosphonate warhead with two aryloxy groups. A peptidic backbone linker, Val-Pro-Val, was used as a recognition sequence (figure 16 – F). Application of the compound with HNE and analysis by SDS-PAGE revealed labeling of characteristic HNE bands around 29kDa and a competition experiment with sivelestat showed that the mechanism is dependent on the enzyme's active site.[188] In a follow-up work, the authors developed an HNE ABP based on the sulfonyloxyphthalimide warhead (figure 16 – G). Upon engagement of the warhead by the enzyme and opening of the heterocyclic ring, a Lossen rearrangement leads to the

formation of an isocyanate, which can also be engaged by the enzyme, leaving it permanently inhibited. The inhibitors were highly potent, with low nanomolar K_i values. Selectivity assays showed strong preference of the ABP for HNE inhibition.[189]

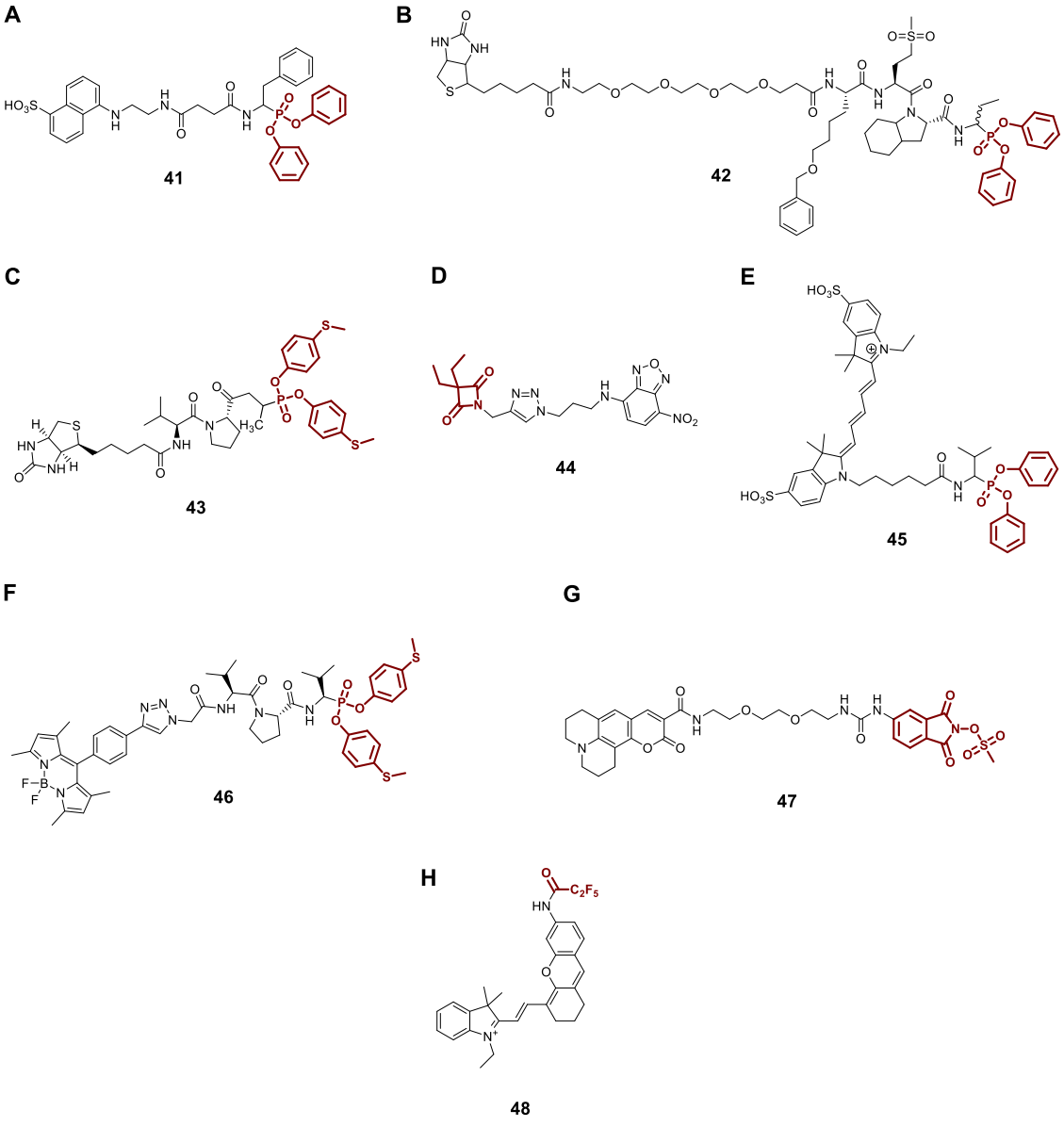

Figure 16 – ABPs for HNE (reactive groups are highlighted in red): A. Diphenyl phosphonate ABP developed by Gilmore et al; B. ABPs based on the optimized tetrapeptides generated by the HyCoSul strategy by Kasperkiewicz et al; C. Peptidic ABP developed by Grzywa et al; D. 4-Oxo-β-Lactam ABPs developed by Ruivo et a; E. Diphenylphosphonate ABPs developed by Edington-Mitchel et al; F. Peptidic ABP developed by Schulz-Fincke et al. G. ABP developed by Schulz-Fincke and coworkers based on a suicide inhibition mechanism dependent on a Lossen rearrangement. H. NIR fluorescence ABP developed by Liu et al.

Liu and coworkers sought to improve HNE detection in living systems to better understand the pathways involved with HNE's destructive role in lung diseases by developing a small-molecule-based near-infrared fluorogenic probe for HNE (figure 16 – H). The probe contained a pentafluoropropanamide as a recognition group and a hemicyanine-based fluorophore.[190]

Overall, these existing studies provided valuable ABPs which seem to be suited for HNE labeling, some of them even when in the presence of a complete proteome. Despite this, the application of these ABPs was limited to gel-based assays for all the described studies, with no mass-spectrometry based ABPP experiments performed in any of the studies. Target identification with mass spectrometry techniques should be used to support gel-based assays whenever possible. In the case of HNE, co-migration of the enzyme is expected to happen with related enzymes like PR3, which shares a very similar molecular weight and substrate specificity.

1.2.1.2. DPP Family of Serine Hydrolases – DPP4, DPP8, DPP9, FAP and PREP

The members of the DPP family are N-terminal dipeptide postproline-cleaving serine proteases. Among them we find dipeptidyl peptidase 4 (DPP4), dipeptidyl peptidase 7 (DPP7), dipeptidyl peptidase 8 (DPP8), dipeptidyl peptidase 9 (DPP9), FAP and prolyl endopeptidase (PREP) (figure 17).[3] The DPP family proteins have a crucial role in the cytoplasmic degradation of proline containing peptides due to their ability to cleave N-terminal dipeptides from peptides containing proline at the second to last position (Xaa-Pro). The proteasome is the entity responsible for the degradation of most cellular proteins but the outcome of the process results in short peptides, which are then degraded by cytosolic peptidases for general cell housekeeping, aminoacid recycling and for antigen presentation by the major histocompatibility complex (MHC) class I.[191] These peptidases struggle with proline containing peptides due to the conformational rigidity of proline's pyrrolidine ring. Among the DPP family members capable of cleaving these problematic peptides we find DPP4, FAP, DPP8 and DPP9. These enzymes are also associated with

cell-extracellular matrix interaction, cell adhesion, migration and apoptosis, with some of these functions being seemingly independent of the catalytic activity.[192]

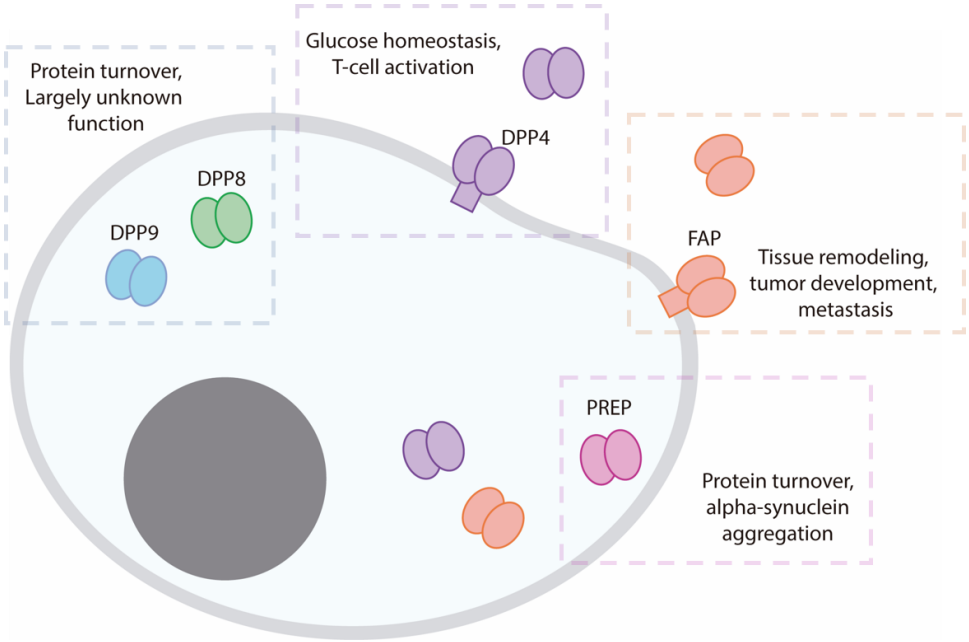

Figure 17 – Overview of selected DPP serine hydrolases and their main localization and functions. Adapted from Waumans et al.[3]

The DPP family of serine hydrolases gained notoriety due to the emergence of DPP4 inhibitors as an oral treatment for type 2 diabetes.[193] DPP4 plays an important role in glucose homeostasis by controling gastrointestinal incretin hormones. The enzyme regulates the endogenous levels of glucagon-like peptide-1 (GLP-1), a gastrointestinal hormone which increases its levels in plasma after food intake. GLP-1 promotes insulin secretion, insulin sensitivity and β-cell proliferation. DPP4 is also described to inhibit an additional incretin hormone, glucose-dependent insulinotropic polypeptide.[194] The GLP-1 duration of action is short due to inactivation by DPP4. The enzyme is a well-established drug target for type II diabetes, with multiple FDA approved drugs currently in the market, including sitagliptin, saxagliptin, linagliptin, and alogliptin.[195] Diabetic patients treated with DPP4 inhibitors have shown a significant decrease in glycated hemoglobin, in glucose levels after meals and in circulating triglycerides. DPP4 has also been studied in the lung. Meyerholz and coworkers have shown an increased immunostaining of DPP4

in chronic lung diseases including COPD. Increased staining was mostly observed in areas of tissue remodeling. The authors found areas of enhanced immunostaining in tissues like airway epithelia, type II cells, pleural mesothelia, and alveolar macrophages.[196] Additionally, Schade et al showed that the induction of asthma in a F344 mouse model is associated with increased DPP4 enzymatic activity in the bronchoalveolar lavage fluid and lung parenchyma, which is associated with T-cell recruitment and activation.[197]

FAP shares 50% homology with DPP4. It is mainly expressed during development, while being rarely expressed in healthy adult tissues. It is highly upregulated at sites of tissue remodeling like wounds, fibrosis and cancer, especially in fibroblasts. Besides the exopeptidase activity common to the DPP family, FAP also has gelatinase activity. FAP activity is intimately associated with cancer due to its pro-tumorigenic nature and has also gained notoriety as a marker of cancer-associated fibroblasts. Inhibition of FAP is pursued as an anti-cancer therapy and FAP expression is of prognostic value in some tumors.[198,199] Pharmacological inhibition of FAP has been shown to lead to a decrease in tumor growth in mouse models.[200] FAP was found to be increased in lung cancers, while being absent in the normal lung. Despite this, it was been considered an indicator of positive outcome in non-small cell lung cancer (NSCLC)-squamous cellcarcinoma.[201]

PREP is involved in regulation of bioactive peptides and regulation of protein-protein interactions with particular emphasis on brain functions and has been associated with neuropsychiatric disorders like autism, schizophrenia and bipolar affective disorder.[202-204] PREP was found to be highly expressed in neutrophils, macrophages and epithelial cells found in lung tissues of COPD patients and in the lungs of mice exposed to cigarette smoke. PREP activity was also found to be increased in patients with cystic fibrosis.[201,205,206]

DPP8 and DPP9 were first described by Abbott et al as dipeptidyl peptidases related to DPP4 and FAP.[207] The authors also worked on the cloning, recombinant expression, biochemistry and tissue expression of DPP8.[207] DPP9 was later studied by Olsen and Wagtmann, who identified it as a novel DPPIV-like protease and showed that it is ubiquitously expressed, with the highest expression in skeletal muscle, heart, and liver.[208] DPP8 and DPP9 are intracellular, mainly localized to the cytoplasm and nucleus, but can also be found associated with the plasma membrane. DPP8 has been described to be

approximately 10-fold less abundant than DPP9 in some cell lines.[209] Crystallographic structures of both DPP8 and DPP9 were only very recently described.[210]

DPP8 and DPP9 share an overall identity of 58% and an identity of 92% of essential active-site residues.[211] DPP8 and DPP9 also share enzymatic specificity, but growing evidence suggests they may have separate physiological roles and potentially interfere in processes that were previously attributed to DPP4. The independent functions of DPP8 and DPP9 remain mostly undefined, in part due to the unavailability of specific inhibitors.[212] Despite this, these serine hydrolases have been implicated in apoptosis, adipogenesis, ROS sensing, spermatogenesis, inflammation, among other functions.[213-215]

There is a conserved general structure between DPP4, DPP8 and DPP9, with all three enzymes having two domains, a C-terminal α/β globular domain, which encompasses the catalytic triad and is the most conserved region between the three enzymes, and an N-terminal β-propeller domain, where most ligand-binding elements are present, and where extensive variations from DPP4 were found, including additional secondary structures, strand exchanges, and loop alterations. The active sites have a conserved S1 subsite, but the S2 subsite diverges significantly, being larger in DPP8 and DPP9 when compared with DPP4 and showing a preference for voluminous hydrophobic groups. Furthermore, the small differences between catalytic site aminoacids have little impact in terms of reactivity since the different aminoacids have analogous structures; lysine 174 in DPP8 is replaced with arginine in DPP9 and isoleucine in DPP8 is replaced with valine in DPP9.[212] Unlike what happens in DPP4, ligand binding in DPP8 induces rearrangement of a region called the R-helix, which participates in the shaping of the substrate binding site, suggesting an induced fit mechanism. When comparing DPP8 and DPP9 structurally, a key difference seems to be a region contained in the R-segment, a solvent exposed loop with two consecutive histidines in DPP9 and aspartic acid and tyrosine in DPP8 in those positions. Regarding the interaction with the protein small ubiquitin-related modifier 1 (SUMO1), the R-segment and R-helix seem to undergo significant structural changes upon ligand binding that disrupt the association of DPP8 or DPP9 with it.[210]

Some DPP8 or DPP9 specific roles have been identified, like the importance of DPP9 in the cytosolic degradation of proline-containing peptides, in a paper published by Geiss-Friedlander et al. The pyrrolidine ring-containing peptides seem to pose a problem for the normal protein turnover mechanisms due to structural constraints. Of the few peptidases

known to be able to cleave these peptides, including PREP, DPP8 and DPP9, only DPP9 seems to be the rate-limiting enzyme in the process. The turnover of substrates containing a proline in the second position was significantly decreased when DPP9 was depleted using siRNAs, but not when the same was done for DPP8 or PREP. This role of DPP9 was also associated with regulation of the presentation of proline-containing peptides by the MHC class I system.[209] DPP9 also seems to have a role in cell adhesion and movement. In a study by Zhang et al it was demonstrated that this function is associated with the focal adhesion proteins integrin-β1 and talin. DPP9 was shown to accumulate with these proteins near the membrane at the edge of migrating cells.[216] Furthermore, the importance of DPP9 in neonatal mice was demonstrated by the generation of gene knock-in mice where the catalytic serine was replaced with an alanine, leading to the production of an inactive form of the enzyme. The homozygote embryos were morphologically indistinguishable from wild type embryos, but died within the first 24 hours of life. These results suggest that the other DPP enzymes are not capable of fulfilling an essential function of DPP9 in the first hours of life.[217] Additional studies suggested that lethality could be due to metabolic impairment. The lack of functional DPP9 was associated with major metabolic challenges mainly related with lipid and glucose metabolism.[218] More recently, it was shown that neonatal lethality is avoided by manual feeding. The lack of DPP9 seems to result in deficient tongue development and a suckling defect.[219]

There is therapeutic potential in inhibiting DPP8 and DPP9. While inhibition of both DPP8 and DPP9 was first thought to be associated with toxicity, continued research with strong and selective DPP8 and DPP9 inhibitors resulted in no toxicity, highlighting that the previously identified effects were probably due to other properties of the compounds and not related with inhibition of DPP8 and DPP9.[220-222] These enzymes have been shown to mediate diverse cancer-related functions like cell migration, tumor cell invasion and metastasis.[223] Smebye et al described two instances of gene fusions involving DPP9 loss-of-function and seem to be associated with ovarian carcinoma. The tumorigenic effect of these gene fusions seem to be associated with the disruption of DPP9-associated cell signaling pathways that are involved with tumor suppressing.[224] Inhibition of DPP8 and DPP9 has been shown to activate the immune system and trigger a proinflammatory type of cell death called pyroptosis via activation of the inflammasome sensor protein Nlrp1b.[213,225] Johnson et al have shown that selective DPP8 and DPP9 inhibition can be used for treatment of acute myeloid leukemia in a process dependent on the induction of

this type of cell death.[226] Additionally, DPP8 and DPP9 inhibition was also shown to have a role in chemosensitivity of leukemia cells to parthenolide.[214] Han et al showed that the inhibition of DPP8 and DPP9 blocked adipogenesis, a function not observed for DPP4 and FAP inhibition. The mechanism involved inhibition of the expression of PPARγ during preadipocyte differentiation.[227] DPP9 has been Shown by Gabrilovac et al to be enzymatically active in fibroblasts and keratinocytes and to positively regulate adhesion and migration of these cells. Inhibition of DPP9 in these cells led to decrease in survival and proliferative capacity.[228]

The roles of DPP8 and DPP9 in lung diseases have also been recently described.[199] DPP8 and DPP9 mRNA levels have been shown to be upregulated during asthma and the localization of their activity in the bronchi suggested the enzymes are responsive to the inflammatory stimulus.[197] Tang et al showed that DPP9 is associated with non-small cell lung cancer. DPP9 expression is increased in NSCLC cells when compared with adjacent non-tumor tissues and promotes proliferation, migration, and invasion of NSCLC cells.[229]

Overall, the inhibition of DPP8 and DPP9 is a hot topic due to the inexistence of selective inhibitors for each of the two enzymes and due to their involvement in several relevant diseases, for which new therapeutic options are heavily sought. The study of the effects of DPP8 and DPP9 inhibition have been crucial to discern the specific functions of these serine hydrolases in the cell. Previous competitive ABPP endeavors with large libraries of compounds that targeted several serine hydrolases failed to hit any of the DPPs, meaning the search for new warhead for their inhibition is an ongoing task.[230]

1.2.1.2.1. Inhibitors and Activity-based Probes of DPPs

Inhibition of DPP enzymes is an important research field. As previously mentioned, inhibition of DPP4 is a therapeutic strategy for treatment of type 2 diabetes, with several approved drugs in the market. Both FAP and PREP have known selective inhibitors reported, namely N-(4-quinolinoyl)-glycyl-(2-cyanopyrrolidine) derivatives[231,232] and xanthine derivatives[233] for FAP, and prolylsulfonylfluoride for PREP.[234] ABPP studies of DPPs have been generally carried out using FP probes.[235,236] Nevertheless, ABPs have been developed to specifically hit selected DPPs, like the case of dipeptidyl phosphonate ABPs for PREP.[237] In this section the focus will be on describing inhibitors of DPP8 and

DPP9 since one of the aims of our project will be the pursuit of selective inhibition of these enzymes, a topic of high interest in current medicinal chemistry. Selective inhibition of DPP8 or DPP9 remains elusive mostly due to the high similarity between these two enzymes and also significant similarity with related members of the DPP family.[238]

While DPP8 and DPP9 inhibition is important due to the relevance of these enzymes in immune response and cancer,[213,225,226] the lack of knockout models or crystallographic structures has hindered the knowledge available regarding the specific functions of the individual enzymes and the development of selective inhibitors for them. Most projects that aimed for specific substrates of either DPP8 or DPP9 resulted in dual inhibition of the enzymes, with varying degrees of concomitant DPP4 and DPP7 inhibition.[239,240] The description of the molecular structures of both DPP8 and DPP9 is a valuable piece of information to guide the design of inhibitors for these enzymes. DPP4 has been extensively studied in the past using X-ray crystallographic methods in unliganded and liganded forms, establishing that the enzyme has two characteristic domains, one α/β catalytic and a β-propeller domain, with the active site located between these structures.[241] DPP8 and DPP9 have similar structures, but their crystallographic data was only very recently published.[210]

Val-BoroPro (figure 18 – A) is a non-selective inhibitor of post-proline-cleaving serine proteases, including DPP4, DPP7, DPP8, DPP9 and FAP, with low nanomolar inhibition for DPP4, DPP8 and DPP9. The compound acts through mediation of the immune system but, until recently, the exact mechanisms of immune activation by Val-BoroPro have not been completely established. Okondo et al showed that the compound induces pyroptosis selectively in monocytes and macrophages via inhibition of DPP8 and DPP9. Canonical pyroptosis involves the formation of cytosolic multiprotein complexes called inflammasomes, which are triggered by pathogen-associated molecular patterns, leading to recruitment and promotion of the proximity-induced autoproteolytic maturation and activation of pro-caspase-1, which leads to the induction of this type of cell death. Inhibition of DPP8 and DPP9 was shown to lead to the activation of the pro-protein form of pro-caspase-1 without autoproteolysis, which then cleaves gasdermin D, the key executor of pyroptosis.[242] Upon cleavage, gasdermin D releases its N-terminal region to form pores in the cell membrane, inducing a lytic type of cell death. The activation of pro-caspase-1 has been shown to be dependent on the inflammasome sensor protein Nlrp1b and also dependent on the proteasome. When associated with DPP8 and DPP9

inhibition, this process results in the induction of pyroptosis in monocytes and macrophages and activation of the immune system.[213,225]

A small molecule inhibitor, 1G244 (figure 18 – B), has been shown to inhibit DPP8 and DPP9 specifically, while showing no activity against DPP4.[243] The isoindoline group fits in the S1 pocket of DPP9, with the amino group interacting with specific side chains (removal of the free amino group is detrimental for inhibitory potency) and the 1-(4-4'-difluorbenzhydryl)-piperazine substituent not being defined in electron density.[210] Extensive optimization of this inhibitor, with the synthesis of numerous variants, has been attempted, with the goal of improving the selectivity for one of the two targets. These studies failed to achieve significant selectivity between both enzymes, highlighting the difficulty in achieving selectivity for either DPP8 or DPP9.[212,238]

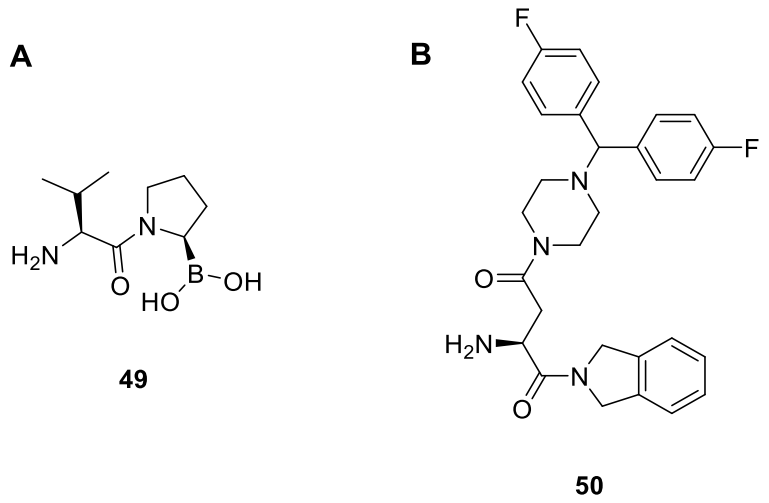

Figure 18 – A. Val-boroPro; B.1G244.

SUMO1 is a small ubiquitin-like protein that has been identified as interaction partner with DPP8 and DPP9. It has been shown that interaction between DPP9 and SUMO1 activates peptidase activity and mutations of the DPP9 arm-like structure responsible for binding to SUMO1 lead to reduced activity. The SUMO1 region associated with the interaction has been mapped, called E67 interacting loop, and based on aminoacids 61 to 67 of SUMO1 – mutation of this motif has been shown to lead to loss of interaction with DPP8 and DPP9 and used to develop a sequence of aminoacids, SLRFLYEG, that functioned as a strong allosteric inhibitor of DPP8 and DPP9, but not DPP4.[244,245] When

the proteins were incubated with the SUMO1 derived peptide SLRFLYEG, the interaction was revealed to happen with the active site and showed tight interaction at P1', P2' and P3'. The phenylalanine seems to have a role in defining specificity for the enzymes, by fitting in pocket that is absent in DPP4. These results were surprising since the peptide was expected to react through binding with the binding site of SUMO1 and not as a competitive inhibitor.[210]

1.2.1.3. ABHD Family Enzymes, overview, inhibitors and Activity-based probes

The mammalian ABHD proteins are a group of at least 19 proteins that are potential regulators of lipid metabolism and signal transduction. A common feature of the ABHD family is the ability to hydrolyze or synthesize glycerophospholipid species. These act as key structural elements for the cell membrane and as intermediates in signaling pathways. They can contain serine, cysteine or asparagine as the nucleophilic catalytic aminoacid.[246] We focus on ABHD2, ABHD6 and α/β hydrolase domain fold family protein 16a (ABHD16a), including relevant examples of their inhibitors and ABPs.

ABHD2 seems to be involved with suppression of smooth muscle cell migration and chronic diseases that involve monocyte and macrophage recruitment like atherosclerosis. ABHD2 has triacylglycerol lipase and ester hydrolase activity and has been implicated in the breakdown of lipids to support the proliferation of cancer cells, suggesting that it is a potential target for cancer therapy.[247] The ABHD2 gene expression has been shown to be upregulated in prostate cancer and associated with cancer growth and resistance to docetaxel chemotherapy.[248] It seems to have a protective role in the lung since deletion of ABHD2 by gene trapping in aged mice has been shown to result in reduction of type II cells in alveolar tissues. Alveolar type II cells produce pulmonary surfactant, a complex mixture of lipids and proteins which regulates lung surface tension during the inflation/deflation cycle. The outcome of ABHD2 deletion involves accumulation of macrophages, increase in cytokines, enhanced apoptosis, reduced pulmonary surfactant and a protease/anti-protease imbalance, which progressively leads to the development of emphysema. This suggests a role for ABHD2 in the protection of lung structural integrity.[246,249] ABHD2 gene polymorphisms have been described to contribute to COPD susceptibility.[249,250] Competitive ABPP experiments using KT195, a known non-selective inhibitor of ABHD6, and an alkynylated version of the same compound identified

ABHD2 as the enzyme responsible for the compound's effect on cell death inhibition via regulation of cytoplasmic calcium concentration.[251]

ABHD6 is a serine hydrolase known to have lipase activity in the central nervous system, where it participates in the hydrolysis of endocannabinoid 2-AG, a function shared with MAGL and ABHD12.[104,252] Outside of the nervous system, ABHD6 has been implicated in glycerophospholipid metabolism and lipid signal transduction, having a prominent role in the development of the metabolic syndrome.[253] ABHD6 has recently been found to negatively regulate the trafficking of postsynaptic glutamate receptors in neurons.[254] ABHD6 inhibitors have potential as therapeutics for obesity, diabetes and non-alcoholic fatty liver disease. Potent and selective inhibitors of ABHD6 have been developed by the Cravatt lab using ABPP tools, including the carbamate derivative (figure 19 – A),[126] piperidyl-1,2,3-triazole ureas (figure 19 – B).[255]

ABHD16A possesses both an esterase catalytic triad and an acyltransferase domain. The enzyme is involved in the conversion of phosphatidylserine to lyso-PS in the brain. Lyso-PS are signaling lipids that regulate macrophage activation and clearance of apoptotic cells. Inhibition of ABHD16A lowers lyso-PS formation and leads to a reduction in inflammation. The enzyme is considered a potential target of inflammation-associated

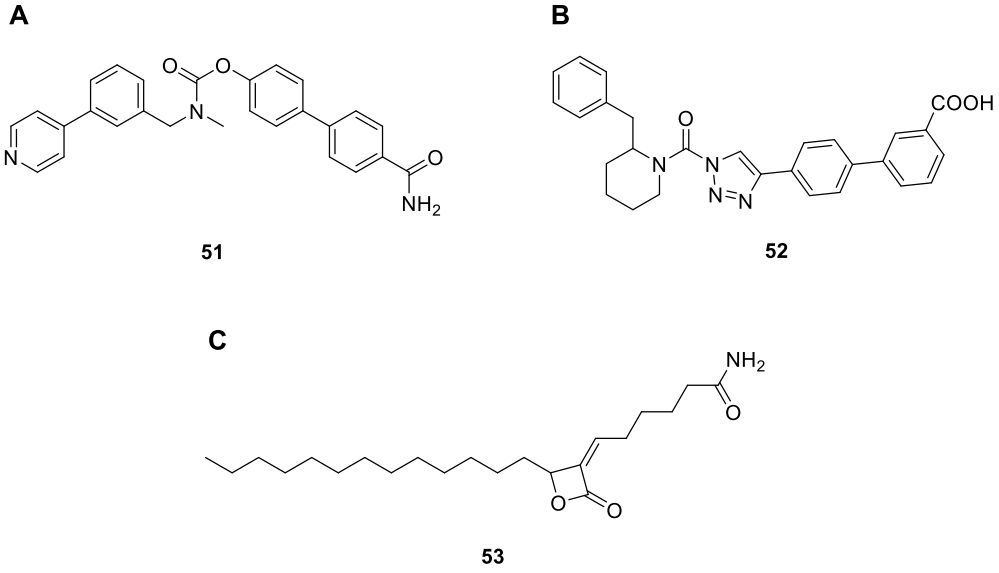

Figure 19 – Carbamate (A) and urea (B) selective inhibitors of ABHD6 developed by the Cravatt lab. C. β-lactone-based inhibitor of ABHD16a.

pain. ABHD16A and ABHD12 jointly regulate lyso-PS levels, with lyso-ps being hydrolyzed by ABHD12 into glycerophosphoserine. Therefore, inhibitors of ABHD16A should avoid concomitant inhibition of ABHD12.[256,257] ABHD12 accounts for ~9% of total hydrolase activity towards 2-AG in the brain. Mutations in ABHD12 have been associated with the progressive neurologic disorder PHARC (polyneuropathy, hearing loss, ataxia, retinitis pigmentosa and cataract) in humans. The derivatization of α-methylene-β-lactones by the Cravatt lab led to the development of an ABHD16a inhibitor (figure 19 – C).[256,258]

1.3. Expanding the ABPP Warhead Toolbox of 4-membered Rings

4-membered ring heterocyclic compounds are very prominent in medicinal chemistry and include chemotypes like β-Lactams, β-Lactones and β-Sultams. These scaffolds have been applied in ABPP experiments to determine their extent of target engagement.

In this work we aimed to expand the knowledge on two underexplored 4-member ring chemotypes, the 3-Oxo-β-Sultam and the 4-Oxo-β-Lactam. These chemotypes are derivatives of β-Lactams, which contain an additional sulfone or carbonyl group, respectively, incorporated into the 4-membered ring structure of the β-Lactam ring.

These warheads have been used in chemical biology for inhibitor development and mechanistic studies but no study involving proteomics have been made to date.

1.3.1. 3-Oxo-β-Sultams

3-Oxo-β-Sultams (scheme 4 – A) are 4-membered rings containing an acyl sulfonamide reactive group. They are both β-Sultams and β-Lactams and have been described to inactivate the PPE as acylating agents.[173] Inhibition was suggested to involve the formation of an enzyme-inhibitor adduct with transient stability by acylation of the active-site serine of PPE.[259]

The 3-Oxo-β-Sultam warhead has been described to be too chemically reactive for therapeutic applications, since its alkaline hydrolysis occurs at a rate much greater than that of clinically useful β-Lactams and the compounds have short half-lives in water. 3-Oxo-β-Sultam-based compounds have found use as scaffolds for poly(acylsulfonamide) polymer formation,[260] ring-enlargement reactions,[261] intermediates in synthetic pathways,[262] and as serine hydrolase inhibitors.[259]

One of our main interests in exploring the 3-Oxo-β-Sultam scaffold is the study of its mechanism of serine hydrolase inhibition. In theory, enzymatic inhibition by 3-Oxo-β-Sultams could involve nucleophilic attack of the enzyme at either the acyl or sulfonyl centers, displacing either a sulfonamide or an amide leaving group, respectively (scheme 4 – B).

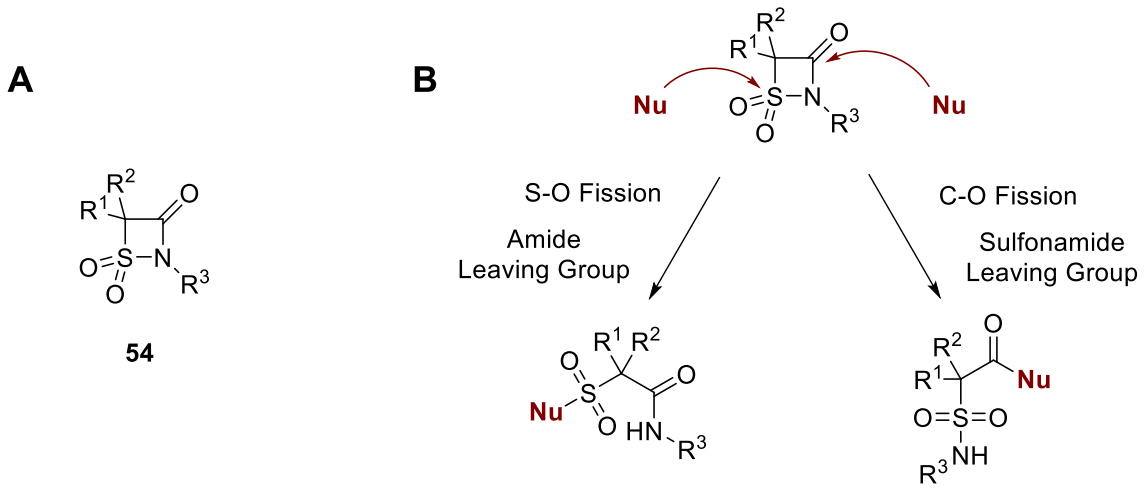

Scheme 4 – A. 3-Oxo-β-Sultam general structure. B. Possible mechanisms of attack of a nucleophile to a 3-Oxo-β-Sultam.

Tsang et al have described that the hydrolysis of the 3-Oxo-β-Sultam warhead and the reaction with the target enzyme occur at different reaction centers, with the enzyme reaction taking place at the carbonyl center and the alkaline hydrolysis occurring at the sulfonyl side.[259,263]

Assuming the attack happens in the carbonyl center, the incoming nucleophile approaches at approximately the tetrahedral angle, while in the sulfonyl attack there is a pentacoordinate trigonal bipyramidal geometry, with the nucleophile taking the apical position. These differences suggest that the nature of the substituents could have an influence in the chemical reactivity of 3-Oxo-β-Sultam inhibitors.[259]

The mechanism for acylation of serine hydrolase enzymes is usually described as a two-step process, with the attack of the nucleophilic serine in the first step forming a tetrahedral intermediate and a second step with the collapse of the intermediate state and displacement of a leaving group.[46] Sulfonylations on the other hand are usually described with a concerted mechanism.[263] Even though the attack at the acyl center displaces a better leaving group, the sulfonamide anion, the nature of the leaving group does not seem to have a drastic effect on reactivity.[264]

Inhibition of serine proteases by sulfonylation is a potential strategy as an alternative to the commonly reported acylation mechanism. However, sulfonyl inhibitors are usually

less reactive that their acyl counterparts and sulfonylation of serine hydrolases remains an underexplored strategy. Tsang et al have reported on β-Sultams, which are unusual in that they undergo sulfonyl transfer faster than the corresponding acylation reaction. X-ray crystallography has shown that an N-benzoyl β-Sultam inhibits elastase by sulfonation of the active site, an irreversible process. N-acylsulfonamides are commonly used to inhibit serine proteases, but the attack of the enzyme occurs in the acyl group, with displacement of a sulfonamide leaving group.[179,265]

Mass spectrometry studies have shown. This, however, does not provide distinction between acylation and sulfonylation, since the products resulting from the attack at either position have the same molecular weight.

In a study of enzymatic inhibition of PPE using 3-Oxo-β-Sultams it was shown that the enzymatic reaction occurs with a 1:1 ratio. The second order rate constant (k_i) for the inactivation of PPE was shown to be nearly 1000 times greater than the inhibition by an N-benzoyl-β-Sultam, which inhibits HNE by a sulfonylation process. The authors concluded that such difference suggests a different inhibition mechanism is taking place, inferring that the acylation of the active site is the probable mechanism of action.[259] On the other hand, NMR studies of the hydrolysis product have shown a cross-peak between the carbonyl carbon and the protons from the methylene group of the N-benzyl substituent, supporting that hydrolysis of the 3-Oxo-β-Sultam ring occurs through attack of the hydroxyl ion at the sulfonyl center.[264]

After inhibition of HNE with a 3-Oxo-β-Sultam there is recovery of enzyme activity within a few hours of 3-Oxo-β-Sultam inhibition, suggesting acylation and formation of a labile ester rather than sulfonylation.[266]

The rate of enzyme inactivation by an N-benzyl 3-Oxo-β-Sultam when compared with a N-benzoyl β-sultam, together with the observed recovery of enzymatic activity suggests different mechanisms for the two processes, leading the authors to conclude that 3-Oxo-β-Sultams inhibit elastase enzymes by forming a reversible acyl enzyme of intermediate stability.[259]

The requirements for attack at sulfonyl centers are inherently different from those at acyl centers. Sulfonyl transfer reactions catalyzed by proteases may offer interesting insights about the flexibility of enzymes, inhibition requirements and information concerning enzyme specificity and selectivity profiles. These characteristics make the 3-Oxo-β-

Sultam warhead an interesting scaffold to study since it might have different selectivity characteristics when compared with related structures.[263]

While the rate of hydrolysis of a β-Lactam is similar to that of its acyclic amide analogs, for the sulfonyl counterparts the rate of hydrolysis of a β-Sultam is estimated to be 10^7-fold higher than that of a sulfonamide.[267] β-Sultams are also hydrolyzed faster than β-Lactams. The alkaline hydrolysis of N-benzoyl β-Sultam occurs exclusively through attack on the sulfur atom with displacement of an amide leaving group, as demonstrated by ^{1}H NMR and MS analysis. [268]

A theoretical study on the alcoholysis of N-benzyl 3-Oxo-β-Sultam confirmed that the S-N bond cleavage has a slightly lower energy barrier than C-N bond cleavage, suggesting the attack at the sulfonyl center is preferential. This seems to involve a stepwise mechanism, with the attack of the alcohol to the sulfur atom as the rate-limiting step.[269]

Even with the added strain in the 3-Oxo-β-Sultam ring, a N-benzyl 4,4-dimethyl 3-Oxo-β-Sultam is only 10-fold more reactive toward alkaline hydrolysis than the corresponding β-Sultam with an exocyclic acyl center (scheme 5).[268,270] Alkaline hydrolysis of the 3-Oxo-β-Sultam occurs exclusively by attack on the sulfonyl center with a second-order rate constant of k_{OH} = 1.83 x 10^5 M^{-1} s^{-1}, which is consistent with the 10^3-fold greater reactivity of β-Sultams compared with β-Lactams towards alkaline hydrolysis.[173] The preference for nucleophilic attack at the sulfonyl group was demonstrated by negative ion ESI-MS, ^{1}H and ^{13}C HMBC NMR. The nature of the leaving group doesn't seem to have a strong enough effect to direct hydrolysis to the acyl center.[263,268,271]

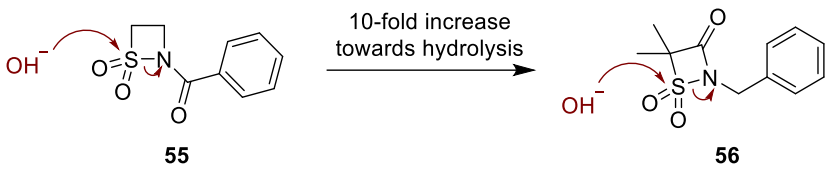

Scheme 5 – Difference in the hydrolysis of an N-benzoyl β-Sultam and a 3-Oxo-β-Sultam.

Modifications to the basic 3-Oxo-β-Sultam structure can be done either at the 4- position or at the nitrogen of the acylsulfonamide group. Modification in the α-substituents and in the nitrogen atom of the 3-Oxo-β-Sultam structure have been shown to result in inhibitors with improved chemical stability, which retain inhibitory activity. Increasing the bulk of the substituent at the 4 position has been shown to decrease the rate of alkaline hydrolysis. Changing the groups from dimethyl to diethyl diminishes hydrolysis 10-fold. A spiro-cyclohexil is 30-fold less reactive. The dimethyl groups show the highest enzymatic inhibition, which decreases 3-fold when changing to diethyl and 100-fold when changing to spiro-cyclohexil. When taking in consideration both the inhibitory activity and the tendency to hydrolyze, the diethyl substitution is the most favorable, since despite being slightly less active than the dimethyl compounds, it possesses greater hydrolytic stability. It has also been shown that a carboxylic acid in the α-position of the nitrogen reduces chemical reactivity 10-fold, which was attributed to the electrostatic repulsion between the incoming nucleophile and the carboxylate group. The enzymatic inhibition is also reduced 25-fold. Overall, a diethyl 3-Oxo-β-Sultam with a carboxylic acid α to the nitrogen, followed by a phenyl group gave the best reactivity/stability ratio and a valine nitrogen leaving group gave the most stable 3-Oxo-β-Sultam, which was still too unstable to be considered therapeutically useful (k_{OH} of 1.74 x 10^3 M^{-1} s^{-1}), proved to be also the less reactive one towards the enzyme, highlighting that the intrinsic reactivity of the 3-Oxo-β-Sultam ring is intimately associated with its activity.[259]

1.3.2. 4-Oxo-β-Lactams

4-Oxo-β-Lactams (scheme 6 – A) are 4-membered ring compounds containing a β-Lactam with an additional carbonyl group at the 4-position. 4-Oxo-β-Lactams are isosteric analogs of 3-Oxo-β-Sultams. They retain the necessary elements for PPE and HNE recognition but have increased stability against hydrolysis. The mechanism of serine hydrolase inhibition by 4-Oxo-β-Lactams involves the attack of the nucleophilic serine residue to one of the carbonyl groups of the 4-Oxo-β-Lactam, forming a tetrahedral intermediate, which is stabilized in the oxyanion hole of the enzyme. The collapse of this intermediate leads to opening of the 4-Oxo-β-Lactam ring, rendering the enzyme inactive

by acylation (scheme 6 – B). The reversibility of this process depends on the stability of the acyl-enzyme complex.

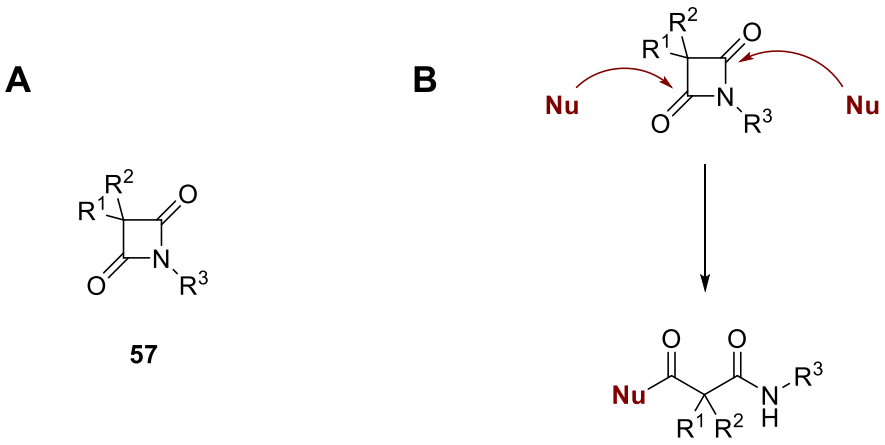

Scheme 6 – A. 4-Oxo-β-Lactam general structure. B. Mechanism of the reaction of 4-Oxo-β-Lactams with nucleophiles.

The 4-Oxo-β-Lactam core is synthesized by reaction of an appropriate amine with 2,2-disubstituted malonic acid chlorides. Yields are low to moderate due the formation of the diamide side-product, which are easily removed by chromatography techniques.[174]

Mulchande et al first described the 4-Oxo-β-Lactam scaffold as a promising structure for the development of HNE inhibitors.[174] The authors designed a small library of 4-Oxo-β-Lactam inhibitors, varying the substituents at the 3-position and at the nitrogen atom, in an effort to establish a basic SAR of common substituents. The compounds were tested against PPE. The rate of acylation of PPE decreased and the rate of deacylation increased when compared with 3-Oxo-β-Sultam inhibitors. Analysis of the second-order rate constants for the alkaline hydrolysis showed that the process is only 7-fold greater than for the corresponding N-benzoyl-β-Lactam. Comparison of the reactivity of 4-Oxo-β-Lactams with similar warheads showed that there is no significant rate enhancement caused by the increased ring strain. When a N-benzyl substituent was replaced with a N-phenyl group the change of leaving group decreased hydrolytic stability, with electron-

withdrawing groups in the aromatic ring decreasing it even more and electron-donating groups having the opposite effect. As for the substituents at the 3-position, PPE inhibition is improved by small hydrophobic substituents, with dimethyl substitution being the most favorable one and 20-fold more active than diethyl. The most potent compounds contained a N-aryl substituent and two ethyl groups at C-3, with N-alkyl inhibitors being inactive or weak inhibitors. Electron-donating groups increase inhibitory activity, with the most potent compound having a 4-CN substituent (figure 20 – A). This compound was also tested against HNE and proved to be very potent and a promising scaffold for the development of HNE inhibitors.

Following the encouraging results for PPE, the authors created a library of inhibitors to test against HNE. Inhibitory activity was shown to be strongly dependent on the nature of C-3 substituents. The diethyl substitution at C-3 seems to be ideal to fit in the small S1 pocket of the enzyme and substituting one of the ethyl groups by a bulkier group like benzyl causes a sharp decrease in activity. There is room for variability, given the fact that one of the most potent inhibitors obtained had an ethyl and a n-butyl group as substituents. Replacing an N-benzyl group with N-phenyl increases the rate of enzymatic inhibition, given the effect of the better leaving group that is generated upon enzyme engagement. Substituents in the ring should be at the para position to have a positive effect in activity. Inhibitors with a thioether substituent in this position present improved inhibitory activity when compared with unfunctionalized counterparts. It seems that the presence of 2-mercaptobenzoxazole is benefic for activity so it might be associated with improved enzyme recognition. A computational study where some inhibitors were modeled with HNE showed that the 3-diethyl substituents are accommodated in the S1 pocket, there are enhanced van der walls interactions between benzothiazole with Leu-99 and His-57 and the carbonyl in close proximity to Ser-195 and involved in H-bonds with the oxyanion hole of the enzyme, which promotes stability of the intermediate tetrahedral state. An inverted binding pose which is detrimental for activity was identified for some compounds and was predominant for compounds with the worst inhibitory activity. As for selectivity, all tested compounds were found to be time-dependent inhibitors of PR3, although with much lower activity than HNE. Most inhibitors were inactive or only weakly active against cathepsin G. This pattern of selectivity might benefit the development of therapeutic molecules since both HNE and PR3 participate in similar pathways of disease and their action is intimately associated. All compounds were

inactive against papain, suggesting good selectivity for serine proteases against cysteine proteases. Compounds were reasonably stable in PBS at 37°C but quickly hydrolyzed in 80% plasma.[272]

Having revealed the great potential of these compounds for the development of HNE inhibitors the authors sought to develop an inhibitor with improved pharmacokinetic properties and that inhibits HNE through a suicide mechanism based on the 4-Oxo-β-Lactam scaffold (figure 20 – B). A sulfone group was added to improve pharmacokinetics and promote the suicide mechanism by inducing departure of phenylsulphinate after attack by Ser-195. An extremely rapid inactivation of HNE by the compound was observed. The compound also inhibited PR3 and CatG with lower potency but didn't show any inhibitory effect against papain. The compound's half-life in PBS was found to be 1.04 ± 0.25 h and in 80% human plasma is 0.11 ± 0.03 h at 37°C, suggesting high susceptibility to plasma esterases. Ex vivo studies in mice showed that the compound distributes to the lungs and spleen, but is not detected in the liver, suggesting high degree of hepatic metabolisation.[175]

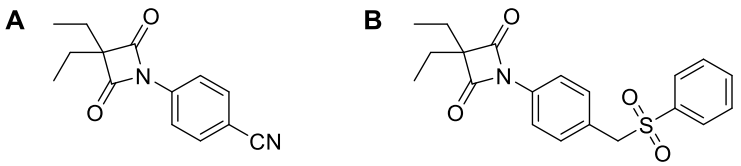

58 59

Figure 20 – 4-Oxo-β-Lactam HNE inhibitors developed by Mulchande et al.

Ruivo et al designed a library of 4-Oxo-β-Lactam inhibitors by derivatization of an alkynylated 4-Oxo-β-Lactam. The compounds resulted in low nanomolar HNE inhibition, including an 82 nM IC_{50} for HNE for the alkynylated compound. Derivatization of this compound by CuAAC afforded fluorescent and biotinylated ABPs with nanomolar potency inhibition against HNE and the application of the fluorescent ABPs in gel-based assays showed HNE labeling, confirming HNE as a target of the compounds. Furthermore, the fluorescent compounds were shown to permeate the cell membrane and allowed for visualization of probe accumulation in cells.[186]

Chavan et al have recently reported an alternative synthesis of 4-Oxo-β-Lactams, specifically for late stage functionalization of the position 3 of the ring. The methodology involves a Sn(II)-catalyzed one-pot reaction via a reaction sequence involving condensation, hydration and cyclization (scheme 7 – A).[273] The proposed mechanism involves the condensation of an aromatic aldehyde with ethyl cyanoacetate In the presence of Sn(II), generating an Sn adduct. The adduct suffers hydrolysis and is stabilized by the Sn catalyst. The carbonyl group of the ester moiety is activated by Sn(II), which favors the cyclization to give a 4-membered ring intermediate, which tautomerizes into the final compound (Scheme 7 – B). This alternative method could provide a versatile way to vary the 3-position substitution pattern.

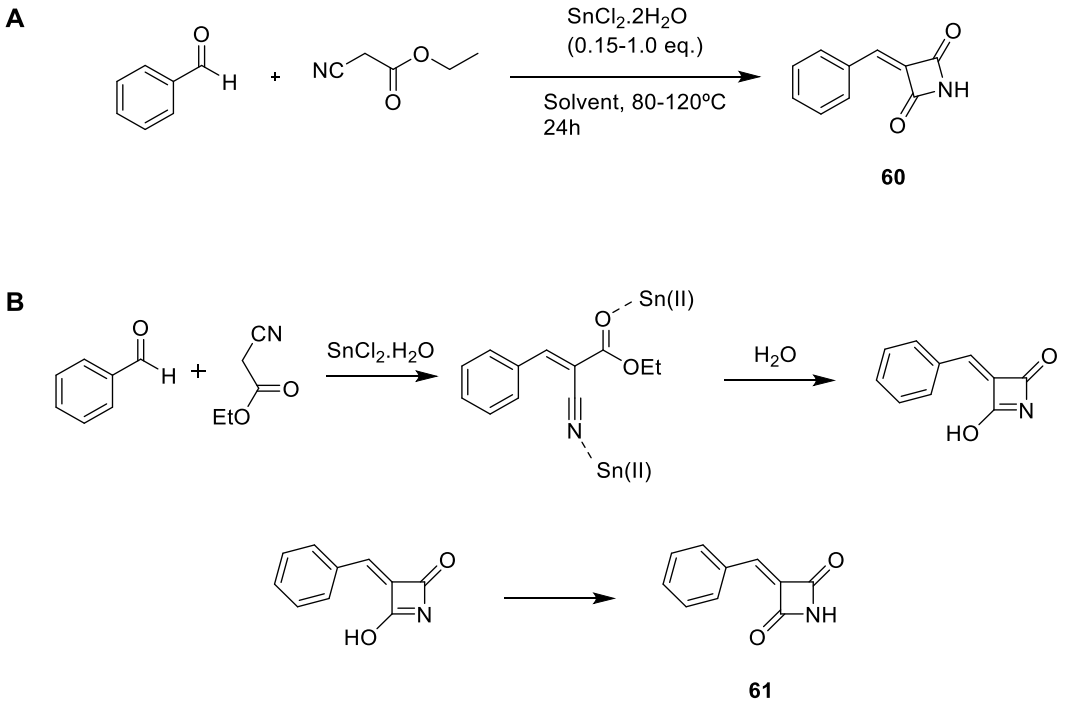

Scheme 7 – A. Synthesis of 4-Oxo-β-Lactams described by Chavan et al; B. Proposed mechanism for the alternative synthesis of 4-Oxo-β-Lactams described by Chavan et al.

1.4. Objectives

The main objective of this project is the evaluation of 3-Oxo-β-Sultams and 4-Oxo-β-Lactams as 4-member ring chemotypes as chemoproteomic tools in chemical biology. These warheads will be developed into libraries of compounds and activity-based probes for application within a selected group of enzymes from the serine hydrolase family. Inhibitor and probe design will be focusing on HNE as a target, but engagement of additional serine hydrolase targets is envisioned.

The project will involve a multi-disciplinary and collaborative approach between Moreira's group at iMed.ULisboa, Penque's group at Instituto Nacional de Saúde Dr. Ricardo Jorge and the Cravatt Group at The Scripps Research Institute, comprising a fully integrated Medicinal Chemistry/Chemical Biology/Proteomics program to streamline the generation, design process and evaluation of novel ABPs with the ultimate goal of establishing target profiles of underexplored 4-membered ring chemotypes for serine hydrolases and develop new inhibitors and tools with diagnostic and biomarker potential (figure 21).

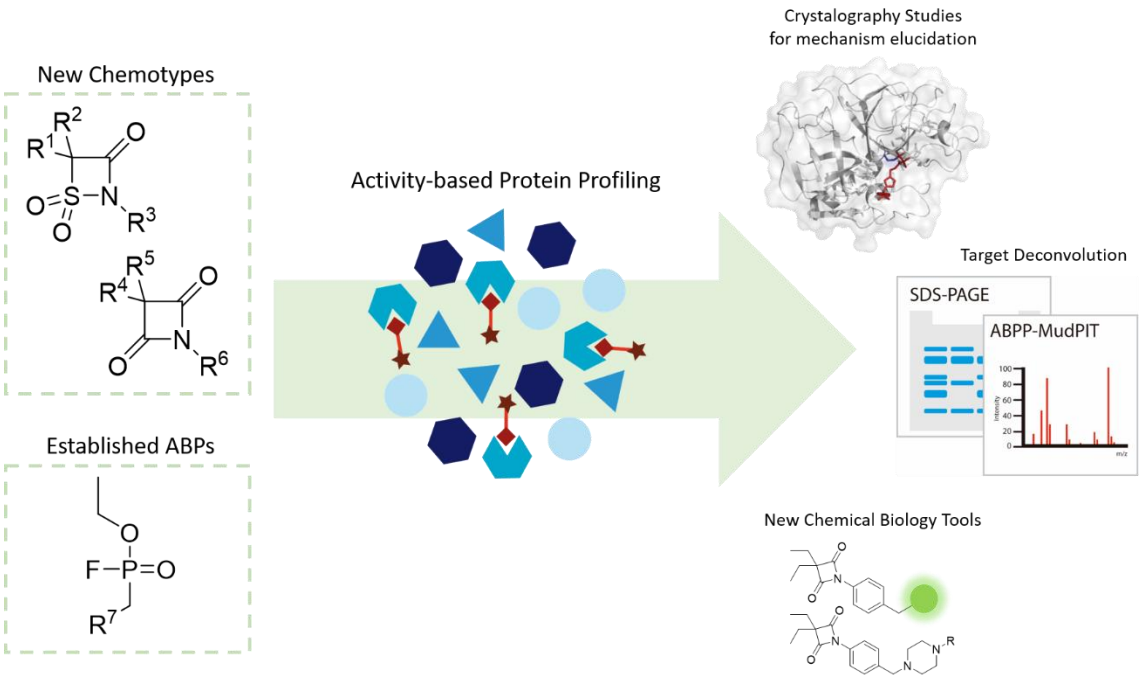

Figure 21 – Overview of the project.

Moreira's group has vast experience on medicinal chemistry, including computer-aided drug design of enzyme inhibitors, while Penque has optimized experimental sets for proteomic studies using state-of-the-art mass-spectrometry platforms. The Cravatt Lab at The Scripps Research Institute in La Jolla, California, is the leading lab in the development and application of ABPs using proteomics approaches. Evaluation of the compound libraries will be performed at the Cravatt lab and supported by a Fulbright grant.

A collaboration with the Archer Lab at Instituto de Tecnologia Química e Biológica António Xavier is envisaged for crystallography studies of the interactions of serine hydrolases with some of the developed molecules. Additional collaborations will be pursued for validation of the identified probe targets and evaluation of new inhibitors for specific serine hydrolases.

The results obtained in this project are reported here and are divided into five main chapters. The first two are associated with the study of the two chemotypes used in this project, the 3-Oxo-β-Sultams and the 4-Oxo-β-Lactams, including synthetic work and proteomics applications. Additional chapters will be devoted to the pursuit of novel inhibitors of the enzymes DPP8 and DPP9, two targets that emerged in competitive ABPP experiments with 4-Oxo-β-Lactam ABPs, and the synthesis and application of other probes to target different enzyme classes associated with some outreaching projects and collaborations. A final chapter will present an overview of the work and the main conclusions and future perspectives.

The main objectives were:

- Synthesis and Evaluation of libraries of inhibitors and ABPs based on the 3-Oxo-β-Sultam and the 4-Oxo-β-Lactam chemotypes, focusing on serine hydrolase as targets and using HNE as the model enzyme;
- Evaluation of HNE inhibition and biochemical selectivity against related serine hydrolases;

- Determination of the HNE and PPE inhibition mechanisms by 3-Oxo-β-Sultam via crystallographic analysis of protein-inhibitor complexes;
- Evaluation of the compounds in a proteomics platform, focusing on gel-based assays and mass-spectrometry based assays to determine compound selectivity, potency and target profile;
- Development of new inhibitors for selected serine hydrolases identified in the ABPP-MudPIT assays and validation via competitive ABPP;
- Study of the 4-Oxo-β-Lactam structure as a novel chemotype for DPP8 and DPP9 inhibition;

Overall, the project will provide unprecedented knowledge on unexplored 4-member rings in ABPP, contributing to the current toolbox of available probes in chemical biology and potentially leading to the establishment of new biomarkers of disease.

Proteomics tools have become indispensable in the evaluation of potential new drugs for the identification of the full extent of target engagement of candidate compounds to prevent potential pitfalls down the pipeline of drug development. This project will mark the first time that proteomics tools are intimately associated with drug development at the Medicinal Chemistry group of iMed.ULisboa and will provide the foundation for future establishment of these techniques in other projects.

Chapter 2 – 3-Oxo-β-Sultams

The experimental part of our project started with the development and evaluation of a library of compounds based on the 3-Oxo-β-Sultam structure. In this chapter we present an overview of the current existing literature on 3-Oxo-β-Sultams, focusing on their potential as enzymatic inhibitors and on the unanswered questions regarding their mechanisms of enzymatic inhibition. We present the optimization and synthesis of 3-Oxo-β-Sultams using CuAAC, the evaluation of these compounds in biochemical assays against HNE and other serine hydrolases and the unprecedented evaluation of these compounds in gel-based and mass-spectrometry-based assays. Furthermore, we attempt to clarify the existing questions regarding the compound's mechanism of action by providing the first crystallographic structures of 3-Oxo-β-Sultams co-crystallized with the serine hydrolases HNE and PPE.

We show that 3-Oxo-β-Sultams are potent inhibitors of HNE, with limited selectivity due their high reactivity, and demonstrate that inhibition of PPE and HNE proceeds through a sulfonylation mechanism.

2.1. Synthetic Procedures

2.1.1. Synthesis of the 3-Oxo-β-Sultam Warhead

3-Oxo-β-Sultams are prepared by ring closure of a (chlorosulfonyl)acetyl chloride with a substituted amine.[259] Scheme 8 depicts an example of the synthesis of a benzylated 3-Oxo-β-Sultam, which was used to optimize the cyclization reaction in this work.

In this work we varied the 3-Oxo-β-Sultam substituents at the 2-position and on the nitrogen atom of the acylsulfonamide. The substituents at the 2-position were introduced prior to the cyclization step, while the N-substitution pattern is determined by changing the amine used for cyclization. We used dimethyl and diethyl substituents at the 2-position, based on previous data of HNE inhibition by 3-Oxo-β-Sultams and related

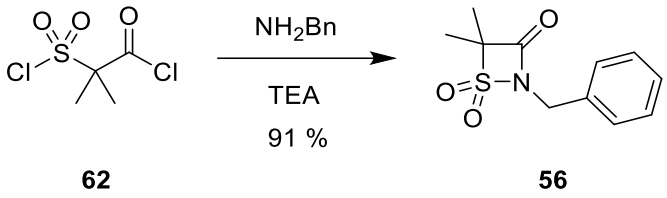

Scheme 8 – Synthesis of a benzylated 4,4-dimethyl 3-Oxo-β-Sultam.

compounds.[259] Bulkier and more varied substitutions have generally resulted in worse activity/stability ratio and have not been explored in this work.

The synthesis of 3-Oxo-β-Sultams started with the introduction of the sulfonyl group by reaction of an appropriate anhydride with sulfuric acid. For the synthesis of the dimethyl derivatives the starting anhydride is isobutyric anhydride, which is commercially available. For the diethyl derivatives, the necessary anhydride is 2-ethylbutanoic anhydride. This chemical was synthesized (Scheme 9) from 2-ethylbutanoic acid prior to being used. A sodium carboxylate salt and an acyl chloride derivative were prepared from 2-ethylbutanoic acid by reacting the acid with sodium ethoxide and thionyl chloride, respectively. Reaction between the sodium salt and the activated acid resulted in the desired anhydride.

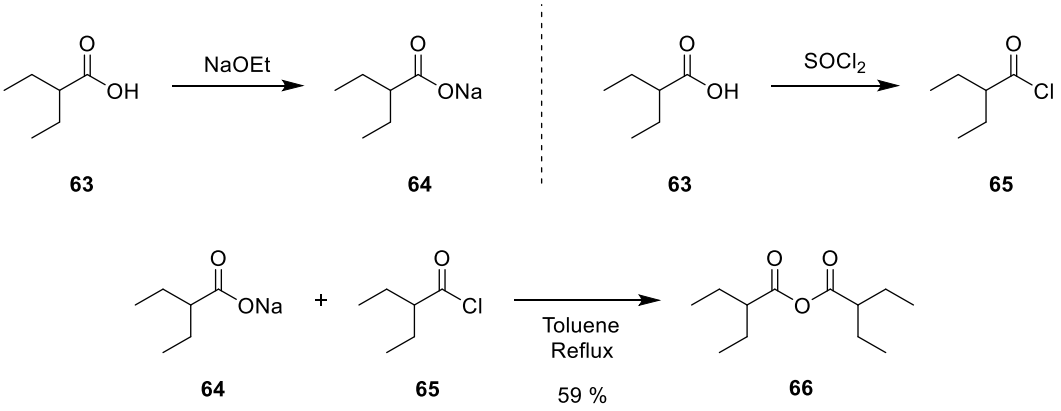

Scheme 9 – Synthesis of 2-ethylbutanoic anhydride from 2-ethylbutanoic acid.

With the appropriate anhydrides in hand the sulfonyl group was introduced by reacting with sulfuric acid overnight at 90°C. The product is precipitated with ethanol from water as a disodium salt in quantitative yield. The disodium salt is derivatized into the dichloride by refluxing in thionyl chloride. The cyclization step is then performed by reacting the dichloride with an appropriate amine. Slow addition of the amine into the reaction is essential to promote cyclization instead of the secondary product that results from the attack of one amine molecule into each of the chlorides.

We have decided to build our library of compounds by taking advantage of CuAAC click chemistry. For this purpose, we prepared an alkyne derivative of the 3-Oxo-β-Sultam core by using propargylamine in the cyclization reaction. The alkynylated 3-Oxo-β-Sultam was obtained in good yield by crystallization in the case of the dimethyl derivative and by column chromatography in the case of the diethyl derivative. Scheme 10 depicts the complete synthesis of compound **70**.

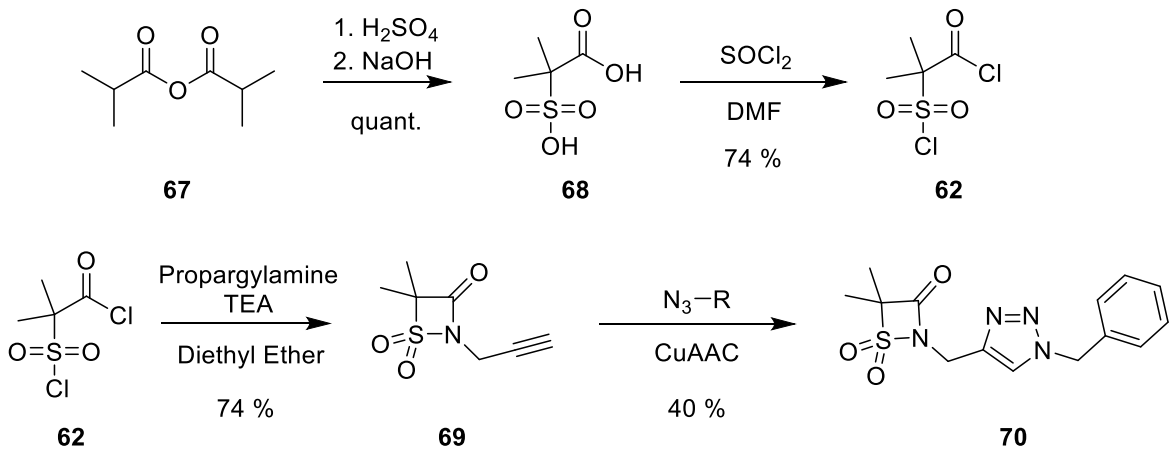

Scheme 10 – Synthesis of a 4,4-diethyl 3-Oxo-β-Sultam alkyne and derivatization by CuAAC.

An alternative strategy for the derivatization of 3-Oxo-β-Sultams was the direct alkylation of a non N-substituted 3-Oxo-β-Sultam, described by Glasl *et al* (scheme 11).[262] The non-substituted 4-membered-ring core was easily obtained by cyclization with liquid ammonia at -78ºC. In a mechanism analogous to other amines, ammonia will attack one of the electrophilic centers in the dichloride and then the cyclization results from the

attack of the amide/sulfonamide formed to the second electrophilic center. A simple extraction work-up from the reaction with dichloromethane yielded the desired product in decent yield.

Alkylation for this type of compound is described by using sodium hydride do deprotonate the acylsulfonamide and then adding an appropriate halogenated compound for alkylation (scheme 11). The proof-of-concept and optimization of this reaction was attempted with benzyl chloride and with 4-Nitrobenzylbromide. When analyzing these reactions, no products were obtained. In NMR analysis, only vestigial amounts of the desired product were identified. This strategy was abandoned for this project, but an optimization is envisaged in the future as a way of increasing N-substitution variability without requiring azides or cyclization with different amines for each pattern of substitution.

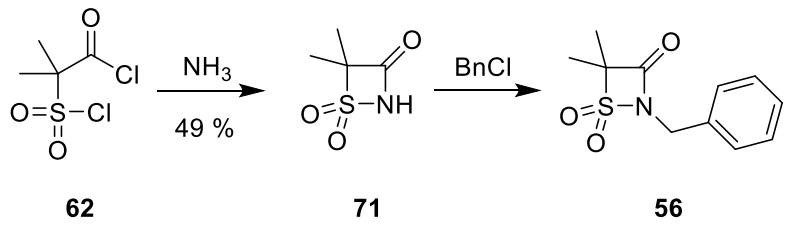

Scheme 11 – Cyclization of a 3-Oxo-β-Sultam with ammonia. Alkylation reactions N-H 3-Oxo-β-Sultams.

2.1.2. Synthesis of Azide Building Blocks

For the derivatization of the 3-Oxo-β-Sultam warhead into a library of compounds click chemistry was used. Click reactions are extremely useful in the fast generation of libraries of compounds. In ABPP the CuAAC click chemistry reaction is very commonly used to attach tags to warheads, generating a triazole linker, which is also associated with favorable properties in the final compounds.[274]

The azides used in this work were either purchased from commercial sources (phenyl azide derivatives and biotin azide – figure 22 – A) or synthesized prior to the CuAAC

reaction (benzyl azide derivatives (figure 22 – B), carbohydrate-based azides (figure 22 – C) and fluorophore azides (scheme 12 and scheme 13).

For the synthesis of benzyl azide building blocks, halogenated benzyl derivatives were stirred overnight with sodium azide in DMSO and the azide derivatives were obtained by extraction from the reaction using diethyl ether and stored as DMSO stocks. The carbohydrate azide was previously synthesized and readily available in Moreira's lab.

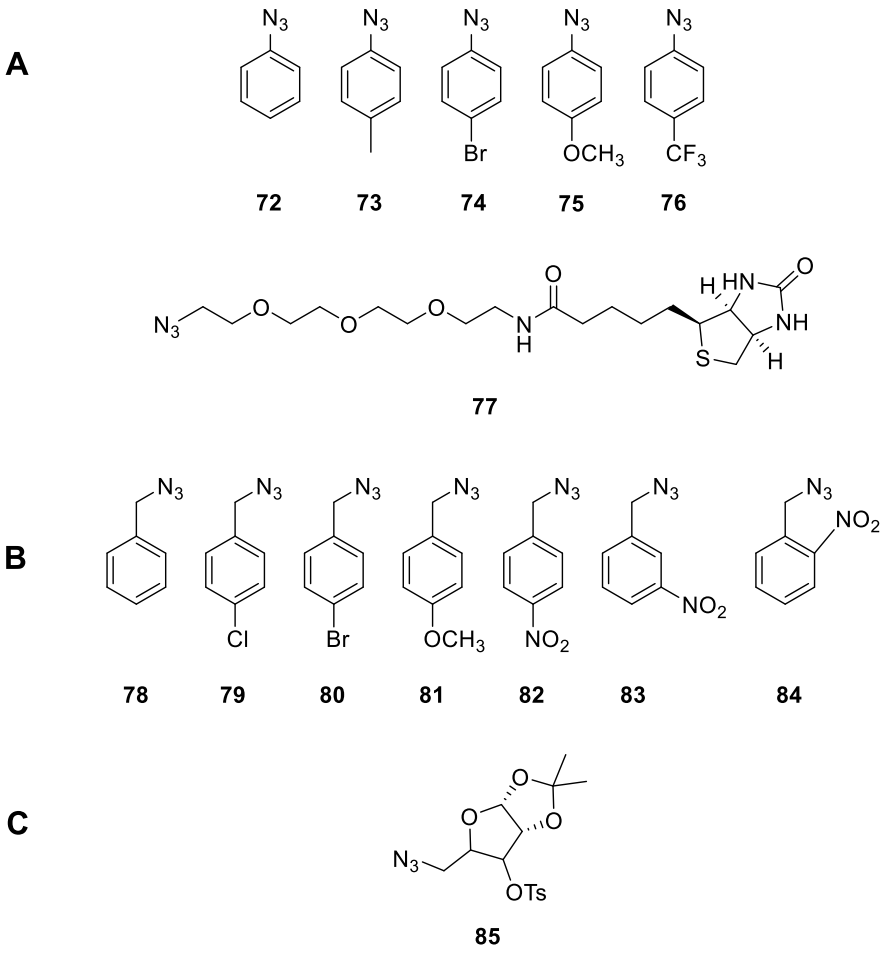

Figure 22 – Azides used in the CuAAC derivatization of 3-Oxo-β-Sultams.

Adding click chemistry handles to complex molecules like fluorophores is less straightforward since the fluorescent properties of the fluorophore should not be negatively affected and the complex structures of most tags make them intrinsically challenging to derivatize. Commercially available azide and alkyne derivatives of a very

large number of different fluorophores and affinity-based tags are plentiful, but the optimization of their synthesis in the lab is important for them to be readily available to use in significant amounts. For fluorescent ABP synthesis we derivatized NBD and Rhodamine.

NBD is purchased as a halogenated derivative. Derivatization of NBD-Cl has been done by adding a linker arm with 3-bromopropylamine hydrobromide, which is then converted into an azide by using sodium azide (scheme 11 – A). In this synthesis, the reaction of the intermediate bromine derivative into the azide derivative is usually incomplete, even after adding an excess of sodium azide into the reaction and prolonging its course through several days. Furthermore, the bromine and the azide derivatives have almost identical Rfs, which makes their chromatographic purification problematic. Given the low overall yield (40% over two steps), an optimization of the reaction was done.

We hypothesized that by synthesizing the azide of the 3-bromopropylamine arm first and then adding NBD-Cl, we could avoid formation of the bromine intermediate and make the product easier to purify and in better yield (scheme 11 – B). A new experiment was made where 3-bromopropylamine was stirred with sodium azide in DMSO overnight and then, without intermediate purification, NBD-Cl and triethylamine were added to the reaction. As predicted, this avoided formation of the bromine derivative and made the final NBD-azide product easier to purify by column chromatography, resulting in a yield of 46%. Despite obtaining only slightly better yield, the new strategy makes the product much easier and faster to obtain.

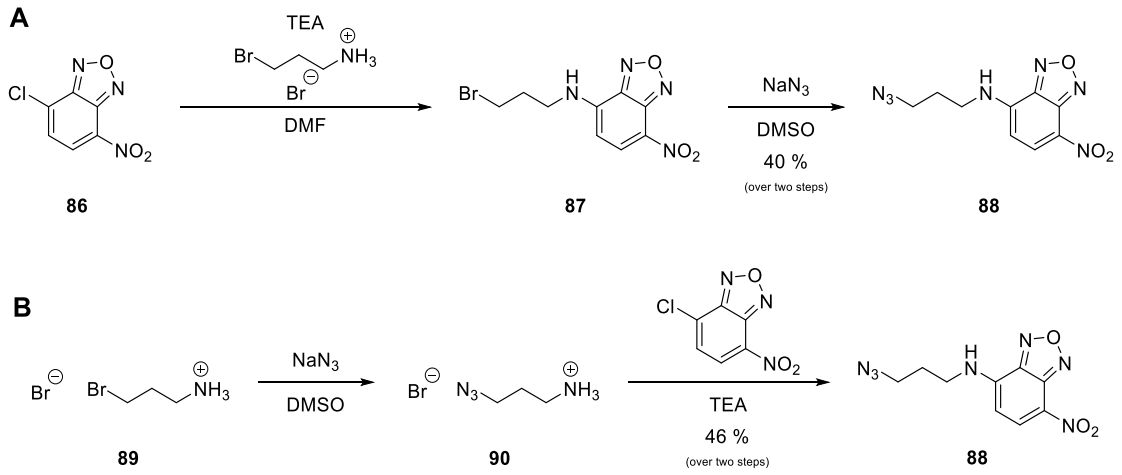

Scheme 12 – Synthesis of an NBD azide.

For rhodamine B the general strategy was to take advantage of the carboxyl group to create an amide bond using different amines that could then be derivatized to include an azide. Rhodamine B was stirred with HOBt, TBTU and DIPEIA in DCM for 30 minutes and then 2-(2-(2-(2-azidoethoxy)ethoxy)ethoxy)ethan-1-amine and DIPEIA were added and the reaction was stirred overnight at 45°C (scheme 12). TLC analysis suggested that there was total consumption of Rhodamine B and formation of a new product. After work-up extractions with water and DCM and a chromatographic purification by preparative TLC, the rhodamine azide was obtained.

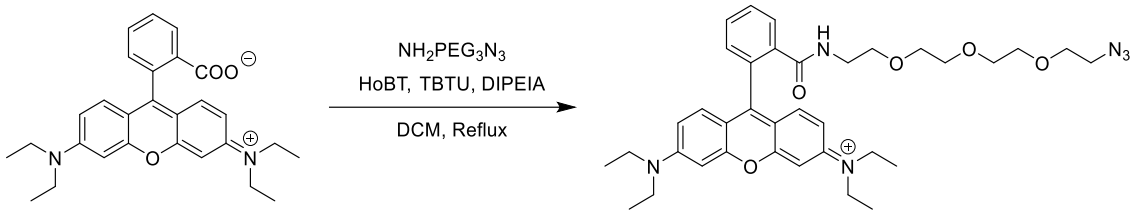

Scheme 13 – Derivatization of Rhodamine B with 2-(2-(2-(2-azidoethoxy)ethoxy)ethoxy)ethan-1-amine.

2.1.3. Derivatization of Alkynylated 3-Oxo-β-Sultam by Click Chemistry

The click chemistry reaction between the 3-Oxo-β-Sultam alkyne and the library of azides had to be optimized. The CuAAC reaction, a click reaction, is usually reliable and provides the desired products in excellent yield with no need for chromatographic purification steps. The first attempts of clicking our 3-Oxo-β-Sultam with different azides failed and no products were obtained. We suspected that the presence of water in the reaction or the extraction-based workup could induce ring-opening of the 3-Oxo-β-Sultam and be responsible for the poor results. An optimization of the synthesis was done, varying reaction times, solvent, sodium ascorbate amounts, copper-ligand and work-up procedure. Additionally, purification of the compounds proved to be complicated, with no elution of the final compounds in silica-based solid media, unless methanol was used, a solvent which can potentially react with the 3-Oxo-β-Sultam ring.

After testing different conditions we concluded that the best results could be obtained by using DMSO and water as solvents; a concentration of sodium ascorbate double to the copper sulfate concentration seemed to improve yields, while the use of a copper ligand (Bathophenanthrolinedisulfonic acid disodium salt hydrate or TBTA[275]) resulted in no apparent improvement. The reaction time was minimized to avoid hydrolysis due to prolonged exposure to aqueous conditions. Using these optimized conditions, dimethyl compounds were easily obtained by precipitation from the reaction by adding water, while diethyl compounds, which did not precipitate via the addition of water, were extracted from the reaction using ethyl acetate and precipitated by washing the resulting crude oil with diethyl ether. The yields were low to moderate but allowed sufficient amounts of the compounds to be available for testing.

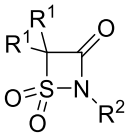

71: R^1 = Me, R^2 = H (49 %)
69: R^1 = Me, R^2 = CH_2CCH (74 %)
92: R^1 = Et, R^2 = CH_2CCH (63 %)

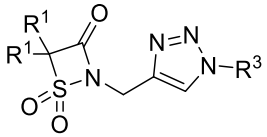

70: R^1 = Me, R^2 = Bn (40 %)
93: R^1 = Me, R^2 = Ph-4-Br (25 %)
94: R^1 = Me, R^2 = Bn-4-Cl (47 %)
95: R^1 = Me, R^2 = Bn-4-Br (60 %)
96: R^1 = Me, R^2 = Bn-4-NO_2 (12 %)
97: R^1 = Me, R^2 = Bn-3-NO_2 (60 %)
98: R^1 = Me, R^2 = Bn-2-NO_2 (44 %)
99: R^1 = Me, R^2 = Bn-4-OCH_3 (63 %)
100: R^1 = Et, R^2 = Ph-4-Br (39 %)
101: R^1 = Et, R^2 = Bn-4-Cl (40 %)
102: R^1 = Et, R^2 = Bn-4-Br (60 %)
103: R^1 = Et, R^2 = Bn-4-NO_2 (47 %)
104: R^1 = Et, R^2 = Bn-4-OCH_3 (41 %)

105: R^1 = Me, R^2 = 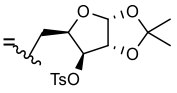
36 %

106: R^1 = Me, R^2 = 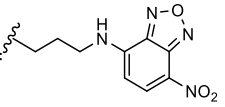
72%

107: R^1 = Et, R^2 = 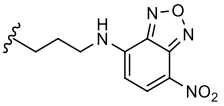
99 %

108: R^1 = Et, R^2 = 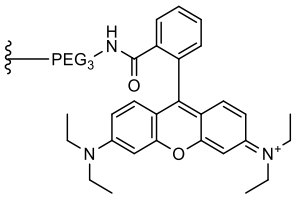
15 %

109: R^1 = Et, R^2 = 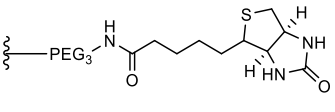
91 %

Figure 23 – 3-Oxo-β-Sultam library of compounds.

3-Oxo-β-Sultam ABPs were synthesized using the same methodology with the fluorophore and biotin azides. Fluorophore containing ABPs were synthesized with NBD and Rhodamine. Biotinylated ABPs were synthesized for mass-spectrometry applications.

Overall, the synthetic route chosen for the synthesis of our library was efficient, with the dimethyl derivatives requiring no chromatographic purification in any of the steps, and the diethyl derivatives requiring only a simple chromatographic step after the cyclization reaction with propargylamine. The yields of most of the steps are good, making it easy to obtain a varied library of 3-Oxo-β-Sultams for testing. The complete library of compounds is presented in figure 23.

2.2. Enzymatic Inhibition Studies

The 3-Oxo-β-Sultam compound library was tested for HNE inhibition, using commercially available pure HNE and an HNE fluorogenic substrate, and for selected serine hydrolases, to establish biochemical selectivity. The assay is based on measuring the conversion of a fluorogenic substrate by the tested enzymes after incubation with the compounds. The fluorescent signal increase is inversely proportional to the compound's potency.

2.2.1. Inhibition of Human Neutrophil Elastase by 3-Oxo-β-Sultams

To test the ability of the 3-Oxo-β-Sultam library to inhibit HNE, a biochemical inhibition assay was performed. Briefly, decreasing concentrations of 3-Oxo-β-Sultam compounds were plated, commercially purchased HNE was added and an incubation of 30 minutes was done. After this, an HNE-specific fluorogenic substrate is added and the fluorescence generation is measured for 30 minutes. If inhibition is efficient, no HNE remains active and there is no increase in fluorescence for the duration of the assay due to no substrate cleavage. As compound concentration decreases, the remaining active HNE in each

reaction cleaves the fluorogenic substrate, generating fluorescence. The remaining HNE activity when compared to a control is plotted against the logarithm of compound concentration for each experimental dataset and the IC_{50} is calculated from the obtained curve. Selected examples of dose-response curves are presented in figure 24. The calculated IC_{50} values for the 3-Oxo-β-Sultam library are presented in table 1. Additionally, ligand efficiency (LE) and ligand-lipophilicity efficiency (LLE) values were calculated and are presented in table 1.

The compounds are potent HNE inhibitors, with some having IC_{50} values in the nanomolar region. A significant difference was observed between dimethyl and diethyl derivatives. When changing from dimethyl to diethyl substitution there is, in general, a ten-fold increase in activity. This is most likely due to a better recognition of the

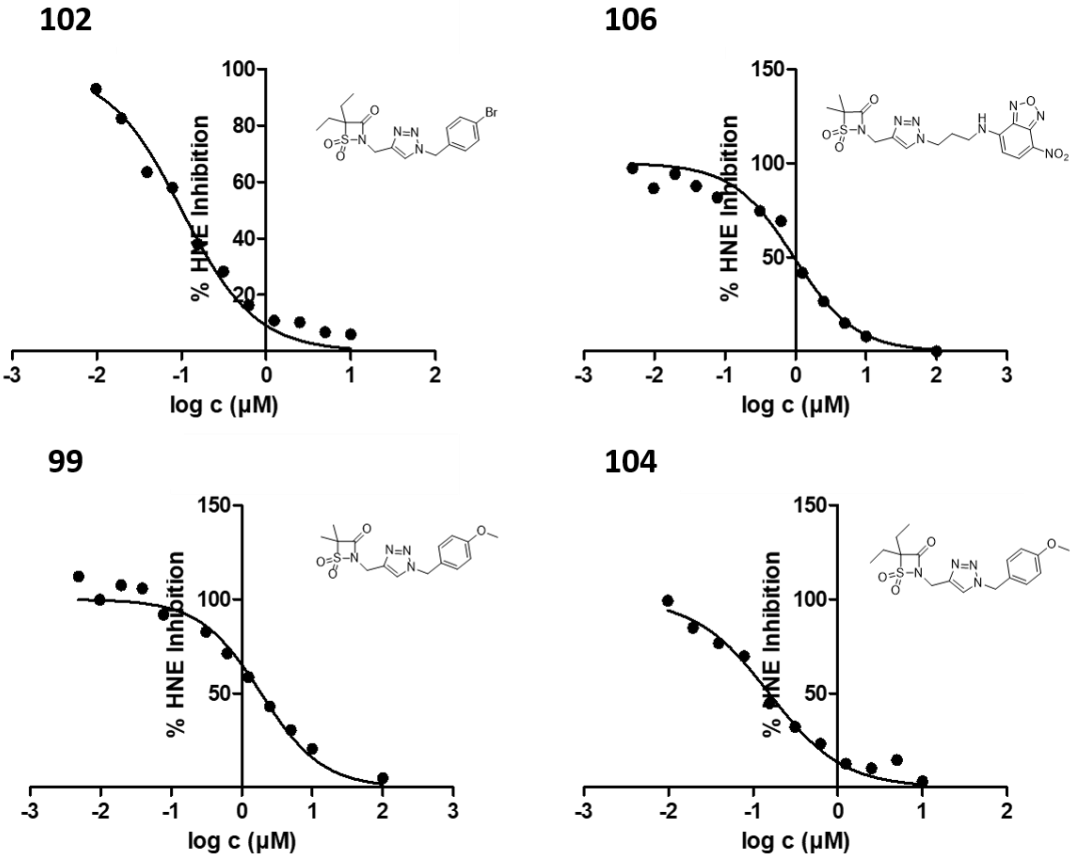

Figure 24 – Dose-response curves for HNE inhibition by selected 3-Oxo-β-Sultams..

Table 1 – IC_{50}, LE and LLE values for HNE inhibition by 3-Oxo-β-Sultams.

	IC_{50} (μM)	LE	LLE		IC_{50} (μM)	LE	LLE
69	3.271	0.64	5.64	**100**	0.184	0.39	3.58
70	3.104	0.35	4.9	**101**	0.296	0.37	4.15
71	10.031	0.78	6.13	**102**	0.156	0.38	4.28
92	0.873	0.61	5.16	**103**	0.199	0.35	5.29
93	1.643	0.37	3.69	**104**	0.309	0.35	4.92
94	1.523	0.35	4.5	**105**	1.040	0.21	5.08
95	1.791	0.35	4.27	**106**	0.528	0.28	5.04
96	4.391	0.3	5.01	**107**	0.188	0.29	4.43
97	1.539	0.33	5.46	**108**	0.011	0.18	6.95
98	1.833	0.32	5.46	**109**	0.603	0.2	7.12
99	3.122	0.32	4.98				

*the compound containing a carbohydrate is (3aR,5R,6S,6aR)-5-((4-((4,4-dimethyl-1,1-dioxido-3-oxo-1,2-thiazetidin-2-yl)methyl)-1H-1,2,3-triazol-1-yl)methyl)-2,2-dimethyltetrahydrofuro[2,3-d][1,3]dioxol-6-yl 4-methylbenzenesulfonate;

compounds by HNE since it has been shown that the 2-diethyl substitution is a better fit for HNE's S1 pocket. A diethyl substitution has been shown to be favorable in 3-Oxo-β-Sultams due to a better k_i/k_{OH} ratio, when compared, for example, with dimethyl or spiro-cyclohexil derivatives. Tsang and coworkers have established the k_i/k_{OH} ratio as a good measurement to evaluate 3-Oxo-β-Sultams since it encompasses both the enzymatic inhibition value and the tendency for alkaline hydrolysis, giving an overall better metric of compound potential.[259] The most potent compound was the Rhodamine ABP **108**, with an 11 nM IC_{50}. Additionally, the biotinylated ABP **109** presents a good IC_{50} of 603 nM, which is a promising value and supports the use of this probe for mass-spectrometry applications. The alkyne derivatives **69** and **92** also showed good IC_{50} values, of 3.271 μM and 0.873 nM, respectively, an encouraging result since these probes can be used for biorthogonal labeling experiments.

LE and LLE are used in drug discovery to guide inhibitor development by providing a simultaneous measurement of both potency and lipophilicity to estimate druglikeness. According to these concepts, compounds should display an LE > 0.3 kcal mol^{-1} per heavy atom and an LLE > 5.[276] The analysis of the LE and LLE values of the 3-Oxo-β-Sultam

compounds revealed a promising outlook, with most compounds fulfilling the recommended values. Practically all the small inhibitors have an LE above 0.3, with most also presenting an LLE above 5 or slightly below this value. Interestingly, all ABPs have an LE below 0.3, clearly reflecting the significant increase in size by inclusion of the bulky tags, which pertain to probe functions and do not necessarily contribute to target engagement, but which also contribute to the excellent LLE values for most of them.

2.2.2. Biochemical Selectivity against Selected Serine Hydrolases

An analogous approach was taken against a group of selected serine hydrolases to determine biochemical selectivity. The tested enzymes were thrombin, urokinase, trypsin, kallikrein and chymotrypsin. The obtained IC_{50} values are presented in table 2.

Table 2 – Biochemical selectivity against selected serine hydrolases (n = 3).

	Thrombin		Urokinase		Trypsin		Kallikrein		Chymotrypsin	
	IC_{50} μM	SD	IC_{50} μM	SD	IC_{50} μM	SD	IC_{50} μM	SD	IC_{50} μM	SD
92	6.2	1.2	2.6	1.1	>100		>100		>100	
107	2.0	1.1	1.7	1.1	>100		2.5	1.1	4.8	1.1
109	6.8	1.2	>100		>100		>100		>100	
108	4.4	1.1	4.1	1.2	>100		>100		>100	
102	1.4	1.1	4.2	1.2	>100		>100		8.1	1.2

The compounds are reasonably selective for HNE when compared with the other studied enzymes. For almost all the tested compounds, micromolar inhibition was measured for thrombin and urokinase. No activity was observed for trypsin. Kallikrein was only inhibited by **107** at micromolar levels and chymotrypsin was inhibited by **107** and **102**. These results reinforce our suspicions that the 3-Oxo-β-Sultam is able to inhibit other hydrolases other than HNE due to its high reactivity, however, there seems to be some selectivity, since some of the tested serine hydrolases were not inhibited by any of the

selected compounds in the biochemical selectivity assay and HNE's inhibition is associated with much lower IC_{50}s. A more in-depth analysis of the protein engagement by the 3-Oxo-β-Sultams will be performed using mass spectrometry and the biotinylated 3-Oxo-β-Sultam.

2.3. Proteomics of 3-Oxo-β-Sultams

The 3-Oxo-β-Sultam library was tested against purified HNE protein, revealing that the compounds are potent HNE inhibitors, with IC_{50} values ranging from low nanomolar to low micromolar values. This was an encouraging result, since it shows that the compounds possess enough stability to engage the targets in aqueous media and can potentially be used in biological applications as probes. Additionally, the most potent compound was the Rhodamine derivative, indicating that the big aromatic structure of rhodamine might be beneficial for target binding and reinforcing the potency of the ABP derivatives. Biochemical inhibition assays provide preliminary information regarding inhibitory properties and allow us to quickly compare between compounds of the same library but fail to mimic the more complex native environment where proteins are encountered in vivo. In our biochemical assays, the limited number of entities present, the target enzyme and the inhibitor, increases the chances of inhibition if no relevant constraints for active site engagement are present. Additionally, the selectivity assays are limited to a selected group of related enzymes, being impossible to simulate the full complexity of a proteome in that type of setting. For these reasons, we employed ABPP techniques to establish, for the first time, the full extent of target engagement and selectivity of the 3-Oxo-β-Sultam warhead and their applicability as chemical biology tools.

2.3.1. Gel Evaluation of 3-Oxo-β-Sultams

Gel-based experiments are one of the pillars of proteomics and ABPP, providing preliminary information regarding proteome reactivity, potency and selectivity of the

compounds against specific targets. Several experiments were done with 3-Oxo-β-Sultams, using different conditions and ABPs. Preliminary studies showed that the signal provided by the rhodamine derivative was much stronger than the signals provided by the NBD ABP. For this reason, we performed the gel studies exclusively with the rhodamine ABP and the diethyl derivatives.

We started by testing the general reactivity of the 3-Oxo-β-Sultam compounds by performing incubations of the alkynylated and rhodamine-derivatized ABPs with complete proteomes of selected cell lines. The diethyl 3-Oxo-β-Sultam-alkyne was incubated for 30 minutes in concentrations ranging from 0.1 to 100 µM with whole cell lysates from the cell lines HEK293T and U937. After incubation, a click reaction with Rhodamine-azide was performed to allow visualization of the labeled proteins. FP-Rhodamine 1 µM labeling was used for comparison (figure 25). Concentration-dependent labeling of proteins was observed for both cell lines. For up to 10 µM of compound,

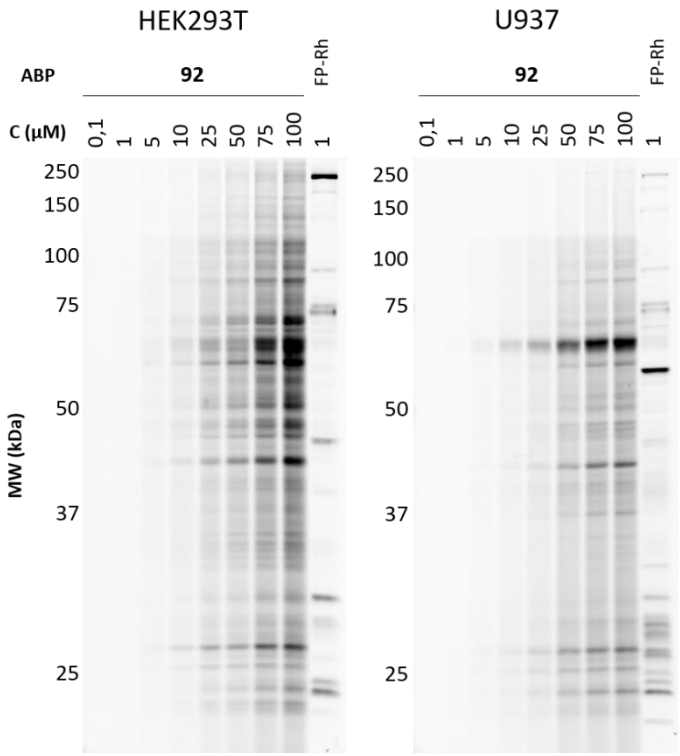

Figure 25 – Concentration range tests for 3-Oxo-β-Sultam ABP **92** in two different whole cell lysates of HEK293T and U937. Labeling of proteins is clearly visible around 5-10 µM and background labeling seems to increase significantly at high concentrations 75-100 µM. FP-Rhodamine (1 µM) labeling is shown for comparison.

labeling is relatively selective, with only a few visible bands, but for higher concentrations, background labeling becomes significant, suggesting non-specific binding. These results suggest the alkynylated 3-Oxo-β-Sultam labels proteins in a biological sample containing a full proteome, but does so with limited selectivity, especially at high concentrations.

In a similar setting, the 3-Oxo-β-Sultam-Rhodamine probe was tested in increasing concentrations (0.1 to 100 µM) in THP-1 and HEK293T whole cell lysates. Like for the alkynylated ABP, concentration-dependent labeling of proteins was observed, with a good degree of apparent selectivity for lower concentrations, but significant background labeling and promiscuity for higher concentrations (figure 26).

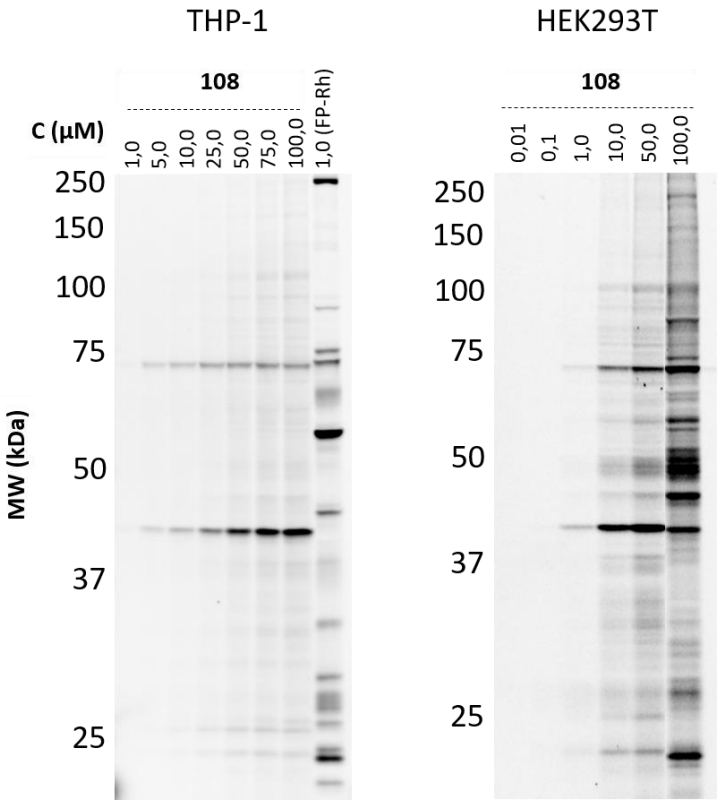

Figure 26 – Labeling of THP-1 and HEK293T whole cell lysates (1 mg/mL) with increasing concentrations of 3-Oxo-β-Sultam **108** in whole cell lysates of THP-1 and HEK293T cell lines. Labeling seems to be reasonably selective up to high concentrations of 50 µM.

To evaluate the ability of the compounds to label HNE, experiments were done where commercially purchased pure HNE was used in PBS as the sample (figure 27). Both the diethyl 3-Oxo-β-Sultam-alkyne and the diethyl 3-Oxo-β-Sultam-rhodamine were incubated at 50 µM with decreasing concentrations of HNE, from 500 nM to 31.25 nM. The alkyne ABP was clicked with rhodamine azide after incubation. For the rhodamine derivative, HNE labeling is observed for all concentrations of enzyme, down to 31.25 nM. In the case of the alkyne ABP a weak signal is only observed for the highest concentration, meaning the compound might not be suitable for tandem-labeling strategies for HNE. These results are consistent with the previously obtained IC_{50} for these two compounds, where the rhodamine derivative showed an IC_{50} value 2 orders of magnitude lower than the alkyne ABP.

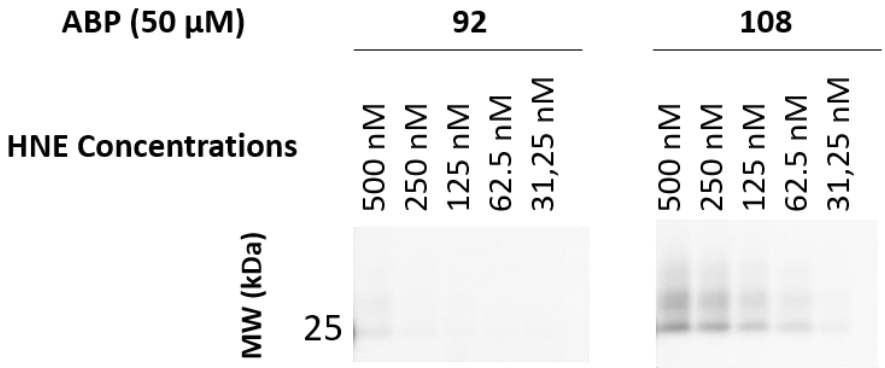

Figure 27 – Labeling of decreasing concentrations of pure HNE by 3-Oxo-β-Sultams **92** and **108** at 50 µM. Compound **92** was clicked with Rhodamine azide after incubation with the proteome. While labeling is clearly observed with the Rhodamine probe, the alkyne probe provides a weak signal, only visible at 500 nM of HNE.

We then spiked the commercial HNE in decreasing concentrations into a full HEK293T proteome to ensure that HNE is present in a detectable amount and tested the labeling of the enzyme using the rhodamine probe. HNE was clearly labeled by the ABP down to 75 nM of HNE but concomitant labeling of additional proteins was observed. This shows the probe labels HNE when in the presence of a complete proteome, but not with absolute specificity. Some bands were observed to increase in labeling as HNE's concentration decreased, suggesting they could be HNE substrates (figure 28).

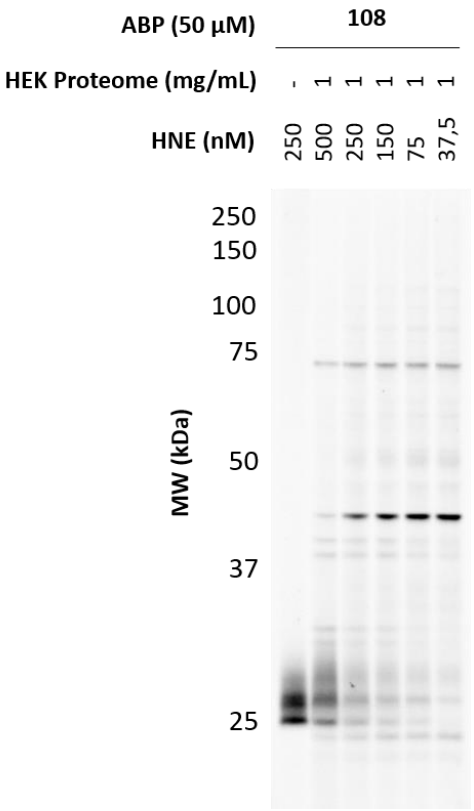

Figure 28 – HNE spiking experiments in HEK293T cells. 3-Oxo-β-Sultam-Rhodamine **108** labeling of pure HNE (first lane) and spiking of pure HNE in decreasing concentrations into HEK293T whole cell lysates (1mg/mL). Labeling of HNE is observed even in the presence of a complete proteome but not completely selective. As spiked HNE concentration decreases, labeling of some proteins clearly increases, indicating these might be HNE substrates.

An additional test was done where HNE labeling was tested in three different situations: pure protein, pure protein spiked into a HEK293T whole cell lysate, and in a native U937 whole cell lysate, a cell line which expresses active HNE.[277] Additionally, in all three experimental conditions a pre-incubation with an HNE-specific active site-dependent inhibitor, ONO-6818,[278] was done to attempt to block HNE labeling and confirm that 3-Oxo-β-Sultam inhibition of HNE is active site dependent. The results are presented in figure 29.

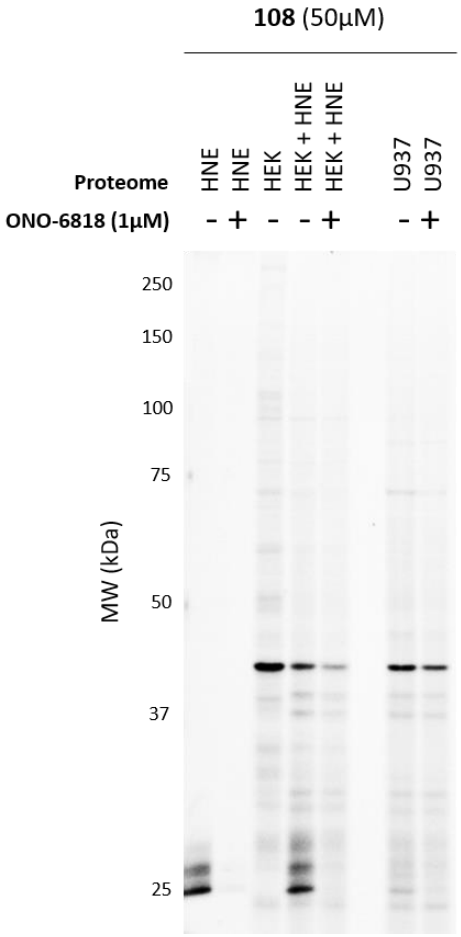

Figure 29 – Testing of HNE labeling in a pure form, spiked into a complete proteome and in a cell line that expresses active HNE with compound **108**. Labeling is clearly visible in all three types of experiments, being suppressed by pre-incubation with ONO-6818. When in the presence of a complete proteome, labeling of additional proteins is visible.

As expected from previous tests, the labeling of pure HNE was efficient and clearly visible as a group of three bands corresponding to different carbohydrate content. Pre-incubation with ONO-6818 blocked labeling, suggesting active site-dependent labeling of HNE by the 3-Oxo-β-Sultam probe. Labeling of HNE when spiked into a full HEK293T proteome was also efficient and inhibited by ONO-6818. In U937 cell lines, labeling of a small band around the molecular weight of HNE is visible. Pre-incubation with ONO-6818 blocked labeling of the protein, indicating it is HNE. This shows that the 3-Oxo-β-Sultam rhodamine ABP is capable of labeling HNE in a complex proteome at native concentrations with enough intensity to be visualized by gel-based ABPP

techniques. These results suggest that the 3-Oxo-β-Sultam ABPs might be suitable for HNE studies in complex proteomes.

To complement these gel studies, we performed competitive ABPP experiments using selected 3-Oxo-β-Sultam compounds. Briefly, the compounds were incubated with U937 whole cell lysates in different concentrations (0.1, 1.0 and 10 µM) for 30 minutes and then the FP or iodoacetamide probe was added and incubated for 30 minutes. The samples were run in SDS-PAGE and compared with a control where DMSO was used as the competitor. The results are presented in figure 30.

Overall, there is no clear strong inhibition of any bands that are labeled by the FP or iodoacetamide probes, suggesting that either the compounds have a selective target profile or that there is no significant inhibition of FP or iodoacetamide targets. For FP

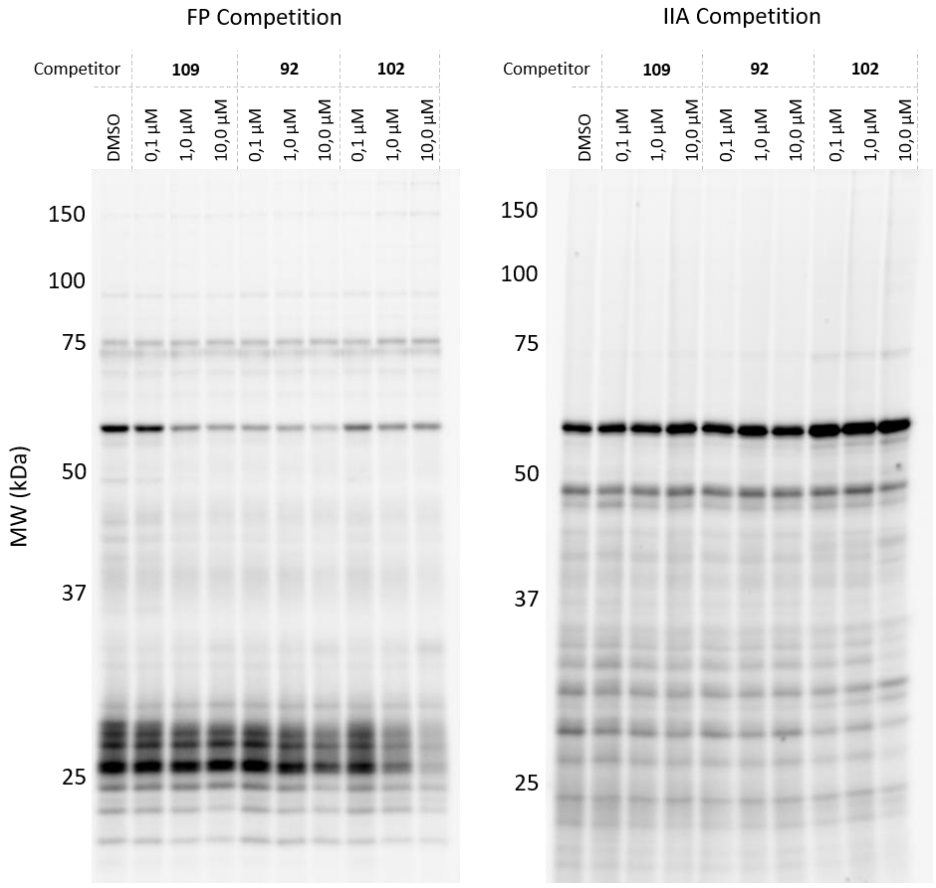

Figure 30 – Competitive ABPP of 3-Oxo-β-Sultam compounds **109**, **92** and **102** against FP-Rhodamine (left) and Iodoacetamide-Rhodamine (right).

competition, when the highest concentrations of compound were tested, there seems to be partial inhibition of some targets (band above 50 kDa for compounds **109** and **92**; bands around 25 kDa for compounds **92** and **102**). This may suggest that inhibition of some serine hydrolase targets is incomplete or occurs with low target occupancy. In the case of the compound **102**, there seems to be a general non-specific reduction of FP labeling, which could indicate a general reactivity for serine hydrolases with low stoichiometry inhibition. In the iodoacetamide competition gel, there are no clear observable targets with the exception of a couple of bands at the highest concentration of compound **102**, suggesting the compounds may be selective against cysteine residues.

Overall, the gel-based assays performed with 3-Oxo-β-Sultam ABPs showed that the compounds seem to be able to efficiently label HNE, even in the presence of a complex proteome, and do so in a process dependent on the active catalytic site of the enzyme. However, the results suggest that selectivity and the stoichiometry of inhibition are limited, which could hinder their applicability as ABPs.

2.3.2. Mass Spectrometry Evaluation of 3-Oxo-β-Sultams

While gel-based experiments are a useful tool to quickly evaluate potency and selectivity of chemical compounds, a more in-depth analysis can be achieved using mass spectrometry. Gel experiments showed us that while 3-Oxo-β-Sultam are able to label HNE in complex proteomes, significant labeling of additional enzymes is present. Mass spectrometry-based ABPP techniques are extremely powerful and are able to provide a comprehensive list of engaged targets by the tested compounds and additional information like target occupancy by using competitive assays.[16,45,73]

For these experiments we used the biotinylated derivative of the 3-Oxo-β-Sultam warhead since labeling of HNE by the alkynylated probe seemed to not be efficient in gel-based assays.

The ABP was first tested in a quantitative protocol using ReDiMe in U937 cell lines. Probe versus DMSO control and probe versus competitor experiments were done, using the rhodamine derivative as competitor, since we had previous data confirming its ability

to label HNE and other proteins in gel-based assays. A summary of the results with the proteins filtered for the serine hydrolase enzyme family is presented in figure 31.

The results showed labeling of HNE in the probe versus DMSO experiments only for the higher concentration of 50 µM of probe. Among the other targets there is clear labeling of several members of the DPP family, including FAP, DPP8 and DPP7, as well other enzymes like acyl-protein thioesterase 2 (LYPLA2), acylamino-acid-releasing enzyme (APEH) and carboxylesterase 1 (CES1), among others. When spiking HNE into a HEK293T proteome the results were more consistent, with HNE being labeled in both concentrations of probe, 10 µM and 50 µM. Among the other targets we find PREP, fatty acid synthase (FASN), acyl-protein thioesterase 1 (LYPLA1), LYPLA2, retinoid-inducible serine carboxypeptidase (SCPEP1), lysosomal Pro-X carboxypeptidase (PRCP), carboxypeptidase (CPVL), ABHD10, among others. Some of these proteins are consistent with the results of the U937 cell line experiments, potentially reinforcing them as targets of our compounds. To validate these results and determine target occupancy we performed probe versus competitor experiments using the rhodamine ABP as competitor. Surprisingly, the results were very variable and none of the labeled proteins was efficiently competed, suggesting low target occupancy of the targets identified in the probe versus DMSO experiments (figure 31).

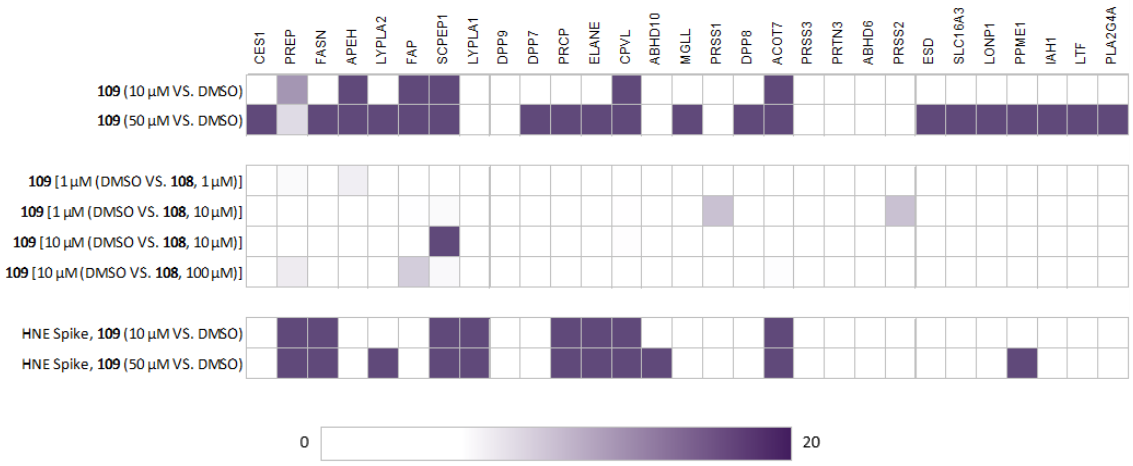

Figure 31 – ReDiMe results for 3-Oxo-β-Sultams. A ratio higher than 3 is considered a hit. The results were filtered to show only the serine hydrolase family of proteins. Each line represents one experiment.

After running the samples and analyzing the data we weren't completely satisfied with the consistency of the results. For this reason, we decided to change our approach to a protocol using SILAC-MudPIT going forward. In SILAC, the control and the tested samples are combined in the beginning of the process after probe labeling and user interference is minimized, which could improve our results. A summary of the obtained results filtered for the serine hydrolase family of enzymes is presented in figure 32.

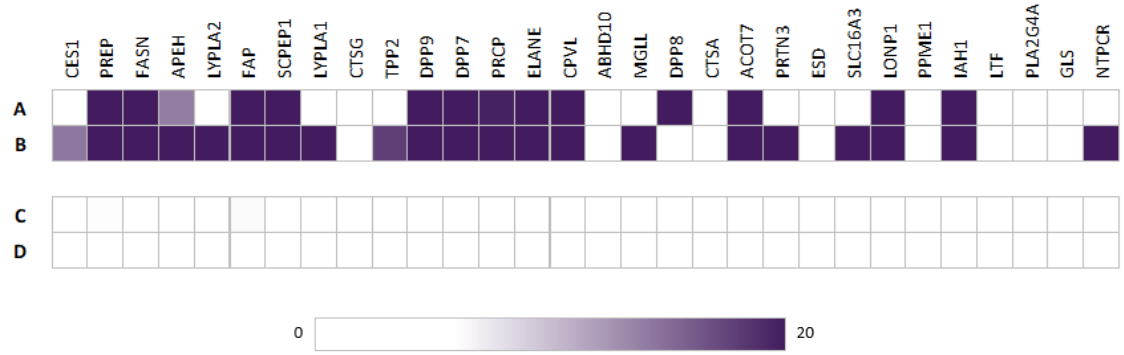

Figure 32 – ABPP-SILAC results for 3-Oxo-β-Sultams. The results were filtered for the serine hydrolase family. Hits were considered when the protein is enriched with a ratio of at least 3 when compared with a DMSO control in at least two experiments. A.**109** [10 µM (Probe VS. DMSO)]; B.**109** [50 µM (Probe VS. DMSO)]; C. [**108** (100µM) VS. DMSO], then **109** (10 µM); D. [(**108** (100µM) VS. DMSO)], then **109** (50 µM).

The results from the experiments using SILAC were more consistent. In probe versus DMSO experiments a large group of serine hydrolases was labeled. HNE was labeled with maximum ratio in all experiments, reinforcing that our compounds are good HNE inhibitors. PREP, FASN, FAP, SCPEP1, LYPLA1, PRCP, CPVL and cytosolic acyl coenzyme A thioester hydrolase (ACOT7) were also consistently labeled in all replicates. Other proteins like CES1, APEH, LYPLA1, DPP7, DPP8, DPP9, PRTN3 were labeled, but not consistently between replicates. When validating these targets in a competitive protocol against the rhodamine ABP there were no high occupancy targets identified consistently. The results presented above were filtered for serine hydrolases due to the high number of proteins identified and our interest in profiling serine hydrolase engagement (figure 32).

When analyzing the entire pool of proteins identified in the assay, we see that approximately 70% of the total enriched proteins were identified as hits of the 3-Oxo-β-Sultam in the 10 µM concentration. Increasing the concentration to 50 µM increases the percentage of proteins hit by the 3-Oxo-β-Sultam to 90%. This shows that the warhead is very reactive and presents low selectivity, which could hinder its applicability in ABPP. When analyzing the results for the probe versus competitor experiments the number of targets with a high ratio decreases significantly for both tested concentrations. (figure 33). While this profile seems to be more fitting for an ABP, with only few proteins showing a ratio of 20, when analyzing the complete list of high ratio proteins these were found to be mostly contaminants from the sample processing steps. No relevant targets with high target occupancy were observed.

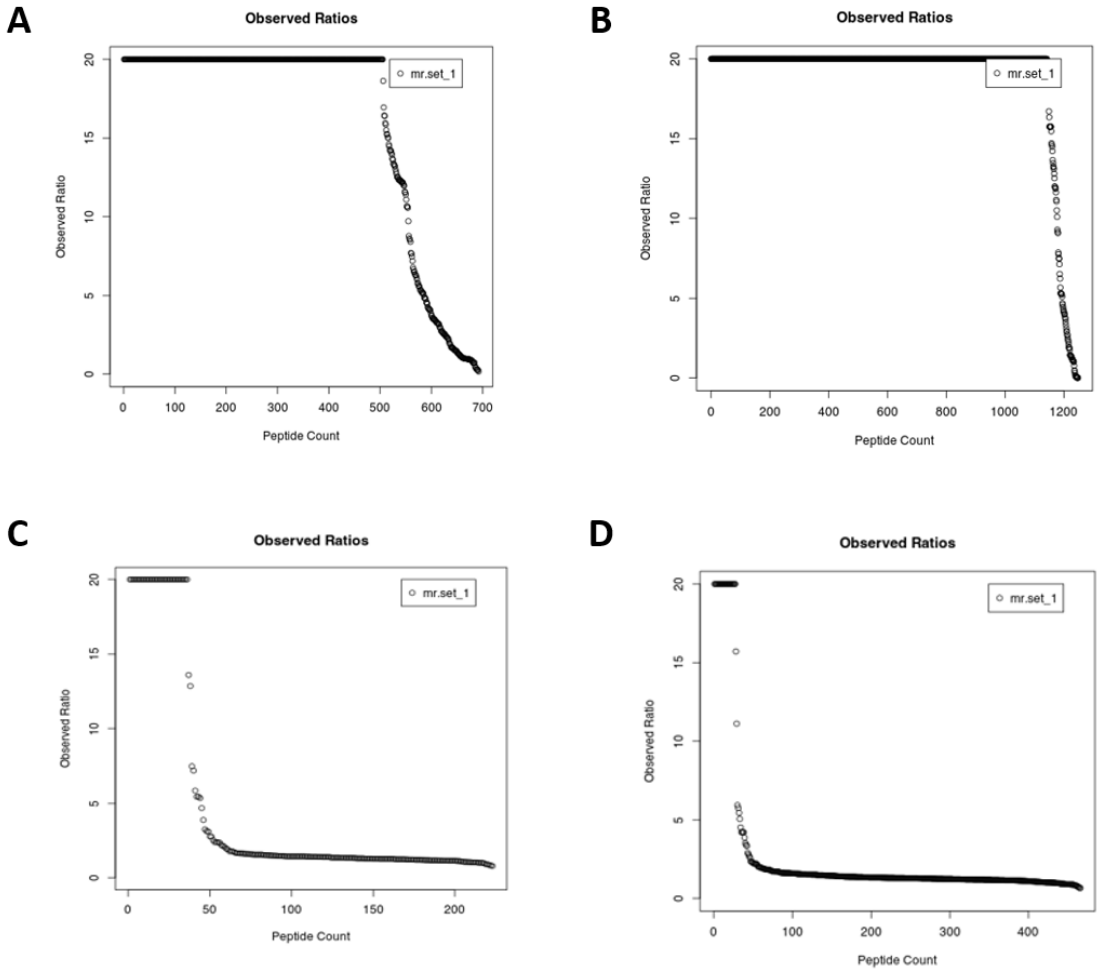

Figure 33 - Example of the peptide count plotted against observed ratios for: A. **109**, 10 uM vs. DMSO experiment; B. **109**, 10 uM vs. DMSO experiment; C. Probe vs. probe experiment. Pre-incubation with **108**, 10 uM or DMSO, and then **109**, 10 uM; D. Probe vs. probe experiment. Pre-incubation with **108**, 50 uM or DMSO, and then **109**, 50 uM.

The analysis of the results shows that while 3-Oxo-β-Sultams hit a diverse group of serine hydrolases and could potentially function as an interesting broad reactivity probe, akin to the FP probes, the target occupancy is very low in virtually all proteins of interest, with very low SILAC ratios, indicating that inhibition is not complete. Only PREP and FAP present ratios higher than 3 and those ratios are inconsistent between replicates. Overall, 3-Oxo-β-Sultams seem to not be suitable for use as ABPs since even though they label a big number of proteins of interest, they react with almost all proteins in the sample and, even when filtered for serine hydrolases, the experiments show that inhibition is very incomplete for these targets. These results also highlight the importance of using a probe vs. probe experiment to complete the information obtained from a probe vs. DMSO experiment.

2.4. Crystallography Studies

The exact mechanism of inhibition of serine hydrolases by 3-Oxo-β-Sultam compounds remains unknown. Several experiments performed by the Page group have led to the conclusion that these compounds inhibit serine hydrolases like PPE by acylation of the active site serine. This, however, was based mostly on kinetic assays and the analysis of reaction reversibility.[173,259]

The mechanism of target inhibition by a 3-Oxo-β-Sultam could, in theory, involve attack at either the acyl or the sulfonyl group, resulting in opening of the ring and displacing of either a sulfonamide or an amide leaving group, respectively (scheme 14).[259]

Inhibition of PPE by a 3-Oxo-β-Sultam was previously studied by Page and coworkers, who concluded that the enzyme inhibition occurs by acylation and expulsion of a sulfonamide leaving group, as demonstrated by analysis of reaction reversibility and kinetic data (see chapter X).[173,259] To the best of our knowledge, a crystal structure of the complex resulting from the reaction of a 3-Oxo-β-Sultam compound with PPE, HNE or other serine hydrolases has never been generated or published. To unequivocally clarify the mechanism of action of 3-Oxo-β-Sultams in serine hydrolase inhibition we performed crystallography experiments between PPE and HNE and selected compounds from the 3-Oxo-β-Sultam library. Our study was focused on PPE and HNE since HNE was our model

target when developing the 3-Oxo-β-Sultams and PPE's inhibition by 3-Oxo-β-Sultams is well-studied.

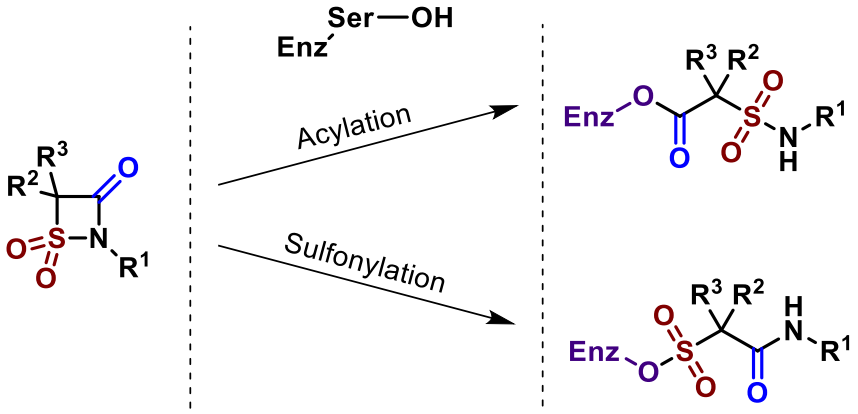

Scheme 14 – Mechanism of inhibition of a putative Serine hydrolase by a 3-Oxo-β-Compound. Inhibition can occur by either acylation or sulfonylation.

The work started with the optimization of the conditions for PPE crystallization (figure 34). Co-crystallization of the compounds with the enzyme was attempted by two techniques, soaking of pre-formed PPE crystals with 3-Oxo-β-Sultam compounds and co-crystallization of 3-Oxo-β-Sultam compounds with PPE. Only the second technique yielded the desired crystals where a positive density corresponding to a 3-Oxo-β-Sultam compound near the active site of PPE was identified.

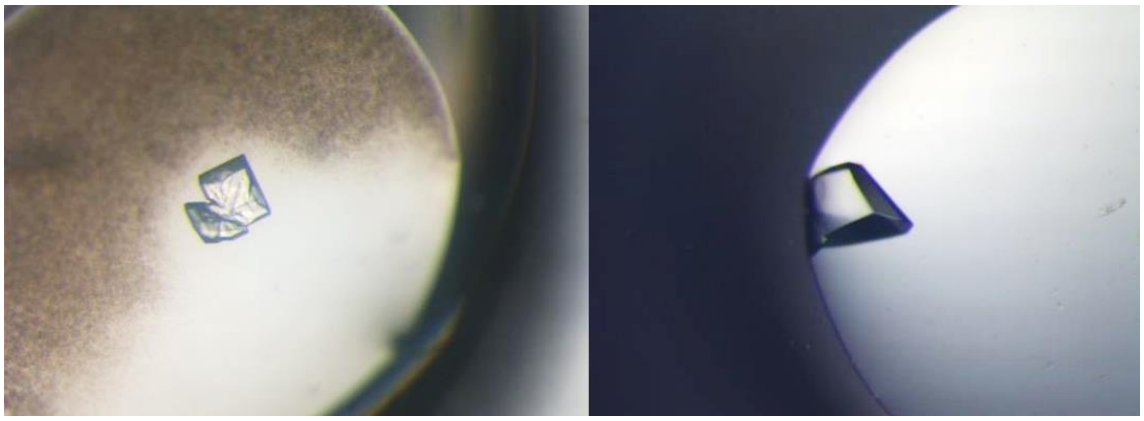

Figure 34 – Native PPE crystals obtained when screening different conditions for PPE crystallization.

One of the first compounds to be successfully co-crystallized with PPE was **94** (figure 35). The compound structure is clearly defined, with the open-ring form after reacting with the catalytic serine from PPE. Surprisingly, the density map showed that PPE is inhibited by sulfonylation of the active site, a result which directly challenges previously published data.[173]

The crystallization process was optimized, and an improved electronic density map technique was developed after refinement of the previous results. Compounds **106**, **94**, **95** and **96** were co-crystallized with PPE. The open 3-Oxo-β-Sultam ring is visibly bound

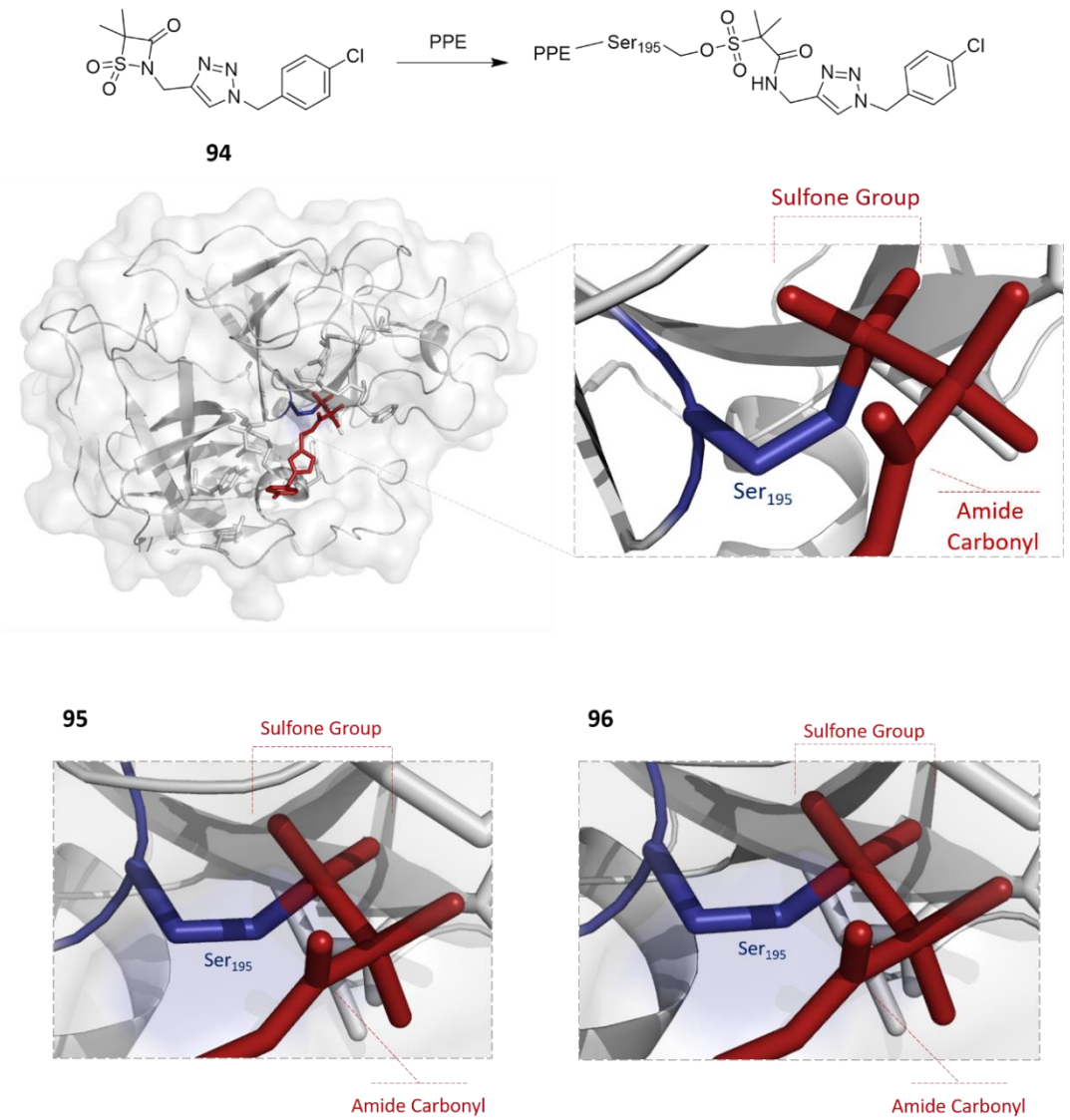

Figure 35 – Reaction of compound **94** with PPE via attack of the catalytic serine to the sulfonyl group of **94**. Active site zoomed view of the complexes between PPE and compounds **94**, **95** and **96** with PPE.

to the active site serine for all enzyme-compound pairs. In all co-crystallization experiments the protein had a positive density corresponding to the density of the ligand in the protein's catalytic center. In all the refined models obtained the electron density suggests that the enzymes are being inhibited by sulfonylation. This was observed due to the presence of two density spheres near the catalytic serine which clearly correspond to the oxygens of the sulfonyl group. The crystallographic structures were refined and are presented in figures 36 and 37.

The results clearly show that the mechanism involves formation of a bond between the catalytic serine oxygen and the sulfur from the 3-Oxo-β-Sultam, displacing an amide leaving group and leaving the enzyme sulfonylated. This was a surprising and promising result since it showed an unexpected mechanism of reaction between a serine hydrolase and the 3-Oxo-β-Sultam warhead. Inhibition of serine hydrolases by sulfonylation is an underexplored strategy and these results might uncover some of the requirements and mechanisms underlying the inhibition of this type of enzyme.

For larger compounds like **106**, electronic density is only well-defined at the catalytic center. This is probably explained by the flexibility and mobility of the distal part of the molecule containing the linker and the NBD fluorophore, given the superficial PPE pocket.

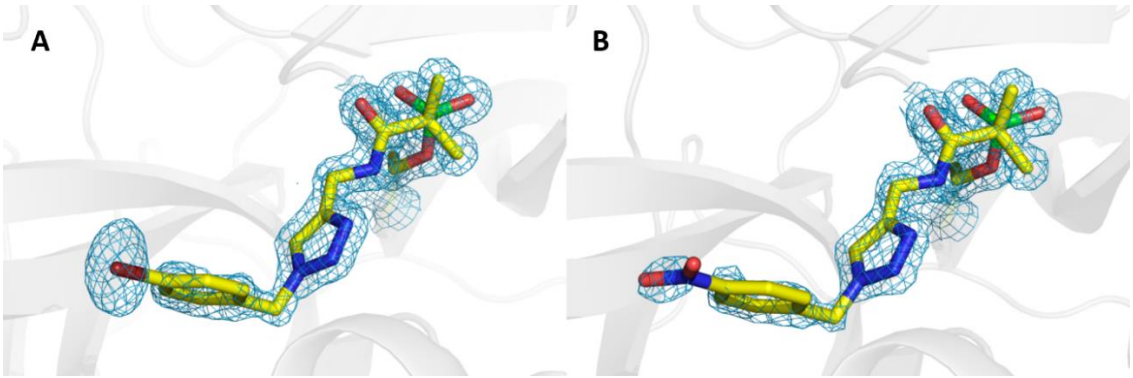

Figure 36 – Electron density map around the covalently bound **95** (A) and **96** (B) ligands of PPE, |2Fo-Fc| map is depicted in blue mesh and contoured at 1σ level. Color code: carbon in yellow, oxygen in red, nitrogen in blue, sulfur in green, and Br atoms in dark red.

Using the COOT program structures of native HNE were superimposed with the obtained structures for PPE-3-Oxo-β-Lactam crystals. The inhibitors were fitted into HNEs active site and bound to Ser195, after which an energy minimized model for this complex was obtained. The results suggest that orientation of the ligand in the HNE-inhibitor complexes should be similar to the ones obtained for the PPE-inhibitor complexes.

The same experiments were performed for HNE. This enzyme proved to be significantly more difficult to co-crystallize with the 3-Oxo-β-Sultam compounds and only one crystal was obtained, for the reaction of compound **102** with HNE. An X-ray structure of the complex at 2.6 Å resolution with R_{cryst} of 20.8 % was obtained. The open-ring compound was clearly defined in HNE's active site, covalently bound to the catalytic serine via the sulfur atom. The results showed that the sulfonyl moiety participates in hydrogen bonds with Gly193, Ser195 and His63, contributing to complex stabilization, along with the expected accommodation of the two ethyl groups in the hydrophobic S1 pocket.

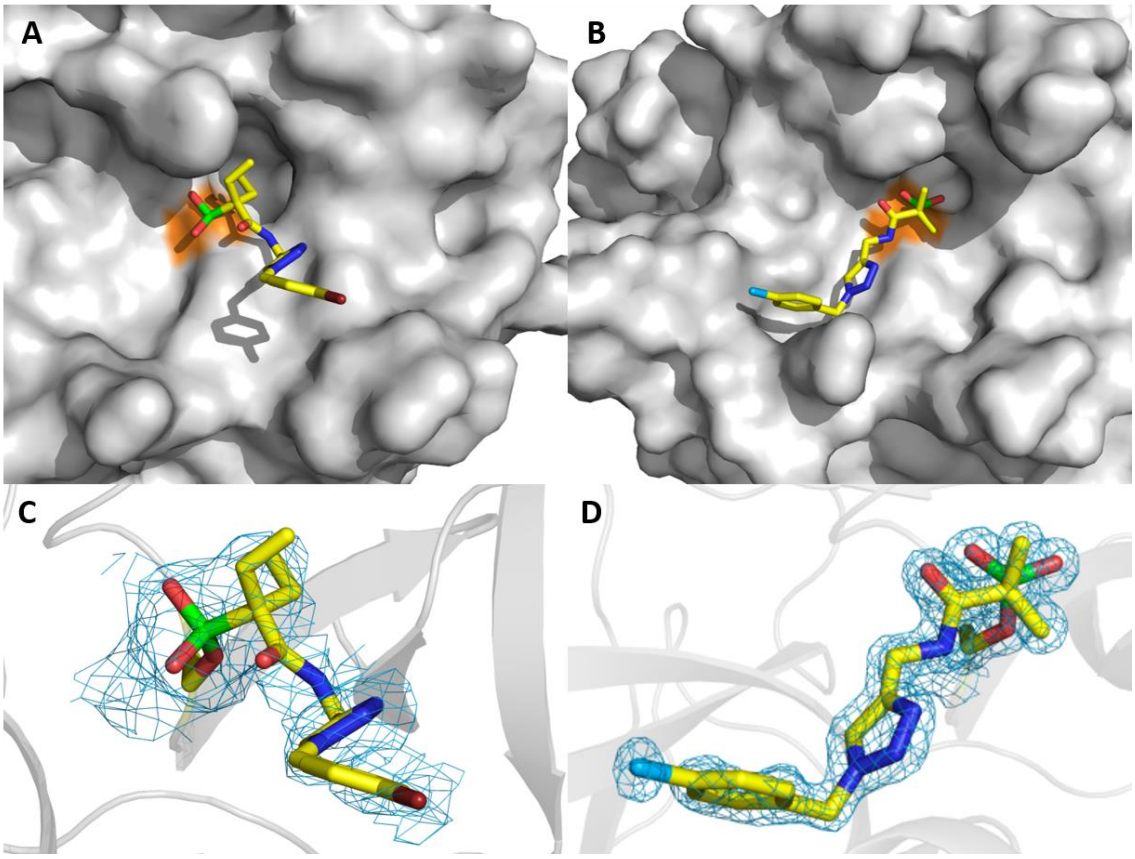

Figure 37 - Surface representation of HNE:**102** (A) and PPE:**94** (B) with ligands depicted in sticks (carbon in yellow, oxygen in red, nitrogen in blue, sulfur in green, and halide atoms in dark red (C) or light blue (D)); catalytic serine is colored in orange. Zoomed view of active site of HNE:**102** (C) and PPE:**94** (D) with |2Fo-Fc| electron density map drawn in blue mesh (at 1σ contour) around the covalently bound 3-Oxo-β-Sultam ligands.

Comparison of the results for PPE and HNE show that **102** seems to interact more extensively with the surface of PPE than **94** interacts with the surface of HNE, which instead extends towards the solvent and shows greater structural flexibility (figures 37 and 38).

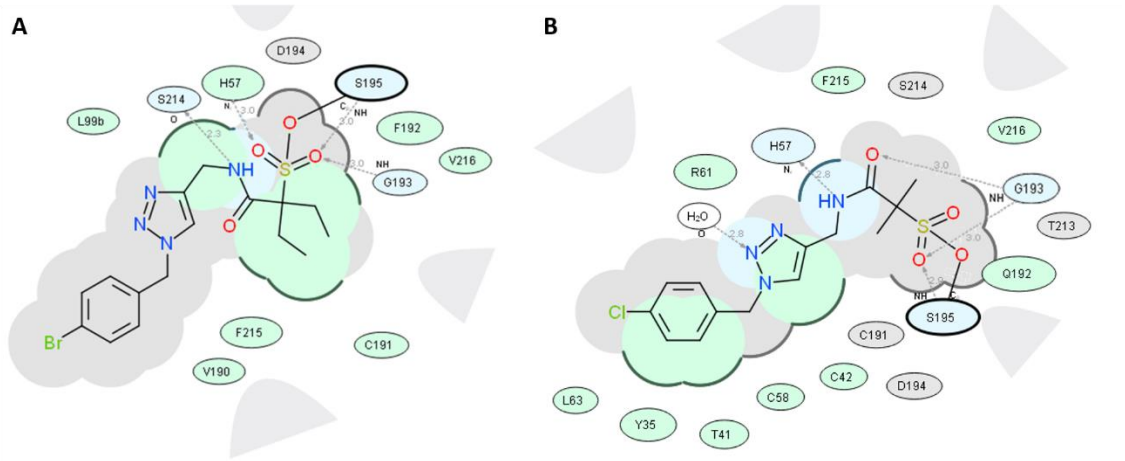

Figure 38 – Atomic interactions around the ligands in HNE:**102** (A) and PPE:**94** (B). Hydrophobic interactions are displayed in green.

Overall, for all tested compound-enzyme pairs, the mechanism of inhibition of PPE and HNE was shown to be sulfonylation of the active site serine. The three compounds crystallized with PPE showed similar crystal structures, with stabilization of the sulfone moiety by hydrogen bonding with neighboring aminoacids. These results suggest a unified mechanism for hydrolysis and serine hydrolase inhibition by 3-Oxo-β-Sultams.

Sulfonylation is an underexplored strategy in enzymatic inhibition and drug discovery, with the β-sultams as the only sulfur (VI)-nitrogen-based warheads to successfully result in selective enzyme inhibitors and ABPs.[114,279-281] The covalent modification of proteins using sulfur-based warheads has focused on sulfur (VI) fluoride exchange chemistry, including sulfonyl fluorides and aryl fluorosulfates.[282-284] The unanticipated preference of a catalytic serine to react with the sulfonyl center of the 3-Oxo-β-Sultam when a theoretically more reactive neighboring acyl center is present, which upon ring opening could expel the better sulfonamide anion leaving group, strongly suggests that the nature of the leaving group does not have a large effect on reactivity. The discovery that 3-Oxo-β-Sultams inhibit serine hydrolases by sulfonylation could provide an opportunity to

expand the available pool of sulfonylating warheads in chemical biology and uncover new enzymatic mechanisms that could guide medicinal chemistry endeavors for drug discovery.

2.5. Overview

The work with 3-Oxo-β-Sultam compounds showed these highly reactive compounds engage a number of targets in complex proteomes, including serine hydrolases, doing so via a sulfonylation mechanism in the case of elastase enzymes.

The synthesis of the compounds was straightforward, allowing some of the inhibitors to be efficiently obtained without relying on any chromatographic purification steps. The compounds also provided good results in biochemical enzymatic assays, showing efficient inhibition of HNE and some selectivity against a panel of related serine hydrolases. More importantly, these assays showed that the compounds presented enough stability for biological experiments.

Gel-based and mass-spectrometry based assays confirmed the compound's potential for labeling of HNE, but also showed significant detrimental reactivity, which results in low stoichiometry engagement of a large portion of the enriched proteome and makes the compounds unsuitable for ABPP applications.

On the other hand, our co-crystallization studies unveiled an unprecedented mechanism of inhibition by the 3-Oxo-β-Sultam compounds, via sulfonylation of the active sites of PPE and HNE. This data directly contradicts the results published by other groups that studied the same process in the past and could provide relevant information regarding the mechanisms of serine hydrolase sulfonylation and the selectivity of the nucleophilic attack of serine hydrolases when in the presence of multiple chemical groups of distinct reactivity.

Medicinal chemistry endeavors by the Page group that focused on the 3-Oxo-β-Sultams have yielded derivatives with greater stability and lower reactivity, which could be suitable for further exploration as serine hydrolase inhibitors. While these contain a

carboxylate alpha to the nitrogen atom of the 3-Oxo-β-Sultam, which will hinder HNE activity, there is potential as a sulfonylating chemotype of other serine hydrolases.

Chapter 3 – 4-Oxo-β-Lactams

The 4-Oxo-β-Lactam chemotype has been discovered and studied by Moreira's group at iMed.ULisboa as an inhibitor of serine hydrolases, namely HNE, and has been developed into libraries of potent enzymatic inhibitors.[174,175,272] The full extent of protein engagement by the 4-Oxo-β-Lactam scaffold remains to be established by proteomics methods. Preliminary work with 4-Oxo-β-Lactam ABPs was previously done in the group but with no mass spectrometry-based ABPP experiments.[186] In this chapter we sought to identify the full extent of targets of the 4-Oxo-β-Lactam chemotype in selected proteomes using fluorophore- and biotin-derivatized 4-Oxo-β-Lactams and to evaluate the scaffold's potential as a warhead for serine hydrolase labeling in competitive ABPP (figure 39).

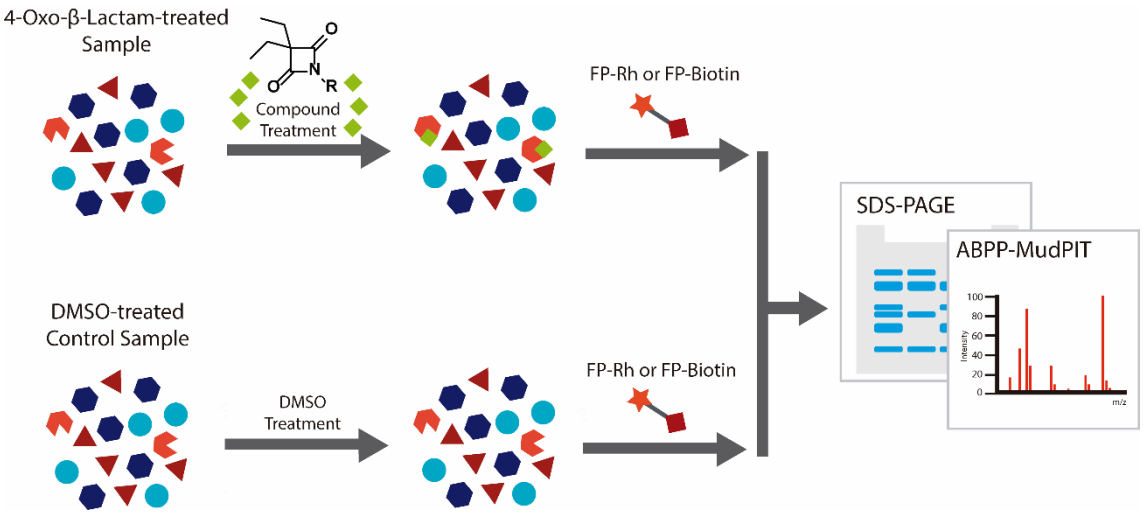

Figure 39 – Competitive ABPP platform for the evaluation of 4-Oxo-β-Lactam compounds.

3.1. Synthesis of 4-Oxo-β-Lactam ABPs

4-Oxo-β-Lactams are synthesized by slow addition of an appropriate amine to a dichloride derivative of a malonic acid.[174,175,272] An alkyne derivative of the 4-Oxo-β-Lactams was synthesized via cyclization of diethyl malonyl dichloride with propargylamine (scheme 15 – A). The 4-Oxo-β-Lactam-alkyne was derivatized into Rhodamine and Biotin ABPs using CuAAC click chemistry (scheme 15 – B, C).[55] The Rhodamine ABP will be used for gel experiments and the biotin compound will be used for mass spectrometry experiments.

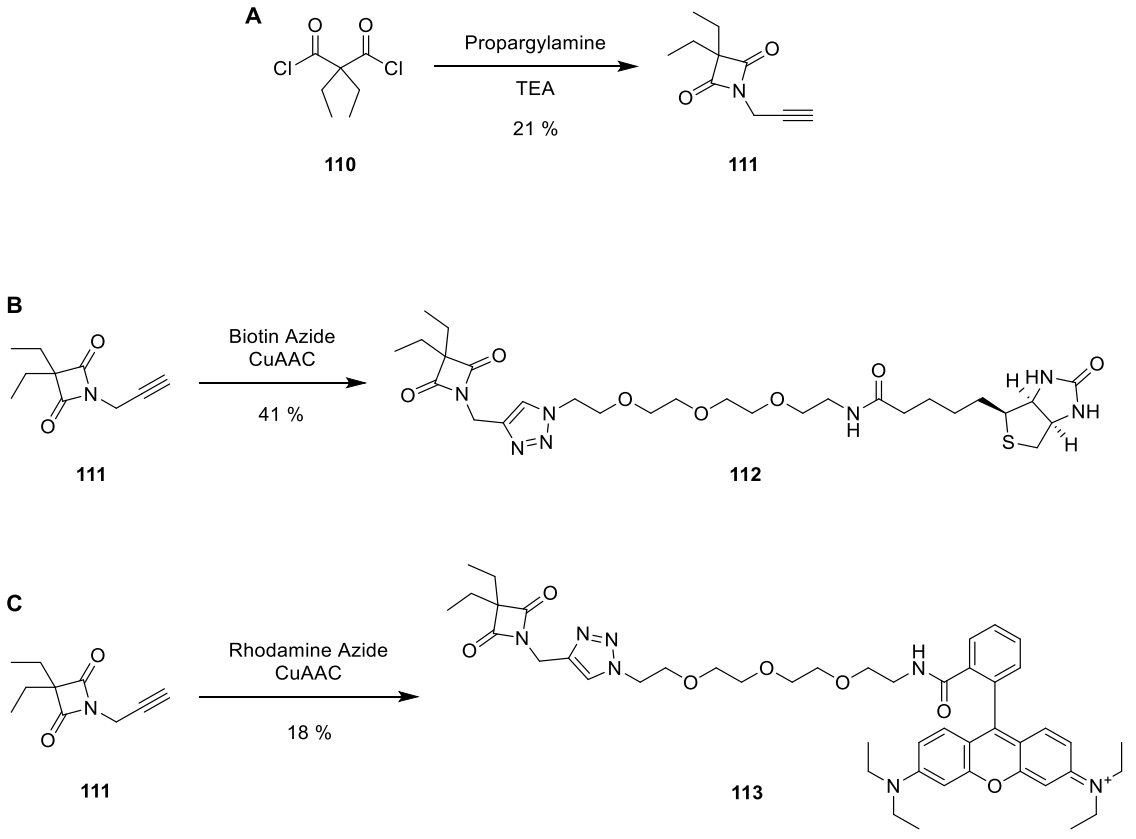

Scheme 15. A. Synthesis of an alkynylated 4-Oxo-β-Lactam; B. Synthesis of a biotinylated 4-Oxo-β-Lactam ABP; C. Synthesis of a rhodamine-derivatized 4-Oxo-β-Lactam ABP.

3.2. Proteomics of 4-Oxo-β-Lactams

Despite having been used to develop potent HNE inhibitors in the past,[186] no proper proteomics approach has been taken to establish the full extent of target engagement by 4-Oxo-β-Lactams. In this work we developed both fluorescent and biotinylated 4-Oxo-β-Lactam ABPs for application in gels and mass spectrometry. Our goal is to validate our previous work with HNE inhibitor development by confirming it as a target of 4-Oxo-β-Lactams and to potentially uncover new targets of interest that will allows us to repurpose the 4-Oxo-β-Lactam warhead to develop inhibitors of other targets. For this purpose, we used the U937 cell line since it natively expressed HNE and had shown to also express a significant group of other serine hydrolases of interest in our work with 3-Oxo-β-Sultams.

3.2.1. Gel Evaluation of 4-Oxo-β-Lactams

We started by evaluating the 4-Oxo-β-Lactam ABPs in gel-based assays. The proteome reactivity of the alkynylated 4-Oxo-β-Lactam, which could potentially be used for tandem-labeling experiments, was tested by labeling HEK293T and U937 whole cell lysates with increasing concentrations of probe, from 0.1 to 100 µM. After incubation, a click chemistry reaction was performed with rhodamine-azide to append a fluorophore to the alkynylated probe. FP-Rhodamine labeling was used as a control reaction (figure 40). Concentration-dependent labeling of proteins is clearly seen, down to 0.1 µM concentration in HEK293T cells. Unlike the 3-Oxo-β-Sultams, increasing the concentrations up to 100 µM doesn't seem to significantly increase non-specific interactions, with no excessive increase in intensity of labeling and number of apparent labeled entities, suggesting that these compounds are more selective. The labeling pattern is also significantly different from FP-rhodamine labeling, suggesting the 4-Oxo-β-Lactam could offer complementing coverage to the FP probes.

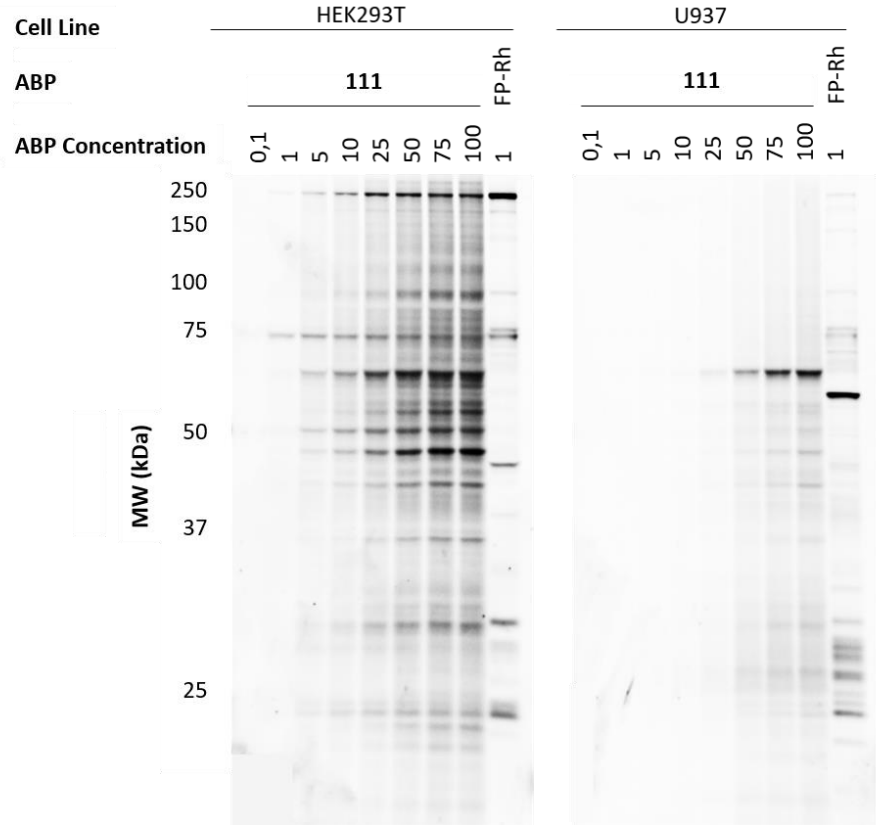

Figure 40 – Concentration range tests for 4-Oxo-β-Lactam-alkyne **111** in HEK293T and U937 whole cell lysates. The ABPs were clicked with Rhodamine-azide after incubation with the proteomes for 30 minutes. Labeling of proteins is clearly visible starting at low concentrations 0.1-1 µM and appears to be concentration-dependent, with little to no background at higher concentrations. FP-Rhodamine (1 µM) labeling is shown for comparison.

Knowing the reactivity of the alkyne ABP we proceeded to test the rhodamine derivative in similar conditions for both cell lines HEK293T and U937 and in the same concentration range. The results are presented in figure 41. Comparable results to the alkyne probe were obtained. Labeling was observed even at the low concentrations of 0.1 and 1 µM. At high concentrations, between 50 and 100 µM, background labeling doesn't seem to increase excessively and the protein target profile seems to be consistent as concentration increases, a promising result, which suggests that 4-Oxo-β-Lactams are much more selective in terms of target engagement when compared with the 3-Oxo-β-Sultams.

Following the gel experiments it seems that a concentration between 1 and 10 µM is ideal to achieve good protein labeling with minimum non-specific background labeling. This range of concentrations will be used for the mass spectrometry-based ABPP experiments.

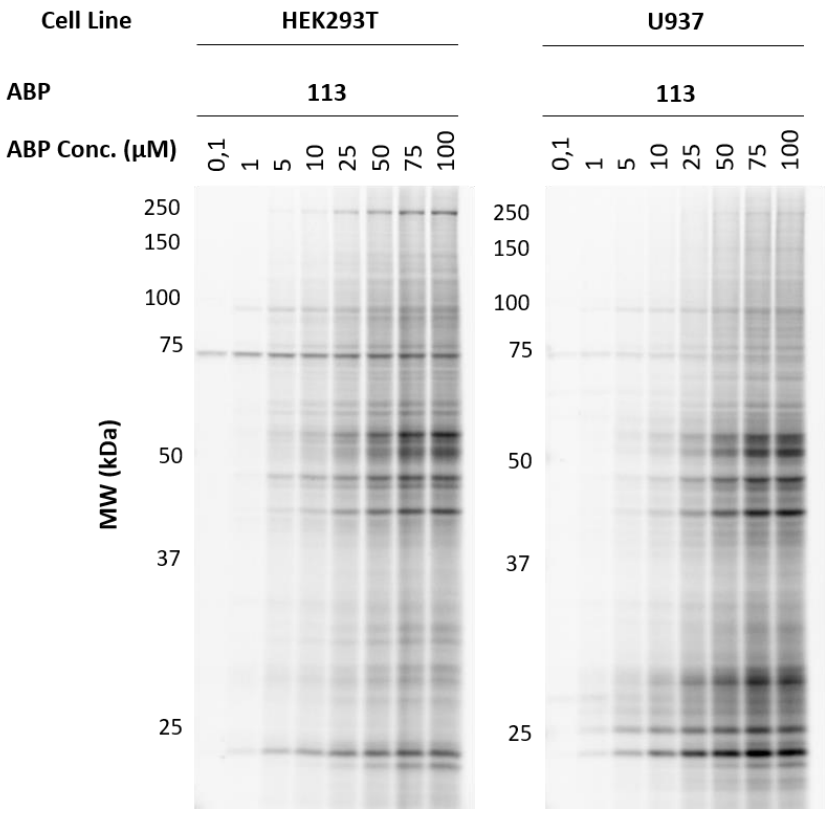

Figure 41 – Concentration range tests for 4-Oxo-β-Lactam-rhodamine **113** in HEK293T and U937 whole cell lysates. The ABPs were incubated with the proteomes for 30 minutes. Labeling of proteins is clearly visible starting at low concentrations 0.1-1 µM and appears to be concentration-dependent, with little to no background at higher concentrations.

The biotinylated 4-Oxo-β-Lactam compound was tested in a competitive ABPP approach (figure 42). The compound was incubated at three different concentrations (0.1, 1.0 and 10.0 µM) in U937 whole cell lysates and fractioned U937 lysates. The proteomes were then labeled with FP-Rhodamine and the samples were run in SDS-PAGE. Only a few proteins are observed to be inhibited by the compound, like the band at approximately 75 kDa, suggesting a selective target profile.

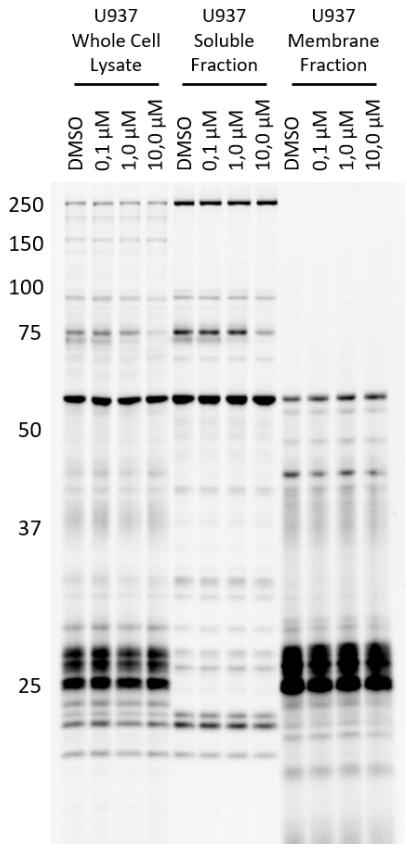

Figure 42 – Competitive ABPP for the biotinylated 4-Oxo-β-Lactam **112** compound in U937 whole cell lysates, U937 soluble protein fraction and U937 membrane protein fraction against FP-Rhodamine.

3.2.2. Mass Spectrometry Evaluation of 4-Oxo-β-Lactams

Gel-based experiments with the alkynylated and the rhodamine derivatives of the 4-Oxo-β-Lactam showed a reasonably selective profile of proteome labeling at low concentrations. We followed these results by performing mass-spectrometry-based ABPP to identify the labeled proteins.

We started by performing probe vs. DMSO control experiments with the 4-Oxo-β-Lactam biotinylated probe in U937 whole cell lysates using ReDiMe. The results, which were filtered for serine hydrolases, are presented in figure 43.

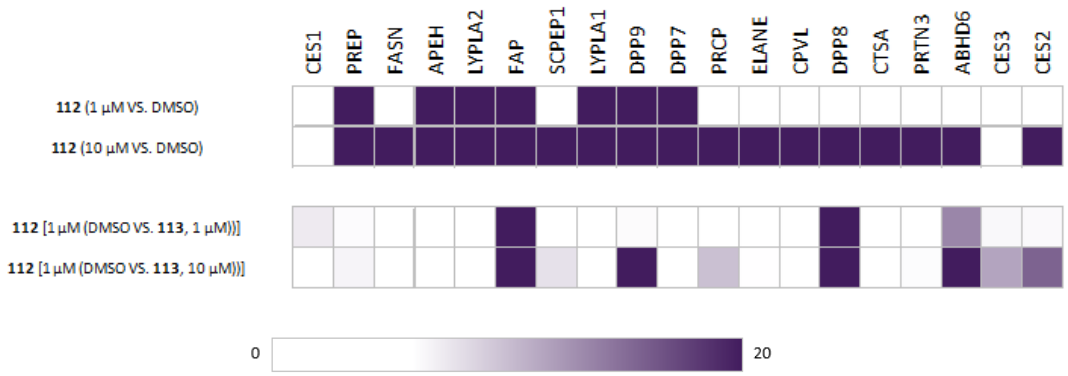

Figure 43 – ReDiMe results for 4-Oxo-β-Lactams. Probe vs. DMSO and competitive experiments. The results were filtered for serine hydrolases. Preliminary results, only one replicate was performed.

The target profile for 4-Oxo-β-Lactams was moderately selective. Approximately 20 potential targets were identified, including HNE, PREP, APEH, LYPLA1, LYPLA2, and members of the DPP family, including DPP7, DPP8, DPP9 and FAP. To validate these targets, we performed probe versus competitor experiments using a rhodamine 4-Oxo-β-Lactam ABP as competitor. The number of targets with high ratio was reduced significantly, indicating that only a few proteins are true hits, with high target occupancy. The target list showed efficient labeling of DPP family members, with DPP8, DPP9 and FAP returning maximum hit ratios. ABHD6, carboxylesterase 2 (CES2), carboxylesterase 3 (CES3), PRCP and SCPEP1 were also identified as hits. Surprisingly, HNE was not identified in these complementary experiments, suggesting it could be a low target occupancy hit for this compound at the tested concentrations. These results show that the 4-Oxo-β-Lactam warhead is very promising for the development of ABPs for a selected group of serine hydrolases. However, these experiments were merely exploratory and only one replicate was done. A more in-depth study was done using SILAC, which previously showed more reliable results.

The experiments were repeated using SILAC U937 cells. Probe versus DMSO experiments with 1 µM of biotinylated 4-Oxo-β-Lactam were performed (figure 44). The results between three replicates were consistent and mostly agreed with the results found in the ReDiMe experiments. Targets like PREP, APEH, PRCP, the members of the DPP

family and the LYPLAs were once again identified. DPP8 was only identified in one of the three experiments. HNE was not identified in any of the replicates, consistent with the ReDiMe results. Increasing probe concentration to 10 µM led to identification of a few additional targets, including FASN, HNE, CPVL, lysosomal protective protein (CTSA), ABHD6 and CES3, but this was based in only one replicate (data not shown).

Competition experiments (figure 44) confirmed that 4-Oxo-β-Lactams inhibit DPP7, DPP8, DPP9 and FAP from the DPP family with high target occupancy, as well as ABHD6 and the CES enzymes. Unlike what the ReDiMe experiments showed, HNE presents a ratio of 20, which identifies the serine protease as a target of 4-Oxo-β-Lactams and is consistent with previous work from our group. Other identified enzymes include PR3, PREP and SCPEP1. The SILAC results confirmed the preliminary results obtained with ReDiMe, revealing a surprisingly selective profile of targets, especially when compared with the results obtained for 3-Oxo-β-Sultams. The identification of several targets as true high occupancy hits shows that the 4-Oxo-β-Lactam warhead is suitable for ABPP applications. These compounds were originally envisaged for the inhibition of HNE, so the identification of additional serine hydrolase targets that are strongly inhibited was surprising and an exciting prospect for the potential of the chemotype in developing enzymatic inhibitors for these targets.

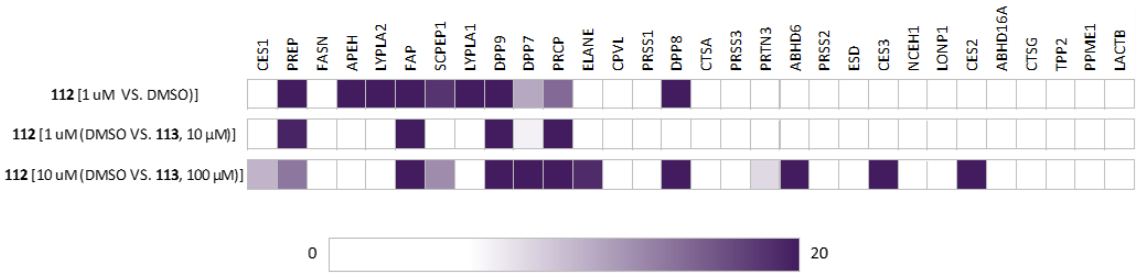

Figure 44 – SILAC-MudPIT results for 4-Oxo-β-Lactams. Results were filtered for serine hydrolases. The results present an average ratio of at least 2 replicates and only when the target was identified in at least two experiments is the target shown.

The output of the LC-MS/MS experiments performed with the biotinylated 4-Oxo-β-Lactam ABP identified several unexpected serine hydrolases as targets, including several

members of the DPP and ABHD family of serine hydrolases. Our biotinylated probe is a simple 4-Oxo-β-Lactam warhead separated from biotin with a PEG_3 linker. Inhibitors with maximum activity for specific targets could potentially be developed by taking advantage of not only molecular recognition of the 4-Oxo-β-Lactam by the catalytic apparatus of the enzyme, but also by exploring favorable noncovalent interactions at the various subsites of the enzymes.

Most of the identified proteins have therapeutic potential, like FAP, whose inhibition is pursued as an anti-cancer therapy.[198,200] DPP8 and DPP9 inhibition is also a hot topic, since these are usually concomitantly inhibited and no selective inhibitors for each have ever been described.[3,212,222,226] Enzymes of the ABHD family are also associated with important pathways, including ABHD2, which could be associated with COPD development.[249]

Given the potential of the 4-Oxo-β-Lactam warhead target profile and the myriad of targets that these compounds could potentially hit, it was decided to pursue the development of inhibitors of the newly identified enzymes focusing on a 4-Oxo-β-Lactam core. A new library of compounds was developed and analyzed by competitive ABPP techniques.

3.3. Synthesis of a Library of 4-Oxo-β-Lactam Inhibitors

The yields for 4-Oxo-β-Lactam cyclization have been historically low, mostly due to the dominant formation of a diamide side-product. For the quick derivatization of the 4-Oxo-β-Lactam scaffold into a varied library of compounds, it was important to optimize the synthetic route to allow a significant amount of 4-Oxo-β-Lactam starting material to be generated and easily derivatized. The synthetic route described in published works consists in performing the reaction in dioxane at room temperature and approximately 1 equivalent of the amine is slowly added to the dichloride malonate derivative (scheme 16 – A). These procedures usually resulted in yields of less than 10% for the cyclization reaction.[174,175,186,272] We performed an optimization of the synthesis of the 4-Oxo-β-Lactam, in which the major factor was changing the reaction solvent from dioxane to DCM, allowing the reaction to be performed at 0°C, instead of room temperature, which was previously required due to dioxane's high melting point. The stoichiometry of the

reagents was also adjusted to promote formation of the compound instead of the side-product. Our optimized conditions dramatically increased the yields of the cyclization reaction to near quantitative values. Specifically, this method resulted in yields of approximately 80, 90 and 100% for cyclization reactions with o-, m- and p- toluidine, respectively, after one chromatographic purification step (scheme 16 – B). This strategy allowed gram amounts of 4-Oxo-β-Lactam starting materials to be generated and is a promising synthetic advance for the generation of 4-Oxo-β-Lactam libraries.

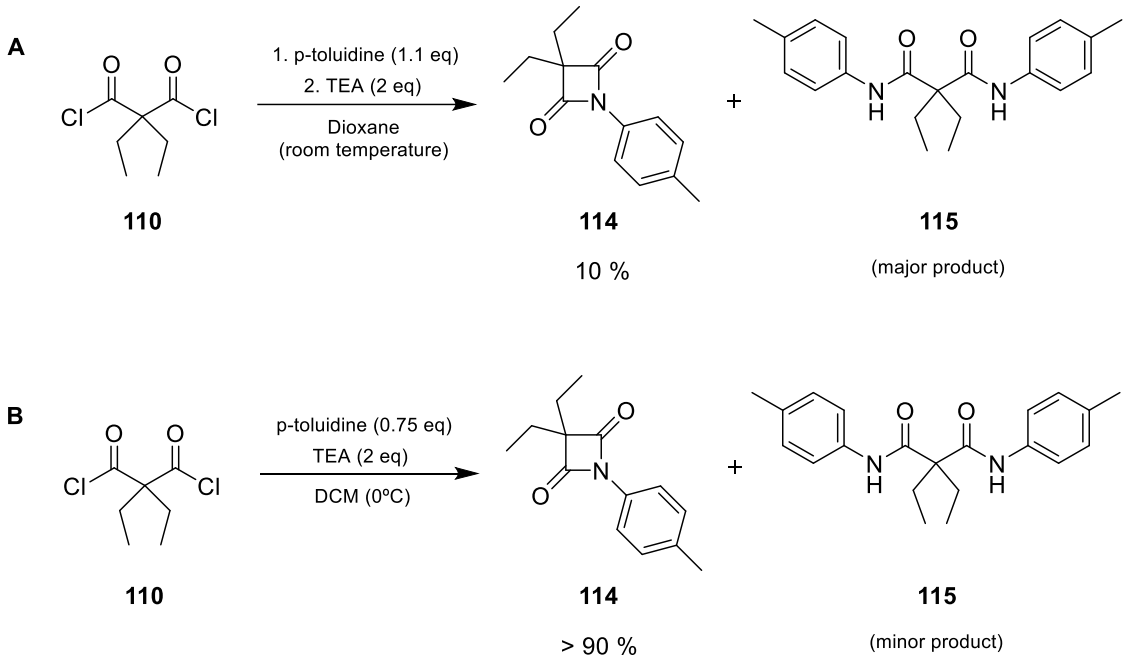

Scheme 16 – Optimization of the synthesis of the 4-Oxo-β-Lactam scaffold using the example of compound **114**: A. the classic synthesis of 4OBLs, which resulted in the unwanted diamide as the major product; B. Optimized synthesis of 4-Oxo-β-Lactams, which results in near-quantitative yields in selected cases.

For this project, a diethyl substitution on the 3-position was used, since this motif has been shown to adequately fit the catalytic sites of specific serine hydrolases and the starting material is commercially available. An N-aryl substitution was chosen for most compounds, since it results in a better leaving group upon opening of the ring when compared to N-alkyl or N-benzyl groups, resulting in increased compound potency.[272] To achieve these structural motifs, (-p, -m or -o) toluidines were used as the amines for cyclization of the commercially available diethyl malonyl dichloride. The methyl group

of the toluidine scaffold was then brominated using N-bromosuccinimide in the presence of benzoyl peroxide and a nucleophilic substitution reaction with a diverse library of amines, mostly piperazine derivatives, was used to obtain the final compounds. Scheme 17 depicts the synthesis of compound **117**. Substituted piperazines containing mostly N-benzyl, but also N-aryl substituents were chosen, containing both electron withdrawing and electron donating groups. Additional variety was introduced with pyridine and piperonal substituents and to achieve geometrical diversity, bulkier and less linear substituents like dibenzylamine and 1-(bis(4-fluorophenyl)methyl)piperazine and other heterocycles were used.

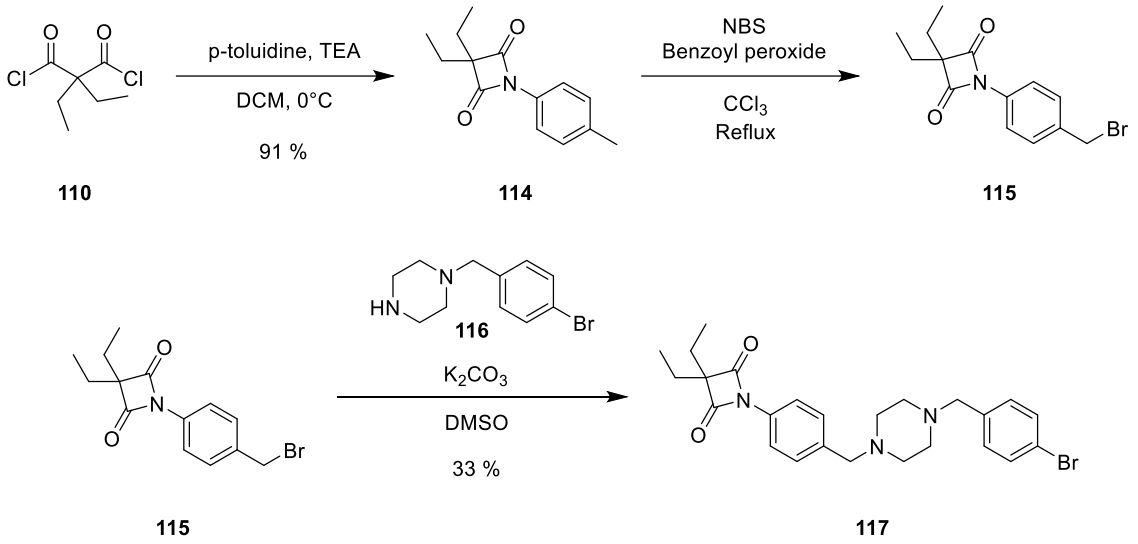

Scheme 17. Synthesis of compound **117**.

Two additional compounds were prepared by cyclization with benzyl 4-(aminomethyl)benzoate, resulting in the corresponding 4-Oxo-β-Lactam (scheme 18 – A). The benzyl group was deprotected by hydrogenation with triethylsilane and palladium in activated charcoal to generate a free carboxylic acid (scheme 18 – B). Both the benzylated and the deprotected compounds were tested in the competitive experiments. These two compounds will allow us to evaluate how critical the N-aryl substitution is for activity and if the presence of a free carboxylic acid significantly changes reactivity and selectivity.

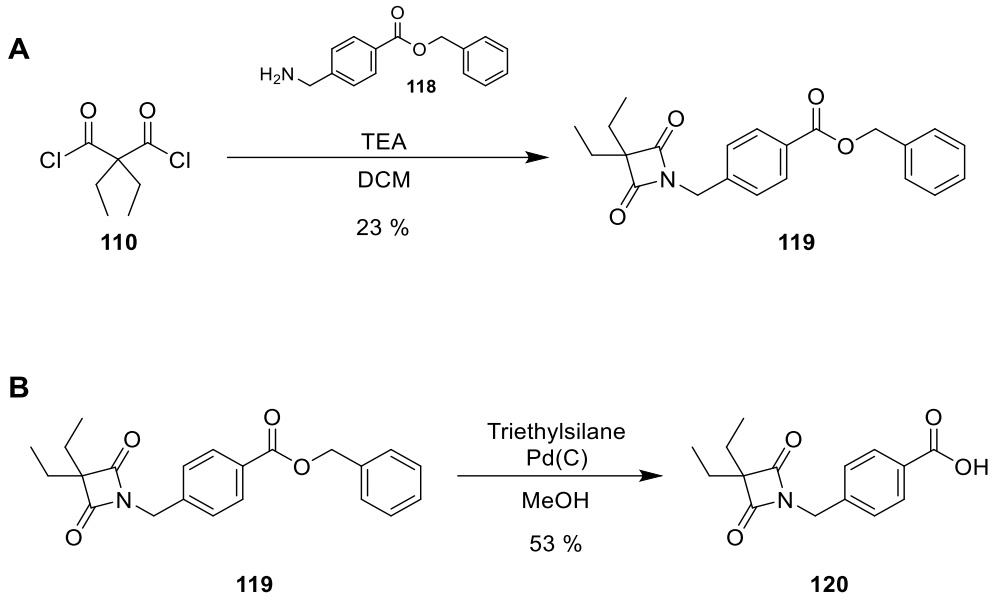

Scheme. 18 – Synthesis of 4-Oxo-β-Lactam compounds **119** and **120**. A. Synthesis of a 4-Oxo-β-Lactam with N-benzyl substituent, **119**, from benzyl 4-(aminomethyl)benzoate; B. Synthesis of a 4-Oxo-β-Lactam with a free carboxylic acid, **120**, by hydrogenation of **120**.

The complete library of 4-Oxo-β-Lactams developed for this project is presented in figure 45.

3.4. Competitive ABPP

With the new library of 4-Oxo-β-Lactams in hand we performed preliminary studies of potency and selectivity by gel-based competitive ABPP against the well-established serine hydrolase-reactive FP probes in U937 cells (figure 39).[285] Briefly, compounds were incubated with U937 whole cell lysates for 30 minutes at 3 different concentrations, 0.1 µM, 1 µM and 10 µM. After 30 minutes, 1 µM of FP-Rhodamine was added. 30 minutes later the reaction was quenched with loading buffer and the mixture was analyzed by SDS-PAGE. Compound reactions were compared against a control sample pre-incubated

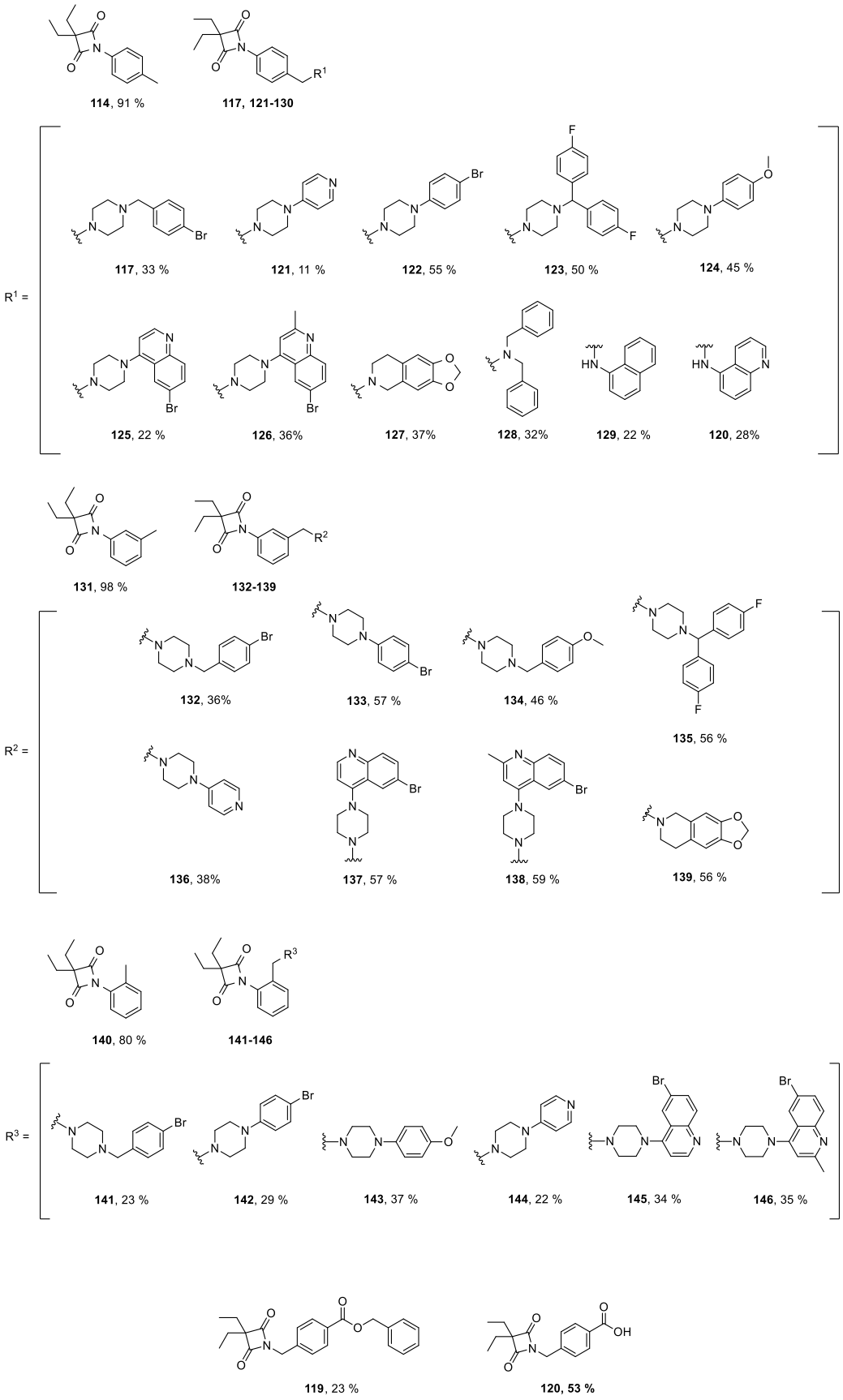

Figure 45 – Library of 4-Oxo-β-Lactams.

with DMSO for 30 minutes and then FP-Rhodamine. Inhibition of an enzyme by the 4-Oxo-β-Lactam compounds results in total or partial blocking of FP-rhodamine labeling, leading to disappearance of a band when compared with the DMSO control. The gels for selected compounds are presented below (figures 46 and 47). The full results for the entire 4-Oxo-β-Lactam library are presented in the sumplementary information. The analysis of the gel shows selective blocking of some targets of the FP probe.

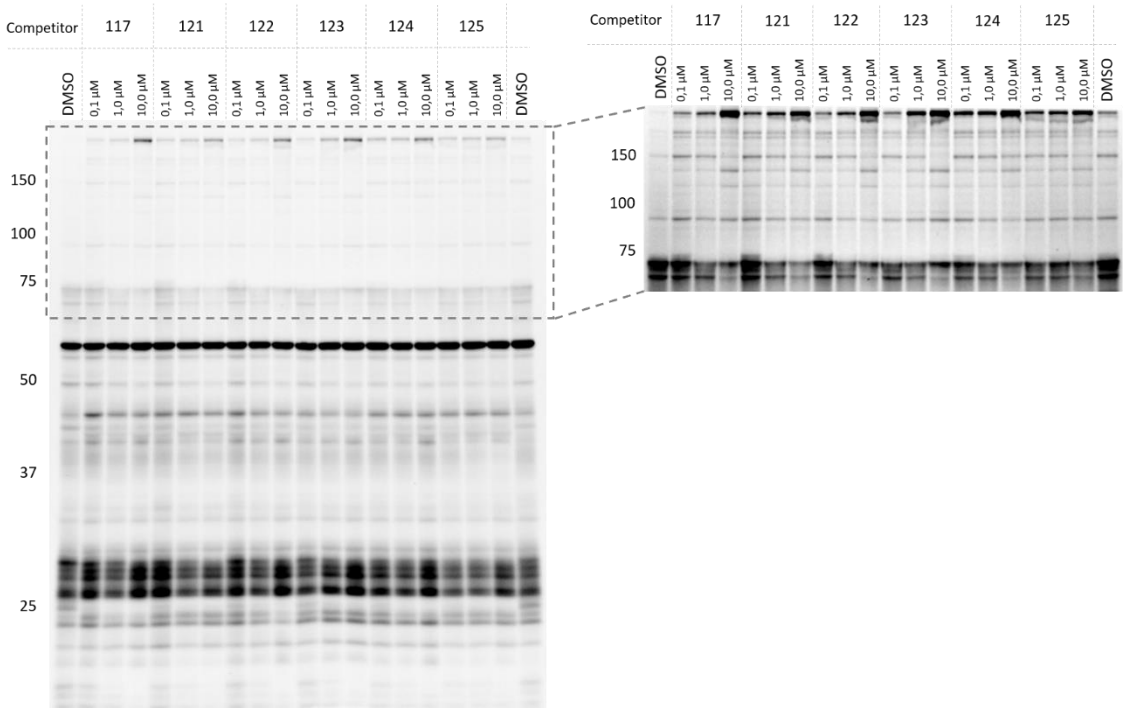

Figure 46 – Example of a competitive ABPP experiment for selected para-substituted 4-Oxo-β-Lactam compounds (**117**, **121**, **122**, **123**, **124**, **125**) compounds in U937 whole cell lysates against FP-Rhodamine (1 µM). The region between 75 and 150 kDa is reproduced on the right with higher contrast.

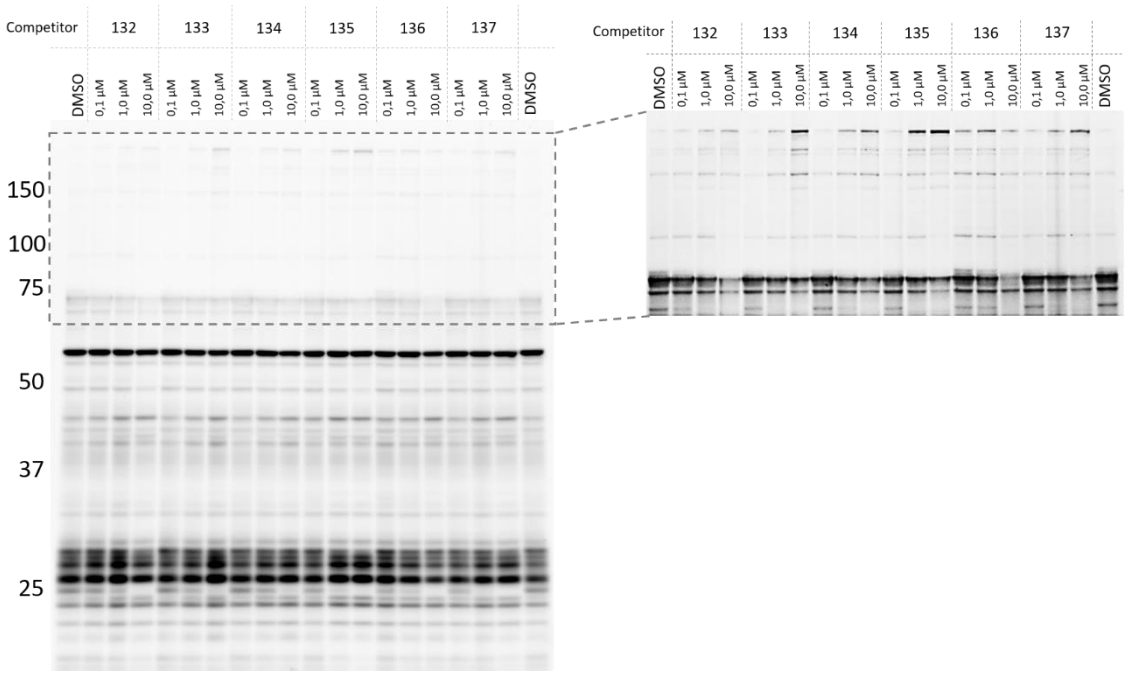

Figure 47 – Example of a competitive ABPP experiments for selected para-substituted 4-Oxo-β-Lactam compounds (**132**, **133**, **134**, **135**, **136**, **137**) compounds in U937 whole cell lysates against FP-Rhodamine (1 µM). The region between 75 and 150 kDa is reproduced on the right with higher contrast.

These gels offer a preliminary glimpse into the reactivity of our compounds, showing a surprisingly selective profile of inhibition, in some cases also with good potency. The para-substituted compounds show very efficient labeling of a protein at 25 kDa, which can potentially be HNE or PR3. Some of the meta-substituted compounds also inhibit this band, but with less potency. The area between 75 kDa and 150 kDa, where most DPP family members fall is difficult to observe but seems to suggest there is more efficient inhibition of these enzymes by the meta-substituted compounds, with compounds **132** and **135** showing inhibition of a band at 100 kDa, which could potentially be either DPP8 or DPP9. Overall, the results seem to be hindered by the lack of resolution in the ~30kDa section, where a lot of proteins overlap, and by different expression of some proteins, which occlude other proteins in regions of high density of FP labeling. For these reasons, the results were repeated using fractioned cell lysates, with separated soluble and membrane fractions of proteins.

The inhibitors were incubated with membrane and soluble lysate fractions of U937 cells for 30 minutes at 3 different concentrations, 0.1 µM, 1 µM and 10 µM. After 30 minutes 1 µM of FP-Rhodamine was added. 30 minutes later the reaction was quenched with loading buffer and the mixture was analyzed by SDS-PAGE. Compound reactions were compared against a control sample pre-incubated with DMSO for 30 minutes and then FP-Rhodamine. The gel of fractioned lysates offers a much more readable profile of protein labeling profile than before. The gels for selected compounds are presented below (figure 48). The full results for the entire 4-Oxo-β-Lactam library are presented in the attachments.

The results suggest that the compounds are potent and selective inhibitors of a selected group of serine hydrolases. A band at approximately 25 kDa in the membrane fraction (potentially HNE) is strongly inhibited by several compounds, even at low concentrations of 100 nM. Bands at approximately 100 kDa in the soluble fraction (likely to be DPP8, DPP9 and/or FAP) seem to be strongly inhibited by some compounds. Bands lower than 25 kDa in the soluble fraction also show some inhibition (probable LYPLA1 and LYPLA2).
Other bands which are harder to identify with confidence also show inhibition when compared with the DMSO control. These identifications are suggested by a combination of previous knowledge of the expected targets of 4-Oxo-β-Lactams and known labeling patterns of FP-probes. The results will be confirmed by additional LC-MS/MS assays.

A significant number of bands seems to increase when compared to the DMSO control. This can be explained by inhibition of serine proteases, which leads to an increase in their substrates, suggesting the increasing bands are potential proteins that are usually cleaved by serine hydrolases that inhibited by the 4-Oxo-β-Lactams.

Overall the results suggest that para-substituted compounds show a remarkably potent inhibition of the band at 25 kDa in the membrane fraction, while the meta-substituted compounds seem to have a much higher potency against the bands around 100 kDa in the soluble fraction, with some compounds, like **135**, showing significant inhibition at 100 nM and complete inhibition at the two higher concentrations. This suggests potential SAR dynamics involving positioning of the substituents in the aromatic ring attached to the 4-Oxo-β-Lactam core. This had previously been suggested in our work with HNE inhibition, where compounds with substituents at the para-position showed higher potency.[272]

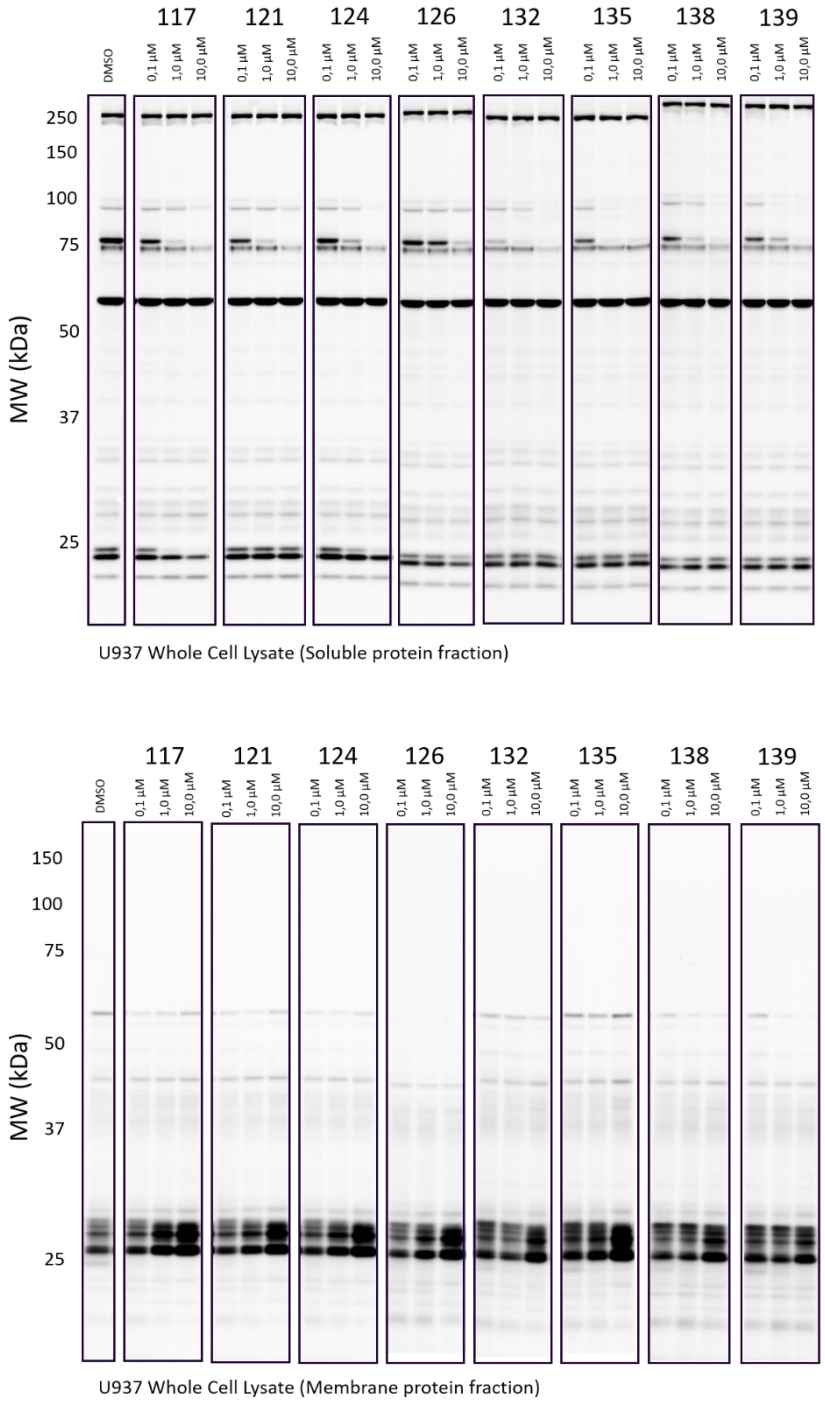

Figure 48 – Competitive ABPP gels with soluble and membrane fractions of U937 cells for selected compounds. Disappearance of a band when compared with DMSO control indicates that band is a target of the compound. Clear inhibition of some targets is observed. Analysis of the molecular weights seems to suggest that the compounds are inhibitors of DPP8 and/or DPP9 (soluble fraction, ~100 kDa), PREP (soluble fraction, ~75 kDa) and HNE (membrane fraction, ~25 kDa).

Ortho-substituted compounds showed almost no blocking of relevant FP-labeled bands and were not presented here, with only some minor bands being partially inhibited at the highest concentration of 4-Oxo-β-Lactam compound (data not shown, complete results are presented in the attachments).

The data presented above was obtained when the compounds were tested in U937 whole cell lysates. To evaluate the capacity of selected compounds to cross the cell membrane and inhibit serine hydrolases as in whole cell lysates we performed a competitive ABPP assay in whole U937 cells. Briefly, U937 cells were diluted to 1 million cells/mL in serum-free media and incubated with selected compounds of the 4-Oxo-β-Lactam library at 1 and 10 μM of concentration. DMSO controls were also performed. The mixtures were incubated at 37°C for one hour. The reactions were stopped by centrifugation, removal of media and PBS wash, followed by resuspension and lysis in PBS. Protein content was normalized to 1 mg/mL and the samples were labeled with FP-Rhodamine. The results are shown in figure 49.

The gel profiles suggest that 4-Oxo-β-Lactam compounds are able to cross the cell membrane in general. This is suggested by the different FP labeling profiles observed when compared with the DMSO control for nearly all compounds at different points in the gels. Some particular bands that were identified in the whole cell lysate assays seem to also be inhibited in these assays, including the band at approximately 25 kDa for compounds **117**, **121** and **126**, for example, and the bands at 75 and 100 kDa for several compounds. Interestingly, multiple bands that are not visible in the DMSO-treated sample are being strongly stained by FP in compound-treated samples, particularly, bands above 150 kDa, which are visible in samples treated with compounds **117**, **122**, **123**, **126**, **128** and **135**. Additional bands present this pattern across the gel. This phenomenon might be the result of inhibition of serine proteases, with the proteins corresponding to bands of increased labeling being potential substrates of these enzymes. Overall, a significant change in the profile of serine hydrolase labeling by FP was observed, indicating that 4-Oxo-β-Lactams efficiently cross the cell membrane, in sufficient concentrations to cause changes in enzymatic behavior that are visible by SDS-PAGE.

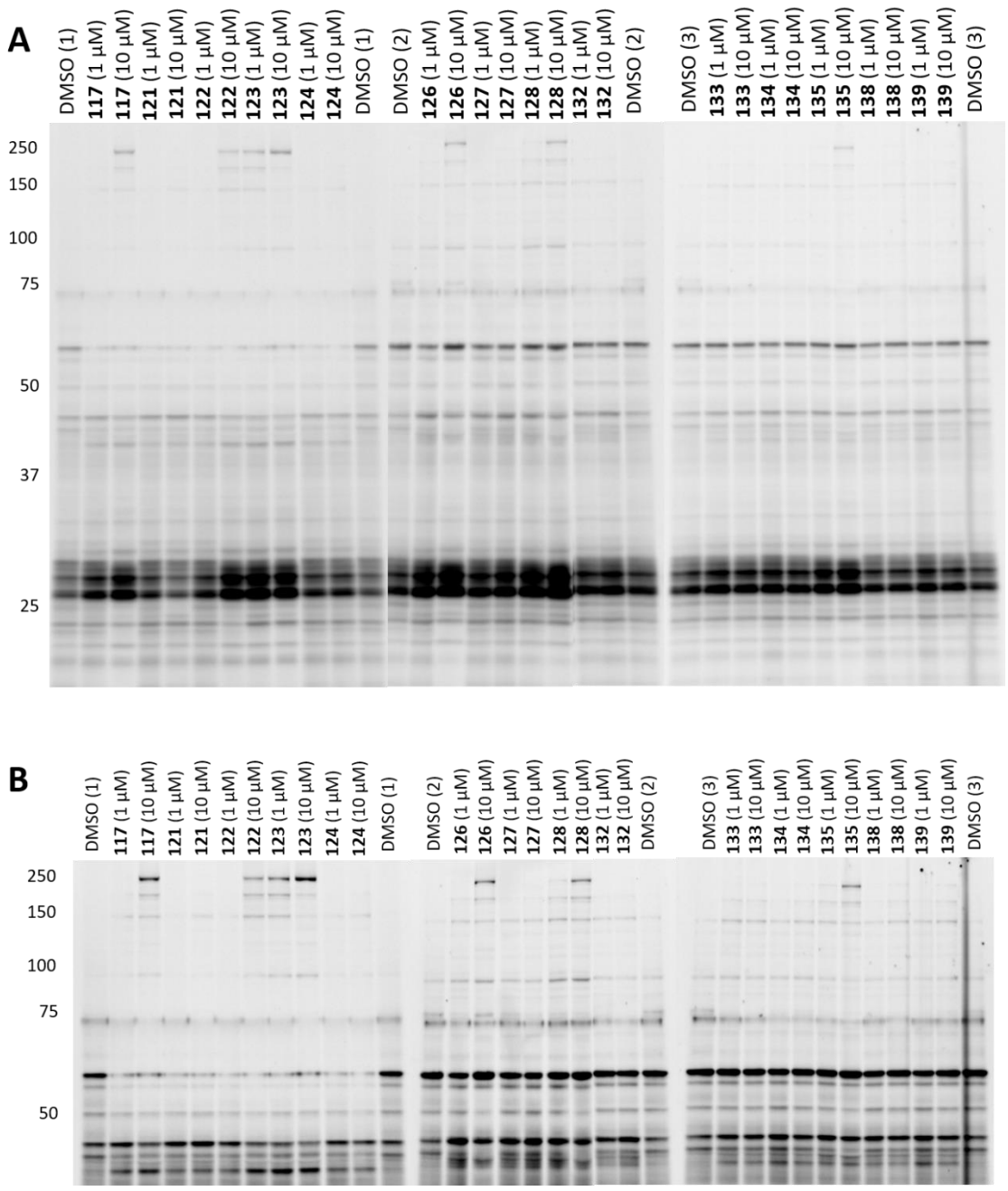

Figure 49 – Competitive ABPP in U937 whole cells using selected compounds from the 4-Oxo-β-Lactam library. The full gels are shown in A. A cropped version with higher contrast to emphasize lower abundance proteins is shown in B.

3.5. Competitive ABPP-MudPIT

The gel-based assays showed us that the compounds have a selective profile of targets within the pool of FP-labeled proteins. The identification of these proteins cannot be made with complete confidence based solely on gel data since proteins with similar molecular weight co-migrate in the gel. In our case, inhibition of HNE could be mistaken with inhibition of PPE. Other enzymes like DPP8, DPP9 and FAP also have similar molecular weights. Mass-spectrometry-based techniques can be applied to confidently identify the

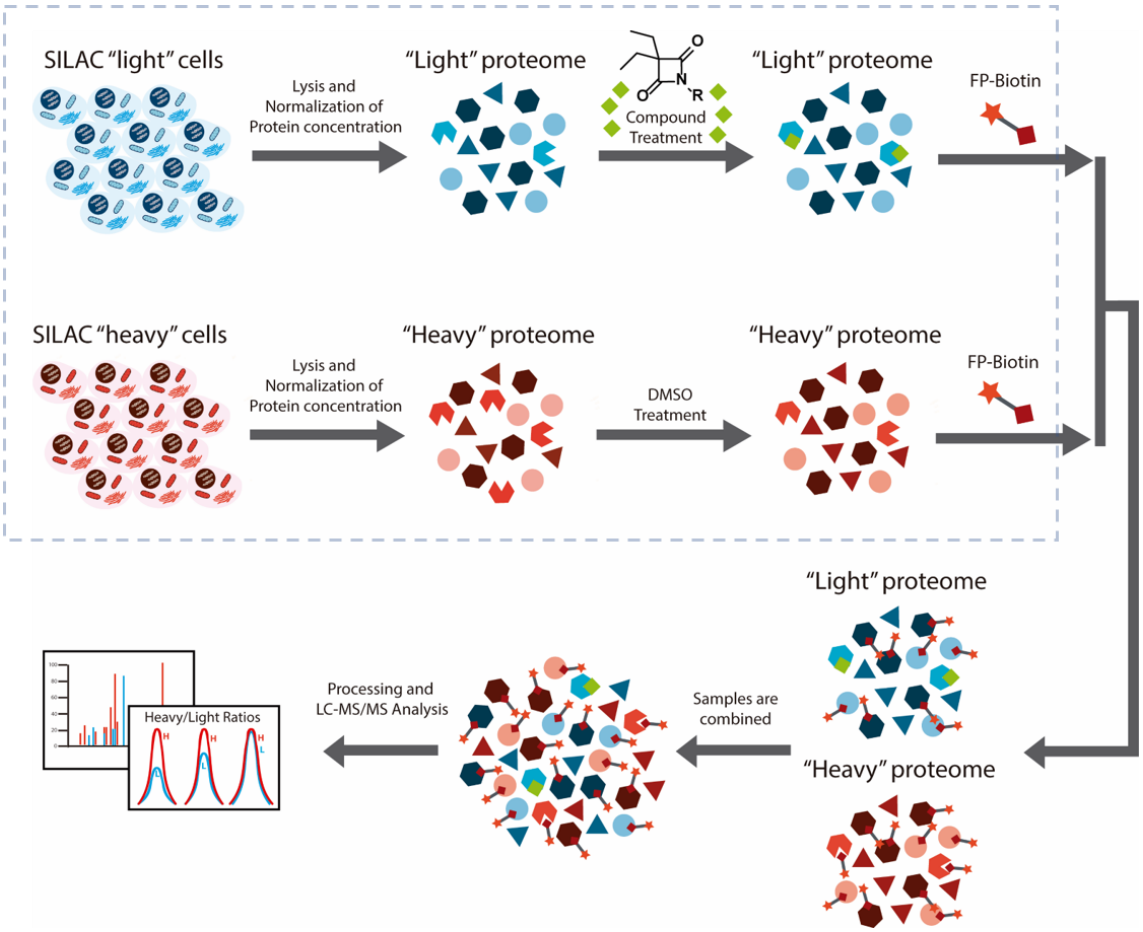

Figure 50 – Overview of a competitive SILAC-ABPP-MudPIT Protocol for 4-Oxo-β-Lactam compounds. The proteomes of SILAC "light" cells and SILAC "heavy" cells are incubated with either 4-Oxo-β-Lactam compound or DMSO. Both samples are then treated with FP-Biotin to label the serine hydrolases that are not inhibited by the 4-Oxo-β-Lactam compound. The reaction is quenched, the samples are combined and processed for LC-MS/MS analysis. Determination of heavy/light ratios gives the IDs of serine hydrolases inhibited by the 4-Oxo-β-Lactam compound.

targets of our compounds, either by extracting bands from gels or simply by analyzing the full proteome via LC-MS/MS. In this work we took the second approach, adapted to a competitive ABPP protocol.

Based on the competitive ABPP gel profile, six compounds were selected for analysis by competitive ABPP-MudPIT, including three para-substituted compounds, **117**, **124** and **126**, and three meta-substituted compounds, **135**, **138** and **139**. SILAC U937 cells were employed; heavy cells were treated with DMSO while light cells were treated with selected compounds at 10 µM concentration for 30 minutes. After this, 5 µM of FP-biotin was added to each sample and incubation was done at room temperature for 1h. Samples were combined and enriched with streptavidin beads for 2.5h, followed by overnight trypsinization. Samples were run in duplicate on an LC-MS/MS experiment and heavy/light ratios were determined (figure 50). The results are presented in figure 51.

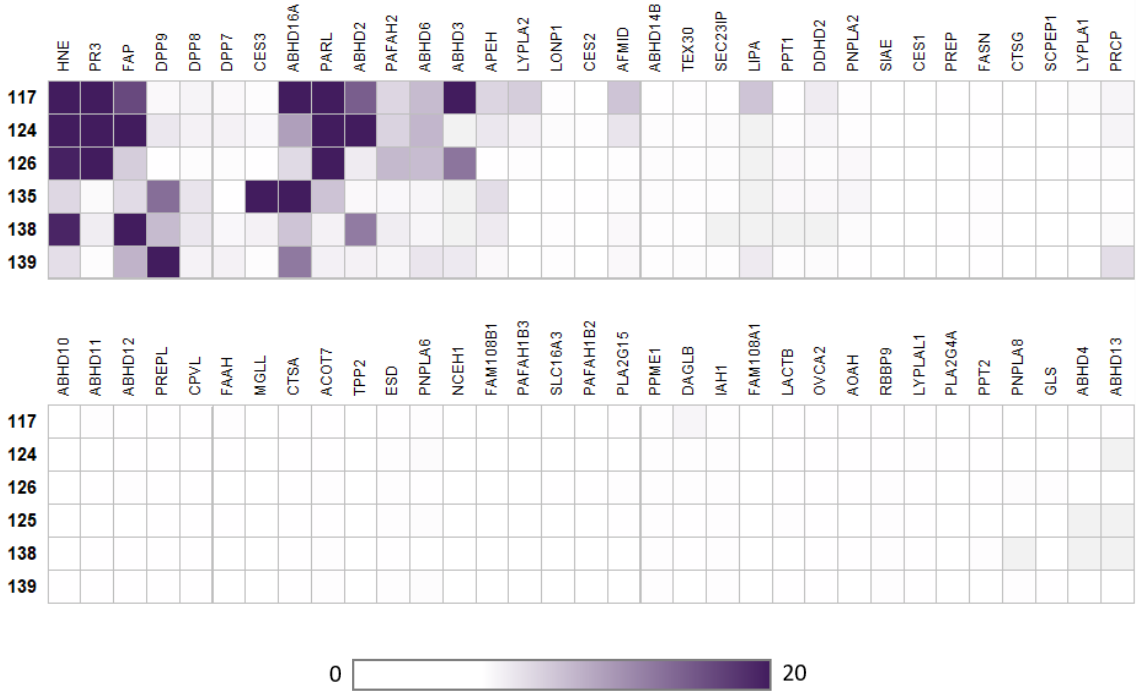

Figure 51 – Competitive ABPP-MudPIT experiments for selected compounds of the 4-Oxo-β-Lactam library. Heavy/light ratios are presented. Values higher than 3 are considered a hit. The results were filtered for serine hydrolases (n = 2).

The results of the mass-spectrometry-based competitive ABPP support the results of the gel-based assays by presenting a relatively selective target profile for all the tested compounds. Meta-substituted compounds seem to be more selective than para-substituted compounds. HNE and PR3 showed maximum ratios for all para-substituted compounds. Meta-substituted compounds, especially compound **138**, show efficient inhibition of HNE and no hit for PR3, suggesting the meta-substitution pattern in the aromatic ring could be exploited to selectively target HNE and not PR3. The DPP family seems to not be significantly inhibited by compounds **117**, **124** and **126**, with the exception of FAP. Meta-substituted compounds inhibit FAP and DPP9, while DPP8 returned minimal ratios to be considered a hit for compounds **138** and **139**. This could suggest some degree of selectivity between DPP9 and DPP8, a desirable characteristic, since there are currently no known selective inhibitors for either of these enzymes. The ABHD family of enzymes is represented by 4 members. All compounds seem to hit ABHD16A and para-substituted compounds hit ABHD6 and ABHD3, while ABHD2 is hit by compounds **117**, **124** and **138**. PARL was hit by all para-substituted compounds with maximum ratio and, to a lesser extent, by compound **135**. Additional hits include CES3 by compound **135**, PAFAH2 by all para-substituted compounds and APEH, LYPLA2, AFMID, LIPA and DDHD2 are all hit by compound **117**.

Following these results, we performed target validation for selected enzymes identified in the competitive mass spectrometry assays, namely HNE, DPP8, DPP9, FAP, ABHD6, DPP4, DPP7, ABHD2, LYPLA1, LYPLA2, ABHD16A, ABHD2, PAFAH2 and PREP.

3.6. Target Validation and IC_{50} calculation

Following the mass spectrometry experiments it is necessary to validate the main proteins identified in the assays as targets of the 4-Oxo-β-Lactam compounds. For this purpose, a competitive ABPP protocol was employed with overexpressed serine hydrolases and IC_{50}s for selected compound-target pairs were developed.

Given the extensive work of the Cravatt Lab with Serine Hydrolases, a library containing plasmid genes in cloning vectors for most of the existing serine hydrolases was readily

available. We overexpressed selected targets of interest to test the compounds and calculate IC_{50}s, including DPP4, DPP7, DPP8, DPP9, FAP, PREP, ABHD2, ABHD3, ABHD6, ABHD16A, SCPEP, CES1, HNE, LYPLA1, LYPLA2, APEH and PAFAH2. Overexpression of METTL7A was used a as mock transfection.

Briefly, the plasmid DNA for each serine hydrolase was transformed into E. coli for amplification and the DNA was obtained using an appropriate DNA extraction miniprep kit. The plasmid DNA was transiently transfected into HEK293T cells using polyethyleneimine (PEI) as the transfection agent (figure 52).[286] The cells were incubated for approximately 48h, after which they were collected and lysed. The protein concentration was normalized to 1 mg/mL. Appropriate overexpression of the serine hydrolases was confirmed by FP-rhodamine labeling (figure 53) and by western blotting using an anti-FLAG tag antibody for selected enzymes.

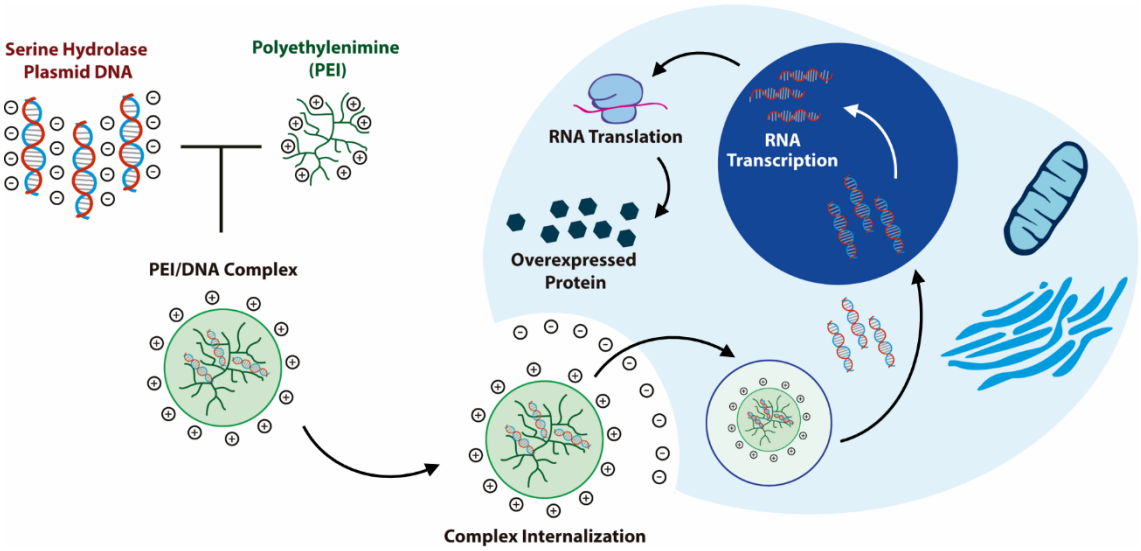

Figure 52 – Overexpression of Serine Hydrolases via PEI-mediated transient transfection of plasmid DNA containing a selected serine hydrolase gene. The PEI/DNA complex is internalized, and the DNA is released in the cell. Transcription of the DNA into mRNA and then mRNA translation leads to the overexpression of the desired serine hydrolase.

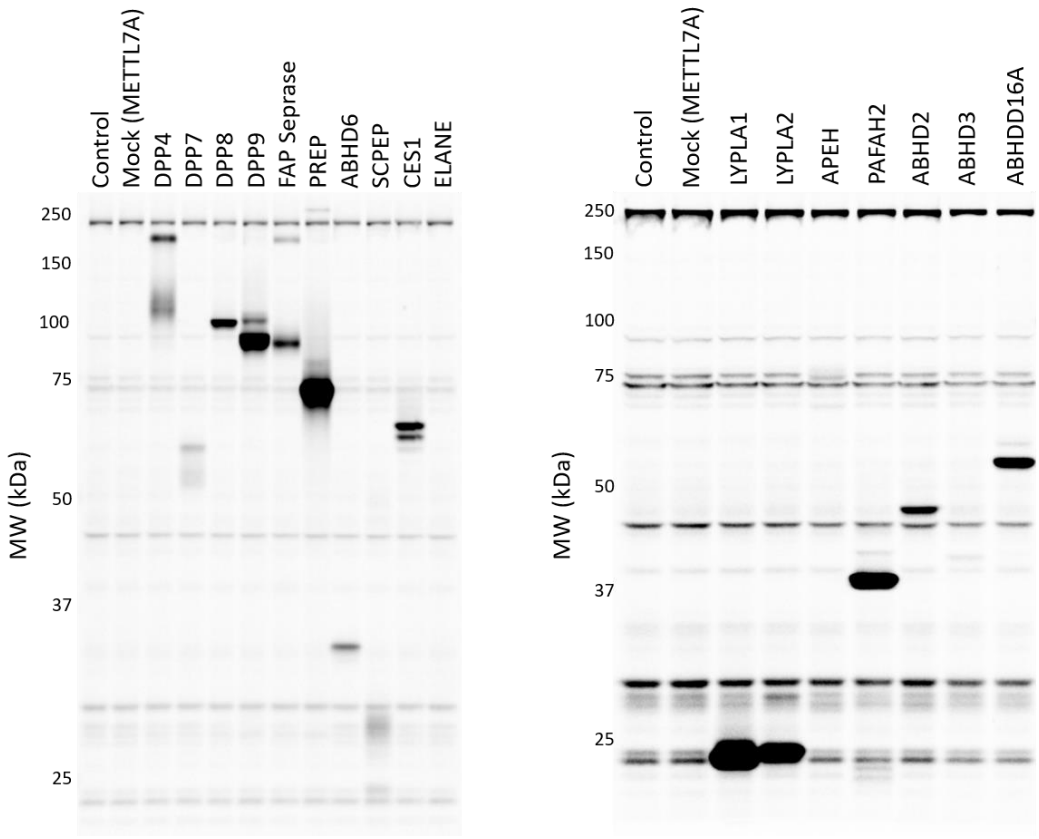

Figure 53 – Overexpression of selected serine hydrolases and labeling by FP-Rhodamine.

Most of the overexpressed serine hydrolases resulted in clear overexpression of the protein, which was confirmed by labeling with FP-Rhodamine. HNE overexpression did not result in the active protease being overexpressed. A western blot analysis using an anti-FLAG tag primary antibody (all overexpressed proteins contained the FLAG tag) confirmed that the protein was overexpressed, but in the inactive form (figure 54). Additionally, APEH and ABHD3 seem to not have been efficiently overexpressed in our assay.

We decided to test the possibility of measuring HNE in the proteome of U937 cells. This cell line was originally chosen due to its native expression of HNE. For this purpose, a western blot analysis was done with an anti-HNE antibody to investigate where HNE located in fractioned U937 cell lysates (figure 55). HNE was only identified in the membrane fraction of U937 lysates. HNE is described to associate with cell membrane receptors upon externalization by HNE-producing cells.[140,142,287]

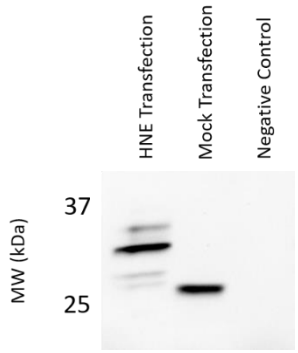

Figure 54 – Western blot of overexpressed HNE using an anti-FLAG antibody. The Mock used was overexpressed METTL7A.

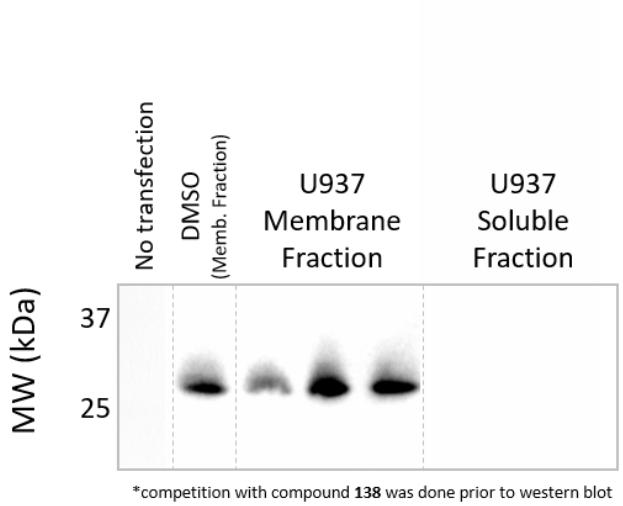

Figure 55 – Western blot of HNE in U937 membrane and soluble fractions using an anti-HNE antibody. The fractioned samples are presented in triplicate.

A preliminary inhibition test with the overexpressed serine hydrolases was done using compounds **117** (para-substituted) and **135** (meta-substituted) to help determine the adequate concentration ranges for the following studies. A range of compound concentrations between 50 nM and 50 µM was tested for a series of overexpressed serine hydrolases. After pre-incubation with the compounds for 30 minutes FP-Rhodamine was used to label the proteins. The results are presented in figure 56.

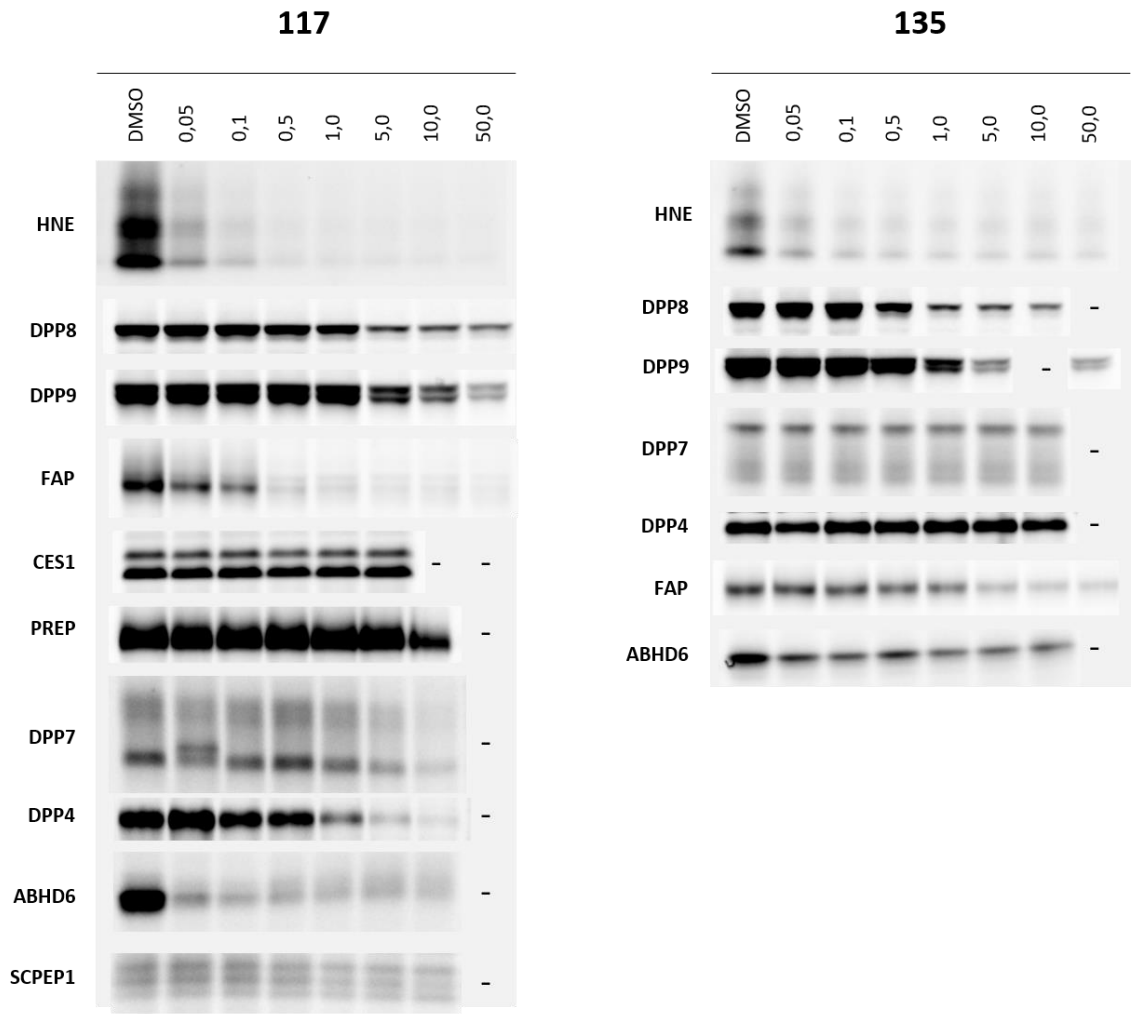

Figure 56 – Preliminary testing of the inhibition of selected serine hydrolases by compounds **117** and **135**.

Selected compound-target pairs were tested for IC_{50} determination by competitive ABPP. Compounds were incubated with whole cell lysate proteomes of HEK293T cells with the individually overexpressed serine hydrolases. HNE was tested in the U937 cell line. Increasing concentrations of compound were incubated with the proteomes for 30 minutes and then labeled with FP-Rhodamine. The samples were run in SDS-PAGE experiments and band intensity of the selected targets was quantified using appropriate software. All samples were run in at least triplicates. In select cases additional experiments were performed to cover a wider range of concentrations. The results were plotted as log [4-Oxo-β-Lactam inhibitor] vs. normalized response and IC_{50}s were

calculated. Selected examples are presented in figure 57 (the complete results are presented in the attchments).

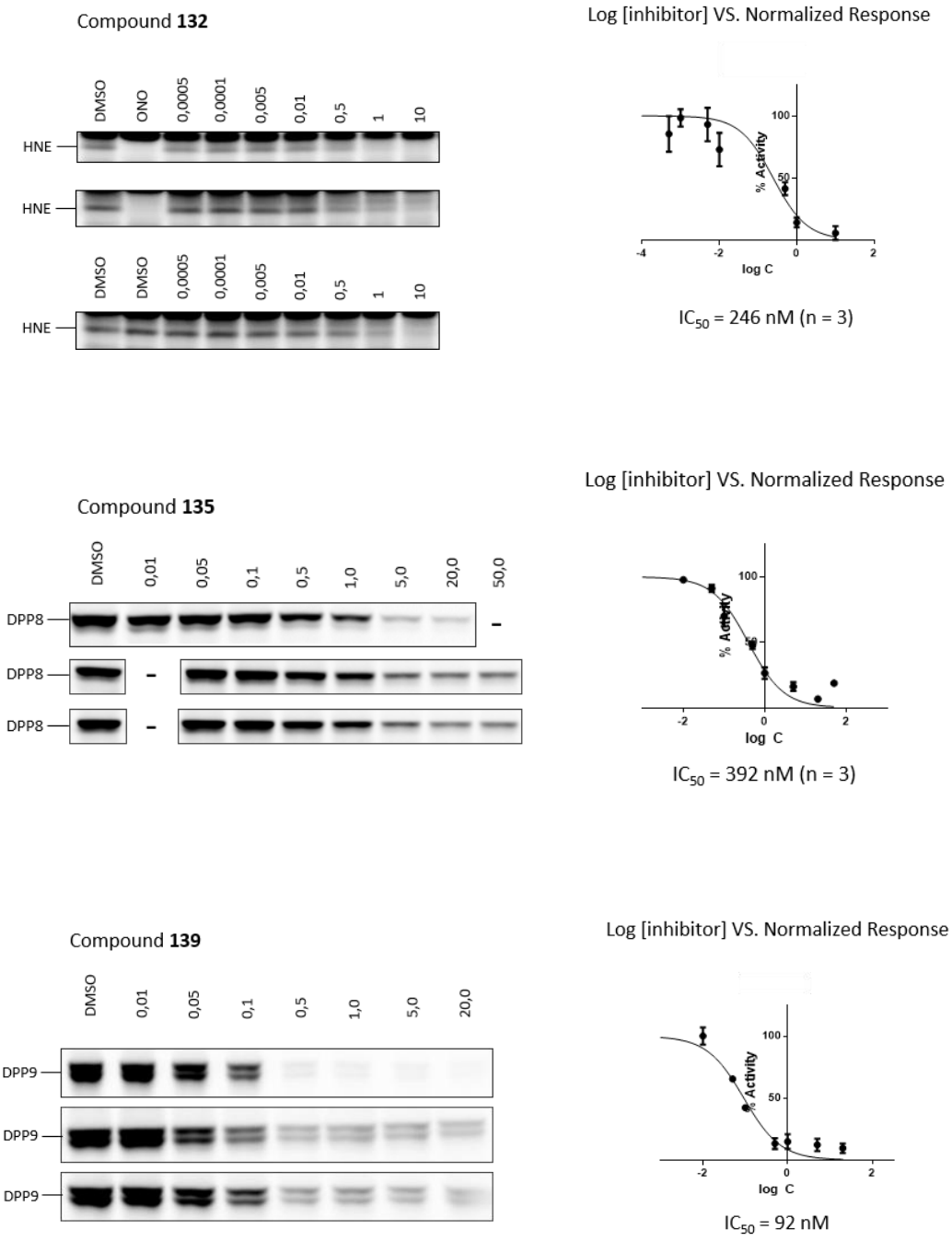

Figure 57 – Examples of determination of the IC_{50} for selected compound-protein pairs: **132**-HNE; **135**-DPP8; **139**-DPP9. FP-labeling blocking is analyzed by SDS-PAGE and gel band intensity is quantified and plotted, allowing the IC_{50} to be calculated from the graphical projection of the remaining enzymatic activity against the logarithm of the inhibitor concentration.

For some serine hydrolases that were not our main interest of study, a preliminary test of inhibition was done where the overexpressed serine hydrolases were incubated with the compounds at 1 µM concentration (figure 58). If inhibition at this concentration was significant, further assays were performed in a range of concentrations. Significant inhibition was only observed for ABHD2 with compounds **117**, **124**, **132**, **138** and **139**, with visible competition of FP-Rhodamine labeling. Additional tests were done for compounds **124**, **132** and **139**, which showed the best ABHD2 inhibition. A summary of the calculated IC_{50}s is presented in table 3.

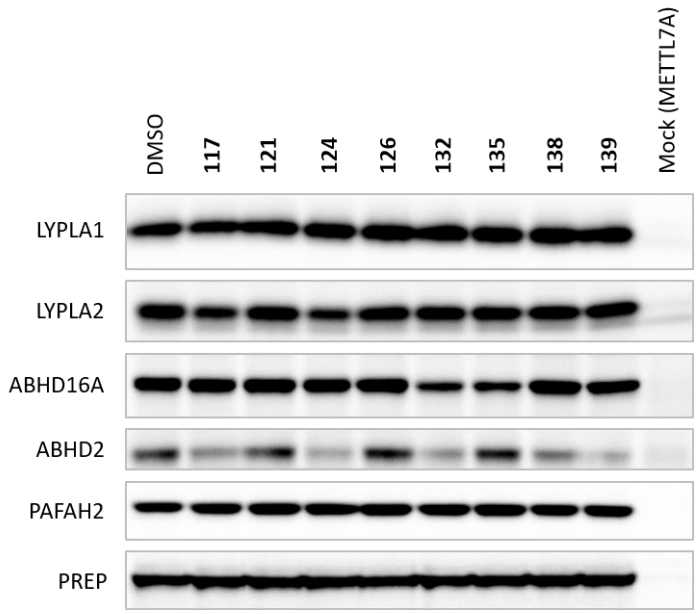

Figure 58 – Preliminary testing for selected serine hydrolase-compound pairs at 1 µM concentration.

Table 3 – Summary of the IC_{50} values determined by competitive ABPP for the tested compound-target pairs.

	117	**121**	**124**	**126**	**132**	**135**	**138**	**139**
HNE	29	6	19	226	246	553	25	483
DPP8	1140	-	404	-	137	392	292	34
DPP9	5171	-	603	-	409	950	1033	92
FAP	219	680	652	2755	147	-	> 10000	-
ABHD6	7	-	253	-	> 10000	320	> 10000	44
DPP4	3446	-	646	-	1398	1182	2699	47
DPP7	> 10000	-	> 10000	-	> 10000	> 10000	> 10000	> 10000
ABHD2	-	-	529	762	-	-	-	740

The results revealed significant differences between the para-substituted compounds, **117**, **121**, **124** and **126**, and the meta-substituted compounds, **132**, **135**, **138** and **139**. All compounds showed sub-micromolar inhibition of HNE, with compounds **117**, **121**, **124** and **138** having an IC_{50} below 30 nM. Inhibition of DPP8 and DPP9 was also efficient and seems to be stronger for meta-substituted compounds, as suggested by the competitive gel-based assays. Compound **139** is especially potent, having IC_{50}s of 34 and 92 for DPP8 and DPP9, respectively. This compound also strongly inhibits DPP4, while most other tested compounds show micromolar inhibition. FAP is overall efficiently inhibited, at varying levels across the tested compounds, with the best IC_{50} corresponding to compound **132**. ABHD6 is very efficiently inhibited at low nanomolar values by compounds **117** and **139**, but with no significant inhibition by some meta-substituted compounds like **132** and **138**. ABH2 showed efficient sub-micromolar inhibition by all three tested compounds. DPP7 was not efficiently inhibited by any of the tested compounds, reflecting the significantly different structure when compared with DPP4, DPP8 and DPP9.[288] Despite not being completely comparable, the results for DPP8 and DPP9 show an interesting pattern, with a generally stronger inhibition of DPP8. These two enzymes share significant similarity, which makes the development of selective inhibitors a difficult task. The apparent preference of 4-Oxo-β-Lactams for DPP8 could guide future SAR studies into the different requirements for DPP8 and DPP9 inhibition, being a promising result from our competitive ABPP studies.

Overall, it seems that compound selectivity can be slightly tuned between the DPP family and HNE/ABHD6, supporting the results that were previously obtained in the LC-MS/MS assays. Compounds with p-substituted N-aryl groups are generally more potent towards HNE and ABHD6, while compounds with m-substituted N-aryl groups are more potent towards DPP8 and DPP9. No ortho compounds were tested since they seem to not have relevant targets at the concentrations tested in competitive ABPP gels.

3.7. Development of a Clickable ABP

A Clickable 4-Oxo-β-Lactam, **151**, carrying a 3-diethyl substitution, an N-aryl group and an alkyne handle for CuAAC was synthesized using a 1-prop-2-ynylpiperazine. The synthesis followed the same path as the rest of the 4-Oxo-β-Lactam library, except for the

alkynylated piperazine building block, which was synthesized from Boc-piperazine and propargylamine and deprotected prior to the reaction with the 4-Oxo-β-Lactam bromide using TFA (scheme 19).

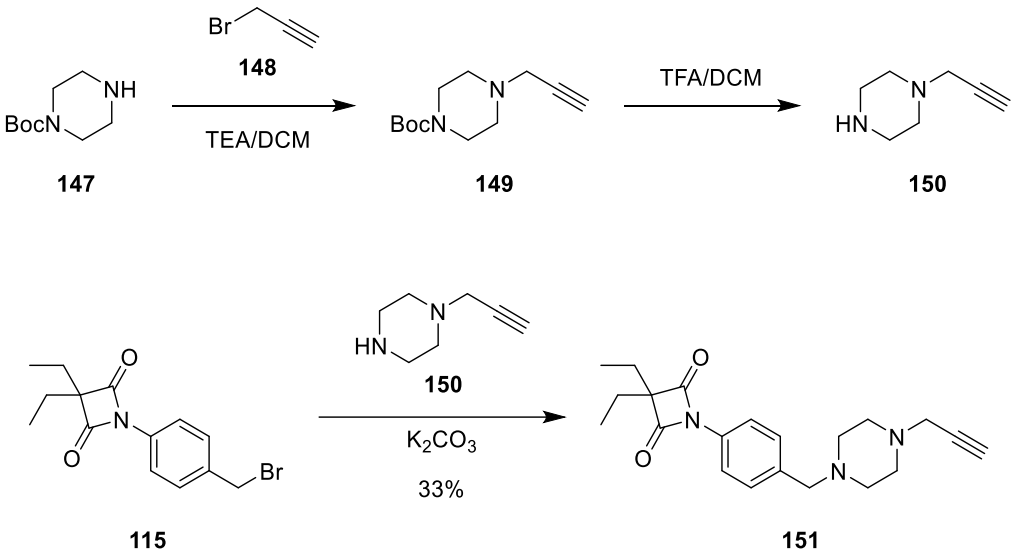

Scheme 19 – Synthesis of a clickable 4-Oxo-β-Lactam **151** using 1-prop-2-ynylpiperazine.

This potential ABP was tested in a competitive ABPP approach against FP-Rhodamine, showing a very selective labeling profile (figure 59 – A). The compound seems to be especially potent against a band at 25 kDa, which is potentially HNE, PR3, or both, showing almost complete supression of FP labeling even at the lowest tested concentration of 0.1 µM. Other than that, only an additional band at 75 kDa is visibly inhibited in the gel, which potentially corresponds to PREP. Labeling of the proteome by **151** was then tested by incubating the proteome with growing concentrations of the probe and clicking it with rhodamine-azide (figure 59 – B). The probe showed a selective labeling pattern up to 1.0 µM concentration, with only a few visible bands at approximately 25 kDa, once again potentially being HNE or PR3, with significant increase in background labeling for higher concentrations. This compound will be

valuable for future derivatization by click chemistry into other compounds and seems to be a potential new ABP for HNE if the identity of the band is confirmed.

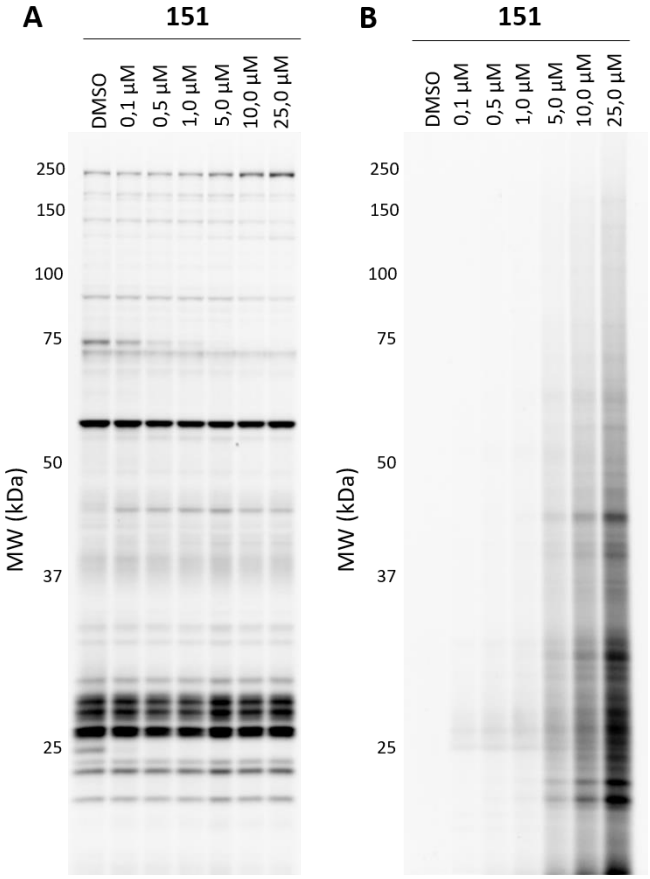

Figure 59 – Competitive ABPP experiment (A) and full proteome reactivity experiment (B) with the 4-Oxo-β-Lactam alkynylated probe **151**.

3.8. Overview

The application of 4-Oxo-β-Lactams in ABPP marks the first time that these compounds were tested with the end goal of establishing a comprehensive list of targets that can potentially be hit by the scaffold.

Starting with an alkynylated 4-Oxo-β-Lactam, the synthesis of ABPs was straightforward using CuAAC chemistry. The compounds showed a reasonably selective protein profile and the LC-MS/MS experiments revealed a surprisingly restricted list of targets that confirmed HNE as a target of the compounds, but also unveiled the potential of 4-Oxo-β-Lactams to inhibit enzymes from the DPP and the ABHD enzyme families, among others. Unlike the case for the 3-Oxo-β-Sultams, these targets were inhibited in high stoichiometry, making the 4-Oxo-β-Lactam warhead the optimal choice to pursue the development and application of ABPs in our project.

The identification of previously unreported 4-Oxo-β-Lactam targets led us to devise a new strategy devoted to the pursuit of selective inhibitors of these targets. A library of 4-Oxo-β-Lactam inhibitors was synthesized and evaluated using competitive ABPP techniques. The N-aryl 4-Oxo-β-Lactam compounds showed a selective profile of FP-target labeling blocking, which preliminarily suggested a good degree of selectivity for these compounds. Mass spectrometry based ABPP revealed that the compounds labeled the previously known targets HNE and PR3, but also hit enzymes from the ABHD and DPP families of serine hydrolases like ABHD6, DPP8, DPP9, DPP4, among other targets. Target validation using overexpressed serine hydrolases confirmed inhibition of these targets and revealed that inhibition of specific enzymes like HNE, DPP8 and DPP9 proceeds with low nanomolar range IC_{50}s, even when measured in the presence of a complete proteome.

The results concerning a few specific targets were also noteworthy, namely the inhibition of DPP8 and DPP9. The 4-Oxo-β-Lactam is a novel chemotype for DPP8 and DPP9 inhibition and is significantly different from previously identified chemotypes that target these enzymes. Additionally, there seems to be a preference for DPP8 inhibition, even though biochemical inhibition assays should be performed to confirm this data.

Our study of the 4-Oxo-β-Lactam warhead has some limitations. The work focused on the U937 cell line proteome, chosen due to its native production of active HNE, which we knew was a target of the 4-Oxo-β-Lactams, and for this reason, the identified proteins are limited to the pool of enzymes present in the U937 proteome. A more in-depth study should analyze additional cell lines. Additionally, our work focused mainly on using whole cell lysates, limiting our knowledge on the cell permeability of the compounds. Chemically, while a diverse group of substituents was appended to the N-aryl moiety, the substitution at the 3-position was kept constant with the diethyl group, potentially

introducing a bias towards enzymes like HNE and leaving one site of potential modification of the compound relatively unexplored in terms of chemical space.

These limitations of our work can be easily addressed in future studies with the 4-Oxo-β-Lactam warhead and even come as an exciting prospect of the additional engageable enzymatic entities that could potentially be addressed by this chemotype. Overall, we provided an unprecedented collection of information regarding the target profile of the 4-Oxo-β-Lactams which will be valuable to guide future inhibitor development and potentially aid in the development of ABPs for applications like biomarker discovery.

Chapter 4 – Pursuing DPP8 and DPP9 Inhibition using 4-Oxo-β-Lactams

DPP8 and DPP9 emerged as targets of the 4-Oxo-β-Lactam warhead during the mass spectrometry experiments we performed with 4-Oxo-β-Lactam ABPs. The competitive approach we then took with the library of N-aryl-4-Oxo-β-Lactams revealed that compounds with meta-substitution in the aromatic ring seem to be particularly suited for DPP8 and DPP9 inhibition. Furthermore, our target validation with overexpressed enzymes suggested that there might be a slight preference for DPP8 inhibition when compared with DPP9, an exciting result since the pursuit of selective DPP8 or DPP9 inhibition is a current area of great interest. There are currently no selective inhibitors for either of these enzymes, despite many efforts to optimize known dual DPP8 and DPP9 selective inhibitors. For these reasons we sought to pursue the inhibition of DPP8 and DPP9 using 4-Oxo-β-Lactams.

4.1. Comparison with known DPP8/DPP9 Inhibitors

The inhibition of DPP8 and DPP9 by structures similar to the 4-Oxo-β-Lactams is, to the best of our knowledge, unprecedented. To compare 4-Oxo-β-Lactams with other known DPP8 and DPP9 structures we analyzed the structural similarity of compound 91 to known DPP8 and DPP9 inhibitors described in ChEMBL v24. To that end, a list of inhibitors was collected and curated, excluding weakly active compounds, whose annotation is potentially skewed by colloidal aggregation.[289] Using the ECFP4-like Morgan fingerprint (radius 2, 2048 bits), we obtained an average Tanimoto index < 0.11 when comparing compound **139** to known ligands of DPP8 and DPP9. In any case had the nearest neighbor a Tanimoto similarity higher than 0.161. For ligands with high similarity, the Tanimoto index approaches 1, whereas if the ligands are substantially different the result is close to 0. Taken together, our data corroborates the 4-Oxo-β-Lactam chemotype as a novel chemotype in DPP inhibitor chemical space. Moreover,

compound **139** also displays an unusual topological pharmacophore feature arrangement, as it does not cluster with DPP8 and DPP9 ligands (figure 60).

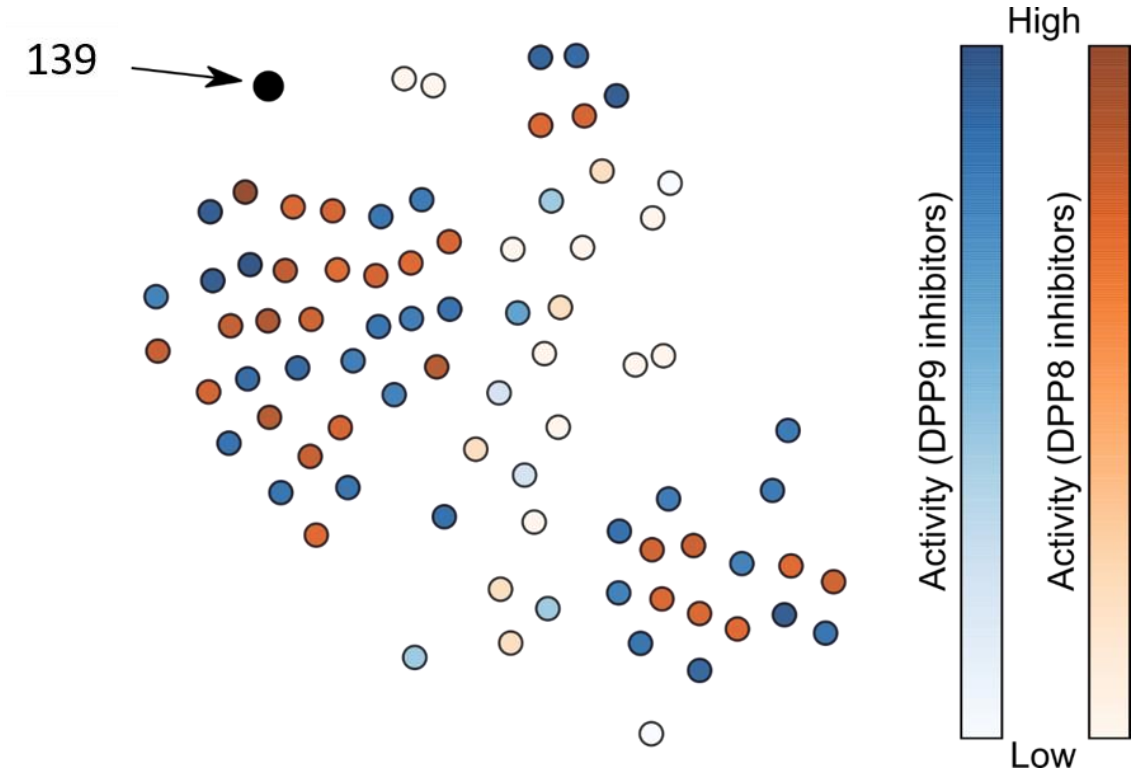

Figure 60 – Projection (t-distributed stochastic neighborhood embedding) of topological pharmacophore descriptor (CATS2) space. Orange: DPP8 ligands; Blue: DPP9 ligands. Gradient depicts activity values for individual compounds. Data shows that compound **139** (black dot) presents an unusual pattern among DDP8 and DPP9 ligands.

4.2. Pyroptosis Induction

The potential of 4-Oxo-β-Lactams to induce pyroptosis was pursued in collaboration with the Bachovchin lab. In a preliminary experiment, a cell viability assay (CellTiter-Glo) was performed with a DPP8/9 inhibitor sensitive AML cell line, MV4;11. CellTiter-Glo measures cell viability by measuring cellular ATP concentrations in the sample. Therefore, cell death results in a decrease in the levels of ATP in the well and a lower CellTiter-Glo signal. The cells were treated with the known DPP8/DPP9 inhibitor Val-

BoroPro as control and 4-Oxo-β-Lactam compounds for 24 h with a top dose of 20 µM. The results are presented in table 4 and figure 61.

Table 4 – Pyroptosys IC_{50}s for selected 4-Oxo-β-Lactam compounds in the AML cell line, MV4;11.

Val-BoroPro	**117**	**123**	**124**	**126**	**127**	**132**	**134**	**135**	**138**	**139**
0,001643	3.895	2.003	1.315	0.957	11,93	5,408	3.013	1.188	1.178	0.7504

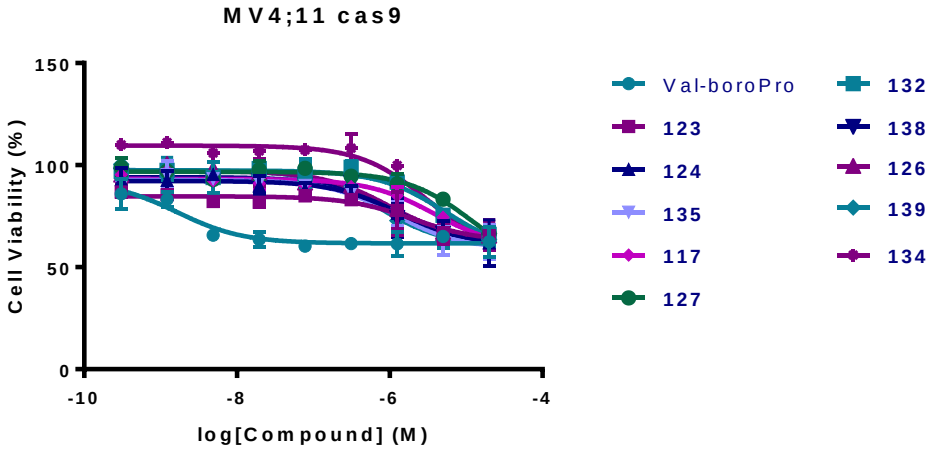

Figure 61 – Graphical representation of the cell viability assay performed for selected 4-Oxo-β-Lactam compounds.

The results showed general micromolar IC_{50}s for pyroptosis for our compounds when compared with the control Val-BoroPro, which showed an IC_{50} of 1 nM. The best compound, **139**, has an IC_{50} of 0,750 µM. This compound showed the best inhibition of DPP8 and DPP9 in the previously described competitive ABPP assays, supporting these results and suggesting that DPP8 and DPP9 inhibition is the process responsible for induction of cell death.

Overall, the results showed an effect in cell viability upon incubation with the 4-Oxo-β-Lactam compounds. This assay has been previously used as a measure of DPP8/DPP9 inhibition-dependent cell death induction by pyroptosis and seems to agree with previous values of DPP8 and DPP9 inhibition for our compounds. Furthermore, these results

support that 4-Oxo-β-Lactam compounds cross the cell membrane and are able to exert their effects in the intracellular environment.

4.3. Kinetic assays and co-crystallization of DPP8 and DPP9 with Selected 4-Oxo-β-Lactam Inhibitors

The crystallographic structures of DPP8 and DPP9 were only recently published.[210] In collaboration with the Huber Lab, which was responsible for this impactful publication in the field of DPP8 and DPP9 inhibition, selected 4-Oxo-β-Lactam compounds were tested in biochemical assays against DPP8 and DPP9 (table 5). These results confirmed the potent inhibition of DPP8 and DPP9 verified by competitive ABPP (see chapter III) and generally agree with the IC_{50}s found in those experiments. With the exception of compound **132**, which shows more potent inhibition for DPP9, all compounds seem to more efficiently inhibit DPP8, with IC_{50} values under 100 nM. An outstanding result is the inhibition of these enzymes by compound **139**. This compound, which had previously resulted in the best IC_{50} values for DPP8 and DPP9 obtained in competitive ABPP, shows the best DPP9/DPP8 inhibition ratio, with approximately 20 times more potent inhibition of DPP8 than DPP9. As frequently mentioned throughout this report, the pursuit of selectivity of inhibition between these enzymes is a highly sought result, emphasizing the importance of these results.

Table 5 – Ki values for DPP8 and DPP9 inhibition by compounds **132**, **135**, **138** and **139** (cleavage of GP-AMC in the presence of inhibitors).

Compound	DPP8, Ki (nM)	DPP9, Ki (nM)
132	230.0	93.3
135	25.7	151.9
138	60.7	372.3
139	44.9	849.1

In addition to kinetic assays, co-crystallization experiments were performed between selected compound-target pairs. Successful co-crystallization was observed between compound **132** and DPP8. A preliminary high-resolution crystal is shown in figure 62.

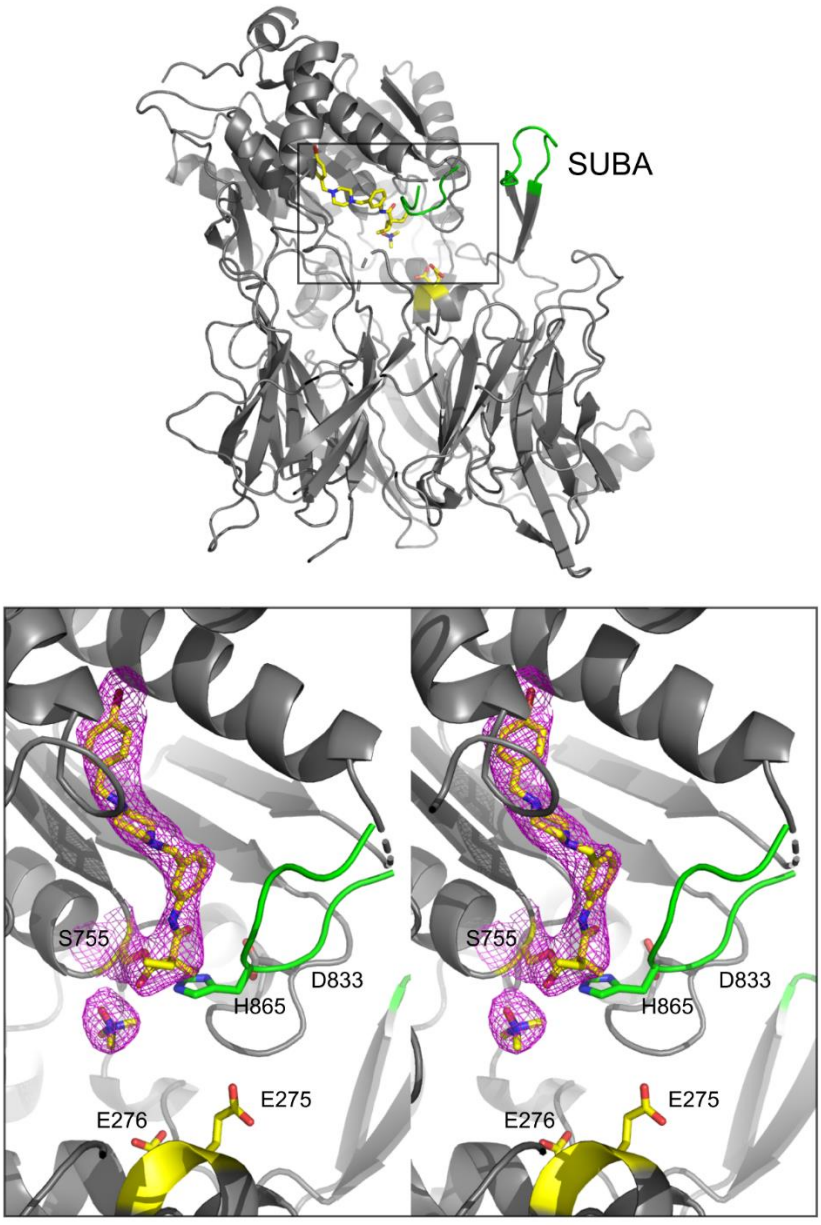

Figure 62 – Co-crystallization of compound **132** with DPP8, revealing a covalent reaction with the catalytic Ser755 and the extension of the inhibitor across a hydrophobic canyon, a novel binding site for extended ligands, different from previously described ligand-DPP8 interactions. Ligand binding induces disordering of structures (colored in green) which were essential for previously studied compounds.

This crystal structure unveiled surprising details regarding DPP8 inhibition by 4-Oxo-β-Lactams. Compound **132** seems to inhibit DPP8 via a different binding mode when compared with previously described inhibitors of DPP8 and DPP9. A covalent bond is clearly defined between the 4-Oxo-β-Lactam and the catalytic serine of DPP8. The inhibition is associated with disordering of the substrate binding site and the catalytic machinery (colored in green in Figure 62), a previously unknown inhibitory mechanism. Additionally, the S1 subsite does not seem to accommodate the diethyl moiety, as is the case for the inhibition of HNE. The distal part of compound 84, containing the piperazine and the 4-bromo benzyl group interacts with a hydrophobic canyon, a novel binding site for extended ligands, which was not used by previously studied inhibitors. Ongoing studies seem to suggest that binding of these compounds with DPP8 and DPP9 seems to exploit different features on each enzyme, an exciting breakthrough which could be crucial for future inhibitor development.

4.4. Overview

In this project we described, for the first time, that 4-Oxo-β-Lactam are inhibitors of enzymes of the DPP family. Following this exciting discovery, we demonstrated through similarity studies, that this warhead was indeed a new chemotype for DPP8 and DPP9 inhibition, with significant differences from previously known inhibitors of these enzymes.

The study of DPP8 and DPP9 inhibition showed that selected compounds from the library have an effect on pyroptosis induction.

The most important conclusion is, however, that 4-Oxo-β-Lactam compounds are able to achieve a level of selectivity between DPP8 and DPP9 inhibition that has been unfruitfully pursued for a long time with other chemotypes, with the exploiting of previously unrecognized binding sites in these enzymes, which will potentially have an important impact in future inhibitor development.

Chapter 5 – Outreaching Projects and Collaborations

In parallel to the main work developed during the PhD project, several side-projects were pursued, including collaborations with other research groups at iMed.ULisboa. These outreaching projects are described in this chapter, including the derivatization of 4-Oxo-β-Lactams with an N-O bond to generate suicide inhibitors, the development of 4-Oxo-β-Lactam on-off probes, the synthesis of peptidic vinyl sulfone ABPs for cysteine targeting and the development of a TUDCA fluorescent probe.

5.1. 4-Oxo-β-Lactams with N-O bond for suicide inhibitor development

The 4-Oxo-β-Lactam chemotype was developed into potential suicide inhibitors by incorporation of an N-O bond. The concept involves the use of the 4-Oxo-β-Lactam core as a warhead (scheme 20 – A) and adding a leaving group via a tosylated N-O bond that will allow the suicide inhibitor mechanism to occur, following a Lossen rearrangement.[290] Upon target engagement and opening of the 4-membered ring, a Lossen rearrangement expels the tosylated hydroxyl group and generates an isocyanate, a new electrophilic center which allows a second nucleophilic attack to render the enzyme irreversibly inhibited (scheme 20 – B).

To synthesize these compounds, we first need to obtain the corresponding malonic esters. Some esters are commercially available or directly available in the lab in large amounts. If not, they can be obtained from mono-substituted malonic esters or by introducing substituents in diethyl malonate. These reactions take advantage of the acidity of the malonic acid alpha protons. Once the malonic ester is ready the two ester groups are hydrolyzed using sodium hydroxide in ethanol to obtain the diacid. The diacid is converted into the diacyl chloride to allow cyclization into the 4-Oxo-β-Lactam by reacting with an appropriate amine. To introduce the N-O bond we used O-benzylhydroxylamine (scheme 21 – A) as the amine for cyclization. The protecting benzyl group from the hydroxylamine is removed by hydrogenation using triethylsilane with

palladium on activated charcoal and the free hydroxyl is protected with a tosyl group, resulting in the final compounds (scheme 21 – B).

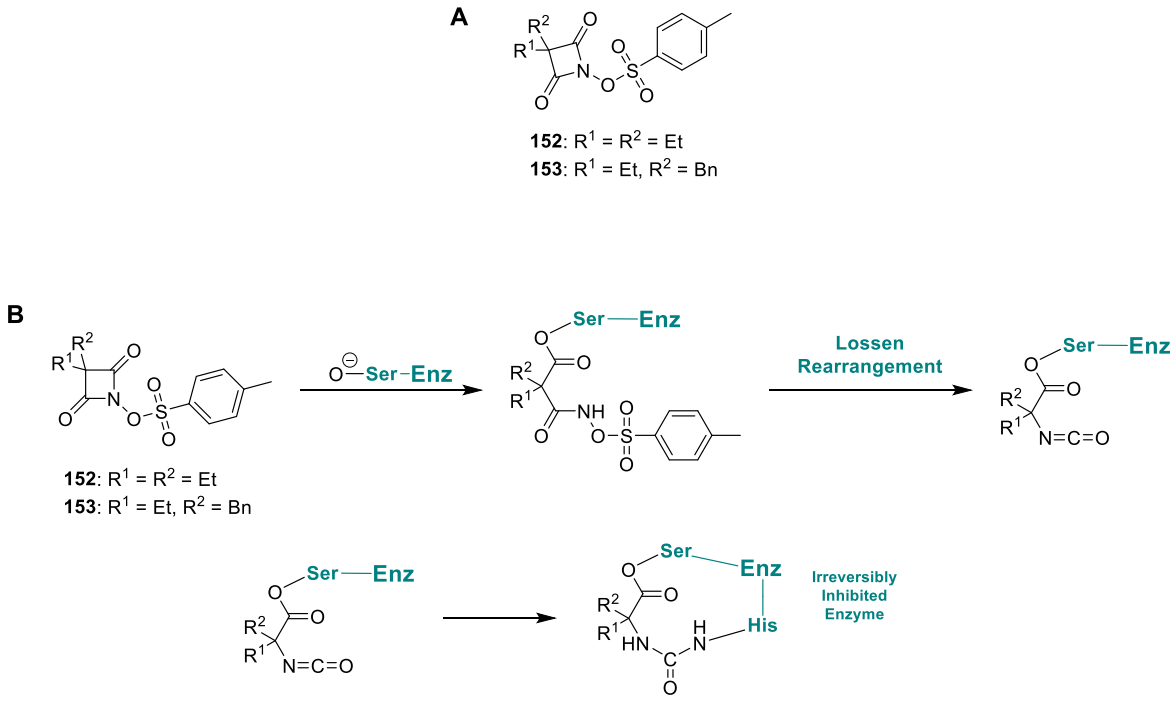

Scheme 20 – A. 4-Oxo-β-Lactam containing an N-O bond; these compounds will take advantage of the Lossen Rearrangement, which will lead to a suicide mechanism. B. Mechanism of HNE inhibition by 4-Oxo-β-Lactam suicide inhibitors. After attack of HNE to the 4-Oxo-β-Lactam ring, a Lossen rearrangement generates an isocyanate, which is then attacked a second time by HNE, leading to an irreversibly inactivated enzyme.

The O-benzylhydroxylamine is obtained starting with N-hydroxyphtalimide. The free hydroxyl group is protected with a benzyl group using benzyl chloride in the presence of sodium bicarbonate and a phase transfer catalyst. The phthalimide group is deprotected in basic medium using hydrochloric acid in acetic acid. The compound is obtained as the hydrochloric salt (scheme 21 – A). Prior to usage, the salt is neutralized by washing with saturated sodium bicarbonate solution.

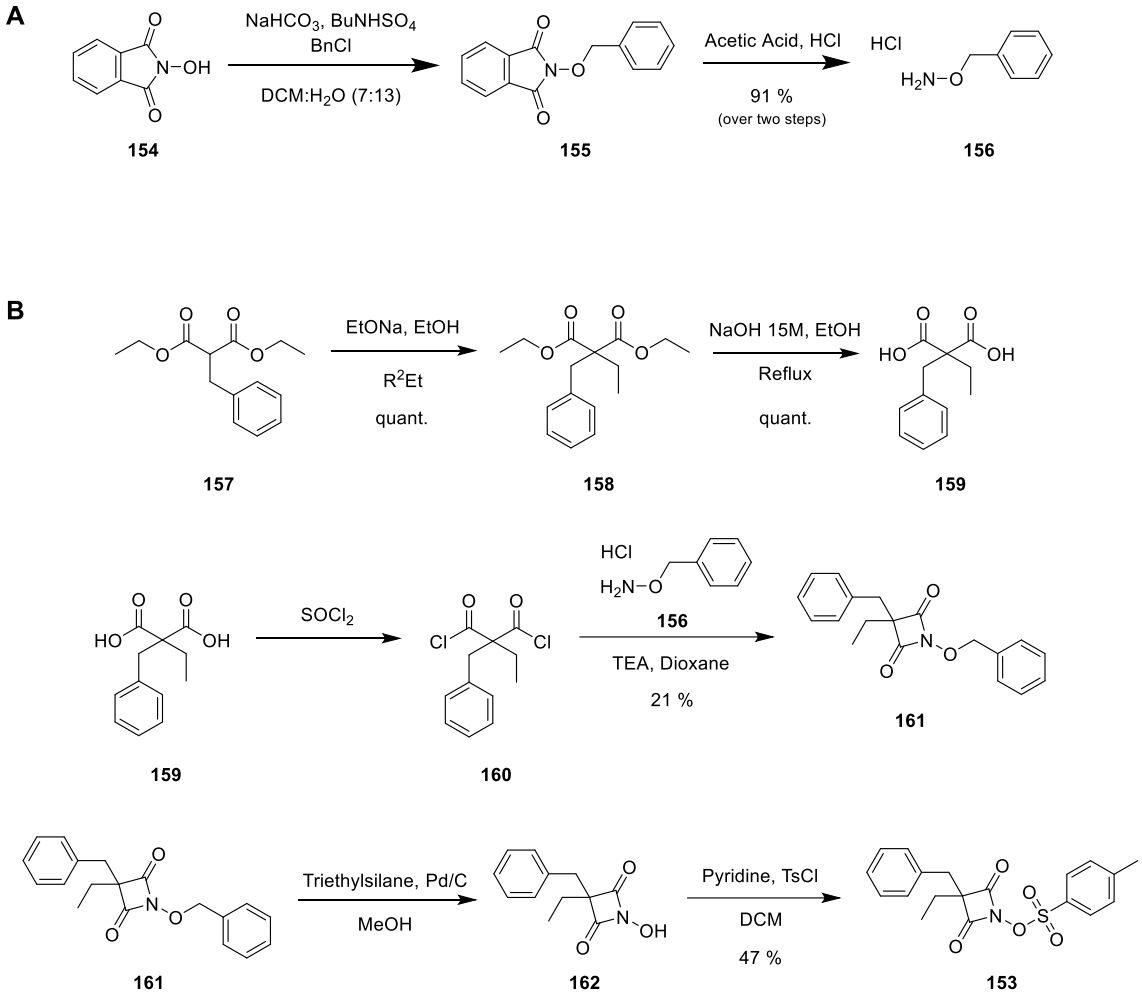

Scheme 21 – Synthesis of compound **153**.

A second inhibitor was prepared with an ethyl and a benzyl groups instead of a diethyl substitution. The synthesis followed a similar pathway after introduction of the benzyl group in the malonic ester.

These two compounds and one of the benzylated intermediates were tested in biochemical assays against HNE using the same assay that was used with 3-Oxo-β-Sultams (see chapter II). The structures and IC_{50} values are presented in figure 63.

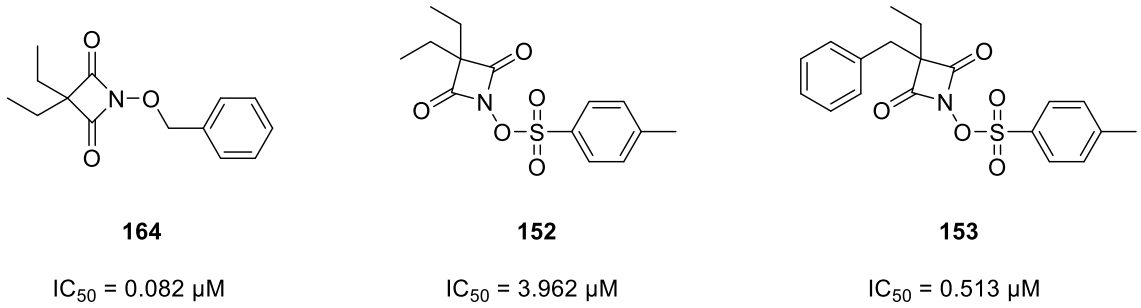

Figure 63 – IC_{50} of N-O derivatives of 4-Oxo-β-Lactams for HNE inhibition.

The IC_{50} for the final compound holding the diethyl substitution was higher than anticipated, falling in the micromolar range, a significantly weaker HNE inhibition than usual for 4-Oxo-β-Lactams with 3-diethyl substitution. On the other hand, the compound containing an ethyl group and a benzyl group displayed sub-micromolar range inhibition, a promising result. The intermediate with the N-O-Bn group presented the best inhibition result, with an IC_{50} of 82 nM. This compound might be suited for HNE inhibition, but the mechanism will not induce a Lossen rearrangement.

Further optimization of these compounds is envisaged. Due to the requirement of the N-O-Ts group for the Lossen Rearrangement-dependent mechanism and the preference of HNE for small substituents at the 3-position, the possibilities of creating chemical diversity with these compounds are limited. The synthesis of variants to target proteasome units and β-Lactamase by taking advantage of specific recognition elements for each of them are envisaged to be developed in the future.

5.2. Synthesis of 4-Oxo-β-Lactam on-off probes

In vivo applications of fluorescent ABPs usually benefit from using on-off probes, so only the fraction of the probe that has engaged a target produces fluorescence, greatly decreasing the background signal from unreacted probe.[53] A 4-Oxo-β-Lactam on-off ABP was synthesized in collaboration with the Nanostructured Systems for Overcoming

Biological Barriers group at iMed.ULisboa. The synthesis of the 4-Oxo-β-Lactam probe followed the previously described strategy of using p-toluidine as the ring-closing amine, radical bromination to introduce a bromine atom at the resulting methyl group and the introduction of the fluorophore via nucleophilic substitution. Umbelliferone was chosen as the fluorophore (scheme 22).

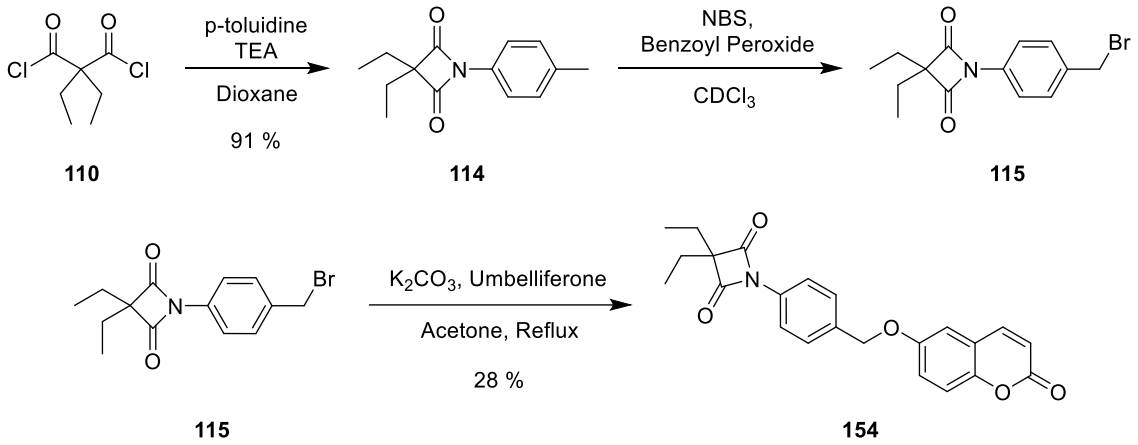

Scheme 22 – Synthesis of compound **154**.

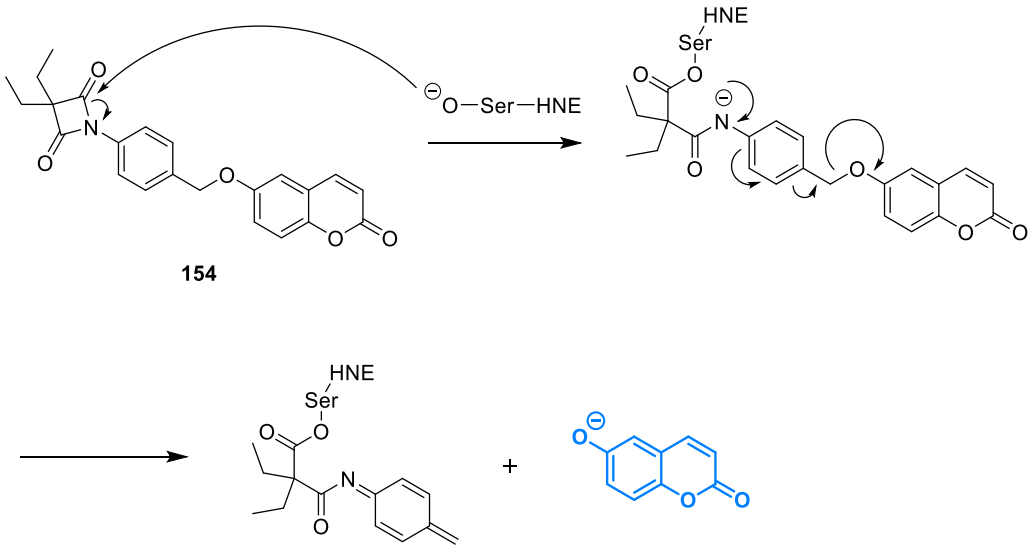

Scheme 23 – Activation mechanism of compound **154** upon attack by HNE.

The probes are expected to release the coumarin tag upon engagement of the target enzyme, leading to the generation of fluorescence. (scheme 23). The application of these ABPs is currently being validated by fluorescence assays.

5.3. Synthesis and purification optimization of a fluorescein tagged 4-Oxo-β-Lactam Activity-based probe

Integrated in a previous project of the group, a 4-Oxo-β-Lactam ABP tagged with fluorescein was synthesized (scheme 24).

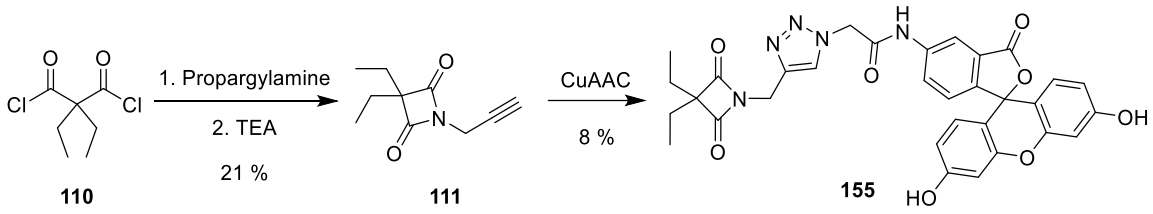

Scheme 24 – Synthesis of a fluorescein tagged 4-Oxo-β-Lactam **155** by CuAAC.

The synthesis followed a similar strategy to the one used for the 3-Oxo-β-Sultam and 4-Oxo-β-Lactam derivatives synthesized in this PhD project, via cyclization of diethyl malonyl dichloride with propargylamine as a way to introduce a click chemistry handle. The alkynylated 4-Oxo-β-Lactam was then derivatized by CuAAC reaction with azidoacetic acid-coupled fluoresceinamine, yielding the desired ABP. Purification of this compound was achieved via a reverse phase combi-flash chromatography column with a water:methanol gradient. This method allowed us to obtain the final compound **155**, nevertheless with a poor yield of 8%.

The compound was tested in biochemical inhibition assays against HNE using the previously described methods, revealing an IC_{50} of 66 nM. Incubation of this ABP with human neutrophils showed the probe permeates the cellular membrane. A gel-based assay showed efficient labeling of pure HNE enzyme.[186]

5.4. Synthesis of a Vinyl Sulfone ABP to target Cysteine Proteases

In collaboration with the Neuron-Glia Biology in Health and Disease group at iMed.ULisboa an ABP based on the vinyl sulfone warhead and tagged with NBD to target cysteine proteases was synthesized.[291] The synthesis of this molecule presented a good opportunity to diversify the set of ABPs synthesized during the PhD project and establish collaborations with other groups at the institute. This probe contained a peptidic linker, Val-HomoPhe, which functions as a recognition element. The complete synthesis of this probe is depicted in scheme 25. Additionally, a non-probe compound capped with morpholine was synthesized.

The synthesis started with the reduction of the carboxylic acid of Boc-protected homo-phenylalanine **156** into an aldehyde, resulting in compound **157**. Coupling of a phenyl-vinyl-sulfone warhead which was readily available at the lab was the following step, yielding compound **158**. After deprotecting the Boc group the peptidic chain was extended by one aminoacid by coupling of Boc-protected leucine, which led to the vinyl sulfone dipeptide **160**. After deprotection of the Boc in the newly introduced leucine, propiolic acid was coupled to introduce an alkyne handle. A CuAAC reaction with the NBD azide led to the final probe **163**.

Compound **163** was delivered, together with the non-probe version **164**, to the Neuron-Glia Biology in Health and Disease group for biologic assays.

These dipeptidyl vinyl sulfone compounds were developed to target the Aβ-inflammatory process associated with Alzheimer's Disease. Inflammatory mediators have gained increased recognition as prominent hallmarks in Alzheimer's disease, involving activation of astrocytes and microglia. The vinyl sulfone warhead is well established for the targeting of cysteine proteases.[292] Particularly, cathepsin S seems to play a role in microglial activation and inhibition of cathepsins S, L, and B reduced the cellular accumulation of Aβ formation.

The compounds were shown to function as effective inhibitors of microglia activation upon treatment with Aβ. Matrix metalloproteinase-9 (MMP-9), matrix metalloproteinase-2 (MMP-2), the alarmin high mobility group box 1 (HMGB1) protein, the NLRP3-inflammasome, IL-1β mRNA levels and miR-155 and miR-146a expression, which are all associated with neuroinflammation, were all found to be at control levels. These results

suggest that vinyl sulfone-based compounds have therapeutic potential to control inflammation in neurodegenerative diseases like Alzheimer's disease.[291]

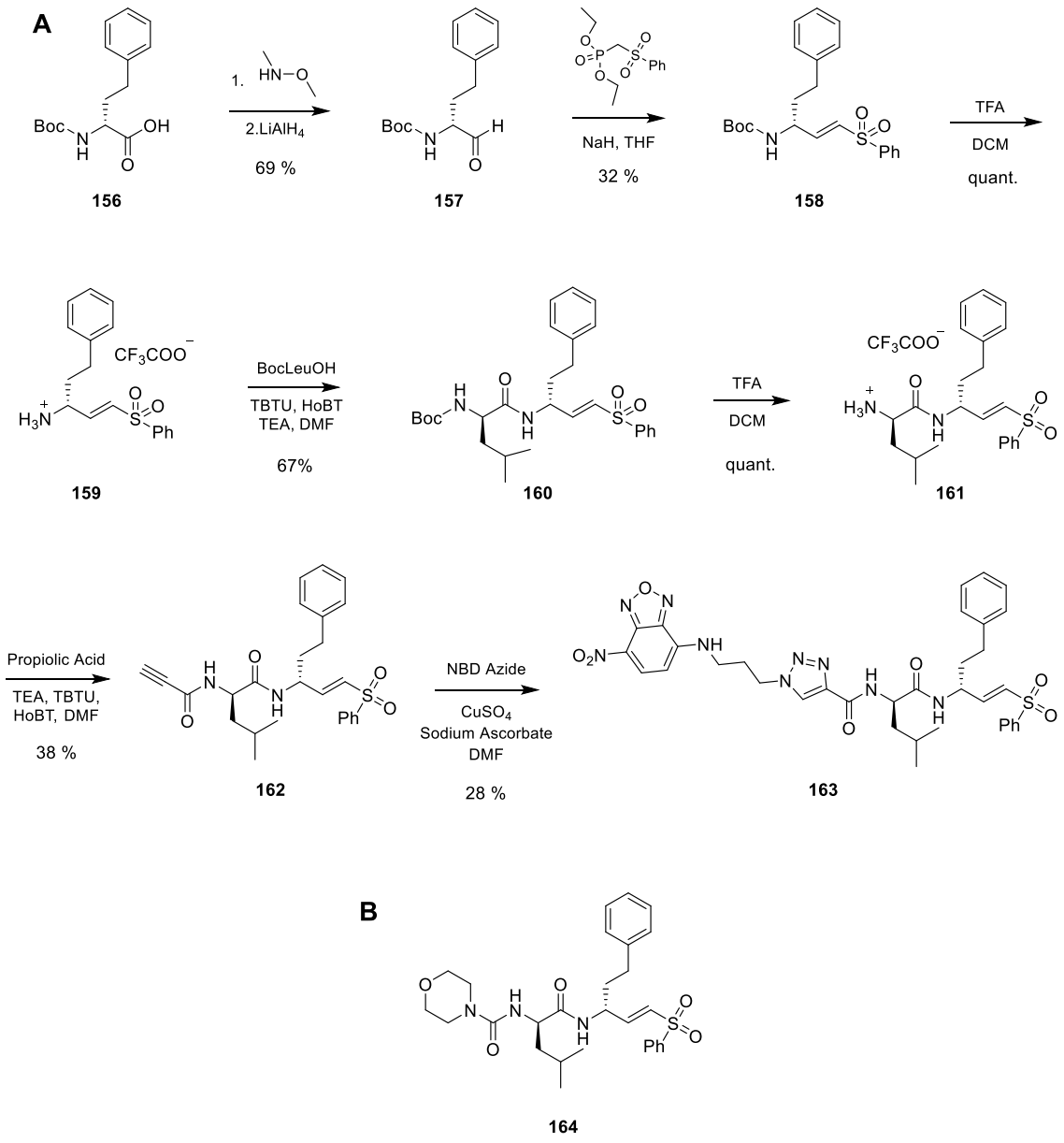

Scheme 25 – Synthesis of an NBD-tagged vinyl sulfone ABP to target cysteine proteases.

More recently Vaz et al developed an amyotrophic lateral sclerosis cellular model based on overexpression of mutated superoxide dismutase 1 in an N9 microglia cell line. The

vinyl sulfone compound was tested in this model and led to promotion of inflammatory resolution, with reduction of TNF-α, IL-1b, high mobility group box 1 protein, S100 calcium-binding protein B, miR-155 expression and MMP-2 and MMP-9 activation. The cellular expression of miR-146a was found to be increased. These results agree with the previously established anti-inflammatory properties of this compound for other cell lines and disease models and further support that vinyl sulfone-based inhibitors are promising modulators of microglia immune response.

5.5. Synthesis of a TUDCA fluorescent Probe

Fluorescent derivatives of bile acids can be used to study the effect of these molecules on cellular membranes. Biologically, bile acids are natural detergents that solubilize lipids for absorption in the digestive system. At micromolar concentrations, some bile acids, like as deoxycholic acid (DCA) or chenodeoxycholic acid (CDCA), have been shown to induce apoptosis through a series of different mechanisms, including activation of cell death receptors, stimulation of p53, induction of mitochondrial disfunction, among other mechanisms, which result in caspase activation and apoptosis. On the other hand, other bile acids, like ursodeoxycholic acid (UDCA) and TUDCA, which are more hydrophilic, have been shown to present anti-apoptotic properties, including prevention of ROS formation, inhibition of mitochondrial disfunction and of death receptor activation.

Mello-Vieira and coworkers used fluorescent derivatives of DCA (more hydrophobic, figure 64 – A) and UDCA (more hydrophilic, figure 64 – B) to characterize the differences in bile acid binding of different bile acids. The study confirmed that hydrophobic bile acids have higher affinity for the cellular membrane and that both hydrophobic and hydrophilic bile acids have higher affinity for disordered membrane structures. Hydrophobic bile acids were shown to prevent the rigidification of lipid membranes induced by cholesterol, potentially affecting the dynamics of structures like lipid rafts, but hydrophilic bile acids showed no significant effect on membrane properties at physiologically relevant concentrations, suggesting a mechanism unrelated with modulation of membrane properties. Importantly, all the studied bile acids were shown

to have limited penetration in the membrane, suggesting a more superficial localization. Our fluorescent derivative of TUDCA will be used in a follow-up to this work.

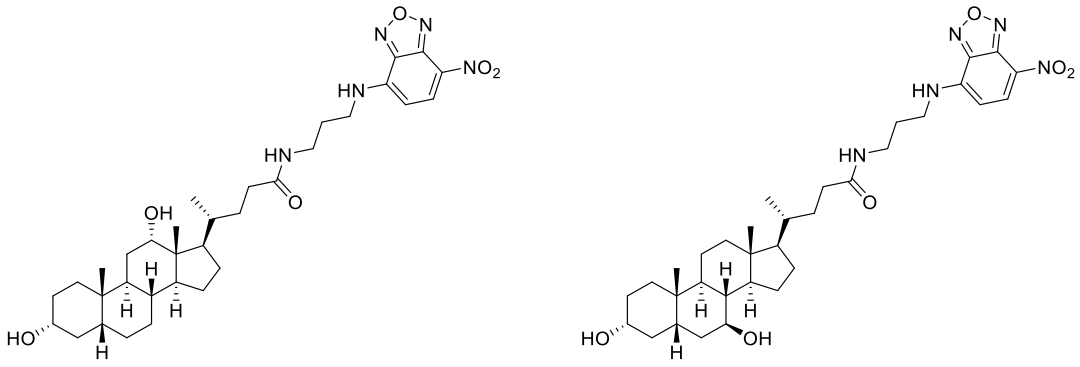

Fig. 64 – Structures of the NBD-derivatized bile acids synthesized by Mello-Vieira et al.

Synthesis of a TUDCA probe was performed in collaboration with the Cellular Function and Therapeutic Targeting group at iMed.ULisboa. The synthetic strategy involved the derivatization of TUDCA with an alkyne moiety, for click chemistry coupling with NBD azide. The synthesis started with 2-(1,3-dioxoisoindolin-2-yl)ethane-1-sulfonyl chloride, to which an alkyne was attached by reaction with propargylamine in the presence of triethylamine. The phthalimide group of this compound is then removed by reaction with hydrazine in ethanol. The coupling of UDCA to the deprotected primary amine was performed via conventional peptide coupling methods using TBTU. The resulting TUDCA alkyne was clicked with NBD azide to provide the final ABP using the same conditions that were optimized for 3-Oxo-β-Sultams (scheme 26). The identity of the final compound was confirmed by mass spectrometry (figure 65). The compound was delivered for biological assays and is currently being tested.

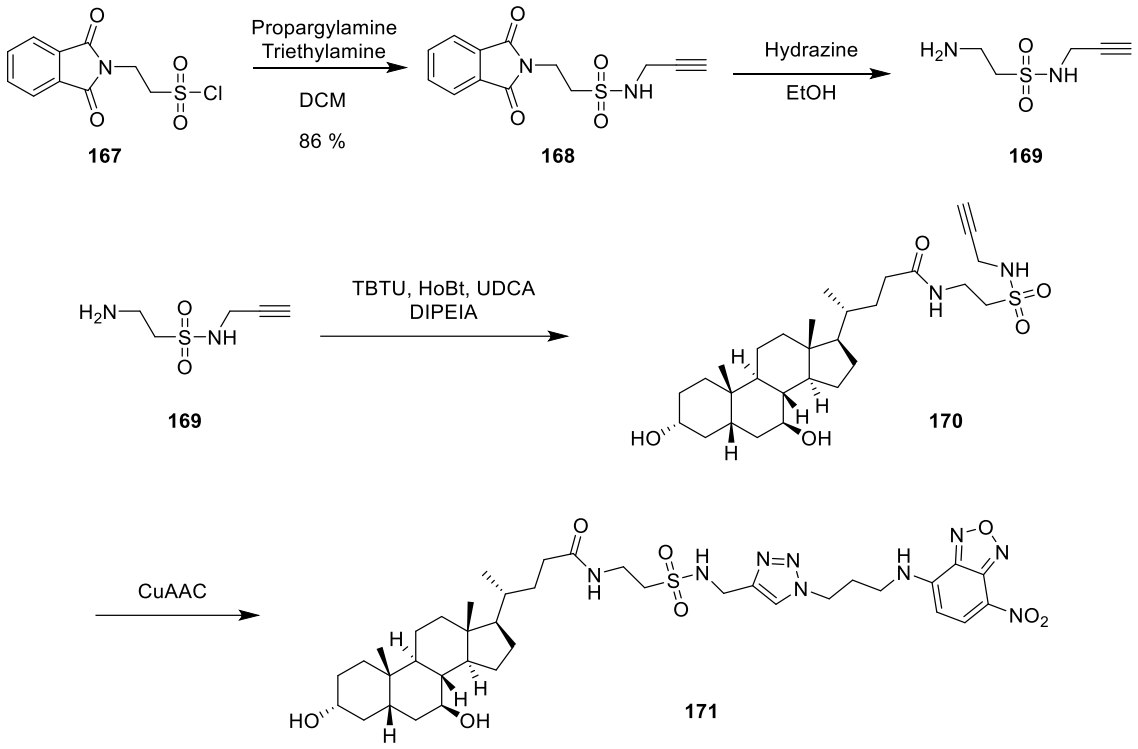

Scheme 26 – Synthesis of a TUDCA ABP.

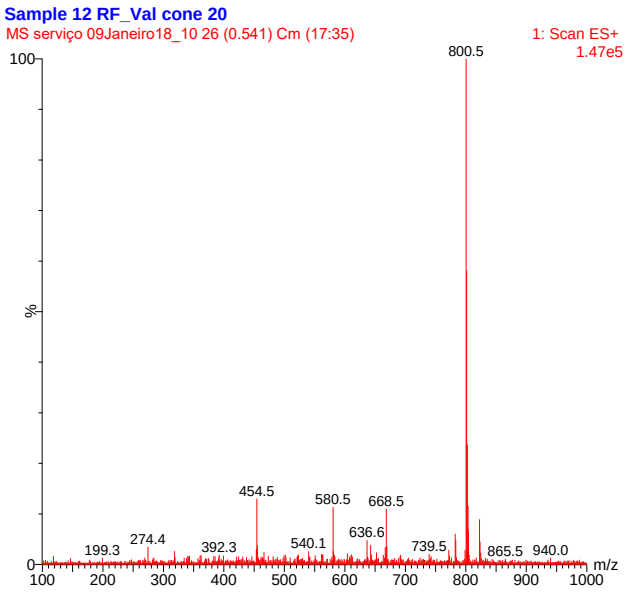

Figure 65 – Mass spectrometry analysis of the TUDCA probe, confirming the identity of the compound.

5.6. Overview

The activities described in this chapter complemented the study on the ABPP of serine hydrolases performed in the main project, allowing different chemistries and targets to be explored. The additional work on 4-Oxo-β-Lactam further showed this warhead's great potential in developing enzymatic inhibitors, with the N-O bond-containing compounds potentially being used in the future for proteasome and β-lactamase targeting via modification of specific recognition moieties. The vinyl sulfone probe allowed us to explore the targeting of the cysteine protease family and contributed to two publications with significant impact in the field. The work with the TUDCA probe in ongoing and will potentially make substantial contributions to the field of studying cellular membranes.

Overall, these works highlight how previously known and established compounds can be further studied by applying ABPP techniques and provide new and exciting results in relevant fields of medicinal chemistry.

Chapter 6 – Conclusions and Future Perspectives

ABPP is a powerful technique that allows the analysis of enzyme dynamics in complex proteomes. The application of ABPP techniques has allowed for significant advances in the study of diverse classes of enzymes and greatly contributed to the annotation of the proteome. By providing a functional readout of enzyme activities instead a simple quantification of protein expression, ABPP has contributed to the elucidation of the role of several enzymes in diverse humane pathologies and for the mapping of enzyme dynamics across different pathologic phenotypes. The analysis of enzymatic activity in disease states has also contributed to biomarker discovery by detecting divergent enzymatic activity fingerprints by comparison with healthy tissues.

In this work we sought to take advantage of ABPP tools to provide unprecedented data regarding underexplored 4-membered-ring warheads, namely 3-Oxo-β-Sultams and 4-Oxo-β-Lactams.

These compounds have shown efficient labeling of serine hydrolases in the past, but their application in ABPP remained unexplored. We aimed for the establishment of target profiles of both 3-Oxo-β-Sultams and 4-Oxo-β-Lactams and to perform a thorough analysis of the possible engageable targets in disease-relevant proteomes. Particularly, we were interested in HNE, a serine protease with a critical role in diseases like COPD and cancer. We had previously studied HNE as a target of 4-Oxo-β-Lactams and 3-Oxo-β-Sultam have been shown to label the porcine variant, PPE. For the purpose of studying HNE activity in disease-relevant proteomes, we developed libraries of 3-Oxo-β-Sultam and 4-Oxo-β-Lactam compounds and ABPs and tested their reactivity and targets in the U937 cell line, which natively expresses HNE.

The 3-Oxo-β-Sultam warhead proved to be a versatile chemotype, easily derivatized for click chemistry applications, and allowed the development of the warhead into a diverse library of compounds with minimal purification hindrances. When analyzing the proteome reactivity of the 3-Oxo-β-Sultam compounds we found that the molecules were highly reactive, labeling a large amount of proteins with limited selectivity. While the labeling of multiple proteins is not a necessarily negative result, given the multiple applications of broad reactivity probes in competitive ABPP and non-directed approaches, the relevant targets of 3-Oxo-β-Sultam compounds were found to be labeled

with low stoichiometry in competitive experiments, which limited their possible applications as broad reactivity ABPs. Despite this, chemical modification of the 3-Oxo-β-Sultam warhead has provided more stable iterations of these compounds in the past, meaning that the 3-Oxo-β-Sultam still has significant potential to be explored.

In addition to defining the target profile of these compounds, we were intrigued by the reaction mechanism of 3-Oxo-β-Sultams with serine hydrolases. Given the presence of two reactive groups in the 3-Oxo-β-Sultam ring, the inhibition mechanism could involve either acylation or sulfonylation of the enzyme's active site. This had been previously studied for PPE, with the authors suggesting an inhibition mechanism by acylation of PPE's active site. We provided, for the first time, crystallographic structures of both PPE and HNE inhibited with 3-Oxo-β-Sultams compounds. Our results contradicted the previously published results, revealing a sulfonylation mechanism for inhibition of PPE. Additionally, we also confirmed that the same mechanism takes place in HNE inhibition. Our unexpected results suggest that 3-Oxo-β-Sultam could be interesting compounds to study serine hydrolase sulfonylation, an underexplored inhibition strategy, and contribute to the pool of available sulfonylation tools in chemical biology.

The 4-Oxo-β-Lactams have previously been developed as low nanomolar HNE inhibitors by our group. We synthesized rhodamine and biotin derivatives and tested them in gel-based and mass-spectrometry-based ABPP. These experiments revealed a much more selective target profile when compared with the 3-Oxo-β-Sultams, but gel analysis showed that there might be additional targets, other than HNE, that could be efficiently labeled by out compounds. Mass-spectrometry-based assays revealed that the 4-Oxo-β-Lactam chemotype is able to efficiently label other members of the serine hydrolase family of enzymes, including enzymes from the ABHD and the DPP families.

Faced with these results we decided to pursue the repurposing of 4-Oxo-β-Lactams as inhibitors of these enzymes, with particular interest in the enzymes DPP8 and DPP9, for which there are currently no selective inhibitors. The synthesis of the 4-Oxo-β-Lactam warhead was optimized into a new method that afforded unprecedented near-quantitative yields, a promising and exciting result for future work with 4-Oxo-β-Lactam libraries.

A library of N-aryl 4-Oxo-β-Lactams was synthesized and evaluated in gel-based competitive ABPP against the well-established FP probes, revealing a selective profile of target inhibition, with only a few targets being efficiently competed by the 4-Oxo-β-

Lactam compounds. Competitive mass spectrometry analysis against FP-biotin of selected compounds confirmed the inhibition of HNE, ABHD and DPP enzymes, with an apparent effect of the N-aryl moiety substitution pattern in determining compound selectivity. Target validation by gel competitive ABPP with overexpressed serine hydrolases confirmed the potent inhibition of these targets, with some compound-target pairs revealing low nanomolar inhibition values. Interestingly, there seems to be a small preference for inhibition of DPP8 when compared with DPP9. This was an exciting result given the fact that the two enzymes share similar structural features and substrate specificity, with no current know selective inhibitors for either of them. For this reason, we envisaged the 4-Oxo-β-Lactam chemotype as a starting point for the development of DPP8 and DPP9 inhibitors. For this purpose, we collaborated with some of the leading machine learning showed us that, when compared with existent DPP8 and DPP9 inhibitors, the 4-Oxo-β-Lactam is novel chemotype that fits an unexplored section of chemical space. A mild effect on the induction of pyroptosis was identified, a process associated with DPP8 and DPP9 inhibition.

Perhaps the most impactful result obtained in the course of this work was the collaboration with the Huber lab. Kinetic assays with DPP8 and DPP9 for selected compounds confirmed low nanomolar K_i values, in general agreement with the IC_{50}s we obtained in competitive ABPP, confirming the high potency of these compounds. One compound, LUSA91, showed a 20-fold preference for DPP8 when compared with DPP9, which is one of the best selectivity ratios ever achieved for DPP8 and DPP9 inhibition, to the best of our knowledge. Co-crystallization experiments allowed us to obtain a crystallographic structure a 4-Oxo-β-Lactam complex with DPP8, which revealed a novel interaction mechanism that had previously not been identified for known DPP8/DPP9 inhibitors. The crystallographic structures of DPP8 and DPP9 were only very recently published, and achieving crystallization of a novel chemotype with these enzymes is a very exciting and promising result, which will certainly be of great value to guide future inhibitor development. The fact that some of our compounds have some of the best selectivity ratios ever achieved between DPP8 and DPP9 and that their mechanism seems to involve previously unidentified enzymatic structures suggests that taking advantage of the interactions with this motif could be the key to develop new and more selective inhibitors for either DPP8 or DPP9.

In addition to these collaborations we are currently studying the inhibition of Rhomboid serine hydrolases by the 4-Oxo-β-Lactam compounds, with preliminary results showing some compounds present submicromolar IC_{50}s for these enzymes, a promising result when compared with current known inhibitors of these enzymes and further proof of the versatility of 4-Oxo-β-Lactams.

One of the potential goals of our project was the application of the best ABPs in the validation of HNE as a biomarker of COPD. The 4-Oxo-β-Lactam ABPs proved to efficiently label HNE, supporting the feasibility of performing this study. Throughout the course of the project, however, new and unexpected targets of the 4-Oxo-β-Lactam scaffold were identified and validated. This was a surprising but exciting result since most of the identified enzymes can be directly or indirectly related to COPD or other relevant respiratory diseases that can co-develop with COPD. Briefly, DPP4 has been shown to present increased immunostaining in the lung with chronic diseases like COPD, particularly in areas of tissue remodeling, while also showing increased activity in mouse models of induced asthma; FAP has been found to be increased in lung cancers, but this goes in line with its general increase in cancer tissues; PREP has been found to be highly expressed in neutrophils, macrophages and epithelial cells found in lung tissues of COPD patients, in the lungs of mice exposed to cigarette smoke and in patients with cystic fibrosis; DPP8 and DPP9 have been found upregulated in asthma and inflammation, with DPP9 also associated with lung cancer. On the other hand, ABHD2 has been shown to have a protective role in the lung, with its inhibition seemingly contributing to the development of chronic lung disease. Collectively, these results emphasize the importance of using ABPP tools when studying new chemotypes given the extent of analysis of target engagement that ABPP provides. Taking the example of using 4-Oxo-β-Lactam ABPs to measure HNE in COPD samples, we now know to evaluate the concomitant inhibition of enzymes like DPP4 and PREP, which can also have clear roles in COPD, but also in a prospective drug development project we know that we should avoid concomitant inhibition of enzymes like ABHD2, which could cause an antagonistic effect, the advantage being that ABPP can simultaneously help guide the development of these new inhibitors and the analysis of undesirable side-hits. Additionally, pathologic states can be more adequately evaluated if multiple variables are measured. It is more valuable to study a profile of enzymatic activities for different enzymatic entities as a hallmark of a disease or disease state than to limit the analysis to a single enzymatic entity. The application of ABPP techniques in the pharmaceutical

industry could, via this path, identify problematic side-targets early in drug development, thus greatly increasing the potential of lead compounds.

Our future work will involve the application of the 4-Oxo-β-Lactam ABPs in human samples of healthy subjects and COPD patients of various disease stages. We will start by identifying HNE in these samples and then quantifying the enzymatic activity between different samples. The measurement of enzymes like DPP4, PREP and ABHD2 will assist in defining a potential panel of biomarkers of COPD stages.

Overall, we believe that 4-membered ring warheads are highly valuable tools in ABPP and chemical biology in general. In particular, the 4-Oxo-β-Lactam chemotype has proven to be highly valuable as a lead for enzymatic inhibitor development and as the warhead in ABP synthesis, which allowed us to identify previously unknown targets and repurpose these compounds as novel inhibitors of DPP8 and DPP9 enzymes with great therapeutic interest.

List of Publications

2015 – L. A. R. Carvalho, E. F. P. Ruivo, S. D. Lucas, R. Moreira, *Activity-based probes as molecular tools for biomarker discovery*, MedChemComm, 2015, 6, 536-546.

[https://pubs.rsc.org/en/content/articlelanding/2015/md/c4md00417e#!divAbstract]

2016 – E. F. P. Ruivo, L. M. Gonçalves, L. A. R. Carvalho, R. C. Guedes, S. Hofbauer, J. A. Brito, M. Archer, R. Moreira, S. D. Lucas, *Clickable 4-oxo-β-lactam-based selective probing for human neutrophil elastase related proteomes*, ChemMedChem, 2016, 11, 2037-2042.

[https://onlinelibrary.wiley.com/doi/full/10.1002/cmdc.201600258]

2016 – A. S. Falcão, L. A. R. Carvalho, G. Lidónio, A. R. Vaz, S. D. Lucas, R. Moreira, D. Brites, *Dipeptidyl vinyl sulfone as a novel chemical tool to inhibit HMGB1/NLRP3-inflamassome and inflamma-miRs in Aβ-mediated microglial inflammation*, ACS Chem. Neuroscience, 2016, 8, 89-99.

[https://pubs.acs.org/doi/10.1021/acschemneuro.6b00250]

2019 - Vaz, A. R.; Pinto, S.; Ezequiel, C.; Cunha, C.; L. A. R., Moreira, R.; Brites, D.; *Phenotypic effects of wild-type and mutant SOD1 expression in N9 murine microglia at steady state, inflammatory and immunomodulatory conditions*, Front. Cell. Neurosci., 2019, accepted.

[https://www.frontiersin.org/articles/10.3389/fncel.2019.00109/full]

Two publications are currently being prepared to report on the findings of the activity-based protein profiling study of 3-Oxo-β-Sultam and 4-Oxo-β-Lactam activity-based probes on the analysis of serine hydrolases.

List of Oral Communications

2015 – L. A. R. Carvalho, S. D. Lucas, R. Moreira, *Acti-Probe: Activity-based probes as chemical tools for biomarker discovery in Chronic Obstructive Pulmonary Disease*. 7th iMed.ULisboa Postgraduate Students Meeting, Lisbon, Portugal, July 15th, 2015.

2017 – L. A. R. Carvalho, L. M. Gonçalves, F. Vaz, S. D. Lucas, D. Penque, R. Moreira, *Activity-Based Probes as Chemical Tools for Biomarker Discovery in Chronic Obstructive Pulmonary Disease by a Proteomics-Based Approach*. Young Investigator Day at Instituto Nacional de Saúde Dr. Ricardo Jorge, Lisbon, Portugal, May 8th, 2017.

2017 – L. A. R. Carvalho, L. M. Gonçalves, F. Vaz, S. D. Lucas, D. Penque, R. Moreira, *Activity-Based Probes as Chemical Tools for Biomarker Discovery in Chronic Obstructive Pulmonary Disease*, IV SEQT Symposium of Medicinal Chemistry Young Researchers, Barcelona, Spain, May 19th, 2017.

2017 – L. A. R. Carvalho, L. M. Gonçalves, F. Vaz, S. D. Lucas, D. Penque, R. Moreira, *Activity-Based Probes as Chemical Tools for Biomarker Discovery in Chronic Obstructive Pulmonary Disease*, European School of Medicinal Chemistry ESMEC, Urbino, Italy, 2-6 of July 2017.

2019 – L. A. R. Carvalho, K. Lum, B. Ross, R. Huber, S. D. Lucas, B. Cravatt, R. Moreira, *Activity-based Protein Profiling of Serine Hydrolases using 4-Oxo-β-Lactams*, ABPP 2019 – Target Discovery and Visualization using Chemical Probes, Leuven, Belgium, 27-29 March 2019.

List of Poster Communications

2015 – E. F. P. Ruivo, L. A. R. Carvalho, L. M. Gonçalves, R. Moreira, S. D. Lucas. *Synthesis of molecular probes toward disease biomarker discovery.* 2nd Young Investigator Symposium of the Spanish Therapeutic Chemistry Society (SEQT), Madrid, Spain, June 12, 2015.

2015 – L. A. R. Carvalho, R. Moreira, S. D. Lucas. *ACTIPROBE: Activity-based probes as chemical tools for biomarker discovery in chronic obstructive pulmonary disease.* 11th National Encounter of Organic Chemistry, 4º National Encounter of Therapeutic Chemistry (Portuguese Society of Chemistry), Porto, Portugal, December 1-3, 2015.

2016 – L. A. R. Carvalho, R. Moreira, S. D. Lucas. *ACTIPROBE: Activity-based probes as chemical tools for biomarker discovery in chronic obstructive pulmonary disease.* 5th Portuguese Young Chemists Meeting, 1st European Young Chemists Meeting, Guimarães, Portugal, April 26-29, 2016.

2017 – L. A. R. Carvalho, L. M. Gonçalves, F. Vaz, S. D. Lucas, D. Penque, R. Moreira. *A Chemoproteomic approach to validate Human Neutrophil Elastase as a Biomarker of Chronic Obstructive Pulmonary Disease*, 9th iMed.ULisboa Postgraduate Students Meeting & 2nd i3DU Meeting, Lisbon, Portugal 13-14th July 2017.

2017 – L. A. R. Carvalho, L. M. Gonçalves, F. Vaz, S. D. Lucas, D. Penque, R. Moreira. *A Chemoproteomic approach to validate Human Neutrophil Elastase as a Biomarker of Chronic Obstructive Pulmonary Disease*, XXV Encontro Nacional da SPQ, Lisbon, Portugal 16-19th July 2017.

2017 – L. A. R. Carvalho, L. M. Gonçalves, F. Vaz, S. D. Lucas, D. Penque, R. Moreira. *A Chemoproteomic approach to validate Human Neutrophil Elastase as a Biomarker of Chronic Obstructive Pulmonary Disease*, 1º Encontro – A Química na Investigação da ULisboa, Lisbon, Portugal 20-21th July 2017.

2019 – L. A. R. Carvalho, K. Lum, B. Ross, S. D. Lucas, R. Huber, B. Cravatt, R. Moreira, *Activity-based Protein Profiling using 4-Oxo-β-Lactams uncovers a new Chemotype for DPP8 and DPP9 Inhibition*, 11th iMed.ULisboa Postgraduate Students Meeting and 4th i3DU Meeting, Lisbon, Portugal, 15th July 2019.

References

1. Weerapana, E., Speers, A.E. & Cravatt, B.F. Tandem orthogonal proteolysis-activity-based protein profiling (TOP-ABPP)--a general method for mapping sites of probe modification in proteomes. *Nat Protoc* **2**, 1414-25 (2007).
2. Shannon, D.A. & Weerapana, E. Covalent protein modification: the current landscape of residue-specific electrophiles. *Curr Opin Chem Biol* **24**, 18-26 (2015).
3. Waumans, Y., Baerts, L., Kehoe, K., Lambeir, A.M. & De Meester, I. The Dipeptidyl Peptidase Family, Prolyl Oligopeptidase, and Prolyl Carboxypeptidase in the Immune System and Inflammatory Disease, Including Atherosclerosis. *Front Immunol* **6**, 387 (2015).
4. Lucas, S.D., Costa, E., Guedes, R.C. & Moreira, R. Targeting COPD: advances on low-molecular-weight inhibitors of human neutrophil. *Med Res Rev* **33 Suppl 1**, E73-e101 (2013).
5. Venter, J.C. et al. The sequence of the human genome. *Science* **291**, 1304-51 (2001).
6. Rohrback, S., Siddoway, B., Liu, C.S. & Chun, J. Genomic mosaicism in the developing and adult brain. *Dev Neurobiol* **78**, 1026-1048 (2018).
7. Greenbaum, D. et al. Chemical approaches for functionally probing the proteome. *Mol Cell Proteomics* **1**, 60-8 (2002).
8. Uttamchandani, M., Li, J., Sun, H. & Yao, S.Q. Activity-based protein profiling: new developments and directions in functional proteomics. *Chembiochem* **9**, 667-75 (2008).
9. Chan, E.W., Chattopadhaya, S., Panicker, R.C., Huang, X. & Yao, S.Q. Developing photoactive affinity probes for proteomic profiling: hydroxamate-based probes for metalloproteases. *J Am Chem Soc* **126**, 14435-46 (2004).
10. Cravatt, B.F., Simon, G.M. & Yates, J.R., 3rd. The biological impact of mass-spectrometry-based proteomics. *Nature* **450**, 991-1000 (2007).
11. Sadaghiani, A.M., Verhelst, S.H. & Bogyo, M. Tagging and detection strategies for activity-based proteomics. *Curr Opin Chem Biol* **11**, 20-8 (2007).
12. Weerapana, E. et al. Quantitative reactivity profiling predicts functional cysteines in proteomes. *Nature* **468**, 790-795 (2010).
13. D'Ascenzio, M. et al. An Activity-Based Probe Targeting Non-Catalytic, Highly Conserved Amino Acid Residues within Bromodomains. *Angew Chem Int Ed Engl* **58**, 1007-1012 (2019).
14. Jessani, N. & Cravatt, B.F. The development and application of methods for activity-based protein profiling. *Current opinion in chemical biology* **8**, 54-59 (2004).
15. Sieber, S.A. & Cravatt, B.F. Analytical platforms for activity-based protein profiling--exploiting the versatility of chemistry for functional proteomics. *Chem Commun (Camb)*, 2311-9 (2006).
16. Speers, A.E. & Cravatt, B.F. Activity-Based Protein Profiling (ABPP) and Click Chemistry (CC)-ABPP by MudPIT Mass Spectrometry. *Curr Protoc Chem Biol* **1**, 29-41 (2009).
17. Evans, M.J. & Cravatt, B.F. Mechanism-based profiling of enzyme families. *Chem Rev* **106**, 3279-301 (2006).

18. Sanman, L.E. & Bogyo, M. Activity-Based Profiling of Proteases. *Annu Rev Biochem* **83**, 249-273 (2014).
19. Doyle, S.K., Pop, M.S., Evans, H.L. & Koehler, A.N. Advances in discovering small molecules to probe protein function in a systems context. *Curr Opin Chem Biol* **30**, 28-36 (2016).
20. Liu, Y., Patricelli, M.P. & Cravatt, B.F. Activity-based protein profiling: The serine hydrolases. *Proceedings of the National Academy of Sciences* **96**, 14694-14699 (1999).
21. Kato, D. et al. Activity-based probes that target diverse cysteine protease families. *Nature Chemical Biology* **1**, 33-38 (2005).
22. Rabilloud, T. Two-dimensional gel electrophoresis in proteomics: old, old fashioned, but it still climbs up the mountains. *Proteomics* **2**, 3-10 (2002).
23. Wang, S., Tian, Y., Wang, M., Sun, G.B. & Sun, X.B. Advanced Activity-Based Protein Profiling Application Strategies for Drug Development. *Front Pharmacol* **9**, 353 (2018).
24. Carvalho, L.A.R., Ruivo, E.F.P., Lucas, S.D. & Moreira, R. Activity-based probes as molecular tools for biomarker discovery. *MedChemComm* (2015).
25. Blum, G., von Degenfeld, G., Merchant, M.J., Blau, H.M. & Bogyo, M. Noninvasive optical imaging of cysteine protease activity using fluorescently quenched activity-based probes. *Nat Chem Biol* **3**, 668-77 (2007).
26. Zuhl, A.M. et al. Competitive activity-based protein profiling identifies aza-beta-lactams as a versatile chemotype for serine hydrolase inhibition. *J Am Chem Soc* **134**, 5068-71 (2012).
27. Cutter, J.L. et al. Topical application of activity-based probes for visualization of brain tumor tissue. *PLoS One* **7**, e33060 (2012).
28. Jessani, N., Liu, Y., Humphrey, M. & Cravatt, B.F. Enzyme activity profiles of the secreted and membrane proteome that depict cancer cell invasiveness. *Proceedings of the National Academy of Sciences* **99**, 10335-10340 (2002).
29. Zhu, Q., Girish, A., Chattopadhaya, S. & Yao, S.Q. Developing novel activity-based fluorescent probes that target different classes of proteases. *Chem Commun (Camb)*, 1512-3 (2004).
30. Blum, G. et al. Dynamic imaging of protease activity with fluorescently quenched activity-based probes. *Nat Chem Biol* **1**, 203-9 (2005).
31. Fonovic, M. & Bogyo, M. Activity based probes for proteases: applications to biomarker discovery, molecular imaging and drug screening. *Curr Pharm Des* **13**, 253-61 (2007).
32. Wilke, K.E., Francis, S. & Carlson, E.E. Activity-based probe for histidine kinase signaling. *J Am Chem Soc* **134**, 9150-3 (2012).
33. Yee, M.C., Fas, S.C., Stohlmeyer, M.M., Wandless, T.J. & Cimprich, K.A. A cell-permeable, activity-based probe for protein and lipid kinases. *J Biol Chem* **280**, 29053-9 (2005).
34. Ratcliffe, S.J., Yi, T. & Khandekar, S.S. Synthesis and characterization of 5'-p-fluorosulfonylbenzoyl-2' (or 3')-(biotinyl)adenosine as an activity-based probe for protein kinases. *J Biomol Screen* **12**, 126-32 (2007).
35. Kumar, S. et al. Activity-based probes for protein tyrosine phosphatases. *Proc Natl Acad Sci U S A* **101**, 7943-8 (2004).
36. Lo, L.C. et al. Design and synthesis of class-selective activity probes for protein tyrosine phosphatases. *J Proteome Res* **1**, 35-40 (2002).
37. Willems, L.I. et al. From covalent glycosidase inhibitors to activity-based glycosidase probes. *Chemistry* **20**, 10864-72 (2014).

38. Vocadlo, D.J. & Bertozzi, C.R. A strategy for functional proteomic analysis of glycosidase activity from cell lysates. *Angew Chem Int Ed Engl* **43**, 5338-42 (2004).
39. Adam, G.C., Sorensen, E.J. & Cravatt, B.F. Proteomic profiling of mechanistically distinct enzyme classes using a common chemotype. *Nat Biotechnol* **20**, 805-9 (2002).
40. Barglow, K.T. & Cravatt, B.F. Discovering disease-associated enzymes by proteome reactivity profiling. *Chem Biol* **11**, 1523-31 (2004).
41. Srinivasan, R., Huang, X., Ng, S.L. & Yao, S.Q. Activity-Based Fingerprinting of Proteases. *ChemBioChem* **7**, 32-36 (2006).
42. Herrera Moro Chao, D. et al. Visualization of Active Glucocerebrosidase in Rodent Brain with High Spatial Resolution following In Situ Labeling with Fluorescent Activity Based Probes. *PLoS One* **10**, e0138107 (2015).
43. Edgington, L.E. et al. Noninvasive optical imaging of apoptosis by caspase-targeted activity-based probes. *Nat Med* **15**, 967-73 (2009).
44. Niphakis, M.J. & Cravatt, B.F. Enzyme inhibitor discovery by activity-based protein profiling. *Annu Rev Biochem* **83**, 341-77 (2014).
45. Jessani, N. et al. A streamlined platform for high-content functional proteomics of primary human specimens. *Nat Methods* **2**, 691-7 (2005).
46. Powers, J.C., Asgian, J.L., Ekici, O.D. & James, K.E. Irreversible inhibitors of serine, cysteine, and threonine proteases. *Chem Rev* **102**, 4639-750 (2002).
47. Saghatelian, A., Jessani, N., Joseph, A., Humphrey, M. & Cravatt, B.F. Activity-based probes for the proteomic profiling of metalloproteases. *Proc Natl Acad Sci U S A* **101**, 10000-5 (2004).
48. Chattopadhaya, S., Chan, E.W.S. & Yao, S.Q. An affinity-based probe for the proteomic profiling of aspartic proteases. *Tetrahedron Letters* **46**, 4053-4056 (2005).
49. Bogyo, M., Verhelst, S., Bellingard-Dubouchaud, V., Toba, S. & Greenbaum, D. Selective targeting of lysosomal cysteine proteases with radiolabeled electrophilic substrate analogs. *Chem Biol* **7**, 27-38 (2000).
50. Chen, X., Wei, S., Ji, Y., Guo, X. & Yang, F. Quantitative proteomics using SILAC: Principles, applications, and developments. *Proteomics* **15**, 3175-3192 (2015).
51. van Swieten, P.F. et al. Development of an isotope-coded activity-based probe for the quantitative profiling of cysteine proteases. *Bioorg Med Chem Lett* **14**, 3131-4 (2004).
52. Bachovchin, D.A., Brown, S.J., Rosen, H. & Cravatt, B.F. Identification of selective inhibitors of uncharacterized enzymes by high-throughput screening with fluorescent activity-based probes. *Nat Biotechnol* **27**, 387-94 (2009).
53. Cheng, Y. et al. Fluorogenic Probes with Substitutions at the 2 and 7 Positions of Cephalosporin are Highly BlaC-Specific for Rapid Mycobacterium Tuberculosis Detection. *Angew Chem Int Ed Engl* **53**, 9360-9364 (2014).
54. Livnah, O., Bayer, E.A., Wilchek, M. & Sussman, J.L. Three-dimensional structures of avidin and the avidin-biotin complex. *Proc Natl Acad Sci U S A* **90**, 5076-80 (1993).
55. Speers, A.E., Adam, G.C. & Cravatt, B.F. Activity-Based Protein Profiling in Vivo Using a Copper(I)-Catalyzed Azide-Alkyne [3 + 2] Cycloaddition. *Journal of the American Chemical Society* **125**, 4686-4687 (2003).
56. Speers, A.E. & Cravatt, B.F. Profiling enzyme activities in vivo using click chemistry methods. *Chem Biol* **11**, 535-46 (2004).

57. Borodovsky, A. et al. A novel active site-directed probe specific for deubiquitylating enzymes reveals proteasome association of USP14. *Embo j* **20**, 5187-96 (2001).
58. Winssinger, N., Ficarro, S., Schultz, P.G. & Harris, J.L. Profiling protein function with small molecule microarrays. *Proc Natl Acad Sci U S A* **99**, 11139-44 (2002).
59. Hesek, D. et al. Design and characterization of a metalloproteinase inhibitor-tethered resin for the detection of active MMPs in biological samples. *Chem Biol* **13**, 379-86 (2006).
60. Alexander, J.P. & Cravatt, B.F. Mechanism of carbamate inactivation of FAAH: implications for the design of covalent inhibitors and in vivo functional probes for enzymes. *Chem Biol* **12**, 1179-87 (2005).
61. Ravindran, M.S. et al. Targeting lipid esterases in mycobacteria grown under different physiological conditions using activity-based profiling with tetrahydrolipstatin (THL). *Mol Cell Proteomics* **13**, 435-48 (2014).
62. Adam, G.C., Sorensen, E.J. & Cravatt, B.F. Trifunctional chemical probes for the consolidated detection and identification of enzyme activities from complex proteomes. *Mol Cell Proteomics* **1**, 828-35 (2002).
63. Borodovsky, A. et al. Chemistry-based functional proteomics reveals novel members of the deubiquitinating enzyme family. *Chem Biol* **9**, 1149-59 (2002).
64. Hemelaar, J. et al. Chemistry-based functional proteomics: mechanism-based activity-profiling tools for ubiquitin and ubiquitin-like specific proteases. *J Proteome Res* **3**, 268-76 (2004).
65. Koehl, C., Knight, C.G. & Bieth, J.G. Compared action of neutrophil proteinase 3 and elastase on model substrates. Favorable effect of S'-P' interactions on proteinase 3 catalysts. *J Biol Chem* **278**, 12609-12 (2003).
66. Kasperkiewicz, P. et al. Design of ultrasensitive probes for human neutrophil elastase through hybrid combinatorial substrate library profiling. *Proc Natl Acad Sci USA* **111**, 2518-23 (2014).
67. Fonovic, M., Verhelst, S.H., Sorum, M.T. & Bogyo, M. Proteomics evaluation of chemically cleavable activity-based probes. *Mol Cell Proteomics* **6**, 1761-70 (2007).
68. Leriche, G., Chisholm, L. & Wagner, A. Cleavable linkers in chemical biology. *Bioorg Med Chem* **20**, 571-82 (2012).
69. Wright, M.H. & Sieber, S.A. Chemical proteomics approaches for identifying the cellular targets of natural products. *Nat Prod Rep* **33**, 681-708 (2016).
70. Speers, A.E. & Cravatt, B.F. A Tandem Orthogonal Proteolysis Strategy for High-Content Chemical Proteomics. *Journal of the American Chemical Society* **127**, 10018-10019 (2005).
71. Qian, Y. & Weerapana, E. A Quantitative Mass-Spectrometry Platform to Monitor Changes in Cysteine Reactivity. *Methods Mol Biol* **1491**, 11-22 (2017).
72. Blancher, C. & Jones, A. SDS -PAGE and Western Blotting Techniques. *Methods Mol Med* **57**, 145-62 (2001).
73. Washburn, M.P., Wolters, D. & Yates, J.R., 3rd. Large-scale analysis of the yeast proteome by multidimensional protein identification technology. *Nat Biotechnol* **19**, 242-7 (2001).
74. Chevalier, F. Highlights on the capacities of "Gel-based" proteomics. *Proteome Sci* **8**, 23 (2010).
75. Cottrell, J.S. Protein identification using MS/MS data. *J Proteomics* **74**, 1842-51 (2011).

76. Gygi, S.P. et al. Quantitative analysis of complex protein mixtures using isotope-coded affinity tags. *Nat Biotechnol* **17**, 994-9 (1999).
77. Tolonen, A.C. & Haas, W. Quantitative proteomics using reductive dimethylation for stable isotope labeling. *J Vis Exp* (2014).
78. Zhang, L. & Elias, J.E. Relative Protein Quantification Using Tandem Mass Tag Mass Spectrometry. *Methods Mol Biol* **1550**, 185-198 (2017).
79. Baggelaar, M.P. & Van der Stelt, M. Competitive ABPP of Serine Hydrolases: A Case Study on DAGL-Alpha. *Methods Mol Biol* **1491**, 161-169 (2017).
80. Kidd, D., Liu, Y. & Cravatt, B.F. Profiling serine hydrolase activities in complex proteomes. *Biochemistry* **40**, 4005-15 (2001).
81. Wang, C., Weerapana, E., Blewett, M.M. & Cravatt, B.F. A chemoproteomic platform to quantitatively map targets of lipid-derived electrophiles. *Nat Methods* **11**, 79-85 (2014).
82. Knuckley, B. et al. A fluopol-ABPP HTS assay to identify PAD inhibitors. *Chem Commun (Camb)* **46**, 7175-7 (2010).
83. Long, J.Z. & Cravatt, B.F. The metabolic serine hydrolases and their functions in mammalian physiology and disease. *Chem Rev* **111**, 6022-63 (2011).
84. Simon, G.M. & Cravatt, B.F. Activity-based proteomics of enzyme superfamilies: serine hydrolases as a case study. *J Biol Chem* **285**, 11051-5 (2010).
85. Bachovchin, D.A. & Cravatt, B.F. The pharmacological landscape and therapeutic potential of serine hydrolases. *Nat Rev Drug Discov* **11**, 52-68 (2012).
86. Botos, I. & Wlodawer, A. The expanding diversity of serine hydrolases. *Curr Opin Struct Biol* **17**, 683-90 (2007).
87. Gilmore, B.F. et al. Expedited solid-phase synthesis of fluorescently labeled and biotinylated aminoalkane diphenyl phosphonate affinity probes for chymotrypsin- and elastase-like serine proteases. *Bioconjug Chem* **20**, 2098-105 (2009).
88. Glynn, P., Read, D.J., Guo, R., Wylie, S. & Johnson, M.K. Synthesis and characterization of a biotinylated organophosphorus ester for detection and affinity purification of a brain serine esterase: neuropathy target esterase. *Biochem J* **301 (Pt 2)**, 551-6 (1994).
89. Staub, I. & Sieber, S.A. Beta-lactam probes as selective chemical-proteomic tools for the identification and functional characterization of resistance associated enzymes in MRSA. *J Am Chem Soc* **131**, 6271-6 (2009).
90. Staub, I. & Sieber, S.A. Beta-lactams as selective chemical probes for the in vivo labeling of bacterial enzymes involved in cell wall biosynthesis, antibiotic resistance, and virulence. *J Am Chem Soc* **130**, 13400-9 (2008).
91. konaklieva, M.I. β-Lactams as Inhibitors of Serine Enzymes. *Current Medicinal Chemistry - Anti-Infective Agents* **1**, 215-238 (2002).
92. Bottcher, T. & Sieber, S.A. Beta-lactones as privileged structures for the active-site labeling of versatile bacterial enzyme classes. *Angew Chem Int Ed Engl* **47**, 4600-3 (2008).
93. Bottcher, T. & Sieber, S.A. β-Lactams and β-lactones as activity-based probes in chemical biology. *MedChemComm* **3**, 408-417 (2012).
94. Shannon, D.A. et al. Sulfonyl fluoride analogues as activity-based probes for serine proteases. *Chembiochem* **13**, 2327-30 (2012).
95. Narayanan, A. & Jones, L.H. Sulfonyl fluorides as privileged warheads in chemical biology. *Chem Sci* **6**, 2650-2659 (2015).
96. Vosyka, O. et al. Activity-based probes for rhomboid proteases discovered in a mass spectrometry-based assay. *Proc Natl Acad Sci U S A* **110**, 2472-7 (2013).

97. Haedke, U., Gotz, M., Baer, P. & Verhelst, S.H. Alkyne derivatives of isocoumarins as clickable activity-based probes for serine proteases. *Bioorg Med Chem* **20**, 633-40 (2012).
98. Chang, J.W., Cognetta, A.B., 3rd, Niphakis, M.J. & Cravatt, B.F. Proteome-wide reactivity profiling identifies diverse carbamate chemotypes tuned for serine hydrolase inhibition. *ACS Chem Biol* **8**, 1590-9 (2013).
99. Adibekian, A. et al. Click-generated triazole ureas as ultrapotent in vivo-active serine hydrolase inhibitors. *Nat Chem Biol* **7**, 469-78 (2011).
100. Patricelli, M.P., Giang, D.K., Stamp, L.M. & Burbaum, J.J. Direct visualization of serine hydrolase activities in complex proteomes using fluorescent active site-directed probes. *Proteomics* **1**, 1067-71 (2001).
101. Jessani, N. et al. Carcinoma and stromal enzyme activity profiles associated with breast tumor growth in vivo. *Proceedings of the National Academy of Sciences of the United States of America* **101**, 13756-13761 (2004).
102. Nomura, D.K. et al. Monoacylglycerol lipase regulates a fatty acid network that promotes cancer pathogenesis. *Cell* **140**, 49-61 (2010).
103. Madsen, M.A., Deryugina, E.I., Niessen, S., Cravatt, B.F. & Quigley, J.P. Activity-based protein profiling implicates urokinase activation as a key step in human fibrosarcoma intravasation. *J Biol Chem* **281**, 15997-6005 (2006).
104. Blankman, J.L., Simon, G.M. & Cravatt, B.F. A comprehensive profile of brain enzymes that hydrolyze the endocannabinoid 2-arachidonoylglycerol. *Chem Biol* **14**, 1347-56 (2007).
105. Viader, A. et al. A chemical proteomic atlas of brain serine hydrolases identifies cell type-specific pathways regulating neuroinflammation. *Elife* **5**, e12345 (2016).
106. Mahrus, S. & Craik, C.S. Selective chemical functional probes of granzymes A and B reveal granzyme B is a major effector of natural killer cell-mediated lysis of target cells. *Chem Biol* **12**, 567-77 (2005).
107. Xing, B., Rao, J. & Liu, R. Novel beta-lactam antibiotics derivatives: their new applications as gene reporters, antitumor prodrugs and enzyme inhibitors. *Mini Rev Med Chem* **8**, 455-71 (2008).
108. Kocaoglu, O. et al. Selective penicillin-binding protein imaging probes reveal substructure in bacterial cell division. *ACS Chem Biol* **7**, 1746-53 (2012).
109. Dargis, M. & Malouin, F. Use of biotinylated beta-lactams and chemiluminescence for study and purification of penicillin-binding proteins in bacteria. *Antimicrob Agents Chemother* **38**, 973-80 (1994).
110. Zhao, G., Meier, T.I., Kahl, S.D., Gee, K.R. & Blaszczak, L.C. BOCILLIN FL, a sensitive and commercially available reagent for detection of penicillin-binding proteins. *Antimicrob Agents Chemother* **43**, 1124-8 (1999).
111. Bottcher, T. & Sieber, S.A. Beta-lactones as specific inhibitors of ClpP attenuate the production of extracellular virulence factors of Staphylococcus aureus. *J Am Chem Soc* **130**, 14400-1 (2008).
112. Krysiak, J. et al. Quantitative Map of beta-Lactone-Induced Virulence Regulation. *J Proteome Res* **16**, 1180-1192 (2017).
113. Lehmann, J. et al. An Antibacterial beta-Lactone Kills Mycobacterium tuberculosis by Disrupting Mycolic Acid Biosynthesis. *Angew Chem Int Ed Engl* **57**, 348-353 (2018).
114. Kolb, R., Bach, N.C. & Sieber, S.A. beta-Sultams exhibit discrete binding preferences for diverse bacterial enzymes with nucleophilic residues. *Chem Commun (Camb)* **50**, 427-9 (2014).

115. Ortega, C. et al. Systematic Survey of Serine Hydrolase Activity in Mycobacterium tuberculosis Defines Changes Associated with Persistence. *Cell Chem Biol* **23**, 290-298 (2016).
116. Nguyen, P.C. et al. Cyclipostins and Cyclophostin analogs as promising compounds in the fight against tuberculosis. *Sci Rep* **7**, 11751 (2017).
117. Seeliger, J.C. et al. Elucidation and chemical modulation of sulfolipid-1 biosynthesis in Mycobacterium tuberculosis. *J Biol Chem* **287**, 7990-8000 (2012).
118. Barry, C.S., Backus, K.M., Barry, C.E., 3rd & Davis, B.G. ESI-MS assay of M. tuberculosis cell wall antigen 85 enzymes permits substrate profiling and design of a mechanism-based inhibitor. *J Am Chem Soc* **133**, 13232-5 (2011).
119. Touchette, M.H. et al. The rv1184c locus encodes Chp2, an acyltransferase in Mycobacterium tuberculosis polyacyltrehalose lipid biosynthesis. *J Bacteriol* **197**, 201-10 (2015).
120. Tallman, K.R., Levine, S.R. & Beatty, K.E. Small-Molecule Probes Reveal Esterases with Persistent Activity in Dormant and Reactivating Mycobacterium tuberculosis. *ACS Infect Dis* **2**, 936-944 (2016).
121. Morak, M. et al. Differential activity-based gel electrophoresis for comparative analysis of lipolytic and esterolytic activities. *J Lipid Res* **50**, 1281-92 (2009).
122. Wolf, E.V., Seybold, M., Hadravova, R., Strisovsky, K. & Verhelst, S.H. Activity-Based Protein Profiling of Rhomboid Proteases in Liposomes. *Chembiochem* **16**, 1616-21 (2015).
123. Sherratt, A.R., Blais, D.R., Ghasriani, H., Pezacki, J.P. & Goto, N.K. Activity-based protein profiling of the Escherichia coli GlpG rhomboid protein delineates the catalytic core. *Biochemistry* **51**, 7794-803 (2012).
124. Wolf, E.V., Zeissler, A. & Verhelst, S.H. Inhibitor Fingerprinting of Rhomboid Proteases by Activity-Based Protein Profiling Reveals Inhibitor Selectivity and Rhomboid Autoprocessing. *ACS Chem Biol* **10**, 2325-33 (2015).
125. Wolf, E.V. et al. A new class of rhomboid protease inhibitors discovered by activity-based fluorescence polarization. *PLoS One* **8**, e72307 (2013).
126. Li, W., Blankman, J.L. & Cravatt, B.F. A functional proteomic strategy to discover inhibitors for uncharacterized hydrolases. *J Am Chem Soc* **129**, 9594-5 (2007).
127. Ahn, K. et al. Novel mechanistic class of fatty acid amide hydrolase inhibitors with remarkable selectivity. *Biochemistry* **46**, 13019-30 (2007).
128. Long, J.Z. et al. Dual blockade of FAAH and MAGL identifies behavioral processes regulated by endocannabinoid crosstalk in vivo. *Proc Natl Acad Sci U S A* **106**, 20270-5 (2009).
129. Leung, D., Hardouin, C., Boger, D.L. & Cravatt, B.F. Discovering potent and selective reversible inhibitors of enzymes in complex proteomes. *Nat Biotechnol* **21**, 687-91 (2003).
130. Chiang, K.P., Niessen, S., Saghatelian, A. & Cravatt, B.F. An enzyme that regulates ether lipid signaling pathways in cancer annotated by multidimensional profiling. *Chem Biol* **13**, 1041-50 (2006).
131. Pham, C.T. Neutrophil serine proteases: specific regulators of inflammation. *Nat Rev Immunol* **6**, 541-50 (2006).
132. Perera, N.C. et al. NSP4, an elastase-related protease in human neutrophils with arginine specificity. *Proc Natl Acad Sci U S A* **109**, 6229-34 (2012).
133. Kasperkiewicz, P. et al. Design of a Selective Substrate and Activity Based Probe for Human Neutrophil Serine Protease 4. *PLoS One* **10**(2015).

134. Takahashi, H. et al. Structure of the human neutrophil elastase gene. *J Biol Chem* **263**, 14739-47 (1988).
135. Korkmaz, B., Horwitz, M.S., Jenne, D.E. & Gauthier, F. Neutrophil elastase, proteinase 3, and cathepsin G as therapeutic targets in human diseases. *Pharmacol Rev* **62**, 726-59 (2010).
136. Campbell, E.J., Campbell, M.A. & Owen, C.A. Bioactive proteinase 3 on the cell surface of human neutrophils: quantification, catalytic activity, and susceptibility to inhibition. *J Immunol* **165**, 3366-74 (2000).
137. Korkmaz, B., Attucci, S., Jourdan, M.L., Juliano, L. & Gauthier, F. Inhibition of neutrophil elastase by alpha1-protease inhibitor at the surface of human polymorphonuclear neutrophils. *J Immunol* **175**, 3329-38 (2005).
138. Owen, C.A., Campbell, M.A., Boukedes, S.S. & Campbell, E.J. Cytokines regulate membrane-bound leukocyte elastase on neutrophils: a novel mechanism for effector activity. *Am J Physiol* **272**, L385-93 (1997).
139. Bode, W. et al. X-ray crystal structure of the complex of human leukocyte elastase (PMN elastase) and the third domain of the turkey ovomucoid inhibitor. *Embo j* **5**, 2453-8 (1986).
140. Korkmaz, B. et al. Measuring elastase, proteinase 3 and cathepsin G activities at the surface of human neutrophils with fluorescence resonance energy transfer substrates. *Nat Protoc* **3**, 991-1000 (2008).
141. Epinette, C. et al. A selective reversible azapeptide inhibitor of human neutrophil proteinase 3 derived from a high affinity FRET substrate. *Biochem Pharmacol* **83**, 788-96 (2012).
142. Owen, C.A., Campbell, M.A., Sannes, P.L., Boukedes, S.S. & Campbell, E.J. Cell surface-bound elastase and cathepsin G on human neutrophils: a novel, non-oxidative mechanism by which neutrophils focus and preserve catalytic activity of serine proteinases. *J Cell Biol* **131**, 775-89 (1995).
143. Liu, J. et al. Advanced Role of Neutrophils in Common Respiratory Diseases. *J Immunol Res* **2017**, 6710278 (2017).
144. Sun, Z. & Yang, P. Role of imbalance between neutrophil elastase and alpha 1-antitrypsin in cancer development and progression. *Lancet Oncol* **5**, 182-90 (2004).
145. Houghton, A.M. et al. Neutrophil elastase-mediated degradation of IRS-1 accelerates lung tumor growth. *Nat Med* **16**, 219-23 (2010).
146. Barnes, P.J. Chronic Obstructive Pulmonary Disease. *New England Journal of Medicine* **343**, 269-280 (2000).
147. Weatherspoon, D., Weatherspoon, C.A. & Abbott, B. Pharmacology Update on Chronic Obstructive Pulmonary Disease, Rheumatoid Arthritis, and Major Depression. *Nurs Clin North Am* **50**, 761-70 (2015).
148. Murray, C.J. & Lopez, A.D. Alternative projections of mortality and disability by cause 1990-2020: Global Burden of Disease Study. *Lancet* **349**, 1498-504 (1997).
149. Lopez-Campos, J.L., Tan, W. & Soriano, J.B. Global burden of COPD. *Respirology* **21**, 14-23 (2016).
150. Berry, C.E. & Wise, R.A. Mortality in COPD: causes, risk factors, and prevention. *Copd* **7**, 375-82 (2010).
151. Daheshia, M. Pathogenesis of chronic obstructive pulmonary disease (COPD). *Clinical and Applied Immunology Reviews* **5**, 339-351 (2005).
152. Köhnlein, T. & Welte, T. Alpha-1 Antitrypsin Deficiency: Pathogenesis, Clinical Presentation, Diagnosis, and Treatment. *The American Journal of Medicine* **121**, 3-9 (2008).

153. MacNee, W. COPD: causes and pathology. *Medicine* **31**, 71-75 (2003).
154. Salvi, S.S. & Barnes, P.J. Chronic obstructive pulmonary disease in non-smokers. *Lancet* **374**, 733-43 (2009).
155. Obermayer, A. et al. New aspects on the structure of neutrophil extracellular traps from chronic obstructive pulmonary disease and in vitro generation. *PLoS One* **9**, e97784 (2014).
156. Shapiro, S.D. et al. Neutrophil elastase contributes to cigarette smoke-induced emphysema in mice. *Am J Pathol* **163**, 2329-35 (2003).
157. Molfino, N.A. & Jeffery, P.K. Chronic obstructive pulmonary disease: histopathology, inflammation and potential therapies. *Pulm Pharmacol Ther* **20**, 462-72 (2007).
158. Jeffery, P.K. Structural and inflammatory changes in COPD: a comparison with asthma. *Thorax* **53**, 129-36 (1998).
159. King, P.T. Inflammation in chronic obstructive pulmonary disease and its role in cardiovascular disease and lung cancer. *Clin Transl Med* **4**, 68 (2015).
160. Barnes, P.J. Immunology of asthma and chronic obstructive pulmonary disease. *Nat Rev Immunol* **8**, 183-92 (2008).
161. Porto, B.N. & Stein, R.T. Neutrophil Extracellular Traps in Pulmonary Diseases: Too Much of a Good Thing? *Front Immunol* **7**, 311 (2016).
162. Farrera, C. & Fadeel, B. Macrophage clearance of neutrophil extracellular traps is a silent process. *J Immunol* **191**, 2647-56 (2013).
163. Iwata, K. et al. Effect of neutrophil elastase inhibitor (sivelestat sodium) in the treatment of acute lung injury (ALI) and acute respiratory distress syndrome (ARDS): a systematic review and meta-analysis. *Intern Med* **49**, 2423-32 (2010).
164. Kawabata, K. et al. ONO-5046, a novel inhibitor of human neutrophil elastase. *Biochemical and Biophysical Research Communications* **177**, 814-820 (1991).
165. Hosseyni, S. & Jarrahpour, A. Recent advances in beta-lactam synthesis. *Org Biomol Chem* **16**, 6840-6852 (2018).
166. Aranda, M.T., Perez-Faginas, P. & Gonzalez-Muniz, R. An Update on the Synthesis of beta-Lactams. *Curr Org Synth* **6**, 325-341 (2009).
167. Doherty, J.B. et al. Cephalosporin antibiotics can be modified to inhibit human leukocyte elastase. *Nature* **322**, 192-4 (1986).
168. Knight, W.B. et al. Mechanism of inhibition of human leukocyte elastase by two cephalosporin derivatives. *Biochemistry* **31**, 4980-6 (1992).
169. Cvetovich, R.J. et al. An Asymmetric Synthesis of L-694,458, a Human Leukocyte Elastase Inhibitor, via Novel Enzyme Resolution of beta-Lactam Esters. *J Org Chem* **61**, 6575-6580 (1996).
170. Clemente, A. et al. Design, synthesis and stability of N-acyloxymethyl- and N-aminocarbonyloxymethyl-2-azetidinones as human leukocyte elastase inhibitors. *Bioorg Med Chem Lett* **11**, 1065-8 (2001).
171. Moreira, R. et al. Design, synthesis, and enzymatic evaluation of N1-acyloxyalkyl- and N1-oxazolidin-2,4-dion-5-yl-substituted beta-lactams as novel inhibitors of human leukocyte elastase. *J Med Chem* **48**, 4861-70 (2005).
172. Beardsell, M. et al. β-Sultams—A novel class of serine protease inhibitors. *Chemical Communications*, 497-498 (2001).
173. Tsang, W.Y. et al. Acylation versus sulfonylation in the inhibition of elastase by 3-oxo-beta-sultams. *J Am Chem Soc* **127**, 8946-7 (2005).
174. Mulchande, J. et al. Azetidine-2,4-diones (4-oxo-beta-lactams) as scaffolds for designing elastase inhibitors. *J Med Chem* **51**, 1783-90 (2008).

175. Mulchande, J. et al. Synthesis, stability, biochemical and pharmacokinetic properties of a new potent and selective 4-oxo-beta-lactam inhibitor of human leukocyte elastase. *J Enzyme Inhib Med Chem* **26**, 169-175 (2011).
176. Macdonald, S.J. et al. Discovery of further pyrrolidine trans-lactams as inhibitors of human neutrophil elastase (HNE) with potential as development candidates and the crystal structure of HNE complexed with an inhibitor (GW475151). *J Med Chem* **45**, 3878-90 (2002).
177. Schramm, V.L. Enzymatic transition states, transition-state analogs, dynamics, thermodynamics, and lifetimes. *Annu Rev Biochem* **80**, 703-32 (2011).
178. Guarnieri, F., Spencer, J.L., Lucey, E.C., Nugent, M.A. & Stone, P.J. A human surfactant peptide-elastase inhibitor construct as a treatment for emphysema. *Proc Natl Acad Sci U S A* **107**, 10661-6 (2010).
179. Sykes, N.O., Macdonald, S.J. & Page, M.I. Acylating agents as enzyme inhibitors and understanding their reactivity for drug design. *J Med Chem* **45**, 2850-6 (2002).
180. Groutas, W.C. et al. Structure-based design of a general class of mechanism-based inhibitors of the serine proteinases employing a novel amino acid-derived heterocyclic scaffold. *Biochemistry* **36**, 4739-50 (1997).
181. Li, Y., Dou, D., He, G., Lushington, G.H. & Groutas, W.C. Mechanism-based inhibitors of serine proteases with high selectivity through optimization of S' subsite binding. *Bioorg Med Chem* **17**, 3536-42 (2009).
182. Taori, K., Matthew, S., Rocca, J.R., Paul, V.J. & Luesch, H. Lyngbyastatins 5-7, potent elastase inhibitors from Floridian marine cyanobacteria, Lyngbya spp. *J Nat Prod* **70**, 1593-600 (2007).
183. Lucas, S.D., Carrasco, M.P., Goncalves, L.M., Moreira, R. & Guedes, R.C. Discovery of C-shaped aurone human neutrophil elastase inhibitors. *MedChemComm* **6**, 1508-1512 (2015).
184. Lechtenberg, B.C., Kasperkiewicz, P., Robinson, H., Drag, M. & Riedl, S.J. The elastase-PK101 structure: mechanism of an ultrasensitive activity-based probe revealed. *ACS Chem Biol* **10**, 945-51 (2015).
185. Grzywa, R. et al. Synthesis of novel phosphonic-type activity-based probes for neutrophil serine proteases and their application in spleen lysates of different organisms. *ChemBioChem* **15**, 2605-12 (2014).
186. Ruivo, E.F. et al. Clickable 4-Oxo-beta-lactam-Based Selective Probing for Human Neutrophil Elastase Related Proteomes. *ChemMedChem* **11**, 2037-42 (2016).
187. Edgington-Mitchell, L.E. et al. Fluorescent diphenylphosphonate-based probes for detection of serine protease activity during inflammation. *Bioorg Med Chem Lett* **27**, 254-60 (2017).
188. Schulz-Fincke, A.C., Blaut, M., Braune, A. & Gutschow, M. A BODIPY-Tagged Phosphono Peptide as Activity-Based Probe for Human Leukocyte Elastase. *ACS Med Chem Lett* **9**, 345-350 (2018).
189. Schulz-Fincke, A.C. et al. Design of an Activity-Based Probe for Human Neutrophil Elastase: Implementation of the Lossen Rearrangement To Induce Forster Resonance Energy Transfers. *Biochemistry* **57**, 742-752 (2018).
190. Liu, S.Y., Xiong, H., Li, R.R., Yang, W.C. & Yang, G.F. Activity-Based Near-Infrared Fluorogenic Probe for Enabling in Vitro and in Vivo Profiling of Neutrophil Elastase. *Anal Chem* **91**, 3877-3884 (2019).
191. Kisselev, A.F., Akopian, T.N., Woo, K.M. & Goldberg, A.L. The sizes of peptides generated from protein by mammalian 26 and 20 S proteasomes. Implications for

understanding the degradative mechanism and antigen presentation. *J Biol Chem* **274**, 3363-71 (1999).
192. Yu, D.M., Wang, X.M., McCaughan, G.W. & Gorrell, M.D. Extraenzymatic functions of the dipeptidyl peptidase IV-related proteins DP8 and DP9 in cell adhesion, migration and apoptosis. *Febs j* **273**, 2447-60 (2006).
193. Deacon, C.F. Dipeptidyl peptidase-4 inhibitors in the treatment of type 2 diabetes: a comparative review. *Diabetes Obes Metab* **13**, 7-18 (2011).
194. Andersen, E.S., Deacon, C.F. & Holst, J.J. Do we know the true mechanism of action of the DPP-4 inhibitors? *Diabetes Obes Metab* **20**, 34-41 (2018).
195. Lambeir, A.M., Scharpe, S. & De Meester, I. DPP4 inhibitors for diabetes--what next? *Biochem Pharmacol* **76**, 1637-43 (2008).
196. Meyerholz, D.K., Lambertz, A.M. & McCray, P.B., Jr. Dipeptidyl Peptidase 4 Distribution in the Human Respiratory Tract: Implications for the Middle East Respiratory Syndrome. *Am J Pathol* **186**, 78-86 (2016).
197. Schade, J. et al. Regulation of expression and function of dipeptidyl peptidase 4 (DP4), DP8/9, and DP10 in allergic responses of the lung in rats. *J Histochem Cytochem* **56**, 147-55 (2008).
198. Pure, E. & Blomberg, R. Pro-tumorigenic roles of fibroblast activation protein in cancer: back to the basics. *Oncogene* **37**, 4343-4357 (2018).
199. Vliegen, G., Raju, T.K., Adriaensen, D., Lambeir, A.M. & De Meester, I. The expression of proline-specific enzymes in the human lung. *Ann Transl Med* **5**, 130 (2017).
200. Santos, A.M., Jung, J., Aziz, N., Kissil, J.L. & Pure, E. Targeting fibroblast activation protein inhibits tumor stromagenesis and growth in mice. *J Clin Invest* **119**, 3613-25 (2009).
201. Kilvaer, T.K. et al. Cancer Associated Fibroblasts in Stage I-IIIA NSCLC: Prognostic Impact and Their Correlations with Tumor Molecular Markers. *PLoS One* **10**, e0134965 (2015).
202. Maes, M. et al. Alterations in plasma prolyl endopeptidase activity in depression, mania, and schizophrenia: effects of antidepressants, mood stabilizers, and antipsychotic drugs. *Psychiatry Res* **58**, 217-25 (1995).
203. Mannisto, P.T. & Garcia-Horsman, J.A. Mechanism of Action of Prolyl Oligopeptidase (PREP) in Degenerative Brain Diseases: Has Peptidase Activity Only a Modulatory Role on the Interactions of PREP with Proteins? *Front Aging Neurosci* **9**, 27 (2017).
204. Svarcbahs, R. et al. New tricks of prolyl oligopeptidase inhibitors - A common drug therapy for several neurodegenerative diseases. *Biochem Pharmacol* **161**, 113-120 (2019).
205. Braber, S. et al. Cigarette smoke-induced lung emphysema in mice is associated with prolyl endopeptidase, an enzyme involved in collagen breakdown. *Am J Physiol Lung Cell Mol Physiol* **300**, L255-65 (2011).
206. Gaggar, A. et al. A novel proteolytic cascade generates an extracellular matrix-derived chemoattractant in chronic neutrophilic inflammation. *J Immunol* **180**, 5662-9 (2008).
207. Abbott, C.A. et al. Cloning, expression and chromosomal localization of a novel human dipeptidyl peptidase (DPP) IV homolog, DPP8. *Eur J Biochem* **267**, 6140-50 (2000).
208. Olsen, C. & Wagtmann, N. Identification and characterization of human DPP9, a novel homologue of dipeptidyl peptidase IV. *Gene* **299**, 185-93 (2002).

209. Geiss-Friedlander, R. et al. The cytoplasmic peptidase DPP9 is rate-limiting for degradation of proline-containing peptides. *J Biol Chem* **284**, 27211-9 (2009).
210. Ross, B. et al. Structures and mechanism of dipeptidyl peptidases 8 and 9, important players in cellular homeostasis and cancer. *Proc Natl Acad Sci U S A* **115**, 1437-1445 (2018).
211. Bjelke, J.R. et al. Dipeptidyl peptidases 8 and 9: specificity and molecular characterization compared with dipeptidyl peptidase IV. *Biochem J* **396**, 391-9 (2006).
212. Van Goethem, S. et al. Structure-activity relationship studies on isoindoline inhibitors of dipeptidyl peptidases 8 and 9 (DPP8, DPP9): is DPP8-selectivity an attainable goal? *J Med Chem* **54**, 5737-46 (2011).
213. Okondo, M.C. et al. DPP8 and DPP9 inhibition induces pro-caspase-1-dependent monocyte and macrophage pyroptosis. *Nat Chem Biol* **13**, 46-53 (2017).
214. Spagnuolo, P.A. et al. Inhibition of intracellular dipeptidyl peptidases 8 and 9 enhances parthenolide's anti-leukemic activity. *Leukemia* **27**, 1236-44 (2013).
215. Lu, C. et al. Dipeptidyl peptidases as survival factors in Ewing sarcoma family of tumors: implications for tumor biology and therapy. *J Biol Chem* **286**, 27494-505 (2011).
216. Zhang, H. et al. Dipeptidyl peptidase 9 subcellular localization and a role in cell adhesion involving focal adhesion kinase and paxillin. *Biochim Biophys Acta* **1853**, 470-80 (2015).
217. Gall, M.G. et al. Targeted inactivation of dipeptidyl peptidase 9 enzymatic activity causes mouse neonate lethality. *PLoS One* **8**, e78378 (2013).
218. Chen, Y. et al. Dipeptidyl peptidase 9 enzymatic activity influences the expression of neonatal metabolic genes. *Exp Cell Res* **342**, 72-82 (2016).
219. Kim, M. et al. DPP9 enzyme activity controls survival of mouse migratory tongue muscle progenitors and its absence leads to neonatal lethality due to suckling defect. *Dev Biol* **431**, 297-308 (2017).
220. Kirby, M., Yu, D.M., O'Connor, S. & Gorrell, M.D. Inhibitor selectivity in the clinical application of dipeptidyl peptidase-4 inhibition. *Clin Sci (Lond)* **118**, 31-41 (2009).
221. Burkey, B.F. et al. Adverse effects of dipeptidyl peptidases 8 and 9 inhibition in rodents revisited. *Diabetes Obes Metab* **10**, 1057-61 (2008).
222. Wu, J.J. et al. Biochemistry, pharmacokinetics, and toxicology of a potent and selective DPP8/9 inhibitor. *Biochem Pharmacol* **78**, 203-10 (2009).
223. Waumans, Y. et al. The Dipeptidyl Peptidases 4, 8, and 9 in Mouse Monocytes and Macrophages: DPP8/9 Inhibition Attenuates M1 Macrophage Activation in Mice. *Inflammation* **39**, 413-424 (2016).
224. Smebye, M.L. et al. Involvement of DPP9 in gene fusions in serous ovarian carcinoma. *BMC Cancer* **17**, 642 (2017).
225. Okondo, M.C. et al. Inhibition of Dpp8/9 Activates the Nlrp1b Inflammasome. *Cell Chem Biol* **25**, 262-267.e5 (2018).
226. Johnson, D.C. et al. DPP8/DPP9 inhibitor-induced pyroptosis for treatment of acute myeloid leukemia. *Nat Med* **24**, 1151-1156 (2018).
227. Han, R., Wang, X., Bachovchin, W., Zukowska, Z. & Osborn, J.W. Inhibition of dipeptidyl peptidase 8/9 impairs preadipocyte differentiation. *Sci Rep* **5**, 12348 (2015).
228. Gabrilovac, J., Cupic, B., Zapletal, E., Kraus, O. & Jakic-Razumovic, J. Dipeptidyl peptidase 9 (DPP9) in human skin cells. *Immunobiology* **222**, 327-342 (2017).

229. Tang, Z. et al. Contribution of upregulated dipeptidyl peptidase 9 (DPP9) in promoting tumoregenicity, metastasis and the prediction of poor prognosis in non-small cell lung cancer (NSCLC). *Int J Cancer* **140**, 1620-1632 (2017).
230. Bachovchin, D.A. et al. Superfamily-wide portrait of serine hydrolase inhibition achieved by library-versus-library screening. *Proc Natl Acad Sci U S A* **107**, 20941-6 (2010).
231. Jansen, K. et al. Extended structure-activity relationship and pharmacokinetic investigation of (4-quinolinoyl)glycyl-2-cyanopyrrolidine inhibitors of fibroblast activation protein (FAP). *J Med Chem* **57**, 3053-74 (2014).
232. Jansen, K. et al. Selective Inhibitors of Fibroblast Activation Protein (FAP) with a (4-Quinolinoyl)-glycyl-2-cyanopyrrolidine Scaffold. *ACS Med Chem Lett* **4**, 491-6 (2013).
233. Jansen, K. et al. Selective inhibitors of fibroblast activation protein (FAP) with a xanthine scaffold. *MedChemComm* **5**, 1700-1707 (2014).
234. Guardiola, S. et al. Targeted Covalent Inhibition of Prolyl Oligopeptidase (POP): Discovery of Sulfonylfluoride Peptidomimetics. *Cell Chem Biol* **25**, 1031-1037.e4 (2018).
235. Gillet, L.C. et al. In-cell selectivity profiling of serine protease inhibitors by activity-based proteomics. *Mol Cell Proteomics* **7**, 1241-53 (2008).
236. Bachovchin, D.A. et al. A high-throughput, multiplexed assay for superfamily-wide profiling of enzyme activity. *Nat Chem Biol* **10**, 656-63 (2014).
237. Sabido, E., Tarrago, T., Niessen, S., Cravatt, B.F. & Giralt, E. Activity-based probes for monitoring postproline protease activity. *Chembiochem* **10**, 2361-6 (2009).
238. Heirbaut, L. et al. Probing for improved selectivity with dipeptide-derived inhibitors of dipeptidyl peptidases 8 and 9: the impact of P1-variation. *MedChemComm* **7**, 433-438 (2016).
239. Van der Veken, P. et al. Inhibitors of dipeptidyl peptidase 8 and dipeptidyl peptidase 9. Part 1: identification of dipeptide derived leads. *Bioorg Med Chem Lett* **18**, 4154-8 (2008).
240. Van Goethem, S. et al. Inhibitors of dipeptidyl peptidase 8 and dipeptidyl peptidase 9. Part 2: isoindoline containing inhibitors. *Bioorg Med Chem Lett* **18**, 4159-62 (2008).
241. Engel, M. et al. The crystal structure of dipeptidyl peptidase IV (CD26) reveals its functional regulation and enzymatic mechanism. *Proc Natl Acad Sci U S A* **100**, 5063-8 (2003).
242. Shi, J. et al. Cleavage of GSDMD by inflammatory caspases determines pyroptotic cell death. *Nature* **526**, 660-5 (2015).
243. Jiaang, W.T. et al. Novel isoindoline compounds for potent and selective inhibition of prolyl dipeptidase DPP8. *Bioorg Med Chem Lett* **15**, 687-91 (2005).
244. Pilla, E. et al. A novel SUMO1-specific interacting motif in dipeptidyl peptidase 9 (DPP9) that is important for enzymatic regulation. *J Biol Chem* **287**, 44320-9 (2012).
245. Pilla, E., Kilisch, M., Lenz, C., Urlaub, H. & Geiss-Friedlander, R. The SUMO1-E67 interacting loop peptide is an allosteric inhibitor of the dipeptidyl peptidases 8 and 9. *J Biol Chem* **288**, 32787-96 (2013).
246. Lord, C.C., Thomas, G. & Brown, J.M. Mammalian alpha beta hydrolase domain (ABHD) proteins: Lipid metabolizing enzymes at the interface of cell signaling and energy metabolism. *Biochim Biophys Acta* **1831**, 792-802 (2013).

247. M, N.K. et al. Molecular characterization of human ABHD2 as TAG lipase and ester hydrolase. *Biosci Rep* **36**(2016).
248. Obinata, D. et al. Abhydrolase domain containing 2, an androgen target gene, promotes prostate cancer cell proliferation and migration. *Eur J Cancer* **57**, 39-49 (2016).
249. Jin, S. et al. Age-related pulmonary emphysema in mice lacking alpha/beta hydrolase domain containing 2 gene. *Biochem Biophys Res Commun* **380**, 419-24 (2009).
250. Guo, Y. et al. Association of genetic polymorphisms with chronic obstructive pulmonary disease in the Chinese Han population: a case-control study. *BMC Med Genomics* **5**, 64 (2012).
251. Yun, B. et al. Regulation of calcium release from the endoplasmic reticulum by the serine hydrolase ABHD2. *Biochem Biophys Res Commun* **490**, 1226-1231 (2017).
252. Marrs, W.R. et al. The serine hydrolase ABHD6 controls the accumulation and efficacy of 2-AG at cannabinoid receptors. *Nat Neurosci* **13**, 951-7 (2010).
253. Thomas, G. et al. The serine hydrolase ABHD6 Is a critical regulator of the metabolic syndrome. *Cell Rep* **5**, 508-20 (2013).
254. Wei, M. et al. alpha/beta-Hydrolase domain-containing 6 (ABHD6) negatively regulates the surface delivery and synaptic function of AMPA receptors. *Proc Natl Acad Sci U S A* **113**, E2695-704 (2016).
255. Hsu, K.L. et al. Discovery and optimization of piperidyl-1,2,3-triazole ureas as potent, selective, and in vivo-active inhibitors of alpha/beta-hydrolase domain containing 6 (ABHD6). *J Med Chem* **56**, 8270-9 (2013).
256. Kamat, S.S. et al. Immunomodulatory lysophosphatidylserines are regulated by ABHD16A and ABHD12 interplay. *Nat Chem Biol* **11**, 164-71 (2015).
257. Ahonen, T.J. et al. Discovery of 12-Thiazole Abietanes as Selective Inhibitors of the Human Metabolic Serine Hydrolase hABHD16A. *ACS Medicinal Chemistry Letters* (2018).
258. Camara, K., Kamat, S.S., Lasota, C.C., Cravatt, B.F. & Howell, A.R. Combining cross-metathesis and activity-based protein profiling: new beta-lactone motifs for targeting serine hydrolases. *Bioorg Med Chem Lett* **25**, 317-21 (2015).
259. Tsang, W.Y., Ahmed, N., Hemming, K. & Page, M.I. Reactivity and selectivity in the inhibition of elastase by 3-oxo-beta-sultams and in their hydrolysis. *Org Biomol Chem* **5**, 3993-4000 (2007).
260. Imai, Y., Ueda, M. & Okuyama, K. Anionic Ring-Opening Polymerization of 4,4-Dimethyl-1,2-thiazetidin-3-one 1,1-Dioxide. *Polymer Journal* **11**, 613-617 (1979).
261. Todorova, T., Linden, A. & Heimgartner, H. Ring-Enlargement and Ring-Opening Reactions of 1,2-Thiazetidin-3-one 1,1-Dioxides with Ammonia and Primary Amines as Nucleophiles. *Helv Chim Acta* **82**, 354-371 (1999).
262. Glasl, D., Otto, H.-H. & Rihs, G. Properties and Reactions of Substituted 1,2-Thiazetidine 1,1-Dioxides: Synthesis of N-Substituted 4,4-dimethyl-1,2-thiazetidin-3-one 1,1-dioxides, and a new base-catalyzed rearrangement to thiazolidin-4-one 1,1-dioxides. *Helvetica Chimica Acta* **80**, 671-683 (1997).
263. Page, M.I., Tsang, W.Y. & Ahmed, N. Comparison of the mechanisms of reactions of β-lactams and β-sultams, including their reactions with some serine enzymes. *Journal of Physical Organic Chemistry* **19**, 446-451 (2006).
264. Ahmed, N., Tsang Wy Fau - Page, M.I. & Page, M.I. Acyl vs sulfonyl transfer in N-acyl beta-sultams and 3-oxo-beta-sultams. *Organic Letters* **6**, 3 (2004).

265. Macdonald, S.J. et al. Intracellular inhibition of human neutrophil elastase by orally active pyrrolidine-trans-lactams. *Bioorg Med Chem Lett* **11**, 243-6 (2001).
266. Page, M.I. Beta-sultams-mechanism of reactions and use as inhibitors of serine proteases. *Acc Chem Res* **37**, 7 (2004).
267. Page, M.I., Tsang, W.Y. & Ahmed, N. Comparison of the mechanisms of reactions of β-lactams and β-sultams, including their reactions with some serine enzymes. *J Phys Org Chem* **19**, 446-451 (2006).
268. Ahmed, N., Tsang, W. & Page, M.I. Acyl vs sulfonyl transfer in N-acyl beta-sultams and 3-oxo-beta-sultams. *Organic Letters* **6**, 201-3 (2004).
269. Maoxia, H., Feng, D., Lingjuan, Y. & Zhengting, C. Theoretical Study for Alcoholysis of N-Benzyl 3-Oxo- β-Sultam. *Struct Chem* **16**, 149-54 (2005).
270. Page, M.I. Beta-sultams-mechanism of reactions and use as inhibitors of serine proteases. *Acc Chem Res* **37**, 297-303 (2004).
271. Tsang, W.Y., Ahmed, N., Hemming, K. & Page, M.I. An activated sulfonylating agent that undergoes general base-catalyzed hydrolysis by amines in preference to aminolysis. *J Org Chem* **73**, 4504-12 (2008).
272. Mulchande, J. et al. 4-Oxo-beta-lactams (Azetidine-2,4-diones) Are Potent and Selective Inhibitors of Human Leukocyte Elastase. *Journal of Medicinal Chemistry* **53**, 241-253 (2010).
273. Chavan, S.S. et al. An efficient Sn(ii)-catalyzed one-pot synthesis of a 3-substituted azetidine-2,4-dione framework. *Org Biomol Chem* **15**, 2385-2391 (2017).
274. Hou, J., Liu, X., Shen, J., Zhao, G. & Wang, P.G. The impact of click chemistry in medicinal chemistry. *Expert Opin Drug Discov* **7**, 489-501 (2012).
275. Chan, T.R., Hilgraf, R., Sharpless, K.B. & Fokin, V.V. Polytriazoles as copper(I)-stabilizing ligands in catalysis. *Org Lett* **6**, 2853-5 (2004).
276. Hopkins, A.L., Keseru, G.M., Leeson, P.D., Rees, D.C. & Reynolds, C.H. The role of ligand efficiency metrics in drug discovery. in *Nat Rev Drug Discov*, Vol. 13 105-21 (England, 2014).
277. Jiang, K.L. et al. Neutrophil elastase and its therapeutic effect on leukemia cells. *Mol Med Rep* **12**, 4165-4172 (2015).
278. Kuraki, T., Ishibashi, M., Takayama, M., Shiraishi, M. & Yoshida, M. A novel oral neutrophil elastase inhibitor (ONO-6818) inhibits human neutrophil elastase-induced emphysema in rats. *Am J Respir Crit Care Med* **166**, 496-500 (2002).
279. Llinas, A. et al. Inactivation of bacterial DD-peptidase by beta-sultams. *Biochemistry* **44**, 7738-7746 (2005).
280. Tsang, W.Y. et al. Different transition-state structures for the reactions of beta-lactams and analogous beta-sultams with serine beta-lactamases. *Journal of the American Chemical Society* **127**, 17556-17564 (2005).
281. Beardsell, M. et al. beta-Sultams - A novel class of serine protease inhibitors. *Chemical Communications*, 497-498 (2001).
282. Dong, J.J., Krasnova, L., Finn, M.G. & Sharpless, K.B. Sulfur(VI) Fluoride Exchange (SuFEx): Another Good Reaction for Click Chemistry. *Angewandte Chemie-International Edition* **53**, 9430-9448 (2014).
283. Narayanan, A. & Jones, L.H. Sulfonyl fluorides as privileged warheads in chemical biology. *Chemical Science* **6**, 2650-2659 (2015).
284. Jones, L.H. Emerging Utility of Fluorosulfate Chemical Probes. *Acs Medicinal Chemistry Letters* **9**, 584-586 (2018).
285. Maes, M.B. et al. Dipeptidyl peptidase 8/9-like activity in human leukocytes. *J Leukoc Biol* **81**, 1252-7 (2007).

286. Longo, P.A., Kavran, J.M., Kim, M.S. & Leahy, D.J. Transient mammalian cell transfection with polyethylenimine (PEI). *Methods Enzymol* **529**, 227-40 (2013).
287. Owen, C.A. Leukocyte cell surface proteinases: regulation of expression, functions, and mechanisms of surface localization. *Int J Biochem Cell Biol* **40**, 1246-72 (2008).
288. Bezerra, G.A. et al. Structures of human DPP7 reveal the molecular basis of specific inhibition and the architectural diversity of proline-specific peptidases. *PLoS One* **7**, e43019 (2012).
289. Reker, D., Bernardes, G.J.L. & Rodrigues, T. Computational advances in combating colloidal aggregation in drug discovery. *Nat Chem* **11**, 402-418 (2019).
290. Chanmiya Sheikh, M. et al. Studies on the Lossen-type rearrangement of N-(3-phenylpropionyloxy) phthalimide and N-tosyloxy derivatives with several nucleophiles. *Tetrahedron* **66**, 2132-2140 (2010).
291. Falcao, A.S. et al. Dipeptidyl Vinyl Sulfone as a Novel Chemical Tool to Inhibit HMGB1/NLRP3-Inflammasome and Inflamma-miRs in Abeta-Mediated Microglial Inflammation. *ACS Chem Neurosci* **8**, 89-99 (2017).
292. Palmer, J.T., Rasnick, D., Klaus, J.L. & Bromme, D. Vinyl sulfones as mechanism-based cysteine protease inhibitors. *J Med Chem* **38**, 3193-6 (1995).

Attachments

S1. General Considerations

Chemicals, enzymes and solvents were purchased from reputable commercial suppliers and used without further purification. Reactions were monitored using Merck silica gel TLC plates (0.25 mm, 60 F_{254}). Compound purification by flash chromatography used SilicaFlash F60 silica gel (40–63 μm, 60 Å). When indicated, flash chromatography was performed in a Combi Flash RF-200 device from Teledyne Isco with RediSep normal- or reverse-phase (C18) silica flash columns. Chemical reactions were followed by thin layer chromatography (TLC) using Merck aluminium backed sheets coated with 60 F_{254} silica gel and visualized in a UV lamp (λ_{max} = 254 nm). Nuclear magnetic resonance experiments (^{1}H and ^{13}C NMR) were performed at room temperature on a Bruker Avance 300, Bruker DRX-500, Varian Inova-400 or Bruker DRX-600 (5 mm DCH Cryoprobe) instruments. Chemical shifts are reported in the δ scale in ppm, relative to tetramethylsilane (TMS). Peak multiplicity is reported as: chemical shift, multiplicity (s = singlet, bs = broad singlet, d = doublet, t = triplet, q = quartet, m = multiplet, bm = broad multiplet), coupling constant (Hz). High-resolution mass spectra (HRMS) were obtained from an Agilent LC/MSD TOF mass spectrometer by electrospray ionization–time-of-flight (ESI-TOF) at the TSRI Center for Mass Spectrometry or from a QqTOF Impact II™ mass spectrometer (Bruker Daltonics) at Instituto Superior Técnico. Low-resolution mass spectra were recorded using Micromass Quattro Micro API mass spectrometer, using electrospray ionization technique. Protein separations by SDS−PAGE were performed using 10% acrylamide gels at 300V and samples were visualized by in-gel fluorescence scanning using a ChemiDoc MP system (Bio-Rad). The resulting data was processed using the Image Lab (5.2.1) software (Bio-Rad), SDS-PAGE images were optimized using appropriate imaging software to enhance contrast when needed or to crop parts of the image without scientific relevance. Culture media and supplements for cell culture were purchased from Life Technologies. Reagents and probes for cell treatment were prepared as stock solutions (1000x) in DMSO and stored at -20°C. Crystallography details for the work developed with the 3-Oxo-β-Sultams are presented in section S3. The crystallography experiments between 4-Oxo-β-Lactams and DPP8/DPP9 are ongoing and are presented in the main text as preliminary results; the experimental methods used the obtain the results will not be presented here. Pyroptosis

induction assays were performed by measuring cell viability of a DPP8/9 inhibitor sensitive AML cell line, MV4;11 using a CellTiter-Glo assay kit.

S2. NMR Characterization

S2.1. 3-Oxo-β-Sultams

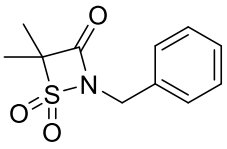

(56) 2-benzyl-4,4-dimethyl-1,2-thiazetidin-3-one 1,1-dioxide. The dichloride **62** (663mg, 2.8mmol) was stirred in dry diethyl ether (7mL) at 0°C under nitrogen atmosphere. Benzylamine (0.920mL, 8.4mmol) in dry diethyl ether (7mL) was very slowly added dropwise. The reaction was stirred at 0°C for 30 minutes and then allowed to reach room temperature and stirred overnight. The precipitate that formed was filtered and washed with hexane. Evaporation of the filtrate yielded **56** as white crystals (612mg, 2.6mmol, 91%). ^{1}H NMR (300 MHz, $CDCl_3$) δ 7.29 (s, 5H), 4.51 (s, 2H), 1.64 (s, 6H). ^{13}C NMR (75 MHz, $CDCl_3$) δ 164.43, 133.26, 129.03, 128.58, 128.16, 83.12, 44.51, 18.45.

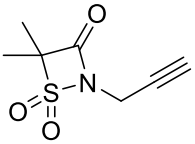

(69) 4,4-dimethyl-2-(prop-2-yn-1-yl)-1,2-thiazetidin-3-one 1,1-dioxide. 2-(chlorosulfonyl)-2-methylpropanoyl chloride (1,568g, 6,6mmol) was stirred in dry diethyl ether (17mL) at 0°C under nitrogen atmosphere. Propargylamine (0.508mL, 7.9mmol) in dry diethyl ether (9mL) was very slowly added dropwise. The reaction was stirred at 0°C for 30 minutes and then triethylamine (2.114mL, 15.2mmol) in dry ether (9mL) was slowly added. The reaction was allowed to reach room temperature and stirred overnight. The precipitate that formed was filtered and washed with diethyl ether. Evaporation of the filtrate yielded **69** as white crystals (920mg, 4.9mmol, 74%). ^{1}H NMR (300 MHz, CDCl3) δ 4.22 (d, J = 2.6 Hz, 2H), 2.44 (t, J = 2.6 Hz, 1H), 1.75 (s, 6H). ^{13}C NMR (75 MHz, CDCl3) δ 163.68, 83.62, 74.55, 73.92, 29.58, 18.36. Accurate mass: 188.0374; HRMS: 188.0376.

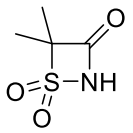

(71) 4,4-dimethyl-1,2-thiazetidin-3-one 1,1-dioxide. Dry diethyl ether was stirred in a pressure tube at -78°C under nitrogen atmosphere. Ammonia gas was bubbled in the solvent, until the desired amount was obtained inside the tube by condensation. The dichloride **62** (xx mg, xx mmol) was added very slowly dropwise through a septum. The reaction was stirred at -78°C for 30 minutes and then left to reach room temperature and react overnight. The system was opened to allow evaporation of the excess ammonia and the solvent. The next day the solid residue that formed was dissolved with DCM and water and poured into an extraction flask. The product was extracted with DCM. The organic layers were dried and concentrated under reduced pressure, yielding the product **71** as white crystals (92mg, 0.62mmol, 49%). ^{1}H NMR (300 MHz, $CDCl_3$) δ 1.76 (s, 1H). ^{13}C NMR (75 MHz, $CDCl_3$) δ 164.05, 82.36, 18.56.

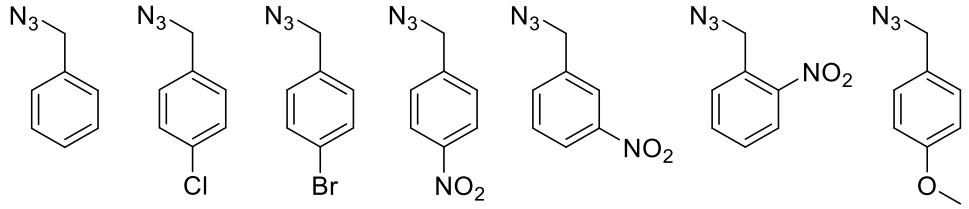

General method for the synthesis of benzylic azides (A): 200mg of an halogenated benzylic compound was dissolved in DMSO (30mL). Sodium Azide (1.3eq) was added and the reaction was stirred overnight at room temperature under nitrogen atmosphere. Full conversion of the starting material was observed by TLC and a single new chemical entity was observed. 50mL of water were added to the solution and the product was extracted with diethyl ether (3 x 10 mL). The organic fractions were combined, dried with anhydrous sodium sulfate and filtered. 1 mL of DMSO was added to the solution and the diethyl ether was evaporated under reduced pressure, resulting in a solution of the respective azide in DMSO. The azides were stored as DMSO solutions and used without

further purification to avoid concentration of potentially explosive azides. A quantitative yield was assumed for the calculation of the concentration of azide solutions. (**Az1**) (azidomethyl)benzene. The compound was purchased from Sigma-Aldricht. (**Az2**) 1-(azidomethyl)-4-chlorobenzene. Synthesized from 1-chloro-4-(chloromethyl)benzene using the general method A. (**Az3**) 1-(azidomethyl)-4-bromobenzene. Synthesized from 1-bromo-4-(bromomethyl)benzene using the general method A. (**Az4**) 1-(azidomethyl)-4-nitrobenzene. Synthesized from 1-(chloromethyl)-4-nitrobenzene using the general method A. (**Az5**) 1-(azidomethyl)-3-nitrobenzene. Synthesized from 1-(chloromethyl)-3-nitrobenzene using the general method A. (**Az6**) 1-(azidomethyl)-2-nitrobenzene. Synthesized from 1-(bromomethyl)-2-nitrobenzene using the general method A. (**Az7**) 1-(azidomethyl)-4-methoxybenzene. Synthesized from 1-(chloromethyl)-4-methoxybenzene using the general method A.

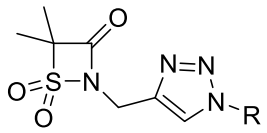

General method for the derivatization of 3-Oxo-β-Sultams by CuAAC (B): Alkyne-derived 3-Oxo-β-Sultam (**69** or **92**) was dissolved in DMSO and stirred at room temperature. $CuSO_4$ (0.1 M, 10% eq.M) and Sodium Ascorbate (0.2 M, 20% eq.M) were added. After 10 minutes the corresponding azide was added. The reaction was stirred overnight at room temperature under nitrogen atmosphere.

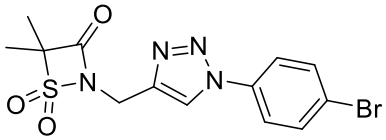

(**93**) **2-((1-(4-bromophenyl)-1H-1,2,3-triazol-4-yl)methyl)-4,4-dimethyl-1,2-thiazetidin-3-one 1,1-dioxide**. From the general method B using azide 1-azido-4-bromobenzene (1.5eq). After stirring overnight, a white solid precipitated in the reaction medium. The solid was filtered and recrystallized from acetonitrile and water, yielding **93** as a white solid (36mg, 0.093mmol, 25%). ^{1}H NMR (300 MHz, DMSO) δ 8.89 (s,

1H), 7.90 (d, J = 9.0 Hz, 2H), 7.82 (d, J = 9.0 Hz, 2H), 4.85 (s, 2H), 1.68 (s, 6H). ^{13}C NMR (75 MHz, DMSO) δ 164.64, 141.79, 136.08, 133.34, 122.50, 122.01, 84.00, 35.44, 18.20. ESI + [M + 1] = 386.81. Accurate mass: 384.9960; HRMS: 384.9964.

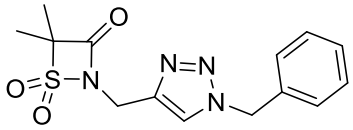

(70) 2-((1-benzyl-1H-1,2,3-triazol-4-yl)methyl)-4,4-dimethyl-1,2-thiazetidin-3-one 1,1-dioxide. From the general method B using azide Az1 (1.2eq). After stirring overnight, the product was precipitated in the reaction medium by adding 5 mL of water. Filtration of the solid yielded **70** as a white solid (48mg, 0.15mmol, 40%). ^{1}H NMR (300 MHz, DMSO) δ 8.21 (s, 1H), 7.39 – 7.26 (m, 5H), 5.63 (s, 2H), 4.75 (s, 2H), 1.64 (s, 6H). ^{13}C NMR (75 MHz, DMSO) δ 164.62, 140.61, 136.46, 129.21, 128.60, 128.26, 124.60, 83.83, 53.26, 35.63, 18.16. ESI + [M + 1] = 321.19. Accurate mass: 321.1012; HRMS: 321.1016.

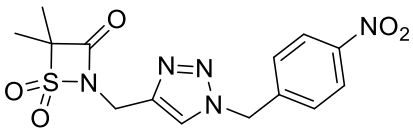

(96) 4,4-dimethyl-2-((1-(4-nitrobenzyl)-1H-1,2,3-triazol-4-yl)methyl)-1,2-thiazetidin-3-one 1,1-dioxide. From the general method B using azide Az4. After reacting overnight 25 mL of water were added to the reaction. The product was extracted with ethyl acetate (3 x 10 mL). The organic fractions were combined, dried with anhydrous sodium sulfate and concentrated under reduced pressure. The product was recrystallized from acetonitrile and water, yielding **96** as a white solid (16mg, 0.044mmol, 12%). ^{1}H NMR (300 MHz, DMSO) δ 8.29 (s, 1H), 8.23 (d, J = 8.8 Hz, 2H), 7.50 (d, J = 8.8Hz, 2H), 5.81 (s, 2H), 4.77 (s, 2H), 1.64 (s, 6H). ^{13}C NMR (75 MHz, Acetone) δ 164.92, 148.72, 144.26, 141.93, 129.70, 125.03, 124.68, 84.11, 53.32, 36.13, 18.28. ESI + [M + 1] = 366.18. Accurate mass: 366.0865; HRMS: 366.0867.

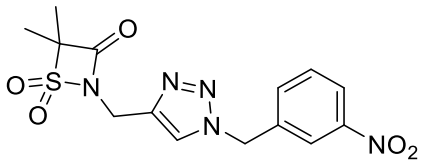

(**97**) DiMe-3-Oxo-β-Sultam-Triazole-Bn-3-NO2. From the general method B using azide Az5. After reacting overnight 10 mL of water were added to the reaction, causing a white solid to precipitate. The solid was filtered and washed with water, yielding **97** as a white solid (94 mg, 0.26 mmol, 60%). ^{1}H NMR (300 MHz, DMSO) δ 8.31 (s, 1H), 8.23 – 8.17 (m, 2H), 7.76 – 7.64 (m, 2H), 5.81 (s, 2H), 4.77 (s, 2H), 1.64 (s, 6H). ^{13}C NMR (75 MHz, DMSO) δ 164.61, 148.33, 140.84, 138.57, 135.05, 130.87, 124.92, 123.61, 123.17, 83.85, 52.22, 35.60, 18.14. ESI + [M + 1] = 366.20. Accurate mass: 366.0866; HRMS: 366.0867.

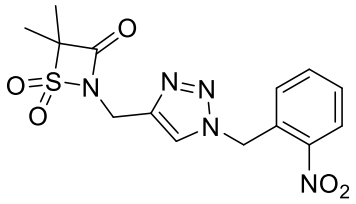

(**98**) DiMe-3-Oxo-β-Sultam-Triazole-Bn-2-NO2. From the general method B using azide Az6. After reacting overnight 10 mL of water were added to the reaction, causing a white solid to precipitate. The solid was filtered and washed with water, yielding **98** as a white solid (69 mg, 0.19 mmol, 44%). ^{1}H NMR (300 MHz, DMSO) δ 8.22 (s, 1H), 8.15 (d, J = 7.8 Hz, 1H), 7.67 (dt, J = 25.6, 7.3 Hz, 2H), 6.94 (d, J = 7.5 Hz, 1H), 6.00 (s, 2H), 4.80 (s, 2H), 1.64 (s, 6H). ^{13}C NMR (75 MHz, DMSO) δ 164.14, 147.45, 140.30, 134.33, 131.08, 129.61, 125.10, 125.03, 83.41, 50.05, 35.20, 17.69. ESI + [M + 1] = 366.20. Accurate mass: 366.0866; HRMS: 366.0867.

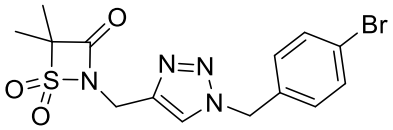

(**95**) **2-((1-(4-bromobenzyl)-1H-1,2,3-triazol-4-yl)methyl)-4,4-dimethyl-1,2-thiazetidin-3-one 1,1-dioxide**. From the general method B using azide Az3. After

reacting overnight 25 mL of water were added. The product was extracted with ethyl acetate (3 x 10 mL). The organic fractions were combined, dried with anhydrous sodium sulfate and concentrated under reduced pressure. The product was recrystallized from acetonitrile and water, yielding **95** as a white solid (176 mg, 0.817 mmol, 60%). ^{1}H NMR (300 MHz, DMSO) δ 8.21 (s, 1H), 7.57 (d, J = 8.4 Hz, 2H), 7.24 (d, J = 8.4 Hz, 2H), 5.61 (s, 2H), 4.75 (s, 2H), 1.64 (s, 6H). ^{13}C NMR (75 MHz, DMSO) δ 164.60, 140.68, 135.86, 132.13, 130.55, 124.66, 121.88, 83.84, 52.52, 35.60, 18.15. ESI + [M + 1] = 401.1. Accurate mass: 399.0120; HRMS: 399.0121.

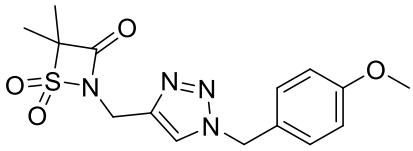

(99) 2-((1-(4-methoxybenzyl)-1H-1,2,3-triazol-4-yl)methyl)-4,4-dimethyl-1,2-thiazetidin-3-one 1,1-dioxide. From the general method B using azide **Az7**. After reacting overnight 25 mL of water were added. The product was extracted with ethyl acetate (3 x 10 mL). The organic fractions were combined, dried with anhydrous sodium sulfate and concentrated under reduced pressure. The product was recrystallized from acetonitrile and water, yielding **99** as a white solid (95mg, 0.27mmol, 63%). ^{1}H NMR (300 MHz, DMSO) δ 8.15 (s, 1H), 7.28 (d, *J* = 8.3 Hz, 2H), 6.92 (d, *J* = 8.4 Hz, 2H), 5.53 (s, 2H), 4.73 (s, 2H), 3.73 (s, 3H), 1.63 (s, 6H). ^{13}C NMR (75 MHz, DMSO) δ 164.17, 159.15, 140.15, 129.54, 127.88, 123.79, 114.11, 83.36, 55.14, 52.39, 35.16, 17.71. ESI + [M + 1] = 351.20. HRMS

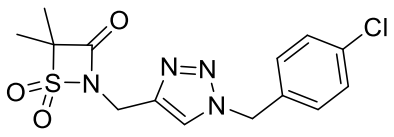

(**94**) **2-((1-(4-chlorobenzyl)-1H-1,2,3-triazol-4-yl)methyl)-4,4-dimethyl-1,2-thiazetidin-3-one 1,1-dioxide**. From the general method B using azide Az2. After reacting overnight a white solid precipitated in the reaction medium. 5 mL of water were added, leading to further precipitation of the solid. The solid was filtered and

recrystallized from ethyl acetate and hexane, yielding **94** as a white solid (71 mg, 0.20 mmol, 47%). ^{1}H NMR (300 MHz, DMSO) δ 8.22 (s, 1H), 7.45 (d, J = 8.6 Hz, 2H), 7.32 (d, J = 8.6 Hz, 2H), 5.63 (s, 2H), 4.75 (s, 2H), 1.64 (s, 6H). ^{13}C NMR (75 MHz, Acetone) δ 164.93, 141.73, 135.88, 134.50, 130.57, 129.70, 124.51, 84.05, 53.42, 36.10, 18.27. ESI + [M + 1] = 355.16. HRMS

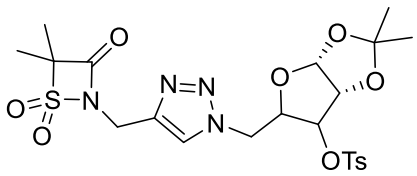

(**105**) **(3aR,6aR)-5-((4-((4,4-dimethyl-1,1-dioxido-3-oxo-1,2-thiazetidin-2-yl)methyl)-1H-1,2,3-triazol-1-yl)methyl)-2,2-dimethyltetrahydrofuro[2,3-d][1,3]dioxol-6-yl 4-methylbenzenesulfonate.** From the general method B and using the azide (3aR,6aR)-5-(azidomethyl)-2,2-dimethyltetrahydrofuro[2,3-d][1,3]dioxol-6-yl 4-methylbenzenesulfonate, which was readily available in the lab. After reacting overnight 25 mL of water were added. The product was extracted with ethyl acetate (3 x 10 mL). The organic layers were combined, dried with anhydrous sodium sulfate and concentrated under reduced pressure. The product was purified by combi flash chromatography (hexane: ethyl acetate gradient, 100% hexane to 100% ethyl acetate), yielding **105** as a white solid (77mg, 0.14mmol, 36%). ^{1}H NMR (300 MHz, CDCl3) δ 7.82 (d, J = 7.4 Hz, 2H), 7.73 (s, 1H), 7.40 (d, J = 6.9 Hz, 2H), 5.93 (s, 1H), 4.88 (s, 1H), 4.76 – 4.63 (m, 3H), 4.58 – 4.31 (m, 3H), 2.47 (s, 3H), 1.71 (s, 6H), 1.38 (s, 3H), 1.25 (s, 3H). ^{13}C NMR (75 MHz, CDCl3) δ 164.10, 146.23, 140.51, 132.37, 130.50, 128.03, 124.26, 113.02, 104.87, 83.43, 83.27, 81.74, 77.52, 49.22, 35.89, 26.57, 26.26, 21.85, 18.48. ESI + [M + 1] = 556.80. Accurate mass: 557.1372; HRMS: 557.1370.

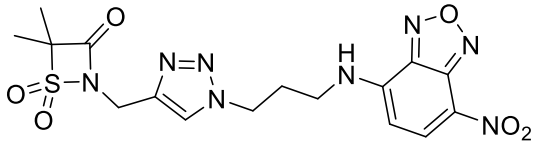

(**106**) **4,4-dimethyl-2-((1-(3-((7-nitrobenzo[c][1,2,5]oxadiazol-4-yl)amino)propyl)-1H-1,2,3-triazol-4-yl)methyl)-1,2-thiazetidin-3-one 1,1-dioxide**. From the general method B and using the azide N-(3-azidopropyl)-7-nitrobenzo[c][1,2,5]oxadiazol-4-amine. After reacting overnight, the solid that formed in the reaction medium was filtered and washed with hexane, yielding **106** as an orange solid (174mg, 0.39mmol, 72%). ^{1}H NMR (300 MHz, DMSO) δ 9.52 (s, 1H), 8.50 (d, J = 8.9 Hz, 1H), 8.19 (s, 1H), 6.33 (d, J = 8.5 Hz, 1H), 4.74 (s, 2H), 4.52 (t, J = 6.9 Hz, 2H), 3.48 (broad, 2H), 2.24 (q, 2H), 1.64 (s, 6H). ^{13}C NMR (75 MHz, DMSO) δ 164.15, 145.13, 144.52, 144.24, 139.91, 137.94, 124.11, 121.04, 99.23, 83.44, 47.17, 35.19, 28.36, 17.71. ESI - [M - 1] = 449.17. Accurate mass: 451.1143; HRMS: 451.1143.

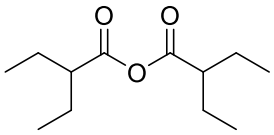

(66) 2-ethylbutanoic anhydride. 2-ethylbutanoic acid (10 mL, 79 mmol) was added to ethanol (40 mL) and then sodium (2.1 g, 91 mmol) was added. The reaction was stirred for 1h and then the solvent was evaporated under reduced pressure to yield sodium 2-ethylbutanoate as a white solid (14.097 g). 2-ethylbutanoic acid (10 mL, 79 mmol) was stirred with thionyl chloride (7 mL) for 1 h. The excess of thionyl chloride was evaporated, yielding 2-ethylbutanoyl chloride as a colorless liquid (9.945 g). Sodium 2-ethylbutanoate was dissolved in toluene (70 mL). 2-ethylbutanoyl chloride was slowly added to the solution. The reaction was refluxed at 115°C for 2h. Ice (70 g) was added to the reaction solution. Upon melting of the ice, the reaction was poured into an extraction vessel and the toluene fraction was collected. This fraction was dried with anhydrous sodium sulfate and evaporated under reduced pressure, yielding 66 as a colorless liquid (9.945 g, 46mmol, 59% yield). ^{1}H NMR (300 MHz, $CDCl_3$) δ 2.22 (tt, *J* = 8.3, 5.7 Hz, 2H), 1.73 – 1.46 (m, 8H), 0.93 (t, *J* = 7.4 Hz, 12H).

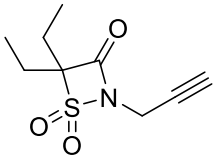

(92) 4,4-diethyl-2-(prop-2-yn-1-yl)-1,2-thiazetidin-3-one 1,1-dioxide. 2-(chlorosulfonyl)-2-ethylbutanoyl chloride (1.08g, 4.6 mmol) was stirred in dry diethyl ether (10 mL) at 0°C under nitrogen atmosphere. Propargylamine (0.330 mL, 5.2 mmol) in dry diethyl ether (10 mL) was very slowly added dropwise. The reaction was stirred at 0°C for 30 minutes and then triethylamine (1.36 mL, 9.8 mmol) in dry ether (10 mL) was slowly added. The reaction was allowed to reach room temperature and stirred overnight. The precipitate that formed was filtered and washed with diethyl ether. The filtrate was evaporated, concentrated under reduced pressure and purified by combi flash chromatography to obtain the product **92** as a colorless oil (0.63 g, 2.9 mmol, 63% yield). ^{1}H NMR (300 MHz, $CDCl_3$) δ 4.21 (d, *J* = 2.6 Hz, 2H), 2.42 (t, *J* = 2.6 Hz, 1H), 2.17 (qd, *J* = 7.5, 1.3 Hz, 4H), 1.13 (t, *J* = 7.5 Hz, 6H). ^{13}C NMR (75 MHz, $CDCl_3$) δ 163.07, 91.25, 74.42, 74.28, 29.31, 22.58, 8.53. Accurate mass: 216.0679; HRMS: 216.0689.

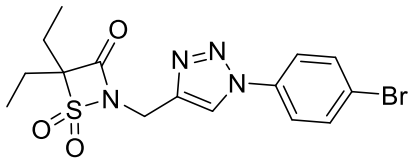

(**100**) **2-((1-(4-bromophenyl)-1H-1,2,3-triazol-4-yl)methyl)-4,4-diethyl-1,2-thiazetidin-3-one 1,1-dioxide**. From the general method B and using azide 1-azido-4-bromobenzene. After reacting overnight 25 mL of water were added. The product was extracted with ethyl acetate (3 x 10 mL). The organic layers were combined, dried with anhydrous sodium sulfate and concentrated under reduced pressure, yielding a green oil. Washing of the crude oil with diethyl ether led to precipitation of **100** as a green solid (74 mg, 0.34 mmol, 39%). ^{1}H NMR (300 MHz, CDCl3) δ 8.06 (s, 1H), 7.64 (q, J = 9.0 Hz, 4H), 4.85 (s, 2H), 2.18 (qd, J = 7.5, 1.2 Hz, 4H), 1.14 (t, J = 7.5 Hz, 6H). ^{13}C NMR (75 MHz, Chloroform-*d*) δ 163.32, 135.72, 132.96, 132.77, 122.75, 122.04, 120.68, 91.01, 35.45, 22.54, 8.44. Accurate mass: 413.0280; HRMS: 413.0277.

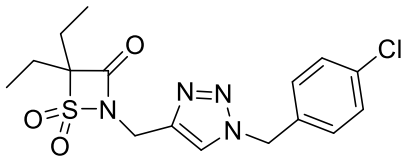

(**101**) **2-((1-(4-chlorobenzyl)-1H-1,2,3-triazol-4-yl)methyl)-4,4-diethyl-1,2-thiazetidin-3-one 1,1-dioxide**. From the general method B and using azide Az2. After reacting overnight 25 mL of water were added. The product was extracted with ethyl acetate (3 x 10 mL). The organic layers were combined, dried with anhydrous sodium sulfate and concentrated under reduced pressure, yielding a colorless oil. Washing of the crude oil with diethyl ether led to precipitation of **101** as a white solid (66 mg, 0.19 mmol, 40%). ^{1}H NMR (300 MHz, Chloroform-*d*) δ 7.56 (s, 0H), 7.35 (d, *J* = 8.5 Hz, 0H), 7.18 (d, *J* = 8.5 Hz, 0H), 5.51 (s, 0H), 4.75 (s, 0H), 2.14 (qd, *J* = 7.5, 1.9 Hz, 1H), 1.10 (t, *J* = 7.5 Hz, 1H). 13C NMR (75 MHz, CDCl3) δ 163.33, 135.74, 133.00, 122.81, 122.07, 91.04, 35.49, 22.56, 8.45. HRMS

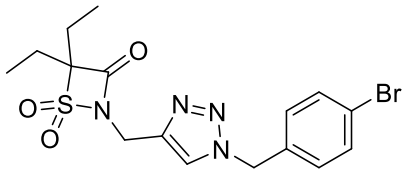

(**102**) DiEt-3-Oxo-β-Sultam-Triazole-PEG3-Bn-4-Br. From the general method B and using azide Az3. After reacting overnight 25 mL of water were added. The product was extracted with ethyl acetate (3 x 10 mL). The organic layers were combined, dried with anhydrous sodium sulfate and concentrated under reduced pressure, yielding a colorless oil. Washing of the crude oil with diethyl ether led to precipitation of **102** as a white solid (176 mg, 0.41 mmol, 60%). ^{1}H NMR (300 MHz, CDCl3) δ 7.69 (s, 1H), 7.50 (d, J = 8.3 Hz, 6H), 7.11 (d, J = 8.3 Hz, 5H), 5.49 (s, 5H), 4.75 (s, 5H), 2.19 – 2.10 (m, 10H), 1.10 (t, J = 7.4 Hz, 16H). ^{13}C NMR (75 MHz, Chloroform-d) δ 163.35, 133.44, 132.44, 129.69, 123.16, 91.05, 54.03, 35.65, 22.69, 8.54. Accurate mass: 427.0435; HRMS: 427.0434.

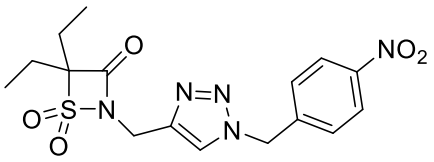

(**103**) **4,4-diethyl-2-((1-(4-nitrobenzyl)-1H-1,2,3-triazol-4-yl)methyl)-1,2-thiazetidin-3-one 1,1-dioxide**. From the general method B and using azide Az4. After reacting overnight 25 mL of water were added. The product was extracted with ethyl acetate (3 x 10 mL). The organic layers were combined, dried with anhydrous sodium sulfate and concentrated under reduced pressure, yielding a brown oil. Washing of the crude oil with diethyl ether led to precipitation of **103** as a brown solid (86 mg, 0,22 mmol, 47%). ^{1}H NMR (300 MHz, CDCl3) δ 8.22 (d, J = 8.5 Hz, 2H), 7.70 (s, 1H), 7.37 (d, J = 8.5 Hz, 2H), 5.66 (s, 2H), 4.78 (s, 2H), 2.15 (q, J = 7.3 Hz, 4H), 1.10 (t, J = 7.4 Hz, 6H). ^{13}C NMR (75 MHz, CDCl3) δ 163.23, 148.11, 141.39, 128.47, 124.34, 91.06, 53.30, 35.60, 22.56, 8.42. Accurate mass: 394.1183; HRMS: 394.1180.

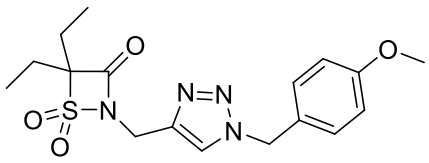

(**104**) **4,4-diethyl-2-((1-(4-methoxybenzyl)-1H-1,2,3-triazol-4-yl)methyl)-1,2-thiazetidin-3-one 1,1-dioxide**. From the general method B and using azide **Az7**. After reacting overnight 25 mL of water were added. The product was extracted with ethyl acetate (3 x 10 mL). The organic layers were combined, dried with anhydrous sodium sulfate and concentrated under reduced pressure, yielding an orange oil. Washing of the crude oil with diethyl ether led to precipitation of **104** as a yellow solid (74 mg, 0.18 mmol, 41%). ^{1}H NMR (300 MHz, CDCl3) δ 7.52 (s, 1H), 7.19 (d, J = 8.6 Hz, 2H), 6.87 (d, J = 8.7 Hz, 2H), 5.44 (s, 2H), 4.71 (s, 2H), 3.78 (s, 3H), 2.12 (qd, J = 7.4, 1.7 Hz, 4H), 1.08 (t, J = 7.5 Hz, 6H). ^{13}C NMR (75 MHz, CDCl3) δ 163.33, 160.03, 129.82, 129.65, 126.40, 122.69, 114.57, 90.91, 55.41, 53.93, 35.67, 22.61, 8.48. Accurate mass: 379.1435; HRMS: 379.1435.

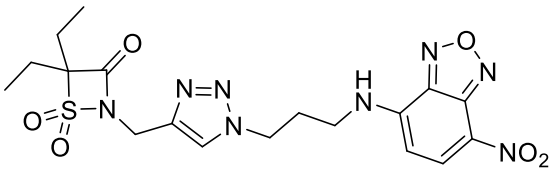

(**107**) **4,4-diethyl-2-((1-(3-((7-nitrobenzo[c][1,2,5]oxadiazol-4-yl)amino)propyl)-1H-1,2,3-triazol-4-yl)methyl)-1,2-thiazetidin-3-one 1,1-dioxide**. From the general method B and using azide **88**. After reacting overnight 25 mL of water were added. The product was extracted with ethyl acetate (4 x 10 mL). The organic layers were combined, dried with anhydrous sodium sulfate and concentrated under reduced pressure, yielding an orange oil. Washing of the crude oil with diethyl ether led to precipitation of **107** as an orange solid (132 mg, 0.27 mmol, 99%). ^{1}H NMR (500 MHz, Chloroform-*d*) δ 8.45 (d, *J* = 8.6 Hz, 0H), 7.75 (s, 0H), 6.96 (s, 0H), 6.16 (d, *J* = 8.6 Hz, 0H), 4.80 (s, 0H), 4.59 (t, *J* = 6.4 Hz, 0H), 3.58 (d, *J* = 6.4 Hz, 0H), 2.44 (t, 0H), 2.16 (qd, *J* = 7.5, 4.8 Hz, 1H), 1.12 (t, *J* = 7.5 Hz, 1H). ^{13}C NMR (75 MHz, CDCl3) δ 163.37, 144.39, 144.10, 143.98, 136.76, 123.87, 99.20, 91.25, 77.36, 47.93, 40.89, 35.73, 28.71, 22.61, 8.53. Accurate mass: 479.1461; HRMS: 479.1556.

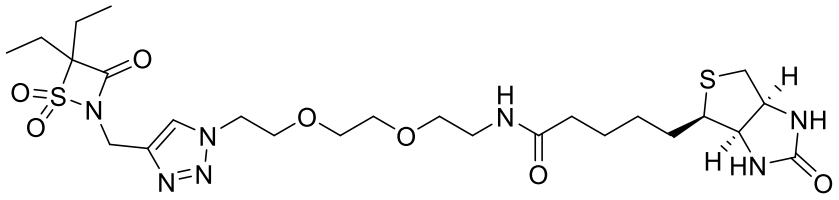

(**109**) **N-(2-(2-(2-(4-((4,4-diethyl-1,1-dioxido-3-oxo-1,2-thiazetidin-2-yl)methyl)-1H-1,2,3-triazol-1-yl)ethoxy)ethoxy)ethyl)-5-((3aR,4R,6aS)-2-oxohexahydro-1H-thieno[3,4-d]imidazol-4-yl)pentanamide**. From the general method B and using a commercially available biotin azide (TCI). 25mL of distilled water were added. The product was extracted with 3 x 10mL of EtOAc. The organic fractions were combined, dried with anhydrous sodium sulfate and concentrated under reduced pressure, resulting in a colorless oil. Washing of the crude oils with diethyl ether resulted in the pure product **109** as a colorless oil (0.07 g, 0.11 mmol, 91% yield); ^{1}H NMR (300 MHz, Chloroform-d) δ 7.82 (s, 0H), 7.28 (s, 0H), 6.59 (t, J = 5.5 Hz, 0H), 6.41 (s, 0H), 5.55 (s, 0H), 4.78 (s, 0H), 4.56 (t, J = 5.0 Hz, 0H), 4.49 (dd, J = 7.9, 4.8 Hz, 0H), 4.31 (dd, J = 8.2, 4.3 Hz, 0H),

3.89 (t, J = 5.1 Hz, 0H), 3.62 – 3.48 (m, 1H), 3.41 (q, J = 5.1 Hz, 0H), 3.15 (td, J = 7.3, 4.5 Hz, 0H), 2.90 (dd, J = 12.8, 4.9 Hz, 0H), 2.72 (d, J = 12.8 Hz, 0H), 2.27 – 2.08 (m, 1H), 1.77 – 1.58 (m, 1H), 1.45 (q, J = 7.5 Hz, 0H), 1.12 (t, J = 7.4 Hz, 1H). ^{13}C NMR (75 MHz, Chloroform-d) δ 173.28, 163.53, 163.31, 140.40, 124.04, 90.91, 70.48, 70.14, 69.96, 69.34, 61.79, 60.12, 55.45, 50.48, 41.01, 40.53, 39.16, 35.85, 35.62, 28.10, 25.53, 22.55, 8.44. HRMS

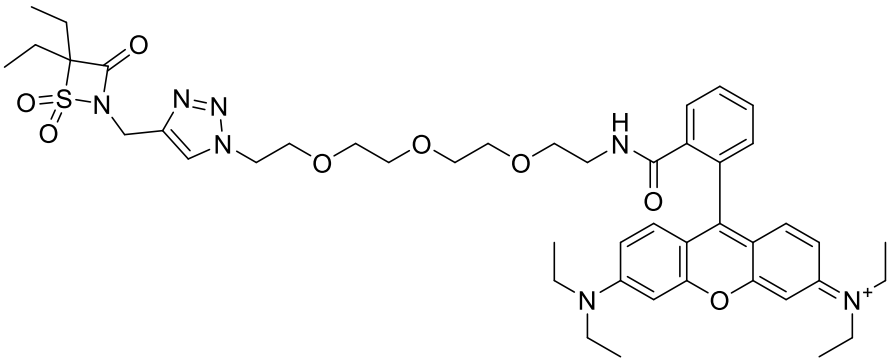

(**108**) **N-(9-(2-((2-(2-(2-(2-(4-((4,4-diethyl-1,1-dioxido-3-oxo-1,2-thiazetidin-2-yl)methyl)-1H-1,2,3-triazol-1-yl)ethoxy)ethoxy)ethoxy)ethyl)carbamoyl)phenyl)-6-(diethylamino)-3H-xanthen-3-ylidene)-N-ethylethanaminium**. From the general method B and using azide N-(9-(2-((2-(2-(2-(2-azidoethoxy)ethoxy)ethoxy)ethyl)carbamoyl)phenyl)-6-(diethylamino)-3H-xanthen-3-ylidene)-N-ethylethanaminium. 25mL of distilled water were added. The product was extracted with 3 x 10mL of EtOAc. The organic fractions were combined, dried with anhydrous sodium sulfate and concentrated under reduced pressure, resulting in a pink oil. The compound was purified using preparative thin layer chromatography (ethyl acetate: methanol – 9:1 eluent). **108** was obtained as a light pink solid (0.018 g, 0.02 mmol, 15% yield). ^{1}H NMR (300 MHz, CDCl3) δ 7.78 – 7.74 (m, 1H), 7.69 (s, 1H), 7.33 – 7.28 (m, J = 5.6, 3.1 Hz, 2H), 6.97 – 6.92 (m, 1H), 6.33 (s, 1H), 6.30 (s, 1H), 6.26 (d, J = 2.5 Hz, 2H), 6.15 (dd, J = 8.9, 2.6 Hz, 2H), 4.63 (s, 2H), 4.39 (t, J = 5.0 Hz, 2H), 3.68 (t, J = 12.8, 7.9 Hz, 2H), 3.43 (s, 4H), 3.39 – 3.31 (m, 2H), 3.31 – 3.15 (m, 12H), 3.05 (t, J = 7.3 Hz, 2H), 2.09 – 1.98 (m, J = 14.8, 7.5, 1.9 Hz, 4H), 1.09 – 0.94 (m, 18H). Add CNMR. Accurate mass: 858.4216; HRMS: 858.4219.

S2.2. 4-Oxo-β-Lactams

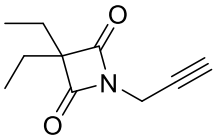

(111) 3,3-diethyl-1-(prop-2-yn-1-yl)azetidine-2,4-dione. Diethylmalonyl dichloride was dissolved in dioxan and cooled to 0ºC. Propargylamine in dioxan was very slowly added to the reaction. The suspension was stirred for 10 minutes and then triethylamine in dioxan was slowly added to the reaction. The reaction was allowed to reach room temperature and stirred overnight under nitrogen atmosphere. The solid in suspension was filtered and the filtrate was evaporated. The crude was purified by combi flash chromatography, yielding **111** as a colorless oil (70mg, 0.39mmol, 21%). ^{1}H NMR (300 MHz, $CDCl_3$) δ 4.02 (d, *J* = 2.6 Hz, 2H), 2.29 (t, *J* = 2.6 Hz, 1H), 1.70 (q, *J* = 7.5 Hz, 4H), 0.94 (t, *J* = 7.5 Hz, 6H). CARBON!

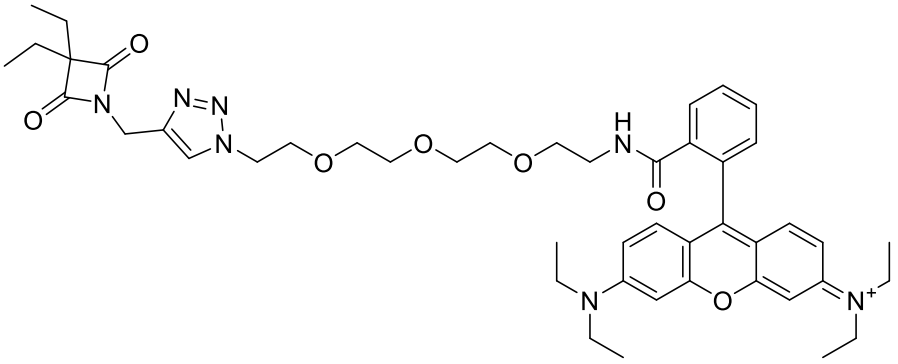

(**113**) **N-(9-(2-((2-(2-(2-(2-(4-((3,3-diethyl-2,4-dioxoazetidin-1-yl)methyl)-1H-1,2,3-triazol-1-yl)ethoxy)ethoxy)ethoxy)ethyl)carbamoyl)phenyl)-6-(diethylamino)-3H-xanthen-3-ylidene)-N-ethylethanaminium**. Compound **111** (30 mg, 0.167 mmol) was dissolved in DMSO (1 mL). $CuSO_4$ (1% (aq.) 10 eq. M) and sodium ascorbate (1% (aq.) 10 eq. M) were added and the solution was stirred for 10 minutes at room temperature. The azide **91** (1.1 eq) was added and the reaction was stirred for one hour. Water (5 mL) was added to the reaction and the product was extracted with 3 x 1 mL of EtOAc. The organic fractions were combined, dried with anhydrous sodium sulfate, and evaporated under reduced pressure. The product was purified via preparative thin layer

chromatography, yielding **113** as a pink oil (25 mg, 0.030 mmol, 18%). ^{1}H NMR (500 MHz, Chloroform-d) δ 7.90 – 7.84 (m, 1H), 7.74 (s, 1H), 7.44 – 7.39 (m, 2H), 7.09 – 7.03 (m, 1H), 6.43 (s, 1H), 6.41 (s, 1H), 6.36 (d, J = 2.6 Hz, 2H), 6.26 (dd, J = 8.9, 2.6 Hz, 2H), 4.60 (s, 2H), 4.50 – 4.46 (m, 2H), 3.79 (dd, J = 5.4, 4.6 Hz, 2H), 3.53 (s, 4H), 3.50 – 3.45 (m, 2H), 3.42 – 3.38 (m, 2H), 3.33 (q, J = 7.1 Hz, 10H), 3.17 (dd, J = 8.0, 6.7 Hz, 2H), 1.72 (q, J = 7.5 Hz, 4H), 1.16 (t, J = 7.0 Hz, 12H), 0.94 (t, J = 7.5 Hz, 6H). ^{13}C NMR (151 MHz, Chloroform-d) δ 173.30, 167.77, 153.31, 152.79, 148.30, 140.63, 131.93, 130.49, 128.37, 127.51, 123.33, 123.24, 122.25, 107.60, 105.06, 97.31, 70.54, 70.09, 70.00, 69.99, 69.50, 68.90, 67.34, 64.35, 52.98, 49.91, 43.90, 38.79, 33.59, 23.07, 12.15, 8.72. Accurate mass: 822.4549; HRMS:

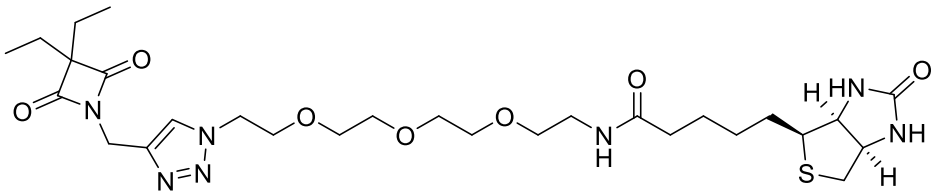

(**112**) **N-(2-(2-(2-(2-(4-((3,3-diethyl-2,4-dioxoazetidin-1-yl)methyl)-1H-1,2,3-triazol-1-yl)ethoxy)ethoxy)ethoxy)ethyl)-5-((3aS,4S,6aR)-2-oxohexahydro-1H-thieno[3,4-d]imidazol-4-yl)pentanamide**. Compound **111** (30 mg, 0.167 mmol) was dissolved in DMSO (1 mL). $CuSO_4$ (1% (aq.) 10 eq. M) and sodium ascorbate (2% (aq.) 10 eq. M) were added and the solution was stirred for 10 minutes at room temperature. A Biotin-PEG_3-azide (1.1 eq) was added and the reaction was stirred for one hour. Water (5 mL) was added to the reaction and the product was extracted with 3 x 1 mL of EtOAc. The organic fractions were combined, dried with anhydrous sodium sulfate, and evaporated under reduced pressure. The crude mixture was washed with diethyl ether, yielding compound **112** as a colorless oil (43 mg, 0.069 mmol, 41%). ^{1}H NMR (500 MHz, Chloroform-d) δ 7.79 (s, 1H), 6.70 (s, 1H), 6.42 (s, 1H), 5.49 (s, 1H), 4.64 (s, 2H), 4.56 (t, J = 5.0 Hz, 1H), 4.52 (dd, J = 7.8, 4.8 Hz, 1H), 4.33 (dd, J = 7.8, 4.5 Hz, 2H), 3.89 (t, J = 5.0 Hz, 6H), 3.61 (s, 2H), 3.58 (t, J = 5.1 Hz, 2H), 3.48 – 3.40 (m, 1H), 3.17 (s, 1H), 2.92 (d, J = 12.2 Hz, 1H), 2.76 (d, J = 12.8 Hz, 2H), 2.24 (t, J = 7.4 Hz, 1H), 1.83 – 1.60 (m, 8H), 1.49 – 1.40 (m, 2H), 0.97 (t, J = 7.5 Hz, 6H). ^{13}C NMR (126 MHz, Chloroform-d) δ 173.84, 173.32, 71.03, 70.57, 70.41, 70.40, 70.07, 69.95, 69.42, 61.81, 60.21, 55.55,

50.41, 40.53, 39.15, 35.93, 34.03, 28.19, 28.11, 25.59, 23.52, 9.21. Accurate mass: 623.3101; HRMS:

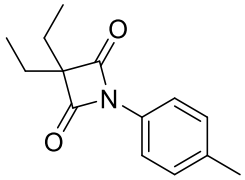

(114) 3,3-diethyl-1-(p-tolyl)azetidine-2,4-dione. Diethyl malonyl dichloride (1.5 g, 7.61 mmol) was dissolved in DCM (15 mL) and the mixture was cooled to 0°C. p-toluidine (0.75 eq.) and triethylamine (2 eq.) were mixed with DCM (30 mL) and added dropwise. The reaction was stirred for 1h at 0°C and then allowed to reach room temperature and stirred for an additional 4h. The solvent was evaporated under reduced pressure. The solid residue was purified by column chromatography (hexane 9:1 ethyl acetate) to yield compound **114** as a colorless oil (1.202 g, 5.20 mmol, 91 %). ^{1}H NMR (500 MHz, Chloroform-*d*) δ 7.71 (d, *J* = 8.4 Hz, 2H), 7.21 (dt, *J* = 8.1, 0.7 Hz, 2H), 2.35 (s, 3H), 1.85 (q, *J* = 7.5 Hz, 4H), 1.06 (t, *J* = 7.5 Hz, 6H). ^{13}C NMR (126 MHz, Chloroform-*d*) δ 172.39, 136.82, 131.47, 129.84, 119.33, 72.14, 24.09, 21.31, 9.37.

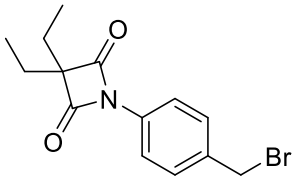

(115) 1-(4-(bromomethyl)phenyl)-3,3-diethylazetidine-2,4-dione. The toluidine-modified 4-Oxo-β-Lactam (1 g, 4.32 mmol) was dissolved in acetonitrile (40 mL). NBS (1.1 eq) and benzoyl peroxide (0.1 eq.). The reaction was refluxed overnight. The solvent was evaporated under reduced pressure. The brominated compound was purified by column chromatography (hexane 9:1 ethyl acetate), which yields the product **115** with trace amount of starting material. The mixture was used without further purification.

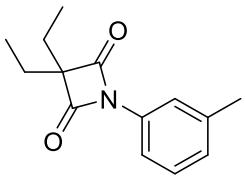

(131) 3,3-diethyl-1-(m-tolyl)azetidine-2,4-dione. Diethyl malonyl dichloride (1.5 g, 7.61 mmol) was dissolved in DCM (15 mL) and the mixture was cooled to 0°C. m-toluidine (0.75 eq.) and triethylamine (2 eq.) were mixed with DCM (30 mL) and added dropwise. The reaction was stirred for 1h at 0°C and then allowed to reach room temperature and stirred for an additional 4h. The solvent was evaporated under reduced pressure. The solid residue was purified by column chromatography (hexane 9:1 ethyl acetate) to yield compound **131** as a colorless oil (1.294 g, 5.59 mmol, 98 %). ^{1}H NMR (300 MHz, Chloroform-d) δ 7.70 – 7.54 (m, 0H), 7.29 (t, J = 7.8 Hz, 0H), 7.08 (ddt, J = 7.6, 1.8, 0.9 Hz, 0H), 2.42 – 2.31 (m, 1H), 1.85 (q, J = 7.5 Hz, 1H), 1.06 (t, J = 7.5 Hz, 1H). CNMR!

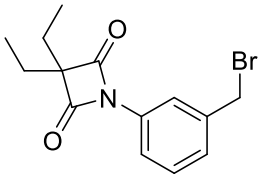

(S1) 1-(3-(bromomethyl)phenyl)-3,3-diethylazetidine-2,4-dione. The toluidine-modified 4-Oxo-β-Lactam (1 g, 4.32 mmol) was dissolved in acetonitrile (40 mL). NBS (1.1 eq.) and benzoyl peroxide (0.1 eq.). The reaction was refluxed overnight. The solvent was evaporated under reduced pressure. The brominated compound was purified by column chromatography (hexane 9:1 ethyl acetate), which yields the product **S1** with remnants on starting material. The mixture was used without further purification.

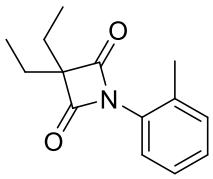

(140) 3,3-diethyl-1-(o-tolyl)azetidine-2,4-dione. Diethyl malonyl dichloride (1.5 g, 7.61 mmol) was dissolved in DCM (15 mL) and the mixture was cooled to 0°C. o-toluidine (0.75 eq.) and triethylamine (2 eq.) were mixed with DCM (30 mL) and added dropwise. The reaction was stirred for 1h at 0°C and then allowed to reach room temperature and stirred for an additional 4h. The solvent was evaporated under reduced pressure. The solid residue was purified by column chromatography (hexane 9:1 ethyl acetate) to yield compound **140** as a colorless oil (1.056 g, 4.57 mmol, 80 %).^{1}H NMR (500 MHz, Chloroform-d) δ 7.29 – 7.27 (m, 0H), 7.25 – 7.23 (m, 0H), 2.35 (s, 0H), 1.88 (q, J = 7.5 Hz, 1H), 1.14 (t, J = 7.5 Hz, 1H). ^{13}C NMR (126 MHz, Chloroform-*d*) δ 172.81, 133.83, 131.42, 129.86, 129.01, 126.67, 125.60, 70.77, 24.11, 18.82, 9.50.

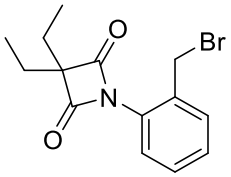

(S2) 1-(2-(bromomethyl)phenyl)-3,3-diethylazetidine-2,4-dione. The toluidine-modified 4-Oxo-β-Lactam (781 mg, 3.38 mmol) was dissolved in acetonitrile (31 mL). NBS (1.1 eq.) and benzoyl peroxide (0.1 eq.). The reaction was refluxed overnight. The solvent was evaporated under reduced pressure. The brominated compound was purified by column chromatography (hexane 9:1 ethyl acetate), which yields product **S2** with remnants on starting material. The mixture was used without further purification.

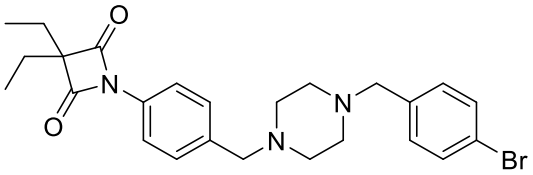

(117) 1-(4-((4-(4-bromobenzyl)piperazin-1-yl)methyl)phenyl)-3,3-diethylazetidine-2,4-dione. Compound **115** (60 mg, 0.19 mmol) was dissolved in acetonitrile (2 mL). 1-(4-bromobenzyl)piperazine (1.1 eq.) was added, followed by K_2CO_3 (1.1 eq.) and the reaction was heated to 60°C for 4h. Water 5 mL was added. The compound was extracted with 3 x 3 mL of ethyl acetate. The organic fractions were collected, combined, dried with anhydrous sodium sulfate and evaporated under reduced pressure. Compound **117** was purified from the crude mixture by preparative thin-layer chromatography (hexane 2:1 EtOAc) and obtained as a colorless oil (31 mg, 0.064 mmol, 33 %). ^{1}H NMR (600 MHz, Chloroform-*d*) δ 7.76 (d, *J* = 8.5 Hz, 2H), 7.42 (d, *J* = 8.3 Hz, 2H), 7.36 (d, *J* = 8.5 Hz, 2H), 7.19 (d, *J* = 8.3 Hz, 2H), 3.50 (s, 2H), 3.45 (s, 2H), 2.45 (s, 4H), 1.85 (q, *J* = 7.5 Hz, 4H), 1.06 (t, *J* = 7.5 Hz, 6H). ^{13}C NMR (151 MHz, Chloroform-*d*) δ 172.32, 137.28, 136.99, 132.76, 131.43, 130.92, 130.03, 120.97, 119.25, 72.22, 62.54, 62.35, 53.09, 53.07, 24.09, 9.37. Accurate mass: 484.1594; HRMS: 484.1599.

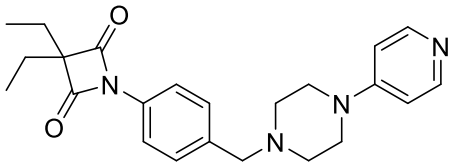

(121) 3,3-diethyl-1-(4-((4-(pyridin-4-yl)piperazin-1-yl)methyl)phenyl)azetidine-2,4-dione. Compound **115** (60 mg, 0.19 mmol) was dissolved in acetonitrile (2 mL). 1-(pyridin-4-yl)piperazine (1.1 eq.) was added, followed by K_2CO_3 (1.1 eq.) and the reaction was heated to 60°C for 4h. Water 5 mL was added. The compound was extracted with 3 x 3 mL of ethyl acetate. The organic fractions were collected, combined, dried with anhydrous sodium sulfate and evaporated under reduced pressure. Product **121** was purified from the crude mixture by preparative thin-layer chromatography (DCM 9:1 MeOH) and obtained as a colorless oil (8.6 mg, 0.022 mmol, 11 %). ^{1}H NMR (500 MHz, Chloroform-*d*) δ 8.26 (d, *J* = 6.0 Hz, 0H), 7.82 (d, *J* = 8.5 Hz, 0H), 7.41 (d, *J* = 8.5 Hz, 0H), 6.70 (d, 0H), 3.57 (s, 0H), 3.43 – 3.40 (m, 1H), 2.60 – 2.57 (m, 1H), 1.88 (q, *J* = 7.5

Hz, 1H), 1.09 (t, *J* = 7.5 Hz, 1H). ^{13}C NMR (126 MHz, Chloroform-*d*) δ 172.35, 155.92, 146.00, 136.27, 133.07, 129.99, 119.45, 107.93, 72.34, 62.34, 52.37, 46.15, 24.10, 9.38. Accurate mass: 393.2285; HRMS: 393.2291.

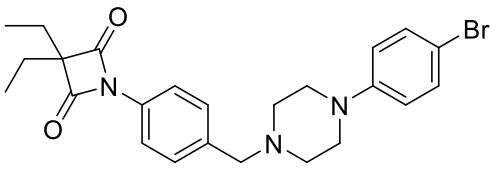

(122) 1-(4-((4-(4-bromophenyl)piperazin-1-yl)methyl)phenyl)-3,3-diethylazetidine-2,4-dione. Compound **115** (60 mg, 0.19 mmol) was dissolved in acetonitrile (2 mL). 1-(4-bromophenyl)piperazine (1.1 eq.) was added, followed by K_2CO_3 (1.1 eq.) and the reaction was heated to 60°C for 4h. Water 5 mL was added. The compound was extracted with 3 x 3 mL of ethyl acetate. The organic fractions were collected, combined, dried with anhydrous sodium sulfate and evaporated under reduced pressure. Product **122** was purified from the crude mixture by preparative thin-layer chromatography (hexane 4:1 EtOAc) and obtained as a colorless oil (50 mg, 0.11 mmol, 55 %). ^{1}H NMR (500 MHz, Chloroform-*d*) δ 7.80 (d, *J* = 8.5 Hz, 0H), 7.42 (d, *J* = 8.1 Hz, 0H), 7.35 – 7.30 (m, 0H), 6.79 – 6.75 (m, 0H), 3.58 (s, 0H), 3.18 (s, 0H), 2.61 (s, 1H), 1.86 (q, *J* = 7.5 Hz, 1H), 1.07 (t, *J* = 7.5 Hz, 1H). ^{13}C NMR (126 MHz, Chloroform-*d*) δ 172.22, 150.32, 132.79, 131.86, 129.94, 119.23, 117.63, 111.78, 72.15, 62.40, 52.85, 48.94, 23.98, 9.27. Accurate mass: 470.1438; HRMS: 470.1444.

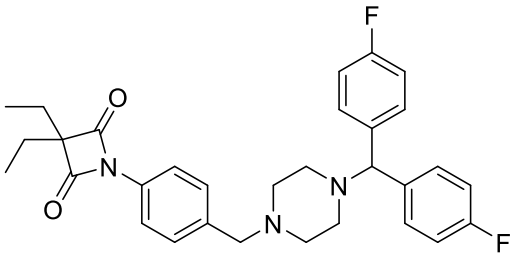

(123) 1-(4-((4-(bis(4-fluorophenyl)methyl)piperazin-1-yl)methyl)phenyl)-3,3-diethylazetidine-2,4-dione. Compound **115** (60 mg, 0.19 mmol) was dissolved in acetonitrile (2 mL). 1-(bis(4-fluorophenyl)methyl)piperazine (1.1 eq.) was added,

followed by K_2CO_3 (1.1 eq.) and the reaction was heated to 60°C for 4h. Water 5 mL was added. The compound was extracted with 3 x 3 mL of ethyl acetate. The organic fractions were collected, combined, dried with anhydrous sodium sulfate and evaporated under reduced pressure. Product **123** was purified from the crude mixture by preparative thin-layer chromatography (hexane 4:1 EtOAc) and obtained as a colorless oil (49.8 mg, 0.096 mmol, 50 %). ^{1}H NMR (600 MHz, Chloroform-*d*) δ 7.76 (d, *J* = 8.5 Hz, 2H), 7.42 (d, *J* = 8.3 Hz, 2H), 7.36 (d, *J* = 8.5 Hz, 2H), 7.19 (d, *J* = 8.4 Hz, 2H), 3.50 (s, 2H), 3.45 (s, 2H), 2.45 (s, 8H), 1.85 (q, *J* = 7.5 Hz, 4H), 1.06 (t, *J* = 7.5 Hz, 6H). ^{13}C NMR (151 MHz, Chloroform-*d*) δ 172.33, 137.33, 137.05, 132.75, 131.43, 130.92, 130.02, 120.95, 119.24, 72.22, 62.55, 62.36, 53.11, 53.09, 24.09, 9.38. Accurate mass: 518.2613; HRMS: 518.2619.

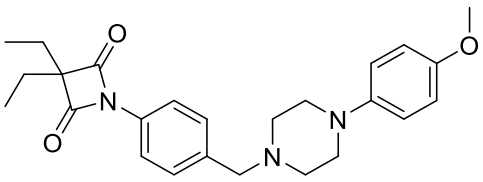

(124) 3,3-diethyl-1-(4-((4-(4-methoxyphenyl)piperazin-1-yl)methyl)phenyl)azetidine-2,4-dione. Compound **115** (60 mg, 0.19 mmol) was dissolved in acetonitrile (2 mL). 1-(4-methoxybenzyl)piperazine (1.1 eq.) was added, followed by K_2CO_3 (1.1 eq.) and the reaction was heated to 60°C for 4h. Water 5 mL was added. The compound was extracted with 3 x 3 mL of ethyl acetate. The organic fractions were collected, combined, dried with anhydrous sodium sulfate and evaporated under reduced pressure. Product **124** was purified from the crude mixture by preparative thin-layer chromatography (hexane 3:1 EtOAc) and obtained as a colorless oil (36.6 mg, 0.087 mmol, 45 %). ^{1}H NMR (500 MHz, Chloroform-*d*) δ 7.83 (d, *J* = 8.3 Hz,2H), 7.45 (d, *J* = 8.0 Hz, 2H), 6.94 – 6.89 (m, 2H), 6.87 – 6.83 (m, 2H), 3.79 (s, 3H), 3.63 (s, 2H), 3.14 (s, 4H), 2.67 (s, 4H), 1.88 (q, *J* = 7.5 Hz, 4H), 1.09 (t, *J* = 7.5 Hz, 6H). ^{13}C NMR (126 MHz, Chloroform-*d*) δ 172.33, 153.89, 145.88, 137.07, 132.80, 130.03, 119.29, 118.31, 114.54, 72.24, 62.60, 55.68, 53.31, 50.75, 24.09, 9.37. Accurate mass: 422.2438; HRMS: 422.2444.

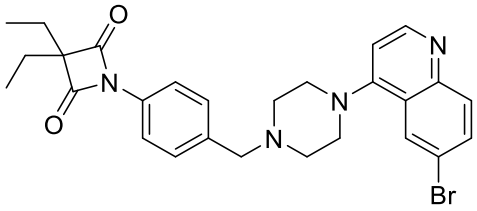

(125) 1-(4-((4-(6-bromoquinolin-4-yl)piperazin-1-yl)methyl)phenyl)-3,3-diethylazetidine-2,4-dione. Compound **115** (60 mg, 0.19 mmol) was dissolved in acetonitrile (2 mL). 6-bromo-4-(piperazin-1-yl)quinoline (1.1 eq.) was added, followed by K_2CO_3 (1.1 eq.) and the reaction was heated to 60°C for 4h. Water 5 mL was added. The compound was extracted with 3 x 3 mL of ethyl acetate. The organic fractions were collected, combined, dried with anhydrous sodium sulfate and evaporated under reduced pressure. Product **125** was purified from the crude mixture by preparative thin-layer chromatography (EtOAC) and obtained as a white solid (22.1 mg, 0.042 mmol, 22 %). ^{1}H NMR (500 MHz, Chloroform-*d*) δ 8.70 (d, *J* = 5.2 Hz, 0H), 8.12 (d, *J* = 2.2 Hz, 0H), 8.00 (d, *J* = 9.0 Hz, 0H), 7.83 (d, *J* = 8.5 Hz, 0H), 7.74 (dd, *J* = 9.0, 2.2 Hz, 0H), 7.47 (d, *J* = 8.3 Hz, 0H), 6.88 (d, *J* = 5.2 Hz, 0H), 3.70 (s, 0H), 3.33 (s, 1H), 2.80 (s, 1H), 1.86 (q, *J* = 7.5 Hz, 1H), 1.07 (t, *J* = 7.5 Hz, 1H). ^{13}C NMR (126 MHz, Chloroform-*d*) δ 172.22, 156.17, 150.96, 147.95, 132.90, 132.60, 131.64, 129.99, 126.09, 124.80, 119.46, 119.28, 109.56, 72.18, 62.40, 52.89, 52.12, 23.98, 9.26. Accurate mass: 521.1547; HRMS: 521.1552.

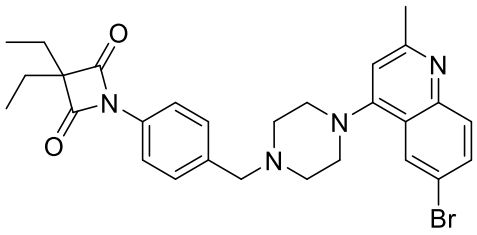

(126) 1-(4-((4-(6-bromo-2-methylquinolin-4-yl)piperazin-1-yl)methyl)phenyl)-3,3-diethylazetidine-2,4-dione. Compound **115** (60 mg, 0.19 mmol) was dissolved in acetonitrile (2 mL). 6-bromo-2-methyl-4-(piperazin-1-yl)quinoline (1.1 eq.) was added, followed by K_2CO_3 (1.1 eq.) and the reaction was heated to 60°C for 4h. Water 5 mL was added. The compound was extracted with 3 x 3 mL of ethyl acetate. The organic fractions were collected, combined, dried with anhydrous sodium sulfate and evaporated under

reduced pressure. Product **126** was purified from the crude mixture by preparative thin-layer chromatography (EtOAc) and obtained as a white solid (37.4 mg, 0.070 mmol, 36 %). ^{1}H NMR (500 MHz, Chloroform-*d*) δ 8.09 (d, *J* = 2.2 Hz, 1H), 7.95 (s, 1H), 7.84 (d, *J* = 8.5 Hz, 2H), 7.72 (dd, *J* = 9.0, 2.2 Hz, 1H), 7.46 (d, *J* = 8.5 Hz, 2H), 6.76 (s, 1H), 3.68 (s, 2H), 3.29 (s,3H), 2.81 – 2.96 (m, 8H), 1.89 (q, *J* = 7.5 Hz, 4H), 1.10 (t, *J* = 7.5 Hz, 6H). ^{13}C NMR (126 MHz, Chloroform-*d*) δ 172.34, 160.10, 156.26, 147.99, 136.83, 132.93, 132.51, 131.10, 130.03, 125.99, 123.44, 119.37, 118.54, 110.41, 72.27, 62.56, 53.09, 52.30, 25.75, 24.09, 9.38. Accurate mass: 535.1703; HRMS: 535.1709.

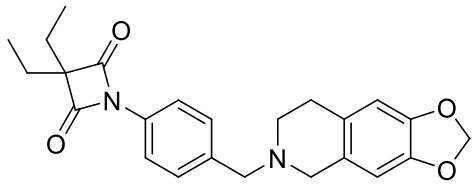

(127) 1-(4-((7,8-dihydro-[1,3]dioxolo[4,5-g]isoquinolin-6(5H)-yl)methyl)phenyl)-3,3-diethylazetidine-2,4-dione. Compound **115** (46 mg, 0.15 mmol) was dissolved in acetonitrile (0.5 mL). 5,6,7,8-tetrahydro-[1,3]dioxolo[4,5-g]isoquinoline (1.1 eq.) was added, followed by K_2CO_3 (1.1 eq.) and the reaction was heated to 60°C for 4h. Water 5 mL was added. The compound was extracted with 3 x 3 mL of ethyl acetate. The organic fractions were collected, combined, dried with anhydrous sodium sulfate and evaporated under reduced pressure. Product **127** was purified from the crude mixture by preparative thin-layer chromatography (hexane 4:1 EtOAc) and obtained as a yellow oil (22 mg, 0.054 mmol, 37 %). ^{1}H NMR (500 MHz, Chloroform-*d*) δ 7.79 (d, *J* = 8.5 Hz, 2H), 7.44 (d, *J* = 8.5 Hz, 2H), 6.56 (s, 1H), 6.44 (s, 1H), 5.87 (s, 2H), 3.67 (s, 2H), 3.54 (s, 2H), 2.75 (dt, *J* = 43.4, 5.8 Hz, 4H), 1.86 (q, *J* = 7.5 Hz, 4H), 1.07 (t, *J* = 7.5 Hz, 6H). ^{13}C NMR (126 MHz, Chloroform-*d*) δ 172.35, 146.27, 145.89, 132.93, 130.03, 127.20, 119.39, 108.59, 106.62, 100.76, 72.26, 62.00, 56.06, 50.55, 29.84, 24.10, 9.38. Accurate mass: 407.1965; HRMS: 407.1970.

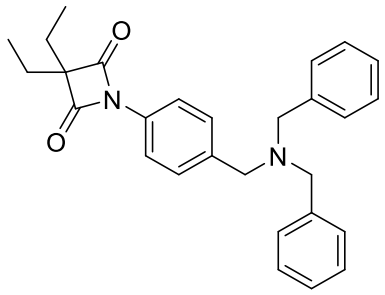

(128) 1-(4-((dibenzylamino)methyl)phenyl)-3,3-diethylazetidine-2,4-dione. Compound **115** (25 mg, 0.081 mmol) was dissolved in acetonitrile (0.5 mL). Dibenzylamine (1.1 eq.) was added, followed by K_2CO_3 (1.1 eq.) and the reaction was heated to 60°C for 4h. Water 5 mL was added. The compound was extracted with 3 x 3 mL of ethyl acetate. The organic fractions were collected, combined, dried with anhydrous sodium sulfate and evaporated under reduced pressure. Product **128** was purified from the crude mixture by preparative thin-layer chromatography (hexane 2:3 EtOAc) and obtained as a white solid (11 mg, 0.026 mmol, 32 %). ^{1}H NMR (500 MHz, Chloroform-*d*) δ 7.79 (d, *J* = 8.5 Hz, 2H), 7.45 (d, *J* = 8.2 Hz, 2H), 7.41 – 7.37 (m, 4H), 7.32 (t, *J* = 7.5 Hz, 4H), 7.26 – 7.22 (m, 2H), 3.55 (s, 1H), 1.85 (q, *J* = 7.5 Hz, 1H), 1.06 (t, *J* = 7.5 Hz, 1H). ^{13}C NMR (126 MHz, Chloroform-*d*) δ 172.23, 139.36, 138.47, 132.56, 129.48, 128.72, 128.29, 126.98, 119.11, 72.10, 57.89, 57.37, 23.98, 9.25. Accurate mass: 427.2386; HRMS: 427.2388.

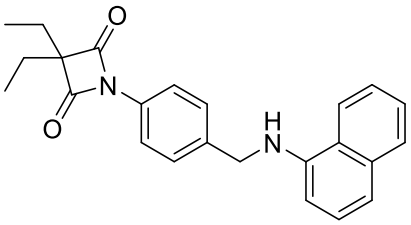

(129) 3,3-diethyl-1-(4-((naphthalen-1-ylamino)methyl)phenyl)azetidine-2,4-dione. Compound **115** (50 mg, 0.16 mmol) was dissolved in acetonitrile (1 mL). Naphthalen-1-amine (1.1 eq.) was added, followed by K_2CO_3 (1.1 eq.) and the reaction was heated to 60°C for 4h. Water 5 mL was added. The compound was extracted with 3 x 3 mL of ethyl acetate. The organic fractions were collected, combined, dried with anhydrous sodium sulfate and evaporated under reduced pressure. Product **129** was purified from the crude mixture by preparative thin-layer chromatography (hexane 1:1 EtOAc) and obtained as a

colorless oil (13 mg, 0.035 mmol, 22 %).[1]H NMR (500 MHz, Chloroform-*d*) δ 7.89 – 7.82 (m, 4H), 7.54 – 7.45 (m, 5H), 7.35 – 7.29 (m, 2H), 6.61 (d, *J* = 6.7 Hz, 1H), 4.55 (s, 2H), 1.89 (q, *J* = 7.5 Hz, 4H), 1.10 (t, *J* = 7.5 Hz, 6H). Accurate mass: 373.1916; HRMS: 373.1915.

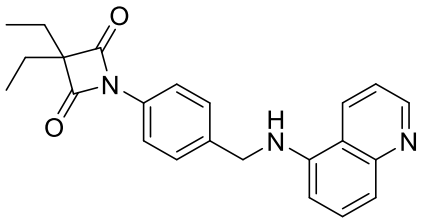

(120) 3,3-diethyl-1-(4-((quinolin-5-ylamino)methyl)phenyl)azetidine-2,4-dione. Compound **115** (50 mg, 0.16 mmol) was dissolved in acetonitrile (1 mL). Quinolin-5-amine (1.1 eq.) was added, followed by K_2CO_3 (1.1 eq.) and the reaction was heated to 60°C for 4h. Water 5 mL was added. The compound was extracted with 3 x 3 mL of ethyl acetate. The organic fractions were collected, combined, dried with anhydrous sodium sulfate and evaporated under reduced pressure. Product **120** was purified from the crude mixture by preparative thin-layer chromatography (EtOAc) and obtained as a yellow oil (17 mg, 0.046 mmol, 28 %). [1]H NMR (500 MHz, Chloroform-*d*) δ 8.63 (dd, *J* = 4.3, 1.6 Hz, 1H), 7.93 (d, *J* = 9.1 Hz, 1H), 7.90 (dd, *J* = 7.2, 1.1 Hz, 1H), 7.84 (d, *J* = 8.5 Hz, 2H), 7.47 (d, *J* = 8.6 Hz, 2H), 7.27 (dd, *J* = 4.2 Hz, 1H), 7.17 (dd, *J* = 9.0, 2.6 Hz, 1H), 6.68 (d, *J* = 2.6 Hz, 1H), 4.47 (s, 0H), 1.87 (q, *J* = 7.5 Hz, 1H), 1.08 (t, *J* = 7.5 Hz, 1H). [13]C NMR (126 MHz, Chloroform-*d*) δ 172.29, 146.20, 145.86, 143.12, 137.47, 134.32, 133.07, 130.27, 130.17, 128.30, 121.55, 121.53, 119.73, 103.60, 72.30, 47.90, 24.07, 9.35. Accurate mass: 374.1863; HRMS: 374.1868.

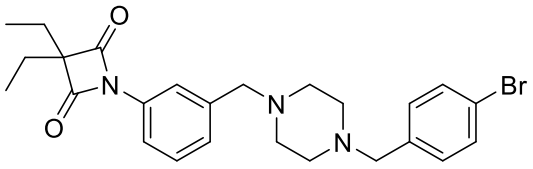

(132) 1-(3-((4-(4-bromobenzyl)piperazin-1-yl)methyl)phenyl)-3,3-diethylazetidine-2,4-dione. Compound **S1** (46 mg, 0.15 mmol) was dissolved in acetonitrile (1 mL). 1-(4-

bromobenzyl)piperazine (1.1 eq.) was added, followed by K_2CO_3 (1.1 eq.) and the reaction was heated to 60°C for 4h. Water 5 mL was added. The compound was extracted with 3 x 3 mL of ethyl acetate. The organic fractions were collected, combined, dried with anhydrous sodium sulfate and evaporated under reduced pressure. Product **132** was purified from the crude mixture by preparative thin-layer chromatography (hexane 2:1 EtOAc) and obtained as a colorless oil (26 mg, 0.054 mmol, 36 %). ^{1}H NMR (500 MHz, Chloroform-*d*) δ 7.77 (t, *J* = 1.9 Hz, 1H), 7.72 (d, *J* = 8.2, 1.6 Hz, 1H), 7.46 – 7.41 (m, 2H), 7.36 (t, *J* = 7.8 Hz, 1H), 7.29 – 7.25 (m, 2H), 7.23 (d, *J* = 8.1 Hz, 2H), 3.56 (s, 2H), 3.51 (s, 2H), 2.55 (s, 8H), 1.86 (q, *J* = 7.5 Hz, 4H), 1.07 (t, *J* = 7.5 Hz, 6H). ^{13}C NMR (126 MHz, Chloroform-*d*) δ 172.40, 140.00, 137.40, 133.88, 131.44, 130.95, 129.22, 127.54, 120.95, 119.89, 118.07, 72.14, 62.57, 62.38, 53.13, 24.06, 9.38. Accurate mass: 484.1594; HRMS: 484.1599.

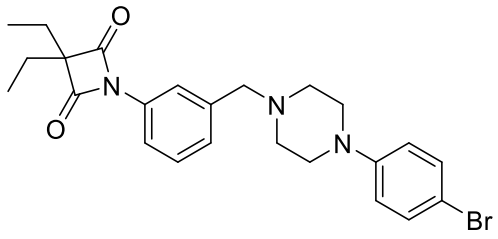

(133) 1-(3-((4-(4-bromophenyl)piperazin-1-yl)methyl)phenyl)-3,3-diethylazetidine-2,4-dione. Compound **S1** (46 mg, 0.15 mmol) was dissolved in acetonitrile (1 mL). 1-(4-bromophenyl)piperazine (1.1 eq.) was added, followed by K_2CO_3 (1.1 eq.) and the reaction was heated to 60°C for 4h. Water 5 mL was added. The compound was extracted with 3 x 3 mL of ethyl acetate. The organic fractions were collected, combined, dried with anhydrous sodium sulfate and evaporated under reduced pressure. Product **133** was purified from the crude mixture by preparative thin-layer chromatography (hexane 4:1 EtOAc) and obtained as a colorless oil (40 mg, 0.085 mmol, 57 %). ^{1}H NMR (500 MHz, Chloroform-*d*) δ 7.81 (s, 1H), 7.75 (d, *J* = 8.0 Hz, 1H), 7.39 (t, *J* = 7.7 Hz, 1H), 7.35 – 7.30 (m, 3H), 6.78 (d, *J* = 9.0 Hz, 2H), 3.62 (s, 2H), 3.20 (s, 4H), 2.65 (s, 4H), 1.86 (q, *J* = 7.5 Hz, 4H), 1.08 (t, *J* = 7.5 Hz, 6H). ^{13}C NMR (126 MHz, Chloroform-*d*) δ 172.39, 150.49, 139.84, 133.95, 131.95, 129.32, 127.48, 119.85, 118.19, 117.72, 111.82, 72.17, 62.55, 53.00, 49.08, 24.05, 9.38. Accurate mass: 470.1438; HRMS: 470.1443.

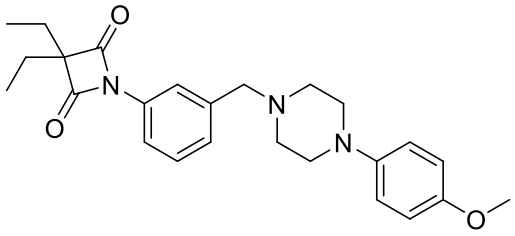

(134) 3,3-diethyl-1-(3-((4-(4-methoxyphenyl)piperazin-1-yl)methyl)phenyl)azetidine-2,4-dione. Compound **S1** (46 mg, 0.15 mmol) was dissolved in acetonitrile (1 mL). 1-(4-methoxybenzyl)piperazine (1.1 eq.) was added, followed by K_2CO_3 (1.1 eq.) and the reaction was heated to 60°C for 4h. Water 5 mL was added. The compound was extracted with 3 x 3 mL of ethyl acetate. The organic fractions were collected, combined, dried with anhydrous sodium sulfate and evaporated under reduced pressure. Product **134** was purified from the crude mixture by preparative thin-layer chromatography (hexane 3:1 EtOAc) and obtained as a colorless oil (29 mg, 0.069 mmol, 46 %). ^{1}H NMR (500 MHz, Chloroform-*d*) δ 7.81 (s, 1H), 7.75 (d, *J* = 7.8 Hz, 1H), 7.43 – 7.30 (m, 2H), 6.92 – 6.88 (m, 2H), 6.85 – 6.80 (m, 2H), 3.76 (s, 3H), 3.64 (s, 2H), 3.14 (s, 4H), 2.68 (s, 4H), 1.86 (q, *J* = 7.5 Hz, 4H), 1.08 (t, *J* = 7.5 Hz, 6H). ^{13}C NMR (126 MHz, Chloroform-*d*) δ 172.40, 153.89, 145.91, 139.95, 133.92, 129.28, 127.56, 119.92, 118.33, 114.54, 72.16, 62.62, 55.69, 53.32, 50.74, 24.06, 9.38. Accurate mass: 422.2438; HRMS: 422.2444.

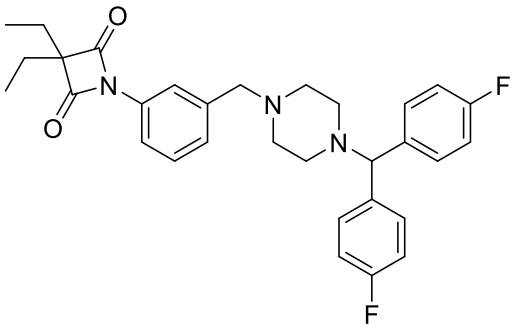

(135) 1-(3-((4-(bis(4-fluorophenyl)methyl)piperazin-1-yl)methyl)phenyl)-3,3-diethylazetidine-2,4-dione. Compound **S1** (46 mg, 0.15 mmol) was dissolved in acetonitrile (1 mL). 1-(bis(4-fluorophenyl)methyl)piperazine (1.1 eq.) was added, followed by K_2CO_3 (1.1 eq.) and the reaction was heated to 60°C for 4h. Water 5 mL was added. The compound was extracted with 3 x 3 mL of ethyl acetate. The organic fractions

were collected, combined, dried with anhydrous sodium sulfate and evaporated under reduced pressure. Product **135** was purified from the crude mixture by preparative thin-layer chromatography (hexane 4:1 EtOAc) and obtained as a colorless oil (43 mg, 0.056 mmol, 56 %). ^{1}H NMR (500 MHz, Chloroform-*d*) δ 7.75 (t, *J* = 1.7 Hz, 1H), 7.72 (d, *J* = 8.0 Hz, 1H), 7.39 – 7.30 (m, 6H), 6.95 (t, *J* = 8.7 Hz, 4H), 4.22 (s, 1H), 3.55 (s, 2H), 2.56 – 2.34 (m, 8H), 1.85 (q, *J* = 7.5 Hz, 4H), 1.06 (t, *J* = 7.5 Hz, 4H). ^{13}C NMR (126 MHz, Chloroform-*d*) δ 172.39, 162.88, 160.93, 139.93, 138.46, 138.44, 133.86, 129.41, 129.34, 129.21, 127.56, 119.90, 118.05, 115.56, 115.39, 74.63, 72.13, 62.58, 53.40, 51.84, 24.04, 9.36. Accurate mass: 518.2613; HRMS: 518.2621.

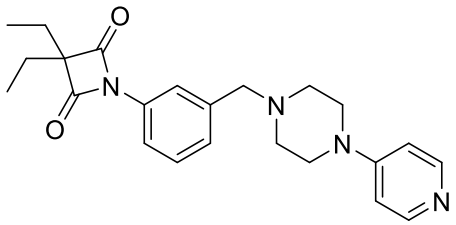

(136) 3,3-diethyl-1-(3-((4-(pyridin-4-yl)piperazin-1-yl)methyl)phenyl)azetidine-2,4-dione. Compound **S1** (46 mg, 0.15 mmol) was dissolved in acetonitrile (1 mL). 1-(pyridin-4-yl)piperazine (1.1 eq.) was added, followed by K_2CO_3 (1.1 eq.) and the reaction was heated to 60°C for 4h. Water 5 mL was added. The compound was extracted with 3 x 3 mL of ethyl acetate. The organic fractions were collected, combined, dried with anhydrous sodium sulfate and evaporated under reduced pressure. Product **136** was purified from the crude mixture by preparative thin-layer chromatography (DCM 9:1 MeOH) and obtained as a yellow oil (22 mg, 0.056 mmol, 38 %). ^{1}H NMR (500 MHz, Chloroform-*d*) δ 8.25 (d, *J* = 6.7 Hz, 2H), 7.82 (t, *J* = 1.9 Hz, 1H), 7.79 – 7.73 (m, 1H), 7.39 (t, *J* = 7.8 Hz, 1H), 7.26 – 7.23 (m, 1H), 6.82 – 6.76 (m, 2H), 3.59 (s, 2H), 3.57 – 3.51 (m, 4H), 2.63 – 2.60 (m, 4H), 1.86 (q, *J* = 7.5 Hz, 4H), 1.07 (t, *J* = 7.5 Hz, 6H). ^{13}C NMR (126 MHz, Chloroform-*d*) δ 172.39, 156.59, 143.29, 139.08, 134.13, 129.52, 127.35, 119.70, 118.48, 107.61, 72.27, 62.22, 52.26, 46.21, 24.05, 9.37. Accurate mass: 393.2285; HRMS: 393.2290.

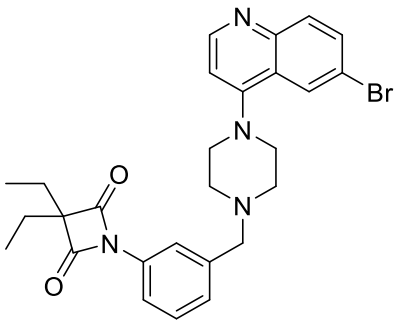

(137) 1-(3-((4-(6-bromoquinolin-4-yl)piperazin-1-yl)methyl)phenyl)-3,3-diethylazetidine-2,4-dione. Compound **S1** (46 mg, 0.15 mmol) was dissolved in acetonitrile (1 mL). 6-bromo-4-(piperazin-1-yl)quinoline (1.1 eq.) was added, followed by K_2CO_3 (1.1 eq.) and the reaction was heated to 60°C for 4h. Water 5 mL was added. The compound was extracted with 3 x 3 mL of ethyl acetate. The organic fractions were collected, combined, dried with anhydrous sodium sulfate and evaporated under reduced pressure. Product **137** was purified from the crude mixture by preparative thin-layer chromatography (EtOAc) and obtained as a white solid (44 mg, 0.084 mmol, 57 %). ^{1}H NMR (500 MHz, Chloroform-*d*) δ 8.69 (d, *J* = 5.2 Hz, 0H), 8.14 (d, *J* = 2.2 Hz, 0H), 8.02 (d, *J* = 8.9 Hz, 0H), 7.86 (d, *J* = 1.9 Hz, 0H), 7.79 – 7.76 (m, 0H), 7.74 (dd, *J* = 8.9, 2.2 Hz, 0H), 7.41 (t, *J* = 7.8 Hz, 0H), 7.35 (d, *J* = 7.8 Hz, 0H), 6.89 (d, *J* = 5.2 Hz, 0H), 3.71 (s, 0H), 3.35 (d, *J* = 5.3 Hz, 1H), 2.82 (s, 1H), 1.87 (q, *J* = 7.5 Hz, 1H), 1.08 (t, *J* = 7.5 Hz, 1H). ^{13}C NMR (126 MHz, Chloroform-*d*) δ 172.29, 156.14, 151.22, 148.21, 139.69, 133.92, 132.46, 131.82, 129.26, 127.37, 126.12, 124.92, 119.71, 119.37, 118.14, 109.64, 72.09, 62.47, 52.97, 52.19, 23.94, 9.27. Accurate mass: 521.1547; HRMS: 521.1552.

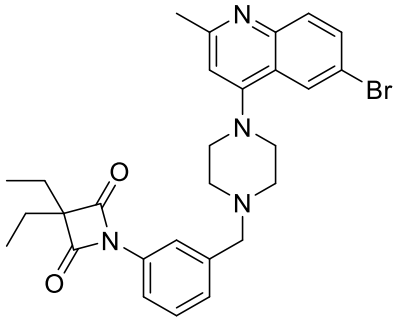

(138) 1-(3-((4-(6-bromo-2-methylquinolin-4-yl)piperazin-1-yl)methyl)phenyl)-3,3-diethylazetidine-2,4-dione. Compound **S1** (46 mg, 0.15 mmol) was dissolved in

acetonitrile (1 mL). 6-bromo-2-methyl-4-(piperazin-1-yl)quinoline (1.1 eq.) was added, followed by K_2CO_3 (1.1 eq.) and the reaction was heated to 60°C for 4h. Water 5 mL was added. The compound was extracted with 3 x 3 mL of ethyl acetate. The organic fractions were collected, combined, dried with anhydrous sodium sulfate and evaporated under reduced pressure. Product **138** was purified from the crude mixture by preparative thin-layer chromatography (EtOAc) and obtained as a white solid (47 mg, 0.088 mmol, 59 %). ^{1}H NMR (500 MHz, Chloroform-*d*) δ 8.08 (d, *J* = 2.2 Hz, 1H), 7.91 – 7.84 (m, 2H), 7.76 (ddd, *J* = 8.0, 2.1, 1.2 Hz, 1H), 7.68 (dd, *J* = 8.9, 2.2 Hz, 1H), 7.40 (t, *J* = 7.8 Hz, 1H), 7.32 – 7.30 (m, 1H), 6.75 (s, 1H), 3.67 (s, 2H), 3.26 (s, 4H), 2.77 (s, 1H), 2.67 (s, 1H), 1.87 (q, *J* = 7.5 Hz, 1H), 1.08 (t, *J* = 7.5 Hz, 1H). ^{13}C NMR (126 MHz, Chloroform-*d*) δ 172.29, 159.97, 156.19, 147.86, 139.74, 133.92, 132.39, 130.97, 129.24, 127.34, 125.90, 123.33, 119.68, 118.42, 118.12, 110.32, 72.08, 62.45, 53.01, 52.18, 25.63, 23.94, 9.27. Accurate mass: 535.1703; HRMS: 535.1706.

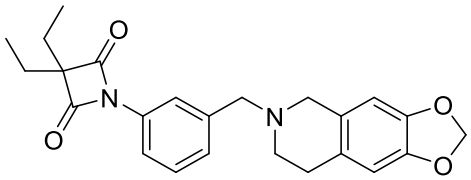

(139) 1-(3-((7,8-dihydro-[1,3]dioxolo[4,5-g]isoquinolin-6(5H)-yl)methyl)phenyl)-3,3-diethylazetidine-2,4-dione. Compound **S1** (46 mg, 0.15 mmol) was dissolved in acetonitrile (1 mL). 5,6,7,8-tetrahydro-[1,3]dioxolo[4,5-g]isoquinoline (1.1 eq.) was added, followed by K_2CO_3 (1.1 eq.) and the reaction was heated to 60°C for 4h. Water 5 mL was added. The compound was extracted with 3 x 3 mL of ethyl acetate. The organic fractions were collected, combined, dried with anhydrous sodium sulfate and evaporated under reduced pressure. Product **139** was purified from the crude mixture by preparative thin-layer chromatography (hexane 4:1 EtOAc) and obtained as a yellow oil (34 mg, 0.084 mmol, 56 %). ^{1}H NMR (500 MHz, Chloroform-*d*) δ 7.82 – 7.81 (m, 1H), 7.78 – 7.73 (m, 1H), 7.41 (d, *J* = 7.4 Hz, 2H), 6.58 (s, 1H), 6.46 (s, 1H), 5.88 (s, 2H), 3.74 (s, 2H), 3.61 (s, 2H), 2.82 (d, *J* = 26.2 Hz, 4H), 1.86 (q, *J* = 7.5 Hz, 4H), 1.07 (t, *J* = 7.5 Hz, 6H). ^{13}C NMR (126 MHz, Chloroform-*d*) δ 172.38, 146.17, 145.81, 140.19, 133.89, 129.34, 127.62, 127.48, 127.37, 119.88, 118.22, 108.59, 106.61, 100.71, 72.14, 62.19, 56.19, 50.67, 29.20, 24.05, 9.38. Accurate mass: 407.1965; HRMS: 407.1973.

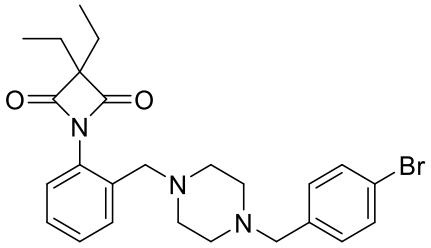

(141) 1-(2-((4-(4-bromobenzyl)piperazin-1-yl)methyl)phenyl)-3,3-diethylazetidine-2,4-dione. Compound **S2** (50 mg, 0.15 mmol) was dissolved in acetonitrile (1 mL). 1-(4-bromobenzyl)piperazine (1.1 eq.) was added, followed by K_2CO_3 (1.1 eq.) and the reaction was heated to 60°C for 4h. Water 5 mL was added. The compound was extracted with 3 x 3 mL of ethyl acetate. The organic fractions were collected, combined, dried with anhydrous sodium sulfate and evaporated under reduced pressure. Product **141** was purified from the crude mixture by preparative thin-layer chromatography (hexane 2:1 EtOAc) and obtained as a colorless oil (18 mg, 0.037 mmol, 23 %). ^{1}H NMR (300 MHz, Chloroform-*d*) δ 7.49 – 7.39 (m, 3H), 7.36 – 7.23 (m, 3H), 7.20 – 7.14 (m, 2H), 3.58 (s, 2H), 3.43 (s, 2H), 2.39 (s, 8H), 1.91 (q, *J* = 7.5 Hz, 4H), 1.13 (t, *J* = 7.5 Hz, 6H). ^{13}C NMR (75 MHz, Chloroform-d) δ 172.88, 137.25, 134.31, 131.44, 131.33, 130.93, 129.98, 128.96, 128.08, 126.21, 120.98, 70.13, 62.38, 60.01, 53.41, 53.04, 23.73, 9.54.
(HRMS SCRIPPS WRONG)

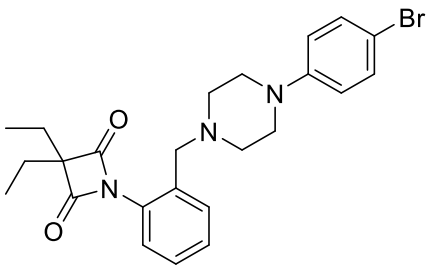

(142) 1-(2-((4-(4-bromophenyl)piperazin-1-yl)methyl)phenyl)-3,3-diethylazetidine-2,4-dione. Compound **S2** (46 mg, 0.15 mmol) was dissolved in acetonitrile (1 mL). 1-(4-bromophenyl)piperazine (1.1 eq.) was added, followed by K_2CO_3 (1.1 eq.) and the reaction was heated to 60°C for 4h. Water 5 mL was added. The compound was extracted with 3 x 3 mL of ethyl acetate. The organic fractions were collected, combined, dried with anhydrous sodium sulfate and evaporated under reduced pressure. Product **142** was purified from the crude mixture by preparative thin-layer chromatography (hexane 4:1

EtOAc) and obtained as a colorless oil (20 mg, 0.043 mmol, 29 %). ^{1}H NMR (500 MHz, Chloroform-*d*) δ 7.58 (d, *J* = 6.7 Hz, 1H), 7.42 – 7.30 (m, 5H), 6.77 – 6.73 (m, 2H), 3.77 (s, 2H), 3.17 (d, *J* = 5.4 Hz, 4H), 2.65 (s, 4H), 1.91 (q, *J* = 7.5 Hz, 4H), 1.13 (t, *J* = 7.5 Hz, 6H). ^{13}C NMR (75 MHz, Chloroform-*d*) δ 172.87, 150.38, 133.87, 131.96, 131.41, 130.08, 129.03, 128.28, 126.26, 117.65, 111.85, 70.20, 59.99, 53.26, 48.93, 23.77, 9.54. Accurate mass: 470.1438; HRMS: 470.1442.

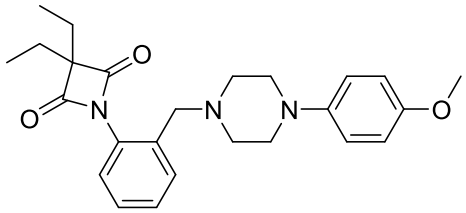

(143) 3,3-diethyl-1-(2-((4-(4-methoxyphenyl)piperazin-1-yl)methyl)phenyl)azetidine-2,4-dione. Compound **S2** (46 mg, 0.15 mmol) was dissolved in acetonitrile (1 mL). 1-(4-methoxybenzyl)piperazine (1.1 eq.) was added, followed by K_2CO_3 (1.1 eq.) and the reaction was heated to 60°C for 4h. Water 5 mL was added. The compound was extracted with 3 x 3 mL of ethyl acetate. The organic fractions were collected, combined, dried with anhydrous sodium sulfate and evaporated under reduced pressure. Product **143** was purified from the crude mixture by preparative thin-layer chromatography (hexane 3:1 EtOAc) and obtained as a colorless oil (23 mg, 0.054 mmol, 37 %). ^{1}H NMR (600 MHz, Chloroform-*d*) δ 7.54 – 7.50 (m, 1H), 7.37 – 7.32 (m, 2H), 7.31 – 7.29 (m, 1H), 6.90 – 6.85 (m, 2H), 6.85 – 6.81 (m, 2H), 3.76 (s, 2H), 3.65 (s, 2H), 3.10 – 2.93 (m, 4H), 2.60 – 2.45 (m, 4H), 1.92 (q, *J* = 7.5 Hz, 4H), 1.14 (t, *J* = 7.5 Hz, 12H). ^{13}C NMR (151 MHz, Chloroform-*d*) δ 172.88, 153.86, 145.80, 134.09, 131.43, 130.04, 128.99, 128.17, 126.20, 118.19, 114.54, 70.17, 60.09, 55.67, 53.60, 50.58, 23.74, 9.54. Accurate mass: 422.2438; HRMS: 422.2444.

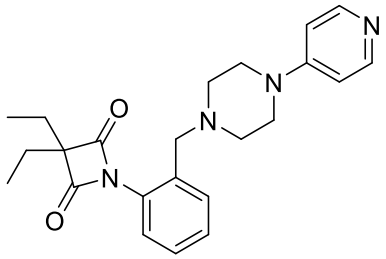

(144) 3,3-diethyl-1-(2-((4-(pyridin-4-yl)piperazin-1-yl)methyl)phenyl)azetidine-2,4-dione. Compound **S2** (46 mg, 0.15 mmol) was dissolved in acetonitrile (1 mL). 1-(pyridin-4-yl)piperazine (1.1 eq.) was added, followed by K_2CO_3 (1.1 eq.) and the reaction was heated to 60°C for 4h. Water 5 mL was added. The compound was extracted with 3 x 3 mL of ethyl acetate. The organic fractions were collected, combined, dried with anhydrous sodium sulfate and evaporated under reduced pressure. Product **144** was purified from the crude mixture by preparative thin-layer chromatography (DCM 9:1 MeOH) and obtained as a colorless oil (13 mg, 0.033 mmol, 22 %). ^{1}H NMR (600 MHz, Chloroform-*d*) δ 7.48 – 7.45 (m, 1H), 7.43 – 7.40 (m, 2H), 7.34 – 7.28 (m, 2H), 7.27 – 7.25 (m, 1H), 7.18 – 7.15 (m, 2H), 3.58 (s, 2H), 3.42 (s, 2H), 2.38 (s, 8H), 1.91 (q, *J* = 7.5 Hz, 4H), 1.13 (t, *J* = 7.5 Hz, 6H). ^{13}C NMR (151 MHz, Chloroform-*d*) δ 172.84, 137.30, 134.28, 131.39, 131.30, 130.88, 129.92, 128.93, 128.04, 126.17, 120.91, 70.09, 62.37, 60.00, 53.42, 53.02, 23.70, 9.52. HREI-MS for $C_{23}H_{28}N_4O_2$ [MH^+]: calculated XXXXX measured XXXXXX. [WRONG SCRIPPS HRMS]

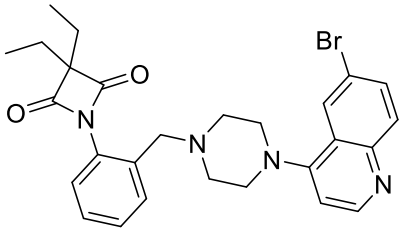

(145) 1-(2-((4-(6-bromoquinolin-4-yl)piperazin-1-yl)methyl)phenyl)-3,3-diethylazetidine-2,4-dione. Compound **S2** (46 mg, 0.15 mmol) was dissolved in acetonitrile (1 mL). 6-bromo-4-(piperazin-1-yl)quinoline (1.1 eq.) was added, followed by K_2CO_3 (1.1 eq.) and the reaction was heated to 60°C for 4h. Water 5 mL was added. The compound was extracted with 3 x 3 mL of ethyl acetate. The organic fractions were collected, combined, dried with anhydrous sodium sulfate and evaporated under reduced

pressure. Product **145** was purified from the crude mixture by preparative thin-layer chromatography (EtOAc) and obtained as a white solid (26 mg, 0.050 mmol, 34 %). ^{1}H NMR (500 MHz, Chloroform-*d*) δ 8.73 (d, *J* = 5.5 Hz, 1H), 8.11 (d, *J* = 2.2 Hz, 1H), 8.03 (d, *J* = 9.0 Hz, 1H), 7.76 (dd, *J* = 9.0, 2.1 Hz, 1H), 7.56 – 7.49 (m, 1H), 7.41 – 7.29 (m, 3H), 6.86 (d, *J* = 5.5 Hz, 1H), 3.75 (s, 2H), 3.45 – 3.23 (m, 4H), 2.69 (t, *J* = 4.7 Hz, 4H), 1.93 (q, *J* = 7.5 Hz, 4H), 1.16 (t, *J* = 7.5 Hz, 6H). ^{13}C NMR (126 MHz, Chloroform-*d*) δ 172.81, 157.49, 148.52, 133.84, 133.29, 131.27, 130.01, 129.35, 129.07, 128.44, 126.48, 126.35, 123.80, 119.97, 108.67, 70.19, 59.66, 52.97, 52.03, 23.72, 9.47. Accurate mass: 521.1547; HRMS: 521.1551.

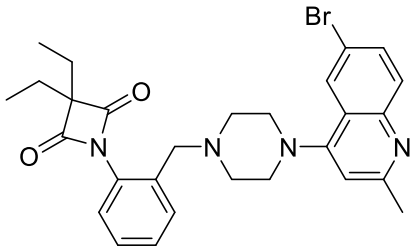

(146) 1-(2-((4-(6-bromo-2-methylquinolin-4-yl)piperazin-1-yl)methyl)phenyl)-3,3-diethylazetidine-2,4-dione. Compound **S2** (46 mg, 0.15 mmol) was dissolved in acetonitrile (1 mL). 6-bromo-2-methyl-4-(piperazin-1-yl)quinoline (1.1 eq.) was added, followed by K_2CO_3 (1.1 eq.) and the reaction was heated to 60°C for 4h. Water 5 mL was added. The compound was extracted with 3 x 3 mL of ethyl acetate. The organic fractions were collected, combined, dried with anhydrous sodium sulfate and evaporated under reduced pressure. Product **146** was purified from the crude mixture by preparative thin-layer chromatography (EtOAc) and obtained as a white solid (28 mg, 0.052 mmol, 35 %). ^{1}H NMR (500 MHz, Chloroform-*d*) δ 8.06 – 7.98 (m, 2H), 7.74 (d, *J* = 8.9 Hz, 1H), 7.54 (d, *J* = 6.8 Hz, 1H), 7.42 – 7.34 (m, 2H), 7.31 (d, *J* = 7.0 Hz, 1H), 6.70 (s, 1H), 3.74 (s, 2H), 3.33 (s, 4H), 2.72 (s, 3H), 2.68 (s, 4H), 1.93 (q, *J* = 7.4 Hz, 4H), 1.16 (t, *J* = 7.4 Hz, 6H). ^{13}C NMR (126 MHz, Chloroform-*d*) δ 172.81, 134.03, 133.38, 131.27, 130.00, 129.07, 128.43, 126.38, 126.31, 122.24, 119.32, 109.41, 70.18, 59.70, 52.97, 51.99, 23.72, 9.47. Accurate mass: 535.1703; HRMS: 535.1712.

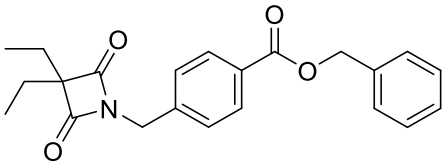

(119) benzyl 4-((3,3-diethyl-2,4-dioxoazetidin-1-yl)methyl)benzoate. Diethyl malonyl dichloride was dissolved in DCM and the mixture was cooled to 0°C. The amine handle benzyl 4-(aminomethyl)benzoate and triethylamine were dissolved in DCM and added to the reaction dropwise. The reaction was stirred for 1h at 0°C and then allowed to reach room temperature and stirred for an additional 4h. The solvent was evaporated under reduced pressure and the crude mixture was purified by flash column chromatography (hexane 9:1 EtOAc to hexane 1:1 EtOAc) to yield the final product **119** as a colorless oil (126 mg, 0.34 mmol, 23 %). ^{1}H NMR (500 MHz, Chloroform-*d*) δ 8.06 (d, *J* = 8.4 Hz, 2H), 7.51 – 7.29 (m, 7H), 5.36 (s, 2H), 4.51 (s, 2H), 1.73 (q, *J* = 7.5 Hz, 4H), 0.92 (t, *J* = 7.5 Hz, 6H). ^{13}C NMR (126 MHz, Chloroform-*d*) δ 174.17, 166.03, 140.05, 136.02, 130.49, 130.16, 128.76, 128.46, 128.42, 128.37, 71.21, 66.99, 42.45, 23.80, 9.34. Accurate mass: 388.1519; HRMS: 388.1527.

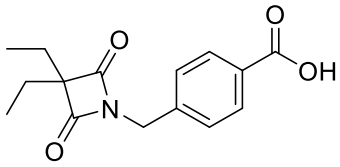

(120) 4-((3,3-diethyl-2,4-dioxoazetidin-1-yl)methyl)benzoic acid. Compound XX (100 mg, 0.27 mmol) was dissolved in MeOH (1 mL). Palladium on activated charcoal (20 mg) was added. Triethylsilane (10 eq.) was slowly added dropwise while the reaction was stirred vigorously. The reaction was stirred at room temperature for 5 minutes. The mixture was diluted with ethyl acetate and filtered. The filtrate was evaporated under reduced pressure. The crude mixture was purified by flash column chromatography and the final product **120** was obtained as a white solid (40 mg, 0.15 mmol, 53 %). ^{1}H NMR (500 MHz, Chloroform-*d*) δ 8.10 (d, *J* = 8.3 Hz, 2H), 7.46 (d, *J* = 8.4 Hz, 2H), 4.54 (s, 2H), 1.74 (q, *J* = 7.5 Hz, 4H), 0.93 (t, *J* = 7.5 Hz, 6H). ^{13}C NMR (126 MHz, Chloroform-*d*) δ 174.21, 171.21, 140.88, 131.02, 129.26, 128.54, 71.26, 42.46, 23.83, 9.34. Accurate mass: 276.123; HRMS: 276.1238.

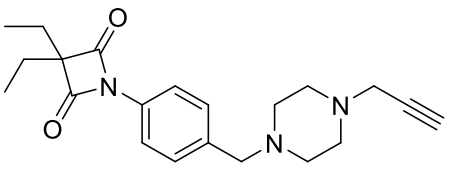

(151) 3,3-diethyl-1-(4-((4-(prop-2-yn-1-yl)piperazin-1-yl)methyl)phenyl)azetidine-2,4-dione. Compound **115** (40 mg, 0.11 mmol) was dissolved in acetonitrile (1 mL). 1-(prop-2-yn-1-yl)piperazine (1.1 eq.) was added, followed by K_2CO_3 (1.1 eq.) and the reaction was heated to 60°C for 4h. Water 5 mL was added. The compound was extracted with 3 x 3 mL of ethyl acetate. The organic fractions were collected, combined, dried with anhydrous sodium sulfate and evaporated under reduced pressure. Product **151** was purified from the crude mixture by preparative thin-layer chromatography (EtOAc) and obtained as a colorless oil (15 mg, 0.042 mmol, 33 %). ^{1}H NMR (300 MHz, Chloroform-*d*) δ 7.77 (d, *J* = 8.5 Hz, 2H), 7.37 (d, *J* = 8.5 Hz, 2H), 3.51 (s, 2H), 3.29 (d, *J* = 2.5 Hz, 2H), 2.65 – 2.44 (m, 8H), 2.24 (t, *J* = 2.4 Hz, 1H), 1.85 (q, *J* = 7.5 Hz, 4H), 1.06 (t, *J* = 7.5 Hz, 6H). ^{13}C NMR (126 MHz, Chloroform-*d*) δ 172.36, 137.07, 132.79, 130.02, 119.28, 78.96, 73.34, 72.26, 62.49, 52.98, 51.98, 46.92, 24.11, 9.38.

S2.3. Fluorophore Derivatization

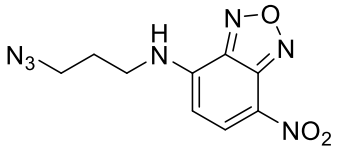

(88) N-(3-azidopropyl)-7-nitrobenzo[c][1,2,5]oxadiazol-4-amine. 3-bromopropan-1-amine hydrobromide (0.75 g, 3.43 mmol) was dissolved in DMSO (30 mL). Sodium azide (0.267 g, 1.2 eq.) was added and the reaction was stirred overnight. The next day NBD-Cl (0.752 g, 3.77 mmol) was added, followed by triethylamine (0.549 mL, 3.94 mmol). The reaction was stirred for 4 h. A dilution was done with water (50 mL) and the product was extracted with 4 x 15 mL of EtOAc. The organic fractions were combined, dried with anhydrous sodium sulfate and concentrated under reduced pressure. The crude was purified by flash column chromatography, to yield product **88** as an orange solid (0.378 g, 1.44 mmol, 46% yield over two steps). ^{1}H NMR (300 MHz, CDCl3) δ 8.47 (d, J = 8.6

Hz, 1H), 6.63 (s, 1H), 6.22 (d, J = 8.7 Hz, 1H), 3.66 (q, J = 6.6 Hz, 2H), 3.61 – 3.56 (m, 2H), 2.16 – 2.00 (m, 2H).

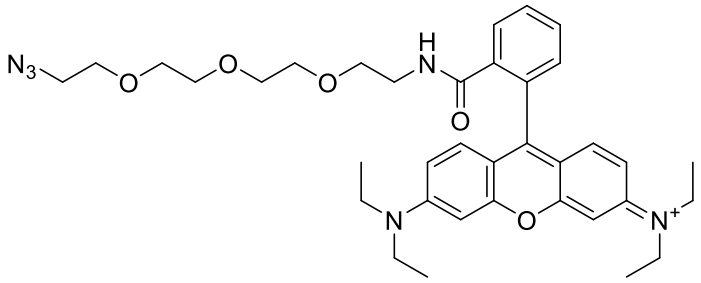

(91) N-(9-(2-((2-(2-(2-(2-azidoethoxy)ethoxy)ethoxy)ethyl)carbamoyl)phenyl)-6-(diethylamino)-3H-xanthen-3-ylidene)-N-ethylethanaminium. Rhodamine B (0.025 g, 0.052 mmol) was dissolved in dry DCM (1 mL) and the solution was cooled to 0°C. HOBt (2 eq.) was added with DIPEIA (1 eq.), followed by TBTU (2eq.). The reaction was stirred for 30 min. **2-(2-(2-(2-azidoethoxy)ethoxy)ethoxy)ethan-1-amine** (3 eq.) was added with DIPEIA (3 eq.) and the reaction was refluxed overnight. The next day the solvent was evaporated under reduced pressure. The product was purified by preparative thin-layer chromatography, yielding product **91** as a pink oil (this reaction was used as a proof-of-concept, no mass of product was determined). ^{1}H NMR (300 MHz, DMSO) δ 7.81 – 7.73 (m, 1H), 7.55 – 7.44 (m, 2H), 7.06 – 6.98 (m, 1H), 6.39 – 6.28 (m, J = 17.9, 8.4 Hz, 6H), 3.56 – 3.52 (m, 2H), 3.50 – 3.38 (m, 11H), 3.37 – 3.26 (m, 4H), 3.20 – 3.08 (m, 4H), 2.99 (t, J = 6.7 Hz, 2H), 1.08 (t, J = 6.8 Hz, 12H).

S2.4. N-tolyl 4-Oxo-β-Lactam with Fluorophore (Coumarin)

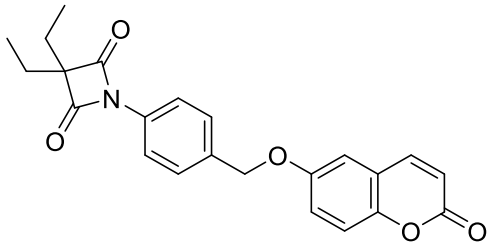

(154) 3,3-diethyl-1-(4-(((2-oxo-2H-chromen-6-yl)oxy)methyl)phenyl)azetidine-2,4-dione. 1-(4-(bromomethyl)phenyl)-3,3-diethylazetidine-2,4-dione was suspended in dry DCM. Umbelliferone (1.1 eq.) and potassium carbonate (1.1 eq.) were added. The reaction was refluxed overnight. The solvent was evaporated under reduced pressure and the product was purified by flash column chromatography. Compound **154** was obtained as a white solid (0.045 g, 0.11 mmol, 28% yield). ^{1}H NMR (300 MHz, CDCl3) δ 7.93 – 7.85 (m, 2H), 7.63 (d, J = 9.5 Hz, 1H), 7.48 (d, J = 8.6 Hz, 2H), 7.38 (d, J = 8.6 Hz, 1H), 6.90 (dd, J = 8.6, 2.4 Hz, 1H), 6.86 (d, J = 2.4 Hz, 1H), 6.26 (d, J = 9.5 Hz, 1H), 5.12 (s, 2H), 1.86 (q, J = 7.5 Hz, 4H), 1.07 (t, J = 7.5 Hz, 6H). ^{13}C NMR (75 MHz, Chloroform-d) δ 172.18, 161.68, 161.16, 155.90, 143.42, 134.39, 133.88, 128.97, 128.48, 119.55, 113.49, 113.30, 112.98, 102.05, 72.37, 69.97, 24.05, 9.32.

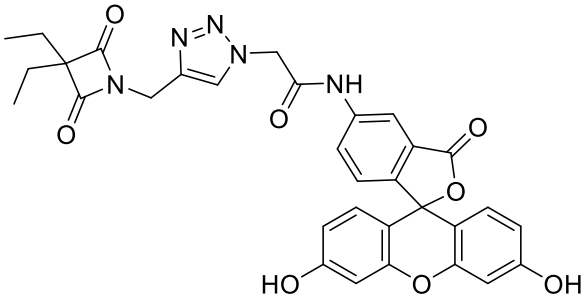

(155) 2-(4-((3,3-diethyl-2,4-dioxoazetidin-1-yl)methyl)-1H-1,2,3-triazol-1-yl)-N-(3',6'-dihydroxy-3-oxo-3H-spiro[isobenzofuran-1,9'-xanthen]-5-yl)acetamide. 3,3-diethyl-1-(prop-2-yn-1-yl)azetidine-2,4-dione (0.07 g, 0.39 mmol) was dissolved in DMSO (2 mL). $CuSO_4$ (400 µL, 0.1 M) and sodium ascorbate (400 µL, 0.2 M) were added and the reaction was stirred for 10 minutes at room temperature. The azide 2-azido-N-(3',6'-dihydroxy-3-oxo-3H-spiro[isobenzofuran-1,9'-xanthen]-5-yl)acetamide (1 eq.)

was then added and the reaction was stirred overnight. The reaction was diluted with water, leading to a yellow precipitate. The solid was filtered and further purification was attempted by recrystallization with different pairs of solvents (EtOAc, hexane, MeOH, acetonitrile and DCM) with no success. The solid was purified using reverse phase combi flash chromatography (100% water to 100% MeOH gradient), yielding compound **155** as a yellow solid (19 mg, 8%). 1 H NMR (300 MHz, (CD3)2SO) δ 10.97 (s, 1H), 8.25 (d, J = 1.8 Hz, 1H), 8.15 (s, 1H), 7.81 (dd, J = 8.4; 1.9 Hz, 1H), 7.24 (d, J = 8.4 Hz, 1H), 6.66 (d, J = 2.3 Hz, 2H), 6.58 (t, J = 8.5 Hz, 3H), 6.53 (dd, J = 8.7; 2.3 Hz, 2H), 5.59 (d, J = 8.0, 1H), 5.41 (s, 2H), 4.63 (s, 2H), 1.68 (q, J = 7.7 Hz, 4H), 0.88 (q, J = 7.7 Hz, 6H). 13C NMR (75 MHz, (CD3)2SO) 173.8, 169.0, 165.3, 157.1, 152.5, 141.1, 140.4, 129.6, 129.3, 127.4, 126.7, 125.5, 125.3, 114.4, 113.4, 110.1, 102.7, 88.7, 70.4, 52.7, 33.8, 23.2, 9.4. ESI (+) m/z: 610.2 [M+H]+ , 649.38 [M+K]+ (Exact mass calcd.: 609.19).

S2.5. N-O 4-Oxo-β-Lactam

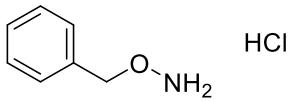

(156) O-benzylhydroxylamine hydrochloride. Sodium bicarbonate (2.1 g, 25 mmol) was suspended in a mixture of DCM (18 mL) and distilled water (34 mL). Tert-butylammonium sulfate (0.42 g, 1.23 mmol) was added, followed by benzyl chloride (1.7 mL, 14.8 mmol). N-hydroxyphtalimide (2 g, 12.3 mmol) was slowly added over 30 minutes. The reaction was refluxed at 45°C for 5h. The benzyl-protected N-hydroxyphthalimide was extracted with 30 x 30 mL of DCM. The organic fractions were combined, dried with sodium sulfate and evaporated under reduced pressure, yielding a white solid. ^{1}H NMR (300 MHz, $CDCl_3$) δ 7.83 – 7.78 (m, 2H), 7.76 – 7.71 (m, 2H), 7.56 – 7.51 (m, 2H), 7.40 – 7.35 (m, 3H), 5.21 (s, 2H). This product was suspended in acetic acid (20 mL) and hydrochloric acid 37% (7.2 mL) was added. The reaction was refluxed at 75°C for 5 hours. The reaction was cooled and DCM was added, causing product **156** to precipitate as a white crystalline solid (0.911 g, 12.4 mol, 91% yield over two steps). Prior to use, this compound is neutralized by washing with sodium bicarbonate. ^{1}H NMR (300 MHz, DMSO) δ 7.42 (s, 5H), 5.01 (s, 2H).

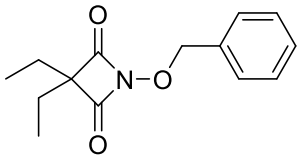

(164) 1-(benzyloxy)-3,3-diethylazetidine-2,4-dione. O-benzylhydroxylamine **156** (1,1 eq.) in dioxane (10mL/eq. of amine) was slowly added to diethylmalonyl dichloride in dioxane (10 mL/eq. of dichloride) at 0°C. Triethylamine (2.1 eq.) in dioxane (5 mL/eq. of TEA) was slowly added to the reaction. The reaction was allowed to reach room temperature and stirred overnight under nitrogen atmosphere. The solid that formed in the reaction medium was filtered and the filtrate evaporated and purified by combi flash chromatography. Compound **164** was obtained as a white solid (0.219 g, 0.89 mmol, 19% yield). ^{1}H NMR (300 MHz, CDCl3) δ 7.39 – 7.25 (m, 5H), 5.04 (s, 2H), 1.54 (q, J = 7.5 Hz, 4H), 0.76 (t, J = 7.5 Hz, 6H).

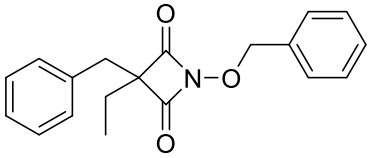

(161) 3-benzyl-1-(benzyloxy)-3-ethylazetidine-2,4-dione. O-benzylhydroxylamine **156** (1,1 eq.) in dioxane (10mL/eq. of amine) was slowly added to 2-benzyl-2-ethylmalonyl dichloride **160** in dioxane (10 mL/eq. of dichloride) at 0°C. Triethylamine (2.1 eq.) in dioxane (5 mL/eq. of TEA) was slowly added to the reaction. The reaction was allowed to reach room temperature and stirred overnight under nitrogen atmosphere. The solid that formed in the reaction medium was filtered and the filtrate evaporated and purified by combi flash chromatography. Compound **161** was obtained as a white solid (0.4 g, 1.3 mmol, 21% yield). ^{1}H NMR (300 MHz, CDCl3) δ 7.40 – 7.17 (m, 10H), 4.52 (s, 2H), 2.96 (s, 2H), 1.78 (q, J = 7.5 Hz, 2H), 0.97 (t, J = 7.5 Hz, 3H).

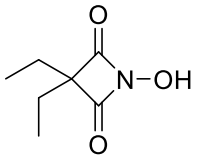

(S3) 3,3-diethyl-1-hydroxyazetidine-2,4-dione. The 4-Oxo-β-Lactam **164** was dissolved in MeOH. Palladium on activated charcoal was added. The reaction was vigorously stirred under nitrogen atmosphere. TES (10 eq.) was slowly added to the reaction, which was stirred for 10 min. The palladium was filtered and washed with ethyl acetate. The filtrate was evaporated under reduced pressure, resulting in a crude colorless oil, which was used without further purification.

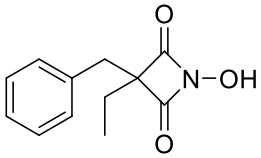

(162) 3-benzyl-3-ethyl-1-hydroxyazetidine-2,4-dione. The benzylated 4-Oxo-β-Lactam **161** was dissolved in MeOH. Palladium on activated charcoal was added. The reaction was vigorously stirred under nitrogen atmosphere. TES (10 eq.) was slowly added to the reaction, which is stirred for 10 min. The palladium was filtered and washed with ethyl acetate. The filtrate was evaporated under reduced pressure, resulting in a crude colorless oil, which was used without further purification.

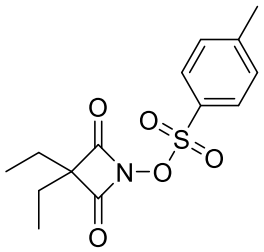

(152) 3,3-diethyl-2,4-dioxoazetidin-1-yl 4-methylbenzenesulfonate. The crude reaction from the TES hydrogenation containing compound **S3** was dissolved in dry DCM. Pyridine (1,1 eq.) was added, followed by 4-methylbenzenesulfonyl chloride (1,1

eq.). The reaction was stirred overnight. The solvent was evaporated under reduced pressure and the product was purified by flash column chromatography. Compound **152** was obtained from 3-benzyl-3-ethyl-1-hydroxyazetidine-2,4-dione as a white solid (0.084 g, 0.22 mmol, 41% yield); ^{1}H NMR (300 MHz, CDCl3) δ 7.56 (d, J = 8.4 Hz, 2H), 7.38 – 7.29 (m, 5H), 7.21 – 7.14 (m, 2H), 2.99 (s, 2H), 2.47 (s, 3H), 1.85 (q, J = 7.5 Hz, 2H), 1.05 (t, J = 7.5 Hz, 3H). ^{13}C NMR (75 MHz, CDCl3) δ 168.29, 147.33, 133.94, 130.32, 130.28, 129.96, 129.32, 128.97, 127.85, 64.76, 36.67, 24.66, 22.05, 9.12.

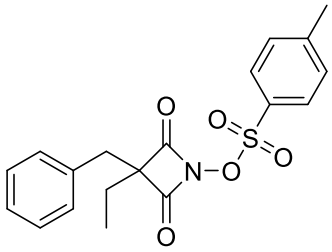

(153) 3-benzyl-3-ethyl-2,4-dioxoazetidin-1-yl 4-methylbenzenesulfonate. The crude reaction from the TES hydrogenation containing compound **162** was dissolved in dry DCM. Pyridine (1,1 eq.) was added, followed by 4-methylbenzenesulfonyl chloride (1,1 eq.). The reaction was stirred overnight. The solvent was evaporated under reduced pressure and the product was purified by flash column chromatography. Compound **153** was obtained as a white solid (0.105 g, 0.34 mmol, 47% yield); ^{1}H NMR (300 MHz, CDCl3) δ 7.94 (dt, 2H), 7.39 (dd, J = 8.6, 0.6 Hz, 2H), 2.45 (s, 3H), 1.80 – 1.65 (m, 4H), 0.56 (t, J = 7.5 Hz, 6H). ^{13}C NMR (75 MHz, CDCl3) δ 172.52, 170.80, 147.50, 132.54, 130.39, 129.24, 54.21, 28.86, 21.95, 8.45.

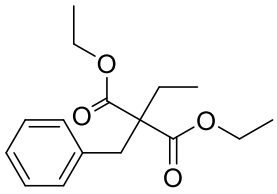

(158) Diethyl 2-benzyl-2-ethylmalonate. Sodium ethoxide (1.1 eq. to malonic ester) was prepared by dissolving sodium in ethanol. Diethyl 2-benzylmalonate (2.5g, 10 mmol) was added, and the reaction was stirred for 30 minutes. Iodoethane (1.1 eq.) was added and

the reaction was refluxed for 5 h. Compound **158** was obtained from diethyl 2-benzylmalonate as a yellow oil (2.689 g, 9.66 mmol, quant. yield). ^{1}H NMR (300 MHz, $CDCl_3$) δ 7.32 – 7.19 (m, 3H), 7.10 (dd, *J* = 7.6, 1.8 Hz, 2H), 4.25 – 4.14 (m, *J* = 9.8, 6.8, 3.1 Hz, 4H), 3.25 (s, 2H), 1.85 (q, *J* = 7.5 Hz, 2H), 1.26 (t, *J* = 7.1 Hz, 6H), 0.94 (t, *J* = 7.5 Hz, 3H).

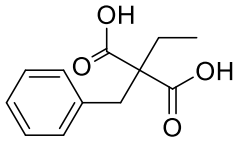

(**159**) 2-benzyl-2-ethylmalonic acid. The disubstituted malonic ester **158** (2.689 g, 9.66 mmol) was dissolved in ethanol (20 mL) and sodium hydroxide (20 mL, 2M) was added. The reaction was refluxed for 5 h. The reaction media was poured into an extraction vessel with 50 mL of water and the remaining starting material was extracted with 3 x 30 mL ethyl acetate. The aqueous fraction was acidified and the product was extracted with 3 x 30 mL ethyl acetate. Concentration of these fractions resulted in the correspondent malonic acid **159**, obtained as a white solid (2.145 g, 9.65 mmol, quant. yield). ^{1}H NMR (300 MHz, CDCl3) δ 7.36 – 7.13 (m, 5H), 3.32 (s, 2H), 2.06 (q, J = 7.4 Hz, 2H), 1.01 (t, J = 7.5 Hz, 3H).

S2.6. Vinyl Sulfone Activity-based Probe

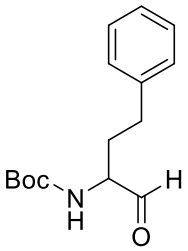

(157) tert-butyl (1-oxo-4-phenylbutan-2-yl)carbamate. 2-((tert-butoxycarbonyl)amino)-4-phenylbutanoic acid (**156**) (500mg, 1.79mmol) was dissolved in dry dichloromethane (DCM) (4mL). Triethylamine (TEA) (0.252µL, 1.8mmol) was added to the solution, which was stirred for 20 minutes. O-(Benzotriazol–1-yl)-

N,N,N′,N′-tetramethyluronium tetrafluoroborate (TBTU) (0.581mg, 1.81mmol) was added to the mixture and the solution was stirred for one hour. N-O-dimethylhydroxylamine (0.195mg, 2,0mmol) was added and the reaction was stirred at room temperature overnight. The reaction mixture was diluted with DCM and washed with hydrochloric acid (3M), followed by washing with potassium hydrogen sulfate and a third washing step with brine. The organic fraction was collected and dried with sodium sulfate, filtered and concentrated under reduced pressure, yielding a crude mass of 440mg, which was dried under vacuum overnight. This mass was dissolved in dry THF (8mL) and cooled to 0°C. Lithium aluminum hydride (70.2mg, 1.85mmol) was added to the solution, which was stirred under nitrogen atmosphere for one hour. The reaction was quenched with 20mL of potassium hydrogen sulfate (10%). The aqueous phase was extracted with diethyl ether until there was no evidence of product remaining in the aqueous phase, as analyzed by TLC. The organic layers were combined and concentrated under reduced pressure, yielding **157** as a colorless oil (325mg, 1.2mmol, 69%).

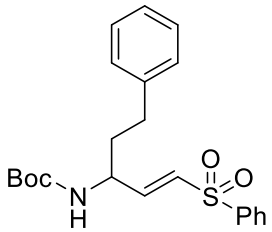

(158) tert-butyl (E)-(5-phenyl-1-(phenylsulfonyl)pent-1-en-3-yl)carbamate. Diethyl ((phenylsulfonyl)methyl)phosphonate (342mg, 1.2mmol) was dissolved in dry THF (8mL) and the solution was cooled to -10°C. Sodium hydride 60% (24mg, 1mmol) was added and the solution was stirred for 10 minutes before a cooled solution of compound **157** was added. The solution was stirred for 4 hours and then diluted with diethyl ether and washed with brine three times. The organic layers were combined, dried with sodium sulfate, filtered and concentrated under reduced pressure, yielding a yellow oil, which was purified by combi flash chromatography, resulting in compound **158** as a colorless oil (152.1mg, 0.4mmol, 32%).

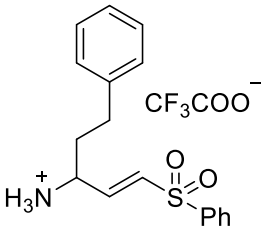

(159) (E)-5-phenyl-1-(phenylsulfonyl)pent-1-en-3-aminium 2,2,2-trifluoroacetate. Compound **158** was dissolved in DCM (3mL). Trifluoroacetic acid (TFA) (3mL, 39.2mmol) was added and the reaction was stirred for 3 hours. The solution was concentrated under reduced pressure. The crude mass was dissolved in DCM and evaporated three times, yielding **159** as a white solid (212mg, 0.5mmol, quantitative yield).

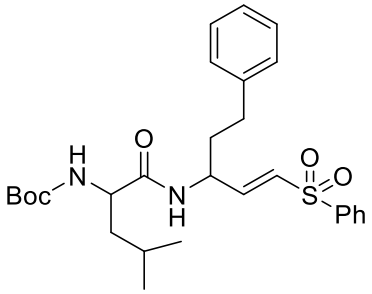

(160) tert-butyl (E)-(4-methyl-1-oxo-1-((5-phenyl-1-(phenylsulfonyl)pent-1-en-3-yl)amino)pentan-2-yl)carbamate. Boc-protected valine (123mg, 0.53mmol) was dissolved in DMF (7.5mL). TEA (75µL, 0.54mmol) was added to the solution, followed by hydroxybenzotriazole (HOBt) (1 eq.) and then TBTU (1 eq.). The mixture was stirred at 0°C for 30 minutes under nitrogen atmosphere. Compound **159** (1.1 eq.) was dissolved in a mixture of DMF (7.5mL) and TEA (1 eq.) and this solution was added to the reaction, which was stirred overnight at room temperature under nitrogen atmosphere. HCl 3M (10 mL) was added to the mixture and the product was extracted with 3 x 3 mL of ethyl acetate. The organic layers were combined, dried with sodium sulfate and concentrated under reduced pressure. The resulting colorless oil was purified by combi flash chromatography, yielding **160** as a white solid (175mg, 0.34mmol, 67%).

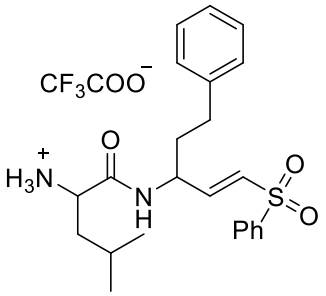

(161) (E)-4-methyl-1-oxo-1-((5-phenyl-1-(phenylsulfonyl)pent-1-en-3-yl)amino)pentan-2-aminium 2,2,2-trifluoroacetate. Compound **160** (175mg, 0.34mmol) was dissolved in DCM (4mL) and TFA (4mL) was added. The solution was stirred at room temperature for 3 hours. The solution was concentrated under reduced pressure. The crude mass was dissolved in DCM and evaporated three times, yielding **161** as a white solid (180.4mg, 0.34mmol, quantitative yield).

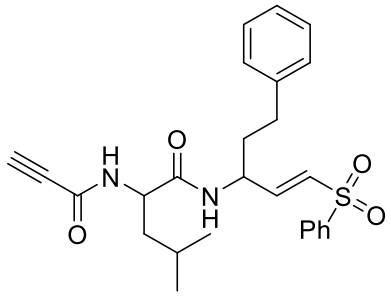

(162) (E)-4-methyl-N-(5-phenyl-1-(phenylsulfonyl)pent-1-en-3-yl)-2-propiolamidopentanamide. Propiolic acid (30µL, 0.49mmol) and TEA (1 eq.) were dissolved in DMF (12mL) and stirred at 0°C. HoBt (1.1 eq.) and TBTU (1.1 eq.) were added and the reaction was stirred for 30 minutes. Compound **161** (180.4mg, 0.34mmol) in DMF (12mL) and TEA (1.1 eq.) was added to the reaction, which was allowed to reach room temperature and stirred overnight. The solution was diluted with HCl 3M (20 mL) and extracted with 3 x 5 mL of EtOAc. The organic phases were combined, dried with sodium sulfate and concentrated under reduced pressure. Combi flash chromatography purification yielded compound **161** as a colorless oil (73mg, 0.15mmol, 38%). ^{1}H NMR (300 MHz, CDCl3) δ 7.85 – 7.79 (m, 2H), 7.50 (m, 3H), 7.24 – 7.11 (m, 3H), 7.06 – 7.01 (m, 2H), 6.90 (dd, J = 15.1, 5.5 Hz, 1H), 6.46 (dd, J = 15.1, 1.4 Hz, 1H), 4.66 – 4.50 (m,

2H), 2.78 (s, 1H), 2.63 – 2.52 (m, 2H), 1.95 – 1.82 (m, 2H), 1.61 – 1.46 (m, 3H), 0.84 (d, J = 5.9 Hz, 3H), 0.80 (d, J = 6.0 Hz, 3H).

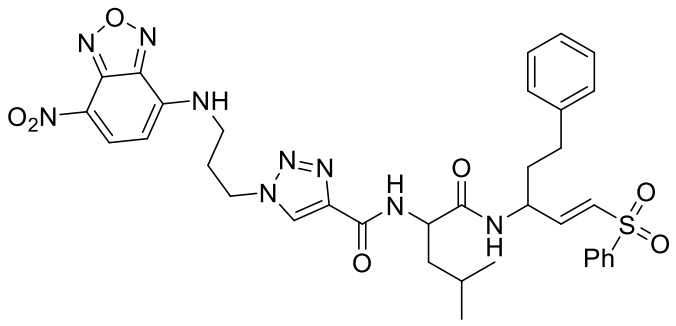

(163) (E)-N-(4-methyl-1-oxo-1-((5-phenyl-1-(phenylsulfonyl)pent-1-en-3-yl)amino)pentan-2-yl)-1-(3-((7-nitrobenzo[c][1,2,5]oxadiazol-4-yl)amino)propyl)-1H-1,2,3-triazole-4-carboxamide. Compound **162** (73mg, 0.15mmol) was dissolved in DMF (0.75mL). $CuSO_4$ (1% (aq.), 10% eq. M) and sodium ascorbate (2% (aq.), 10% eq. M) were added to the solution, which was stirred under nitrogen atmosphere for 10 minutes. NBD-azide **88** (1.1 eq.) was added to the reaction, which was stirred overnight. Water (10 mL) was added to the reaction medium and the product was extracted with 3 x 5 mL ethyl acetate. The organic fractions were combined, dried with anhydrous sodium sulfate and concentrated under reduced pressure. The crude was purified by combi flash chromatography, yielding compound **163** as an orange solid (30mg, 0.04mmol, 28%). ^{1}H NMR (500 MHz, Acetone) δ 8.51 (d, J = 8.8 Hz, 1H), 8.48 (s, 1H), 8.35 (s, 1H), 7.90 – 7.86 (m, 2H), 7.86 – 7.81 (m, 1H), 7.78 (d, J = 8.2 Hz, 1H), 7.73 – 7.69 (m, 1H), 7.65 – 7.61 (m, 2H), 7.22 (t, J = 7.4 Hz, 2H), 7.18 – 7.13 (m, 3H), 6.98 (dd, J = 15.1, 4.9 Hz, 1H), 6.70 (d, J = 15.1 Hz, 1H), 6.48 (d, J = 8.7 Hz, 1H), 4.78 – 4.68 (m, 3H), 4.70 – 4.62 (m, 1H), 3.79 (s, 2H), 2.79 – 2.60 (m, 2H), 2.59 – 2.52 (quint, J = 6.9 Hz, 2H), 1.92 – 1.66 (m, 5H), 0.94 (dd, J = 16.0, 6.1 Hz, 6H). ^{13}C NMR (126 MHz, Acetone) δ 172.6 (C-3), 160.9 (C-24), 147.4 (C-19), 145.6 (C-34), 145.2 (C-38), 143.7 (C-26), 142.2 (C-13), 142.0 (C-44), 137.8 (C-37), 134.3 (C-47), 131.6 (C-20), 130.3 (C-45, C-49), 129.3 (C-15, C-17), 129.3 (C-14, C-18), 128.3 (C-46, C-48), 127.2 (C-30), 126.8 (C-16), 52.8 (C-10), 50.1 (C-2), 48.7 (C-35), 42.0 (C-32), 36.2 (C-11), 32.8 (C-12), 25.7 (C-5), 23.4 (C-6), 22.2 (C-7). Accurate mass: 729.2603; HRMS (m/z): found 730.2777 [M+1].

S2.7. TUDCA Probe

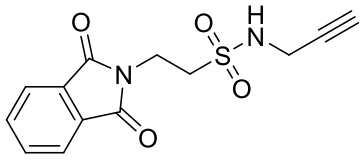

(168) 2-(1,3-dioxoisoindolin-2-yl)-N-(prop-2-yn-1-yl)ethane-1-sulfonamide. 2-(1,3-dioxoisoindolin-2-yl)ethane-1-sulfonyl chloride (0.3 g, 1.1 mmol) was dissolved in dry DCM (10 mL). Triethylamine (0.153 mL, 1.1 mmol) was added, followed by propargylamine (0.07 g, 1.1 mmol). The reaction was stirred for 2 h. The solvent was evaporated under reduced pressure and the product was purified by combi flash chromatography, yielding a white solid (0.28 g, 0.96 mmol, 86% yield). ^{1}H NMR (300 MHz, Acetone) δ 7.86 (s, 4H), 6.67 (t, J = 5.7 Hz, 1H), 4.15 (t, J = 7.0 Hz, 2H), 4.03 – 3.98 (m, 2H), 3.58 (t, J = 7.0 Hz, 2H), 2.87 (t, 1H). ^{13}C NMR (75 MHz, Acetone) δ 168.40, 135.13, 133.04, 123.87, 80.38, 74.16, 50.75, 33.33, 32.82.

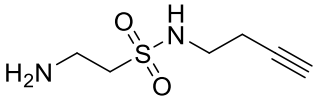

(169) 2-amino-N-(but-3-yn-1-yl)ethane-1-sulfonamide. N-(but-3-yn-1-yl)-2-(1,3-dioxoisoindolin-2-yl)ethane-1-sulfonamide (0.27 g, 0.92 mmol) was dissolved in EtOH (5 mL). Hydrazine 98% (0.05 mL, 2.23 mmol) was added and the reaction was refluxed for 5 h. The solvent was evaporated under reduced pressure and the compound was used without further purification.

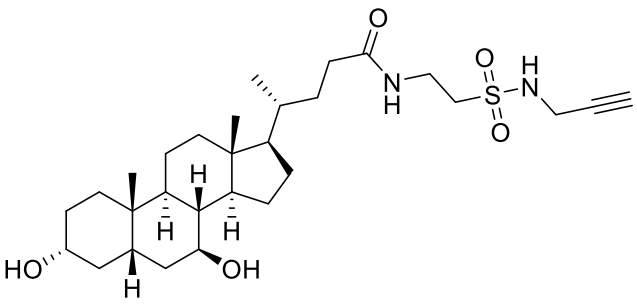

(170) (R)-4-((3R,5S,7S,8R,9S,10S,13R,14S,17R)-3,7-dihydroxy-10,13-dimethylhexadecahydro-1H-cyclopenta[a]phenanthren-17-yl)-N-(2-(N-(prop-2-yn-1-yl)sulfamoyl)ethyl)pentanamide. UDCA (0.435 g, 1.11 mmol) was dissolved in DMSO (4 mL). HOBt (1.1 eq.) was added, followed by TBTU (1.1 eq.) and the reaction was stirred for 30 min. The crude from the phthalimide deprotection reaction of N-(but-3-yn-1-yl)-2-(1,3-dioxoisoindolin-2-yl)ethane-1-sulfonamide was added and the reaction was stirred overnight. Water (20 mL) was added and the product was extracted with 3 x 5 mL of EtOAc. The organic fractions were combined, dried with anhydrous sodium sulfate, and concentrated under reduced pressure. The crude mixture obtained was used without further purification.

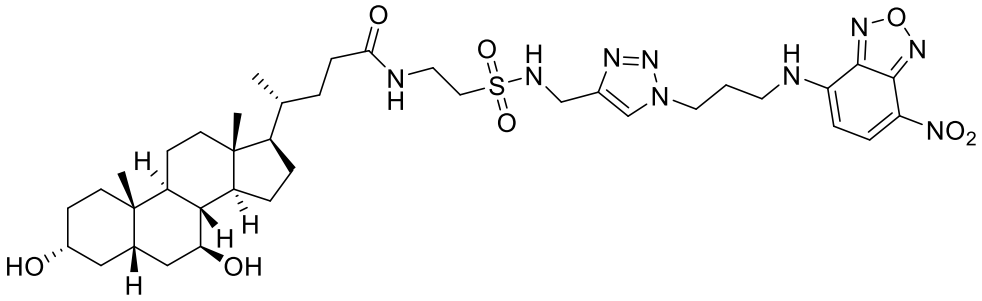

(171) (R)-4-((3R,5S,7S,8R,9S,10S,13R,14S,17R)-3,7-dihydroxy-10,13-dimethylhexadecahydro-1H-cyclopenta[a]phenanthren-17-yl)-N-(2-(N-((1-(3-((7-nitrobenzo[c][1,2,5]oxadiazol-4-yl)amino)propyl)-1H-1,2,3-triazol-4-yl)methyl)sulfamoyl)ethyl)pentanamide. The crude mixture containing **170** (100 mg) was dissolved in DMF (0.75mL). $CuSO_4$ (1% (aq.), 10% eq. M) and sodium ascorbate (2% (aq.), 10% eq. M) were added to the solution, which was stirred under nitrogen atmosphere for 10 minutes. NBD-azide **88** (1.1 eq.) was added to the reaction, which was stirred overnight. Water (10 mL) was added to the reaction medium and the product was

extracted with 3 x 5 mL ethyl acetate. The organic fractions were combined, dried with anhydrous sodium sulfate and concentrated under reduced pressure. The crude was purified by flash chromatography, yielding compound **171** as a yellow solid (12 mg, 0.015 mmol).

S3. Crystallography Section

Crystals of Porcine Pancreatic Elastase (PPE), were obtained as previously described.[3, 4] In summary, PPE (SERVA Electrophoresis GmbH, Heidelberg, Germany), was dissolved in Milli-Q water to a final concentration of 20 $mg.mL^{-1}$ (~0.8 mM), and used for crystallization trials without further purification. 100 mM stock solutions were prepared for ligands **94, 95, 96** and **102** in 100% (*V*/*V*) dimethyl sulfoxide (DMSO). PPE crystals were obtained at 20^{o}C using the sitting-drop vapor diffusion method by mixing equal volumes of protein and crystallization solution consisting of 70 % (*V*/*V*) MPD (2-methyl-2,4-pentanediol), 10 mM sodium/potassium phosphate buffer pH 5.9 (this solution was chosen based on previous crystallization reports of PPE).[5] HNE (Elastin Products Co., Inc. Owensville, Missouri, USA , No. SE563) was crystallized in 24% PEG Smear Broad, 0.1 M Tris-HCl pH 7.2, 0.1 M potassium thiocyanate and 0.1M sodium bromide.

Complexes of PPE and HNE with inhibitors were obtained by co-crystallization. Elastases were first incubated with each inhibitor in 5X molar excess for 15-30 min (PPE) or 60-90 min (HNE), at room temperature, with final DMSO concentration around 3% (*V*/*V*). Crystals of putative complexes of both enzymes were grown under similar crystallization conditions as for the apo-protein, testing various concentrations and ratios of protein:precipitant and drop volumes (at 20^{o}C). In some of the drops, nucleation had to be promoted using seeding techniques, namely microseeding.[6]

For X-ray diffraction data collection, crystals were harvested from the drops and directly flash-cooled in liquid nitrogen. The crystallization solution of PPE with 70% MPD is already cryoprotectant, whereas for HNE, ethylene glycol was added to the crystallization solution to a final concentration of 20% (*V*/*V*). In alternative, 25% (*V*/*V*) PEG Smear High, 0.1 M sodium acetate pH 4.5 and 20% (*V*/*V*) ethylene glycol was tested.

Data were collected at beamlines ID23 and ID30A-3 at the European Synchrotron Radiation Facility (ESRF, Grenoble, France), and I03 and I24 at the Diamond Light Source (Didcot, Oxfordshire, UK), synchrotrons. The programs *XDS*,[7] *POINTLESS*[8] and *AIMLESS*,[9] all within the *autoPROC* pipeline,[10] were used to integrate, determine space group and scale the data, respectively. *STARANISO*,[11] also within the *autoPROC* pipeline, was used to analyze the anisotropy of the data and, eventually, extend the resolution to a higher limit. Data collection and reduction statistics are depicted in Table SX. Molecular replacement solutions for PPE and HNE datasets were obtained with

PHASER,[12] as implemented in the *PHENIX* suite of programs,[13, 14] using the coordinates of 4YM9 (PDB entry[3, 4]) for PPE and 1HNE for HNE (PDB entry),[15] devoid of any ligands and solvent molecules, as search models. Initial crystallographic refinement was performed with *BUSTER-TNT*[16] using the macro "Missing Atoms" and "-L" flag ("presence of an unknown ligand"), to render clear electron density for the putative ligands. Iterative model building and refinement were carried out with programs *COOT*[17] and *BUSTER-TNT*[16] until model convergence and satisfactory overall quality statistics were achieved. Hydrogen atoms were added with zero occupancy before each refinement cycle with the program *HYDROGENATE*, which uses *reduce* from the *MolProbity* suite.[18] Final refinements were performed with *phenix.refine*[14] from the *PHENIX* suite of programs.[13] Structure validation was carried out with *MolProbity*[18] as implemented in *phenix.refine*. Final refinement and validation statistics are shown in tables S1 and S2. All figures were rendered with PyMol.[19]

Accession codes: The atomic coordinates and structure factor amplitudes of PPE:**94**, PPE:**95**, PPE:**96** and HNE:**102** complex structures were deposited in the Protein Data Bank (PDB) as entries 6QBU, 6QEN, 6QEO, and XYWZ (being deposited), respectively.

Table S1. Data collection and refinement statistics for complexes PPE:7 and PPE:8.

	PPE:94		**PPE:95**	
PDB Entry	6QBU		6QEN	
	autoPROC/STARANISO	autoPROC/AIMLESS	autoPROC/STARANISO	autoPROC/AIMLESS
Data collection				
Synchrotron	ESRF (Grenoble – France)		DLS (Oxford – UK)	
Beamline	ID30A-3		I03	
Wavelength (Å)	0.976		0.976	
Resolution range (Å)[a]	45.57 – 1.38 (1.45 – 1.38)	45.57 – 1.53 (1.56 – 1.53)	34.05 – 1.20 (1.30 – 1.20)	34.05 – 1.41 (1.44 – 1.41)
Space group	$P\,2_1\,2_1\,2_1$		$P\,2_1\,2_1\,2_1$	
Unit cell				
***a, b, c* (Å)**	50.55, 57.55, 74.59		51.13, 57.71, 74.65	

***α, β, γ* (°)**	90.0, 90.0, 90.0		90.0, 90.0, 90.0	
Total no. of reflections	154 232 (6 552)	129 339 (6 576)	198 534 (11 131)	164 442 (8 329)
No. of unique reflections	38 592 (1 929)	32 333 (1 617)	49 274 (2 466)	42 081 (2 116)
Multiplicity	4.0 (3.4)	4.0 (4.1)	4.0 (4.5)	3.9 (3.9)
Completeness spherical (%)	84.3 (28.2)	97.2 (99.9)	70.0 (15.6)	98.0 (98.4)
Completeness ellipsoidal (%)	91.8 (57.6)	-	93.5 (70.2)	-
<*I*/σ(*I*)>	11.4 (1.2)	13.3 (2.1)	14.5 (1.5)	16.7 (2.2)
R_{merge} (%)[b]	5.4 (73.3)	5.0 (49.2)	3.4 (75.0)	3.2 (43.6)
R_{pim} (%)[c]	2.9 (44.6)	2.6 (25.7)	1.9 (39.1)	1.8 (24.7)
$CC_{1/2}$ (%)[d]	99.9 (57.8)	99.9 (81.9)	99.9 (65.7)	99.9 (86.1)
Refinement				
R_{cryst} (%)[e]	13.32 (21.31)	-	14.20 (21.65)	-
R_{free} (%)[f]	16.34 (26.00)	-	17.40 (27.39)	-
RMSD bonds (Å)[g]	0.007	-	0.008	-
RMSD angles (°)	0.98	-	0.98	-
Protein residues	Val16 – Asn245	-	Val16 – Asn245	-
Ramachandran plot				
Most favoured (%)	97.9	-	97.5	-
Outliers (%)	0.0	-	0.0	-
Rotamer outliers (%)	0.0	-	0.5	-
Clashscore[h]	0.81	-	2.72	-
MolProbity score[i]	0.78	-	1.16	-
***B*-factors (Å^2)**				
Protein	18.81	-	23.42	-
Ligands/ions	27.94	-	28.21	-

[a] Information in parenthesis refers to the last resolution shell.

[b] $R_{merge} = \sum_{hkl}\sum_i |I_i(hkl) - \overline{I(hkl)}| \,/\, \sum_{hkl}\sum_i I_i(hkl)$.

[c] $R_{p.i.m} = \sum_{hkl}[1/(N-1)^{\frac{1}{2}} \sum_i |I_i(hkl) - \overline{I(hkl)}| / \sum_{hkl}\sum_i I_i(hkl)$.

[d] $CC_{1/2}$ as described in Karplus & Diederichs (2012). Science, 336(6084): 1030–1033.

[e] $R_{cryst} = \sum_h \sum_k \sum_l \frac{\{||F_o(h,k,l)|-|F_c(h,k,l)||\}}{\sum_h \sum_k \sum_l |F_o(h,k,l)|}$, where F_o and F_c are the observed and calculated structure factors for reflection *h*, respectively.

[f] R_{free} was calculated the same way as R_{cryst} but using only 5% of the reflections which were selected randomly and omitted from refinement.

[g] RMSD, root mean square deviation.

[h] Clashscore is the number of unfavourable all-atom steric overlaps ≥ 0.4Å per 1000 atoms. Word *et al.*,(1999). Mol Biol, 285(4):1711-33.

[i] *MolProbity* score provides a single number that represents the central *MolProbity* protein quality statistics; it is a log-weighted combination of clashscore, Ramachandran not favoured and bad side-chain rotamers, giving one number that reflects the crystallographic resolution at which those values would be expected.

Table S2. Data collection and refinement statistics for complexes PPE:9 and HNE:17.

	PPE:96		**HNE:102**
PDB Entry	6QEO		XXXX
	autoPROC/STARANISO	autoPROC/AIMLESS	autoPROC/AIMLESS
Data collection			
Synchrotron	ESRF (Grenoble – France)		DLS (Oxford – UK)
Beamline	ID23		I24
Wavelength (Å)	0.967		1.649
Resolution range (Å)[a]	33.94 – 1.30 (1.35 – 1.30)	33.94 – 1.42 (1.44 – 1.42)	62.83 – 2.59 (2.63 – 2.59)
Space group	*P* 2_1 2_1 2_1		*C2*
Unit cell			
***a, b, c* (Å)**	50.74, 57.71, 74.66		116.67, 105.91, 79.47
***α, β, γ* (º)**	90.0, 90.0, 90.0		90.0, 121.1, 90.0
Total no. of reflections	210 764 (6 935)	187 811 (6 811)	85 806 (4 020)
No. of unique reflections	49 091 (2 456)	41 396 (1 917)	24 564 (1 254)
Multiplicity	4.3 (2.8)	4.5 (3.6)	3.5 (3.2)
Completeness spherical (%)	88.9 (40.6)	98.0 (91.5)	95.1 (97.3)
Completeness ellipsoidal (%)	91.8 (52.0)	-	-
<*I*/σ(*I*)>	13.4 (1.2)	15.7 (2.2)	6.6 (1.8)
R_{merge} (%)[b]	4.5 (65.2)	4.4 (42.8)	23.4 (126.4)

R_{pim} (%)[c]	2.4 (44.4)	2.2 (24.6)	13.3 (75.5)
$CC_{1/2}$ (%)[d]	99.9 (62.8)	99.9 (83.8)	96.6 (36.7)
Refinement			
R_{cryst} (%)[e]	13.01 (21.55)	-	20.79 (27.19)
R_{free} (%)[f]	16.74 (26.07)	-	25.76 (31.39)
RMSD bonds (Å)[g]	0.009	-	0.002
RMSD angles (°)	1.17	-	0.547
Protein residues	Val16 – Asn245	-	Ile16 – Gln233
Ramachandran plot			
Most favoured (%)	97.5	-	97.4
Outliers (%)	0.0	-	0.0
Rotamer outliers (%)	0.5	-	0.2
Clashscore[h]	1.59	-	3.50
MolProbity score[i]	1.01	-	1.27
B-factors (Å^2)			
Protein	17.70	-	40.93
Ligands/ions	22.94	-	57.54

[a] Information in parenthesis refers to the last resolution shell.

[b] $R_{merge} = \sum_{hkl}\sum_i |I_i(hkl) - \overline{I(hkl)}| / \sum_{hkl}\sum_i I_i(hkl)$.

[c] $R_{p.i.m} = \sum_{hkl}[1/(N-1)^{\frac{1}{2}} \sum_i |I_i(hkl) - \overline{I(hkl)}| / \sum_{hkl}\sum_i I_i(hkl)$.

[d] $CC_{1/2}$ as described in Karplus & Diederichs (2012). Science, 336(6084): 1030–1033.

[e] $R_{cryst} = \sum_h \sum_k \sum_l \frac{\{||F_o(h,k,l)|-|F_c(h,k,l)||\}}{\sum_h \sum_k \sum_l |F_o(h,k,l)|}$, where F_o and F_c are the observed and calculated structure factors for reflection *h*, respectively.

[f] R_{free} was calculated the same way as R_{cryst} but using only 5% of the reflections which were selected randomly and omitted from refinement.

[g] RMSD, root mean square deviation.

[h] Clashscore is the number of unfavourable all-atom steric overlaps ≥ 0.4Å per 1000 atoms. Word *et al.*,(1999). Mol Biol, 285(4):1711-33.

[i] *MolProbity* score provides a single number that represents the central *MolProbity* protein quality statistics; it is a log-weighted combination of clashscore, Ramachandran not favoured and bad side-chain rotamers, giving one number that reflects the crystallographic resolution at which those values would be expected.

S4. Enzymatic Assays

S4.1. Enzymatic Inhibition Assays for Human Neutrophil Elastase

HNE assays were carried out in a total volume of 200µL per well. Each assay well contained 155 µL of 0.1 M HEPES pH 6.9, 20 µL of HNE (stock solution 1.7 µM in 0.05 M acetate buffer, pH 5.5) and 5 µL of the tested compound. After incubation at room temperature for 30 minutes, 20 µL of fluorogenic substrate (MeO-Suc-Ala-Ala-Pro-Val-AMC, Merck, Germany) is added. DMSO was used as control. Enzymatic inhibition assays were carried out at 25ºC for a period of 30 minutes. The reaction was monitored with a FLUOstar Omega (BMG Lactech, Germany) microplate reader, at the excitation wavelength of 360 nM and emission wavelength of 460 nM. IC50s were determined by non-linear regression using GraphPad PRISM software. For all experiments, stock solutions of the tested compounds were prepared and diluted in DMSO.

S4.2. Inhibition Assay for Chymotrypsin

Inhibition assays for chymotrypsin (Calbiochem) were performed in 0.05 M Tris-HCl, 0.138 M NaCl, pH 8.0 with 30 nM human pancreas chymotrypsin, test compounds in pre-determined concentrations, and 100 µM substrate (Suc-Ala-Ala-Pro-Phe-7-amino-4-methylcoumarin, Bachem). DMSO was used as control. The reaction was monitored like for HNE (see S4.1).

S4.3. Inhibition Assay for Urokinase

Inhibition assays for urokinase (Calbiochem) were performed in 0.05 M Tris-HCl, 0.138 M NaCl, pH 8.0, with 30 U/mL human urine urokinase, test compounds in pre-determined concentrations, and 50 µM substrate (Z-Gly-Gly-Arg-AMC.HCl, Bachem). DMSO was used as control. The reaction was monitored like for HNE (see S4.1).

S4.4. Inhibition Assay for Trypsin

Inhibition assays for trypsin (Calbiochem) were performed in 0.05 M Tris-HCl, 0.138 M NaCl, pH 8.0, with 30nM human pancreas Trypsin, test compounds in pre-determined

concentrations, and 50 μM substrate (Z-Gly-Gly-Arg-AMC.HCl, Bachem). DMSO was used as control. The reaction was monitored like for HNE (see S4.1).

S4.5. Inhibition Assay for Thrombin

Inhibition assays for thrombin (Calbiochem) were performed in 0.01 M sodium phosphate, 0.138 M NaCl, 0.1% PEG 6000, pH 7.0, with 1.7 U/mL human plasma thrombin, test compounds in pre-determined concentrations, and 50 μM substrate (Z-Gly-Gly-Arg-AMC.HCl, Bachem). DMSO was used as control. The reaction was monitored like for HNE (see S4.1).

S4.6. Inhibition Assay for Kallikrein

Inhibition assays for kallikrein (Calbiochem) were performed in 0.05 M Tris-HCl, 0.138 M NaCl, pH 8.0, with 2 nM human plasma kallikrein, test compounds in pre-determined concentrations, and 50 μM substrate (H-Pro-Phe-Arg-AMC acetate salt, Bachem). DMSO was used as control. A positive control was also used (Gabexate mesylate, Aldrich). The reaction was monitored like for HNE (see S4.1).

S4.7. Inhibition Assay for DPP8/DPP9

Inhibition assays for DPP8 and DPP9 were performed at the lab of Robert Huber. The results were obtained by measurement of the release of fluorescence by GP-AMC when cleaved by DPP8 or DPP9 in the presence of 4-Oxo-β-Lactam inhibitors.

S4.8. Progress curve determination for HNE

The rates of inhibition of HNE by compound 20 were determined by the progress curve method. Inactivation of HLE was studied at 25 °C by mixing 10 μL of HLE stock solution (2 μM in 0.05 M acetate buffer, pH 5.5) to a solution containing 10 μL of inhibitor in DMSO, 20 μL of the MeOSuc-Ala-Ala-Pro-Val-p-nitroanilide substrate (50 mM in DMSO), and 960 μL of 0.1 MpH 6.9 HEPES buffer, and the absorbance was monitored continuously at 410 nm for 20 min. Control assays, where no inhibitor was used, ran

linearly. Inhibition of HLE was rapid even at very low inhibitor concentrations. In these experimental conditions, progress curves at different inhibitor concentrations were fitted to equation S1, which accounted for the tight-binding nature of the inhibition.

$$A = v_s t + \left[\frac{(v_i - v_s)(1 - y)}{k_{obs}\gamma}\right] ln\left\{\frac{[1 - \gamma \exp(-k_{obs} t)]}{(1 - \gamma)}\right\} + A_0$$

Equation S1

A represents the absorbance at 410 nm (formation of 4-nitroaniline upon hydrolysis of the MeOSuc-Ala-Ala-Pro-Val-*p*-NA through an extinction coefficient of 8250 M^{-1} cm^{-1}), A_0 represents the absorbance at $t = 0$, v_i and v_s represent the initial and final rates of product formation, k_{obs} represents the pseudo-first-order rate constant for the approach to the steady-state;γ is defined by equation S2.

$$\gamma = ([E]/[I])[1 - (v_s/v_i)]^2$$

Equation S2

S5. Proteomics

S5.1. Cell Culture and Handling

U937 cells were cultured in tissue culture flasks using RPMI-1640 medium, supplemented with fetal bovine serum (final concentration of 10%) and L-Glutamine. Cells were seeded at 2 X 105 viable cells/mL and cultured by addition of fresh media every 2 to 3 days, maintaining cell density below 2 X 106 viable cells/mL. Cells were cultured in 95% air and 5% carbon dioxide, at 37°C. SILAC-U937 cells were generated by culturing U937 cells in RPMI-1640 medium supplemented with isotopically labeled arginine for a minimum of 5-8 passages. Aliquots were frozen after in the corresponding SILAC media and stored in liquid nitrogen for future use. After thawing, cells were passaged a minimum of three times before being used in experiments.
HEK293T cells were cultured in tissue culture plates using DMEM medium, supplemented with fetal bovine serum (final concentration of 10%) and L-glutamine. A subcultivation ratio of 1:3 to 1:5 was used for passaging cells every 2 to 3 days when the cells reached approximately 80% confluency. Cells were cultured in 95% air and 5% carbon dioxide, at 37°C.

S5.2. E. coli transformation with serine hydrolase plasmid DNA and Transfection into HEK293T for transient expression of Serine Hydrolases

The plasmids encoding the serine hydrolases that were overexpressed were readily available in the Cravatt lab. The plasmids were transformed into E. coli. Briefly, 16 uL of E. coli suspension were mixed with 2 uL of DNA. The mixture was incubated at 0°C for 30 minutes. Heat-shock at 42°C was done for 30 seconds to induce internalization of the DNA. The cells were put back in ice for 5 minutes. S. O. C. media (600uL) was added and the mixture was incubated at 37°C for 1h. After this, 10uL were plated (100uL SOC media was added to increase the volume) in an LB-CARB (ampicilin) plate and incubated overnight at 37°C. The next day ampicilin resistant colonies had grown. A single colony was picked and suspended in 5mL of LB media. The suspension was incubated overnight with shaking at 37°C. The next day a miniprep was done to extract the DNA. The DNA samples were quantified using a nanodrop equipment (nucleic acid measurement). All constructs were sequenced prior to use.

HEK293T cells were seeded at 5 X 10^5 cells/mL and grown for 48h. A transfection mixture was prepared: per transfection experiment, 200 µL of serum-free DMEM media were mixed gently with 2 µg of plasmid DNA. 6 µg of PEI (1 mg/mL solution) were added and the mixture was mixed vigorously and incubated for 30 minutes. The mixture was added dropwise to the cell plate. The cells were grown for 24-48h before harvesting.

S5.3. SDS-PAGE

1 µL of the tested compound (50 X concentrated) or DMSO was incubated for 30 minutes with 50 µL of whole cell lysate, which was normalized to 1 mg/mL of protein concentration. In case of a competitive experiment, 1 µL of probe (50 X concentrated) is added and incubated for 30 minutes. The reaction is quenched by adding 18 µL of loading buffer mixture. The samples are loaded into a 10% polyacrylamide gel (14% in the competitive ABPP gels to determine the IC50 of HNE). Gels were run at constant voltage of 300 V for 3 to 3.5h. In-gel fluorescence scanning was done to obtain the labelled protein profile.

S5.3.1. Click-chemistry for gel-based assays

A premix of click reagents is prepared by adding (for 110 µL) TBTA (60 µL of 1.7 mM), $CuSO_4$ (20 µL of 50 mM in dH2O), biotin or rhodamine azide (10 µL of 10 mM in DMSO) and TCEP (20 µL x 50mM [14 mg/ mL] in PBS), mixing well between each reagent. 6 µL of premix are added per sample and allowed to react for 1h at room temperature. The reaction is quenched by adding loading buffer.

S5.4. SILAC ABPP-MudPIT

SILAC U937 whole cell lysates were normalized to a concentration of 1 mg/mL. The tested compound and the control are incubated with either light or heavy SILAC whole cell lysates for 30 minutes. (If the experiment is competitive, both samples are then treated with biotinylated probe for 30 minutes) The reaction is quenched by adding each sample to cold MeOH on ice. Both samples are combined in this step by adding to the MeOH. 0.5 mL of cold CHCl3 are then added and the sample is vortexed. 1 mL of cold PBS is added, and the mixture is vortexed, causing the proteins to precipitate. A centrifugation

at 5000 rpm for 10 minutes yields a protein disc in the interface between PBS and the organic solvents. The protein disc is isolated and washed with cold 1:1 mixture of MeOH and CHCl3 (1mL, 3 X). 2 mL of cold MeOH are added and the protein disc is sonicated. 0.5 mL of CHCl3 is added. Centrifugation at 5000 rpm for 10 minutes yields a protein pellet.

Denature, Reduce, Alkylate:

500 µL of 6M urea in PBS are added. 50 µL of a mixture of TCEP (200 mM in PBS) and K2CO3 (600 mM in PBS), to give a final concentration of TCEP of 100 mM, was added and the protein pellet is sonicated into suspension. 20 µL of 10% SDS is added and the suspension is incubated for 30 minutes at 37°C while shaking. 70 µL of iodoacetamide (400 mM) are added and the mixture is incubated at room temperature in the dark for 30 minutes. 120 µL of 10% SDS are added and then the sample is diluted with 5 mL of PBS, giving a final concentration of 0.25% SDS.

Streptavidin Enrichment:

100 µL of streptavidin beads per sample are washed 3 times with 0.25% SDS in PBS and then the total volume of bead suspension is diluted to 500 µL per sample. 500 µL of bead suspension is added to each sample. An incubation for 2.5h at room temperature while rotating is performed. After enrichment, a centrifugation (1400 rpm, 3 minutes) is done to pellet the beads. The supernatant is removed, and the beads are washed 3 times with 10 mL of 0.25% SDS in PBS. The beads are transferred to a low-bind tube and washed 3 times with 1 mL of PBS and 3 times with 1 mL of ddH2O.

Trypsinization:

A trypsin premix is prepared by diluting trypsin (20 ug) with 2mL of 2M urea and adding TEAB for a final concentration of 100 mM (TEAB). 200 µL of trypsin mix is added to each sample. The samples are incubated overnight (14h) at 37°C.

The reaction is transferred into a biospin column and eluted into a LoBind tube. 16 µL of formic acid are added to a final formic acid concentration of 5%. The sample is then run in a LC-MS/MS or stored at -20°C.

Digested peptides are pressure-loaded on to a biphasic capillary column containing a strong cation exchange resin and then reverse phase stationary phase. Loaded samples were analyzed by LC-MS/MS on an LTQ-Orbitrap (Thermo Scientific). The results were searched using the ProLuCID algorithm against a human reverse-concatenated non-redundant (gene-centric) FASTA database, assembled from the Uniprot database. SILAC ratios were quantified using CIMAGE software (described in Weerapana et al., 2010).

5.4.1. ReDiMe Variation

If the procedure uses a ReDiMe protocol the samples are not combined after incubation in the probes and all the sample processing, including denaturation, reduction, alkylation, streptavidin enrichment and trypsinization.

For each final ReDiMe sample, two separate samples need to be prepared for the two conditions being tested, usually treated sample and control, one will be the light sample and one will be the heavy sample. To the light sample light formaldehyde (8 µL of 4% stock solution) is added and to the heavy sample heavy formaldehyde (8 µL of 4% stock solution) is added. 8 µL of 0.6M $NaBH_3CN$ is added to both samples. 1h of incubation at room temperature is done while shaking and then 32 µL of 1% NH_4OH in water is added, followed by 16 µL of formic acid to a final formic acid concentration of 5%. Light and heavy samples and combined, including beads. The supernatant is transferred to a biospin column and eluted into a LoBind tube. The sample is then run in a LC-MS/MS or stored at -20ºC.

S6. Competitive ABPP Gels

S6.1. U937 Whole Cell Lysates

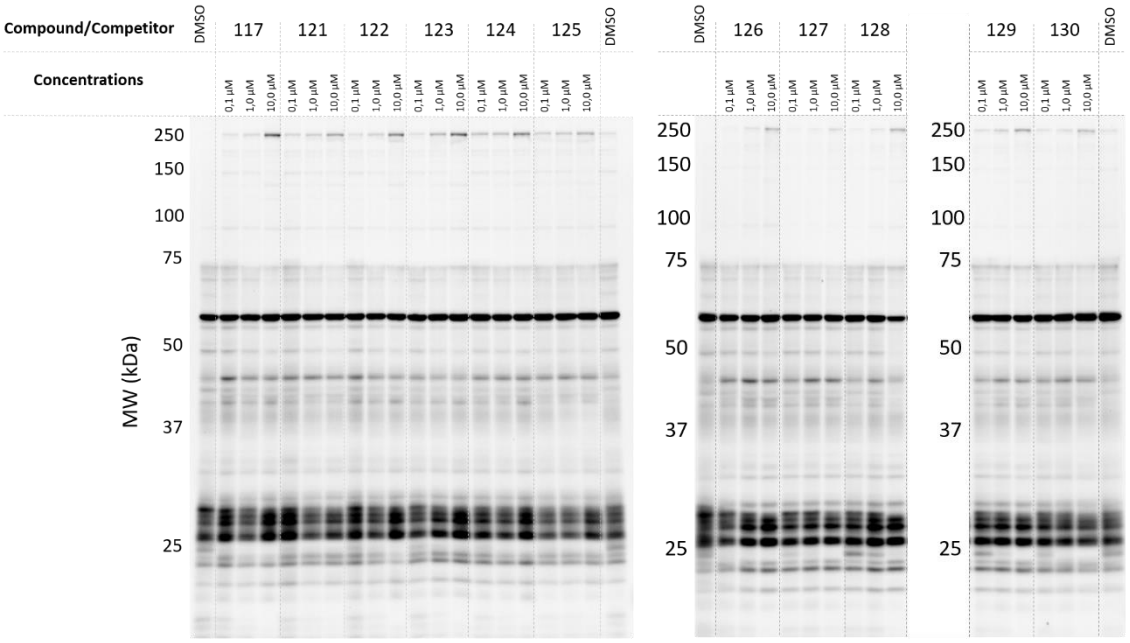

Fig SX – Competitive ABPP in U937 whole cell lysates for compounds **117**, **121-130**.

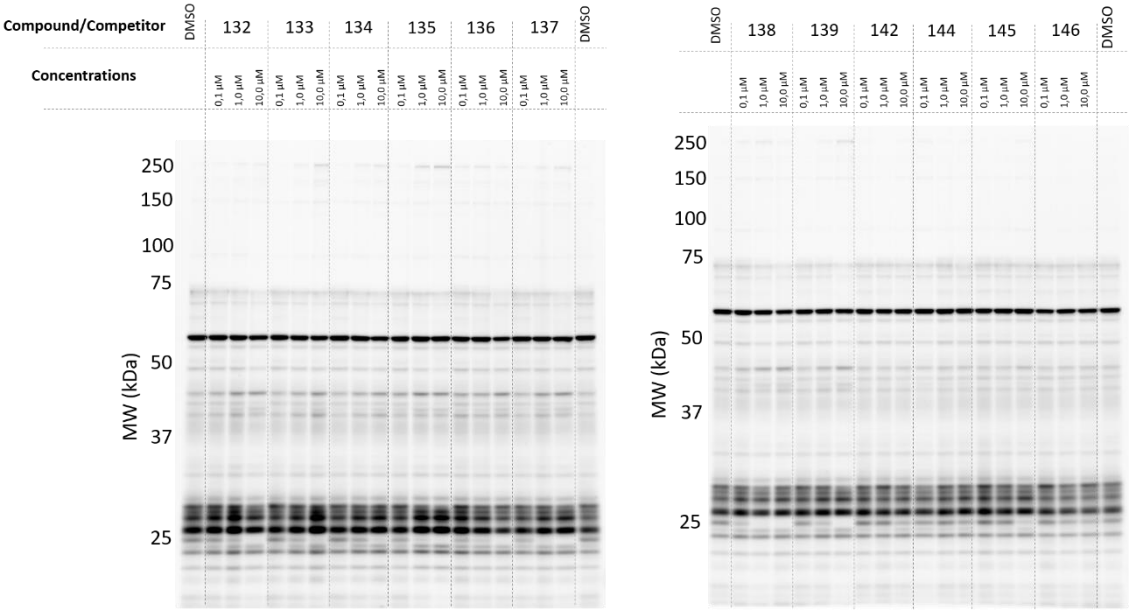

Fig SX – Competitive ABPP in U937 whole cell lysates for compounds **132-139**, **142**, **144-146**.

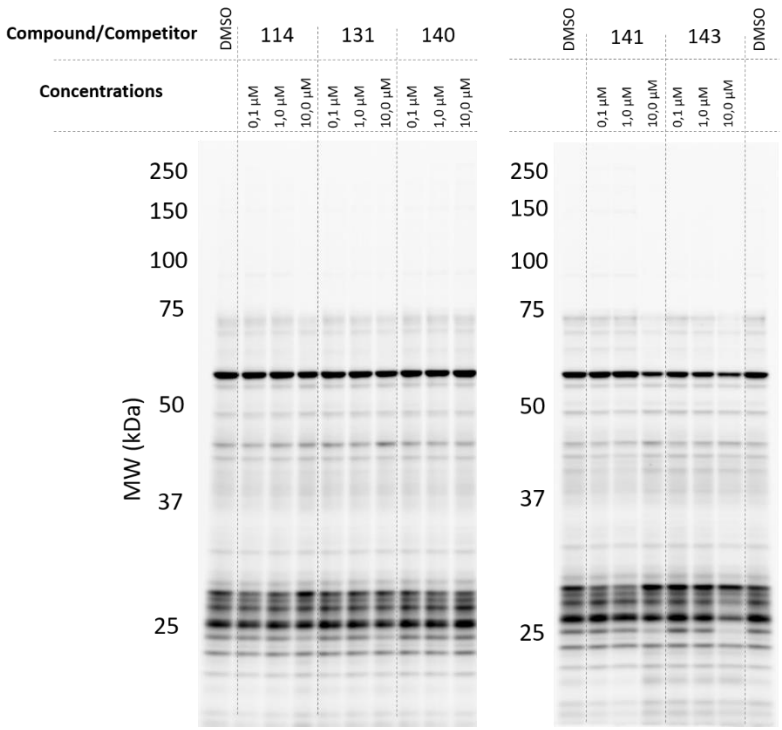

Fig SX – Competitive ABPP in U937 whole cell lysates for compounds **114**, **131**, **140**, **141**, **143**.

S6.2. Fractioned U937 Lysates

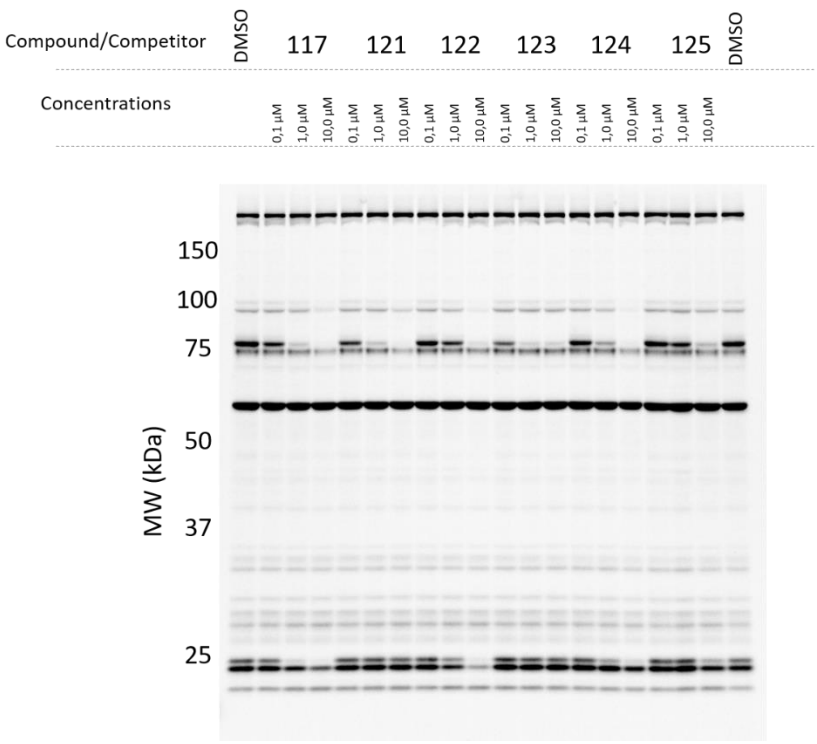

Fig SX – Competitive ABPP; U937 soluble fraction; compounds **117**, **121-125**.

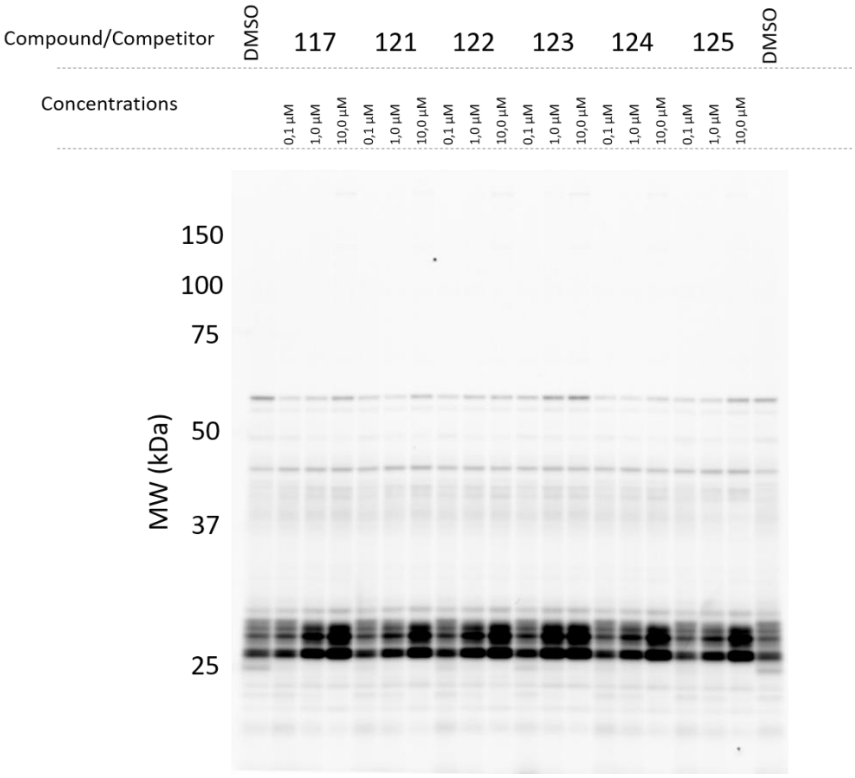

Fig. SX – Competitive ABPP; U937 membrane fraction; compounds **117**, **121-125**.

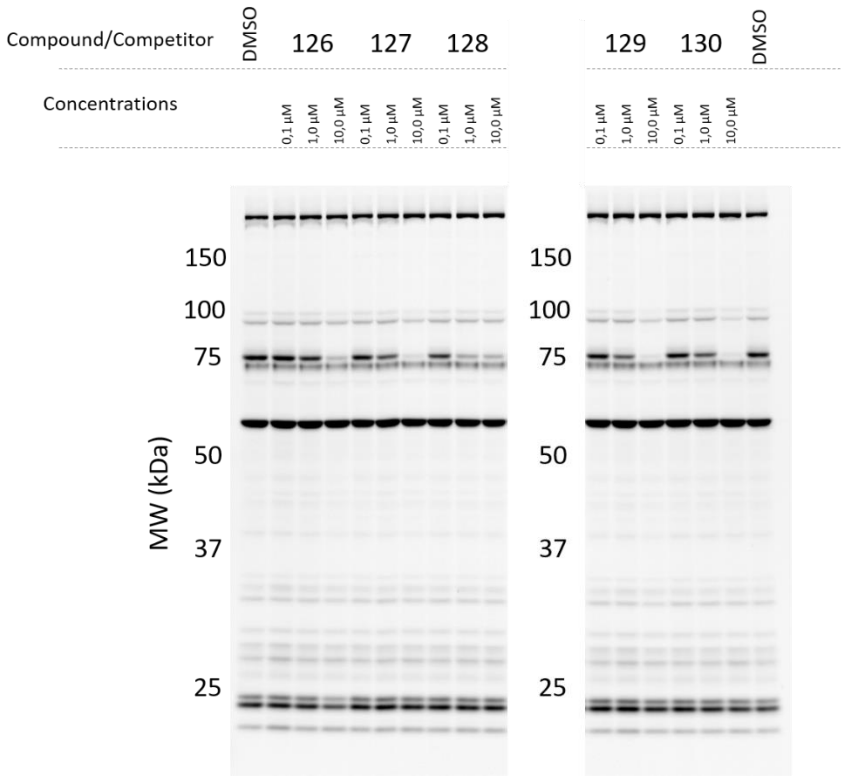

Fig SX - Competitive ABPP; U937 soluble fraction; compounds **126**-**130**.

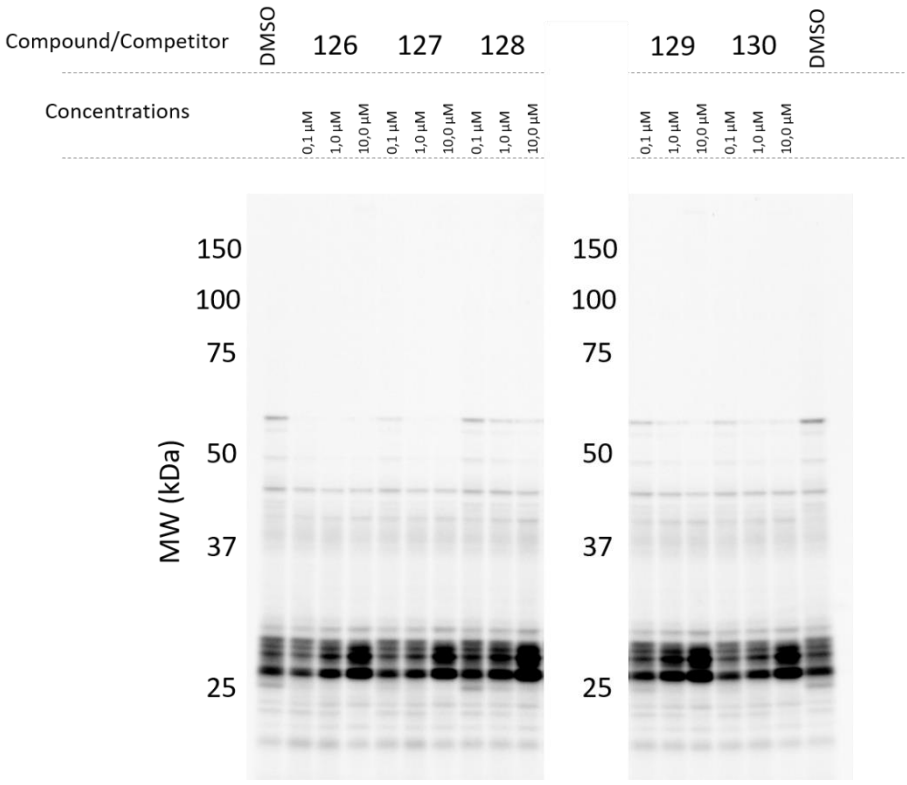

Fig SX - Competitive ABPP; U937 membrane fraction; compounds **126**-**130**.

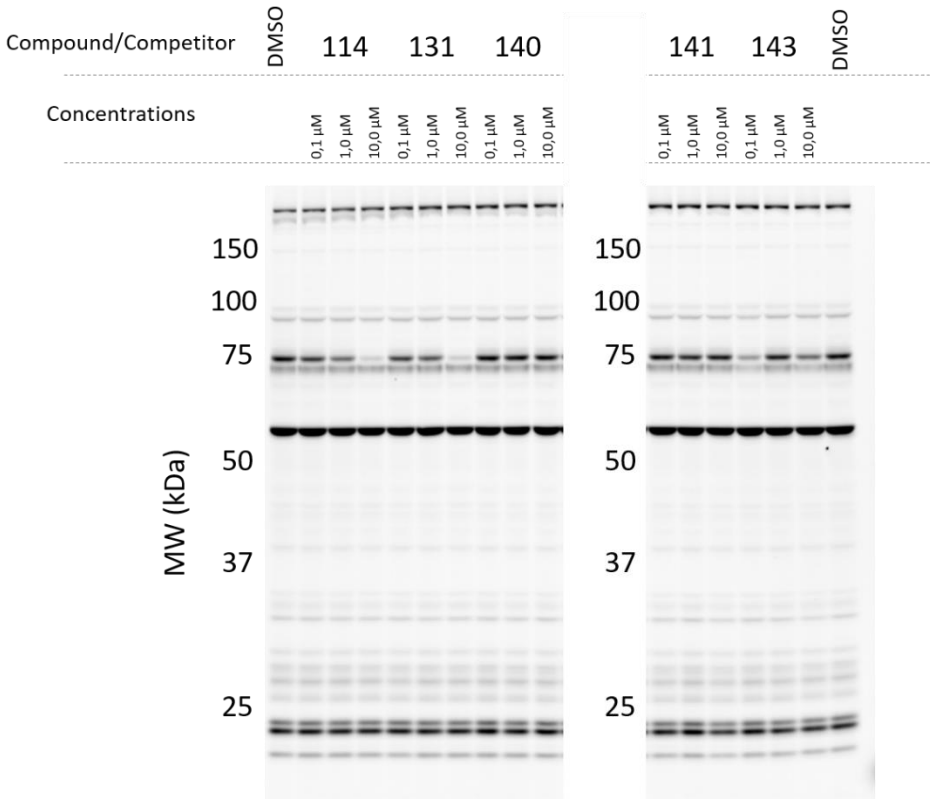

Fig SX - Competitive ABPP; U937 soluble fraction; compounds **114**, **131**, **140**, **141**, **143**.

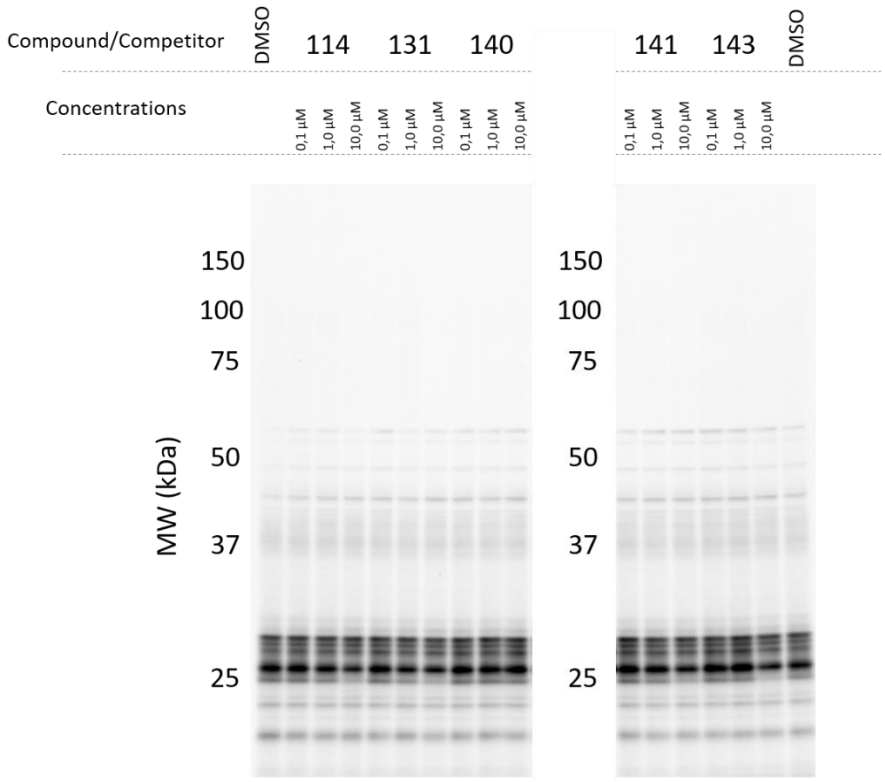

Fig SX - Competitive ABPP; U937 membrane fraction; compounds **114**, **131**, **140**, **141**, **143**.

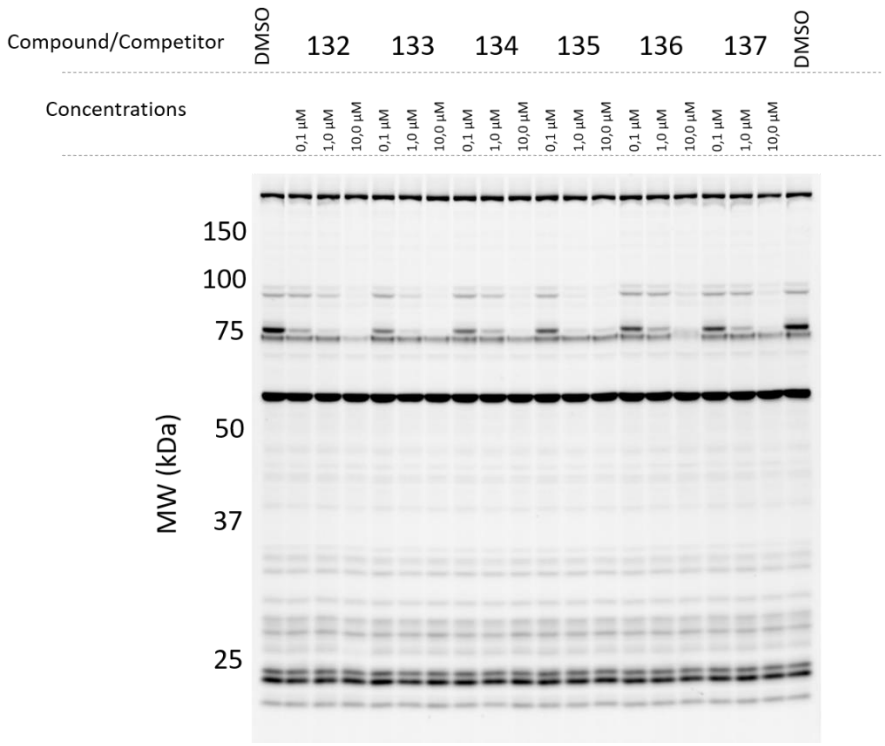

Fig SX - Competitive ABPP; U937 soluble fraction; compounds **132-137**.

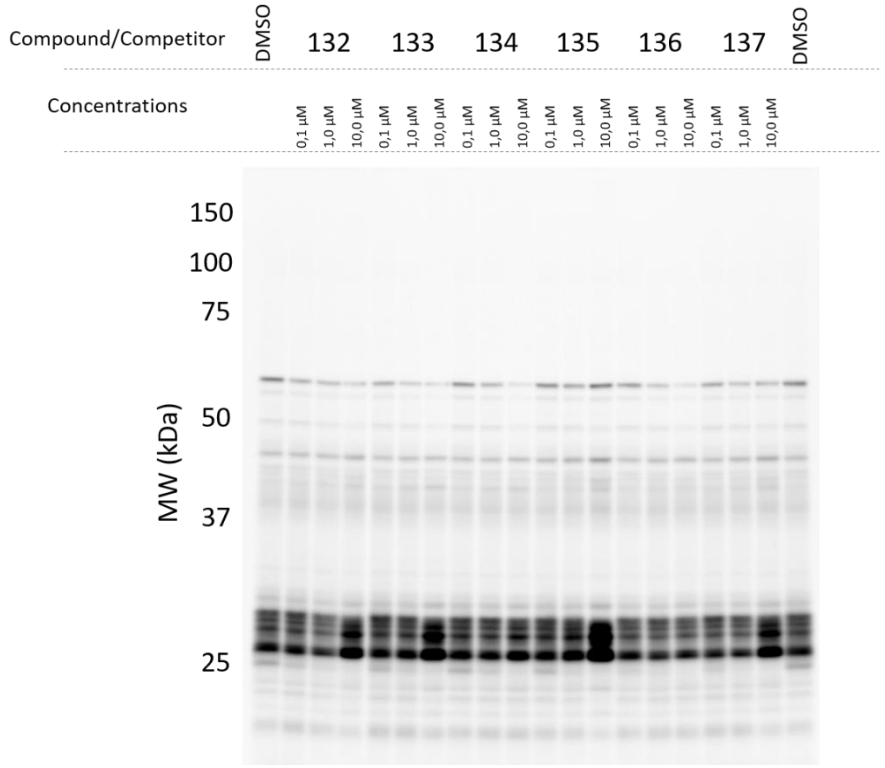

Fig SX - Competitive ABPP; U937 membrane fraction; compounds **132**-**137**.

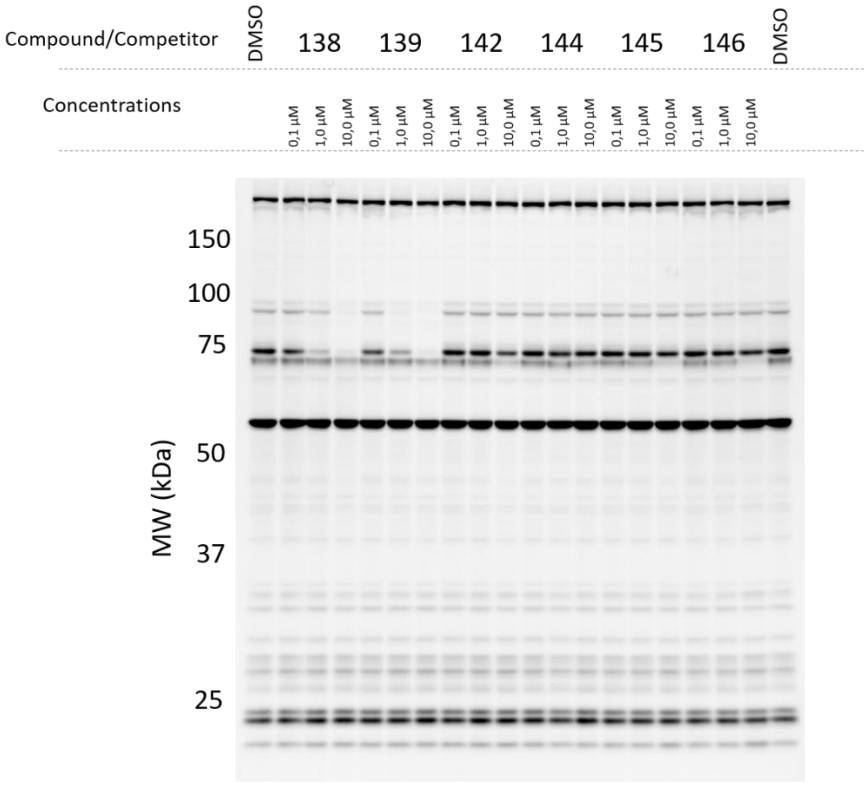

Fig SX - Competitive ABPP; U937 soluble fraction; compounds **138**, **139**, **142**, **144**-**146**.

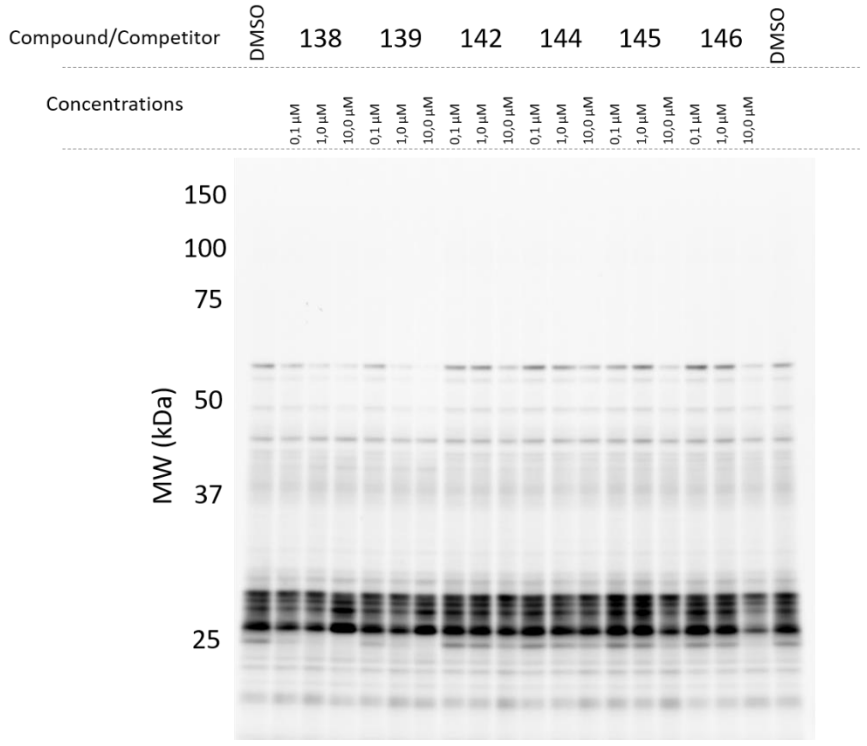

Fig SX - Competitive ABPP; U937 membrane fraction; compounds **138**, **139**, **142**, **144-146**.

S7. Target Validation by Competitive ABPP

S7.1. HNE

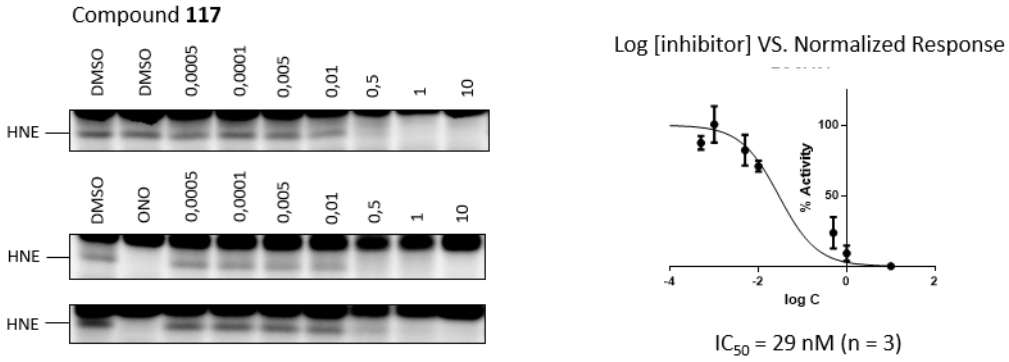

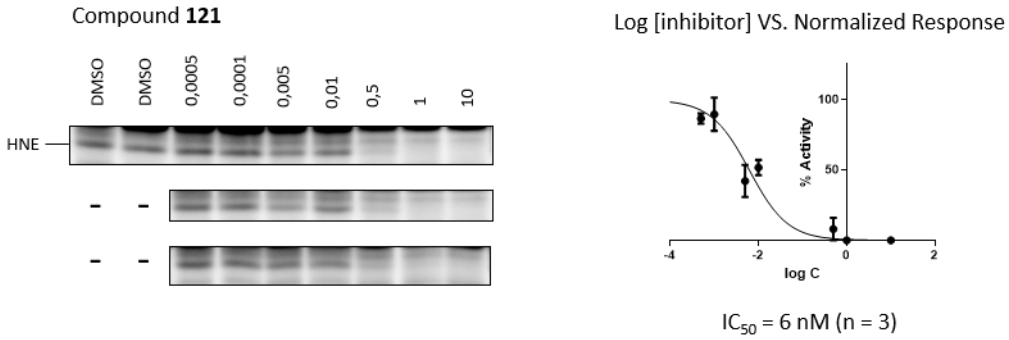

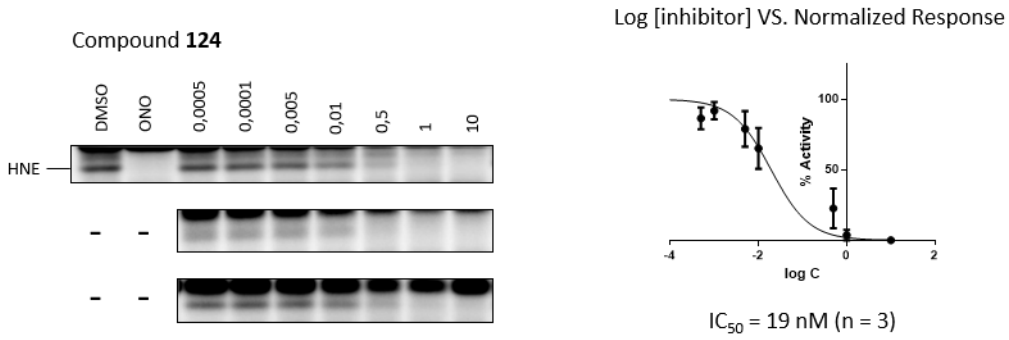

Fig. SX – HNE IC_{50} determination by competitive ABPP for compounds **117**, **121** and **124**.

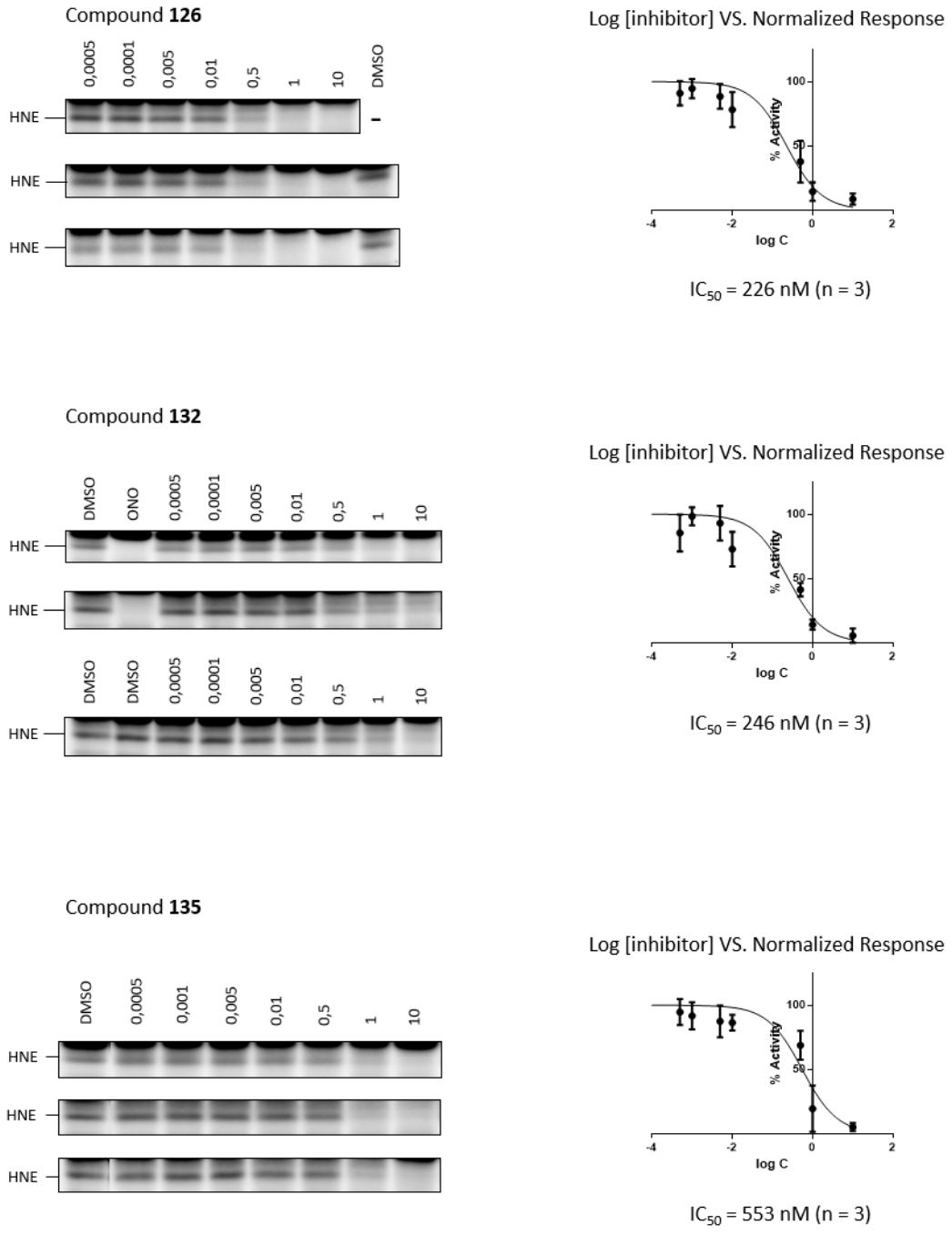

Fig. SX – HNE IC_{50} determination by competitive ABPP for compounds **126**, **132** and **135**.

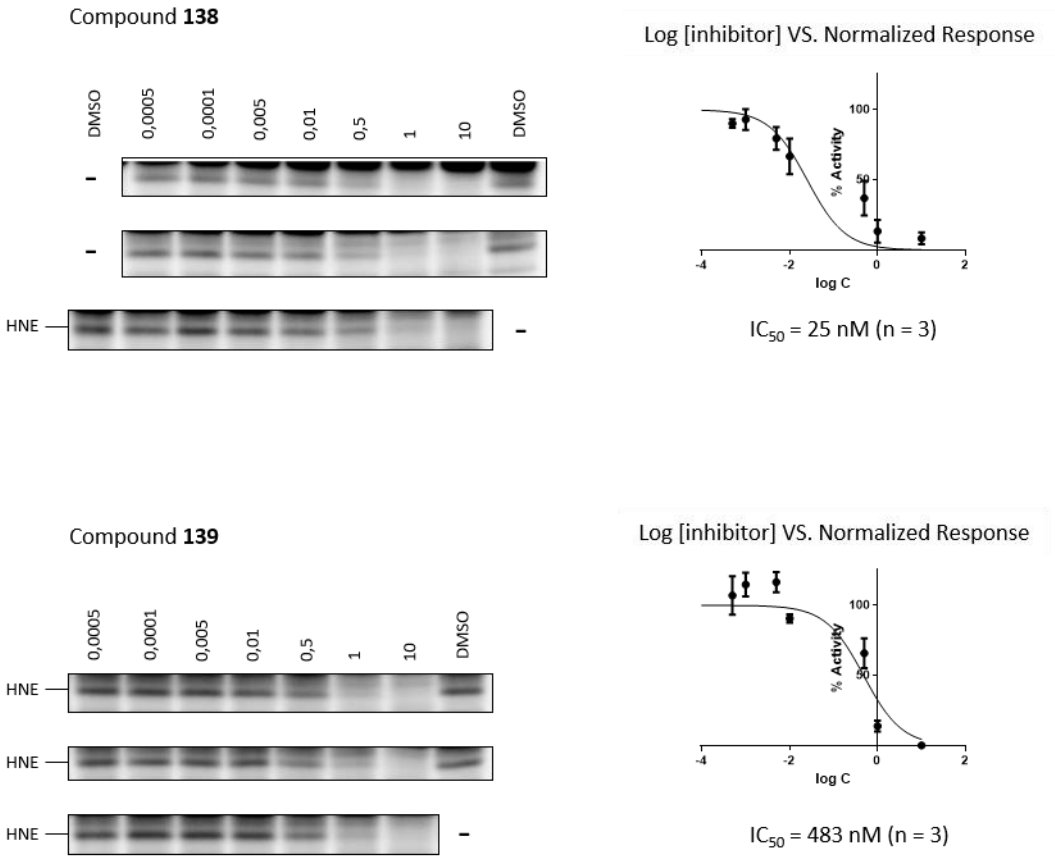

Fig. SX – HNE IC_{50} determination by competitive ABPP for compounds **138** and **139**.

S7.2. DPP8

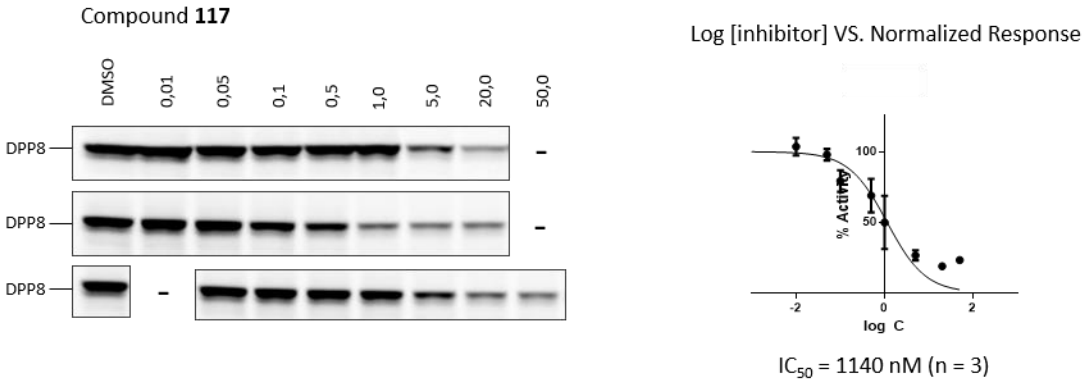

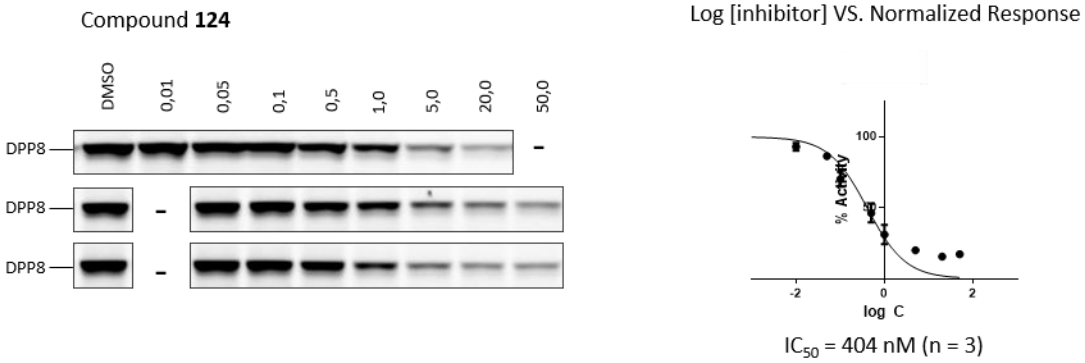

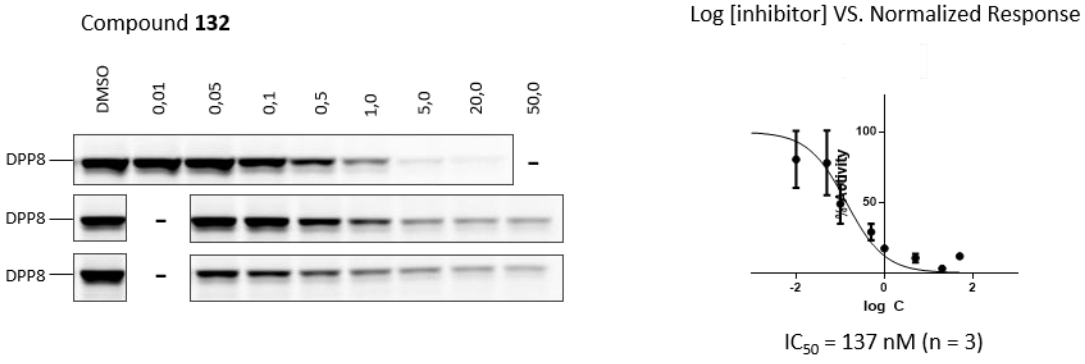

Fig. SX – DPP8 IC_{50} determination by competitive ABPP for compounds **117**, **124** and **132**.

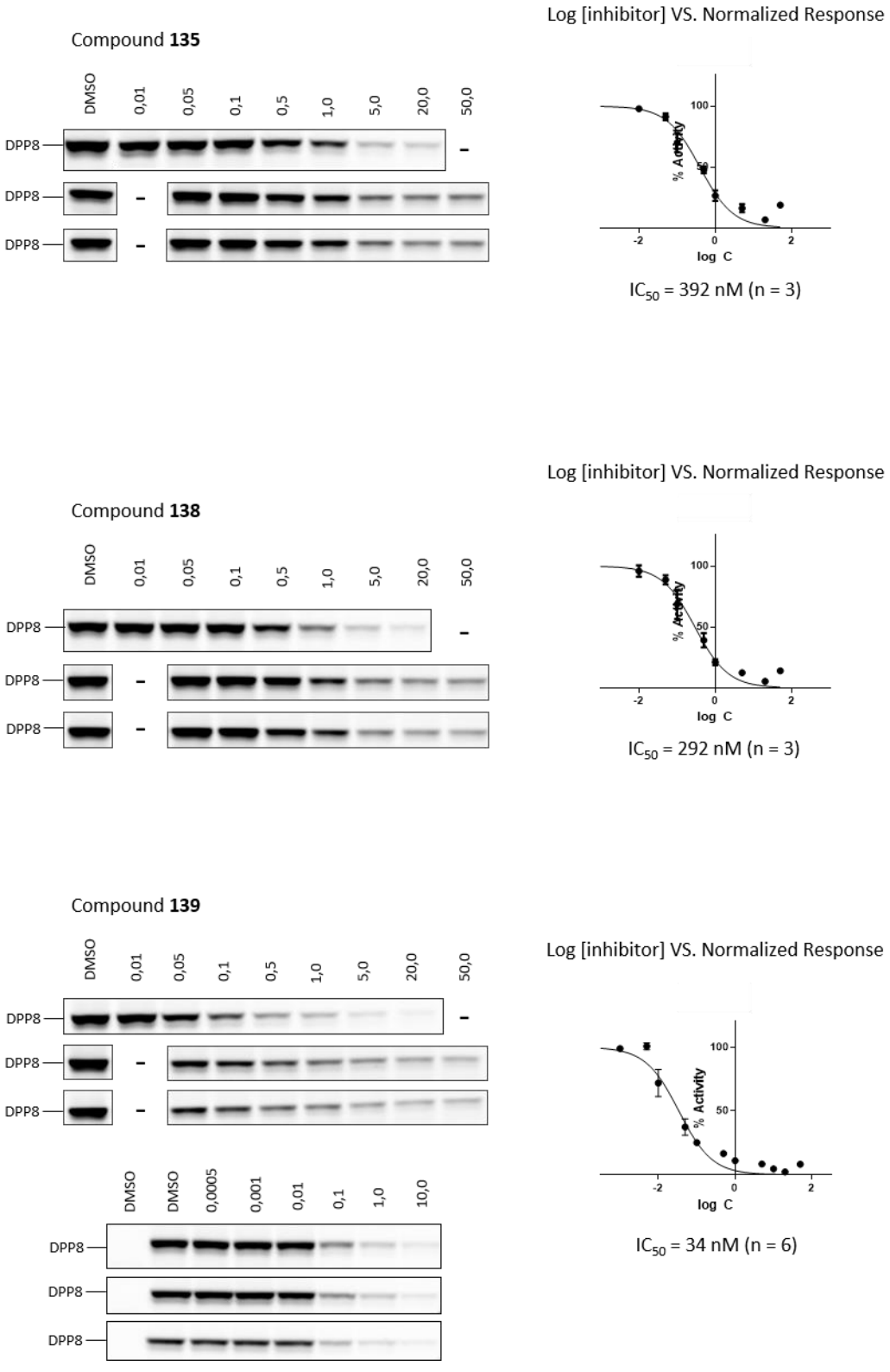

Fig. SX – DPP8 IC_{50} determination by competitive ABPP for compounds **135**, **138** and **139**.

S7.3. DPP9

Compound **117**

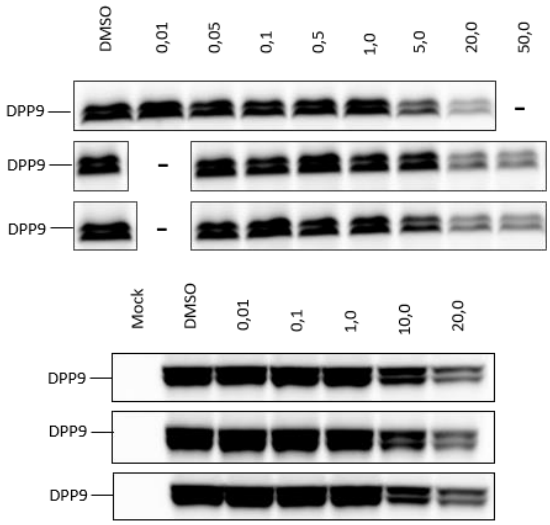

Log [inhibitor] VS. Normalized Response

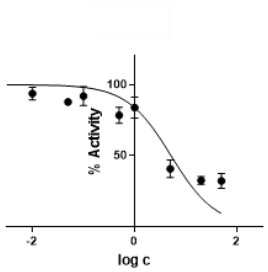

IC_{50} = 5171 nM (n = 6)

Compound **124**

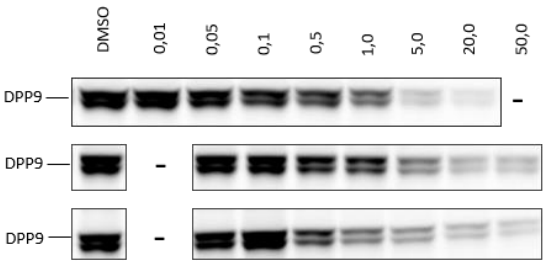

Log [inhibitor] VS. Normalized Response

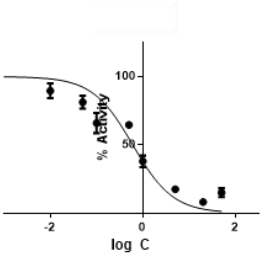

IC_{50} = 603 nM (n = 3)

Compound **132**

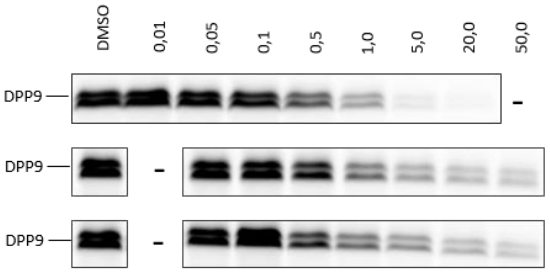

Log [inhibitor] VS. Normalized Response

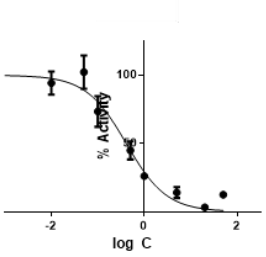

IC_{50} = 409 nM (n = 3)

Fig. SX – DPP9 IC_{50} determination by competitive ABPP for compounds **117**, **124** and **132**.

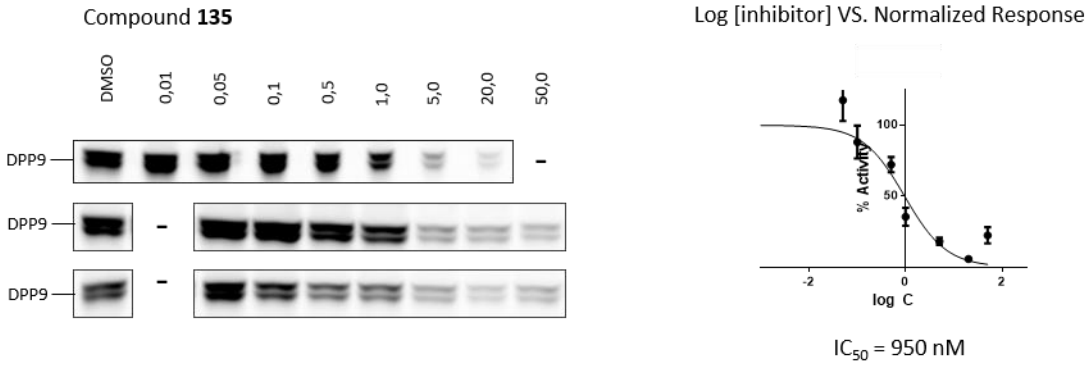

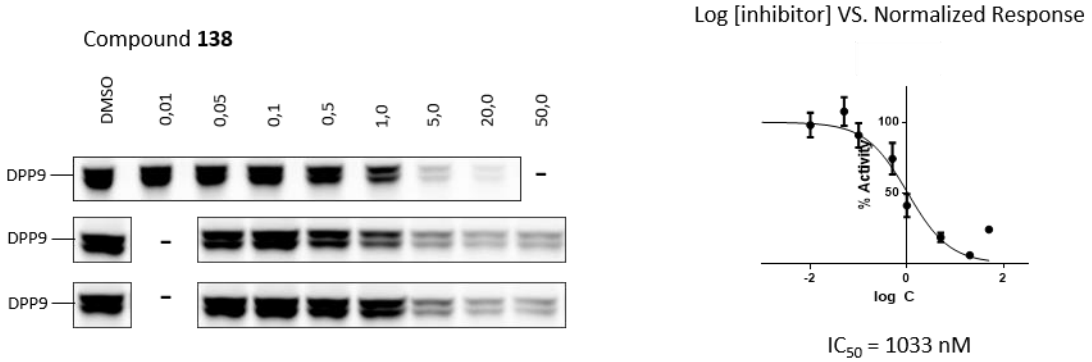

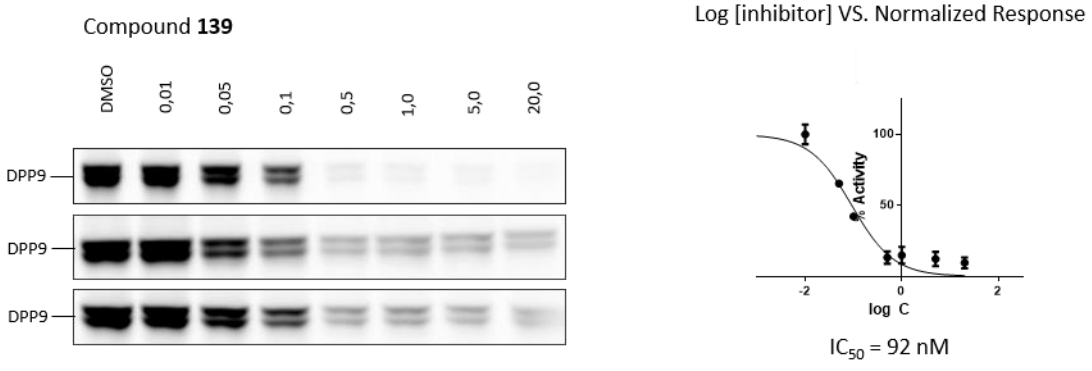

Fig. SX – DPP9 IC_{50} determination by competitive ABPP for compounds **135**, **128** and **139**.

S7.4. FAP

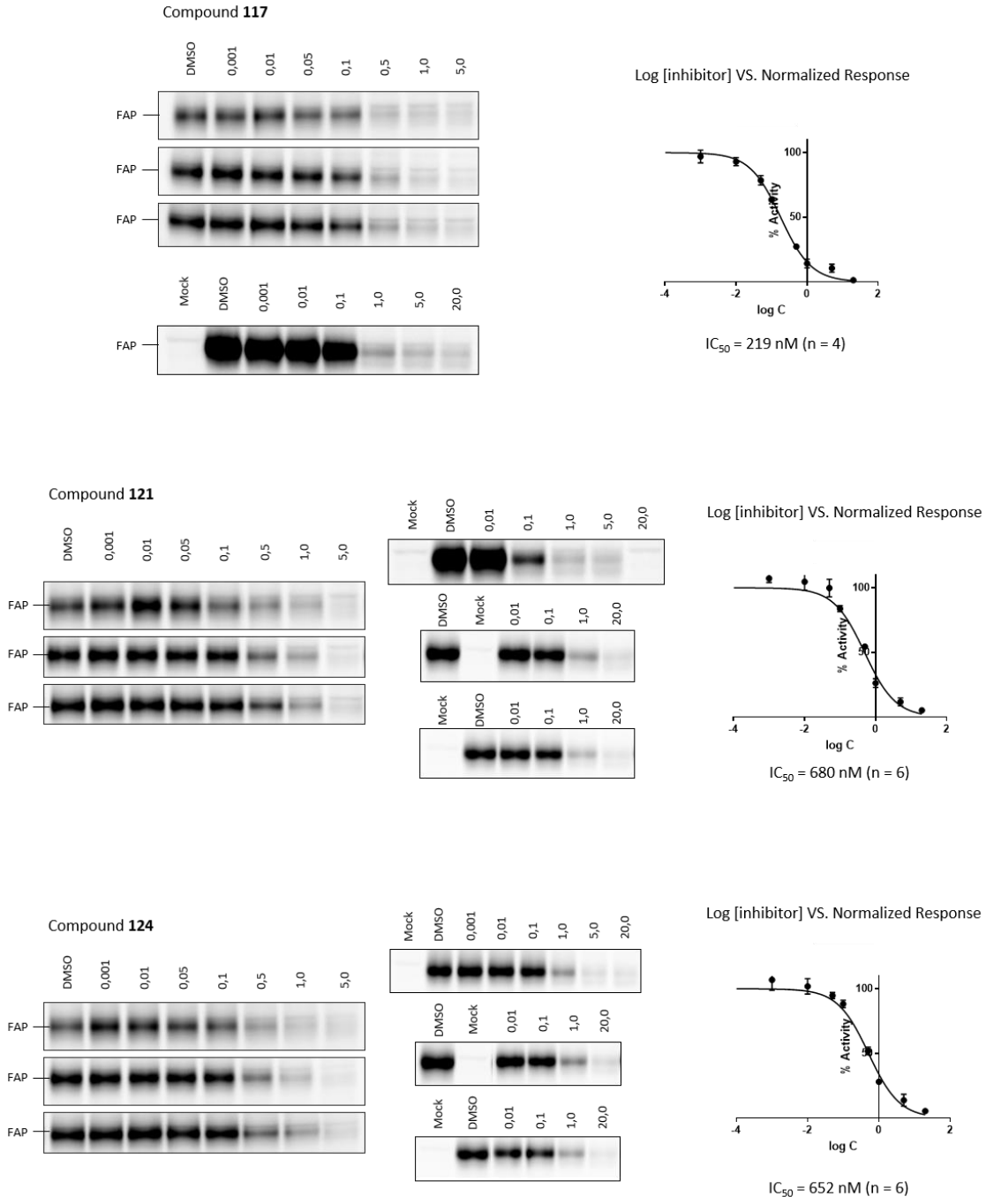

Fig. SX – FAP IC_{50} determination by competitive ABPP for compounds **117**, **121** and **124**.

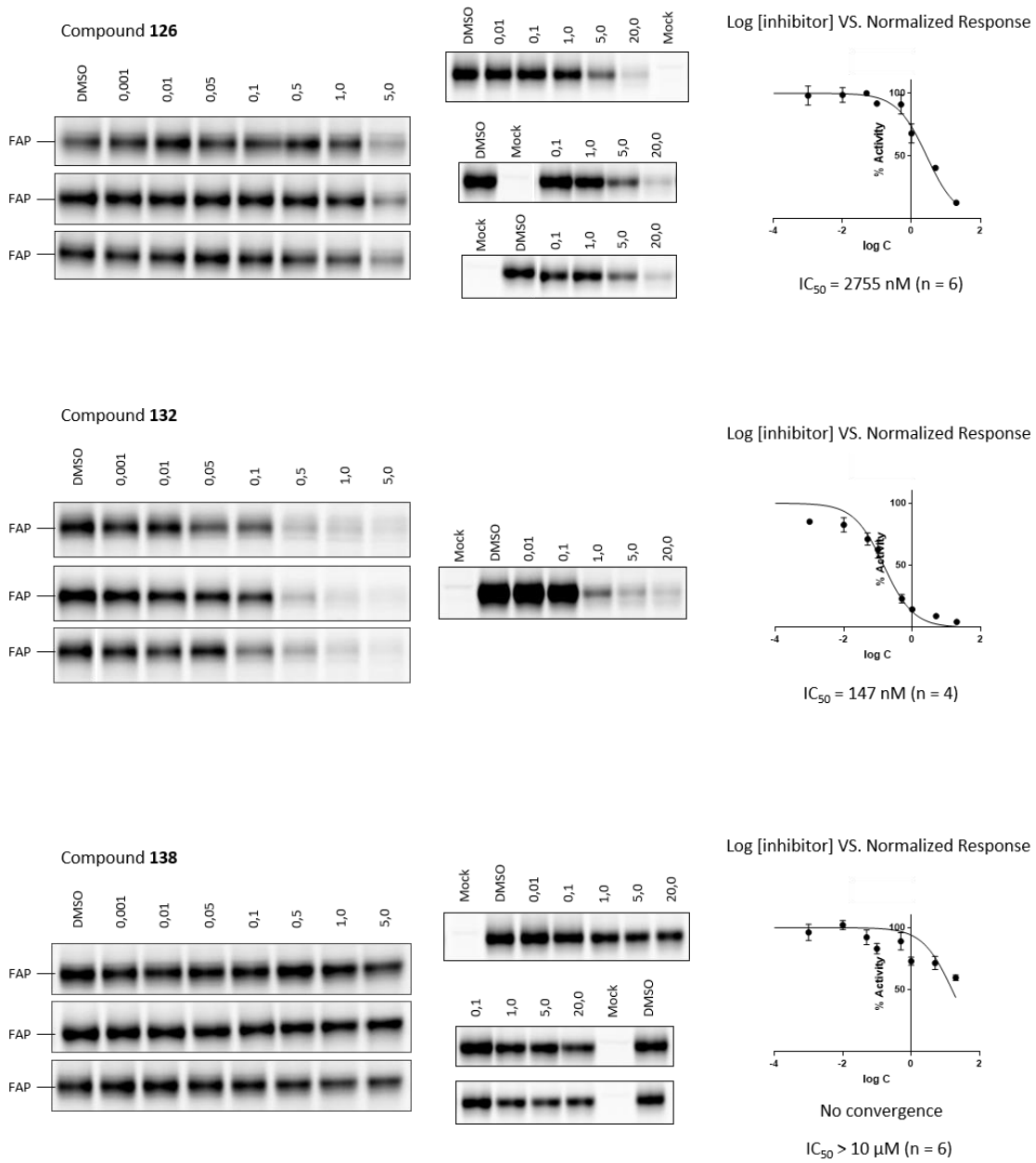

Fig. SX – FAP IC_{50} determination by competitive ABPP for compounds **126**, **132** and **138**.

S7.5. DPP4

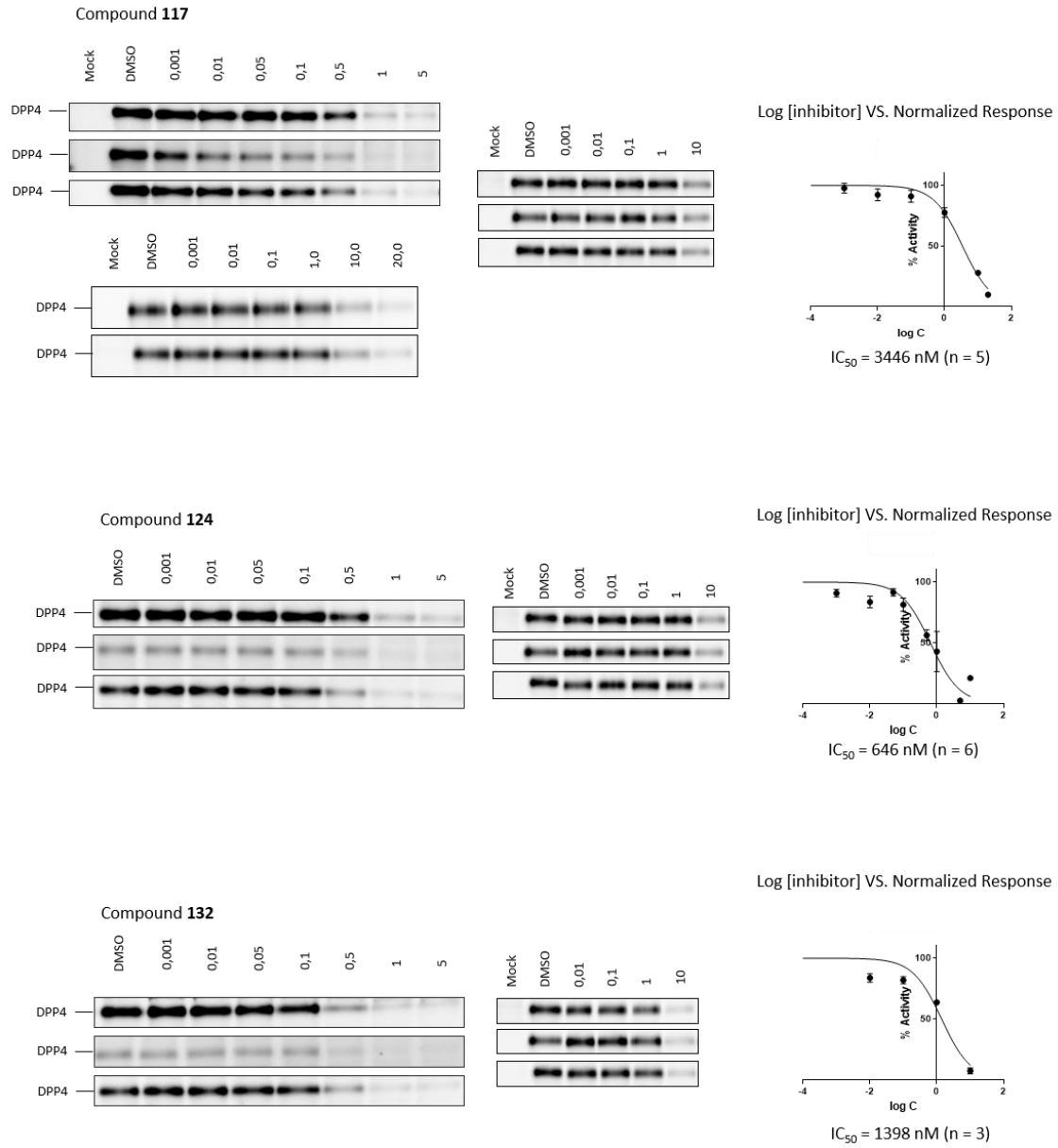

Fig. SX – DPP4 IC_{50} determination by competitive ABPP for compounds **117**, **124** and **132**.

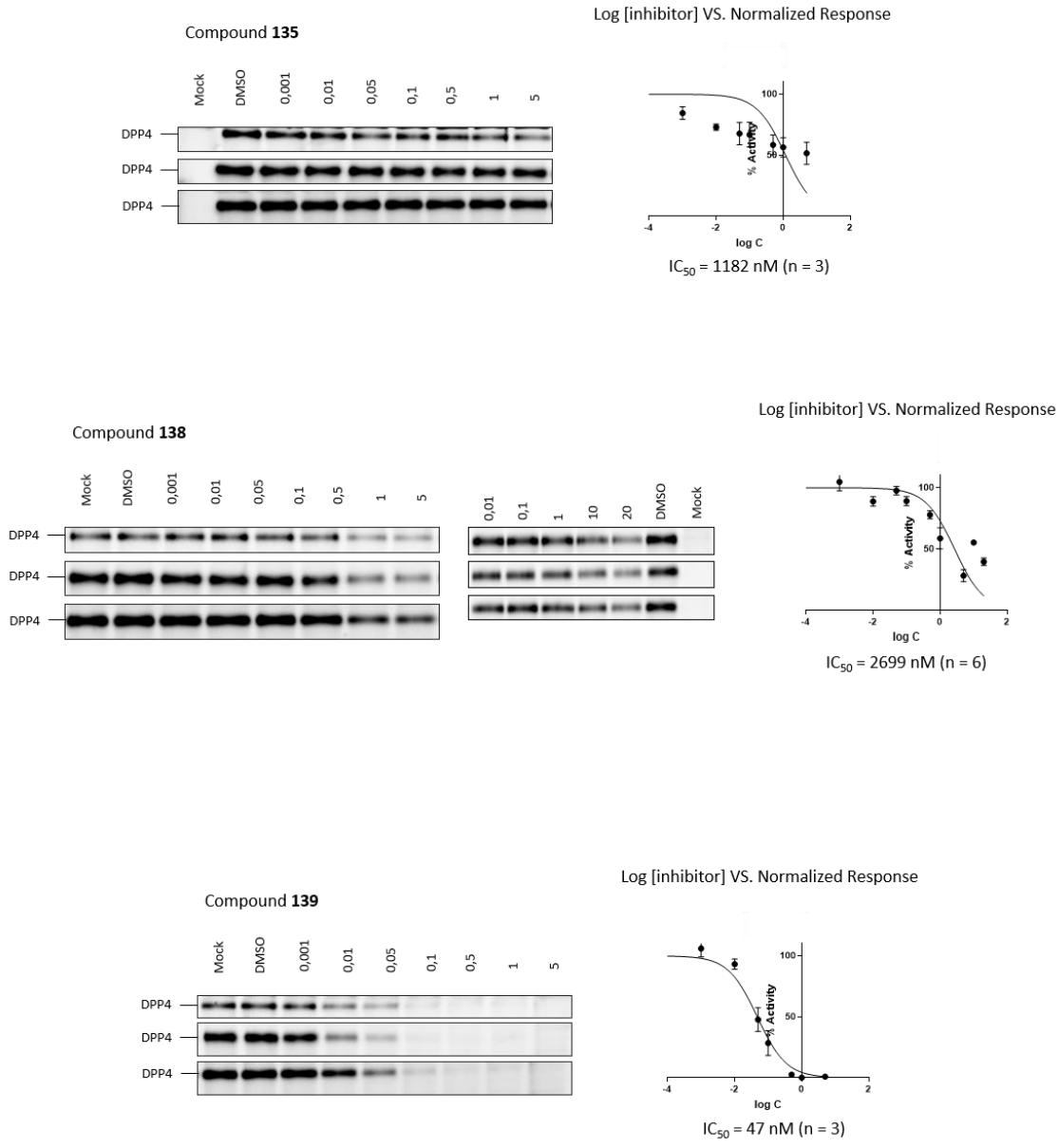

Fig. SX – DPP4 IC_{50} determination by competitive ABPP for compounds **135**, **138** and **139**.

S7.6. DPP7

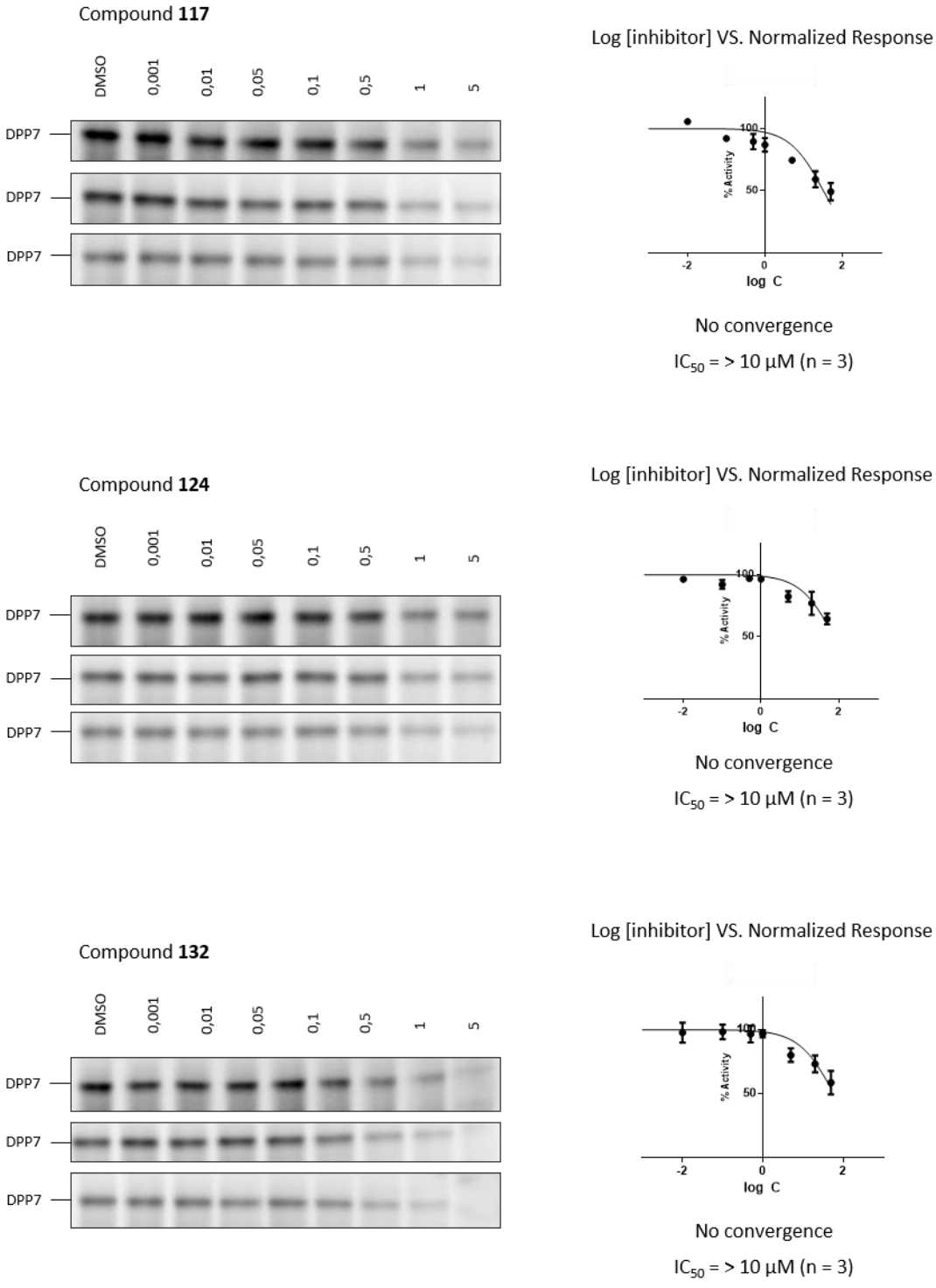

Fig. SX – DPP7 IC_{50} determination by competitive ABPP for compounds **117**, **124** and **132**.

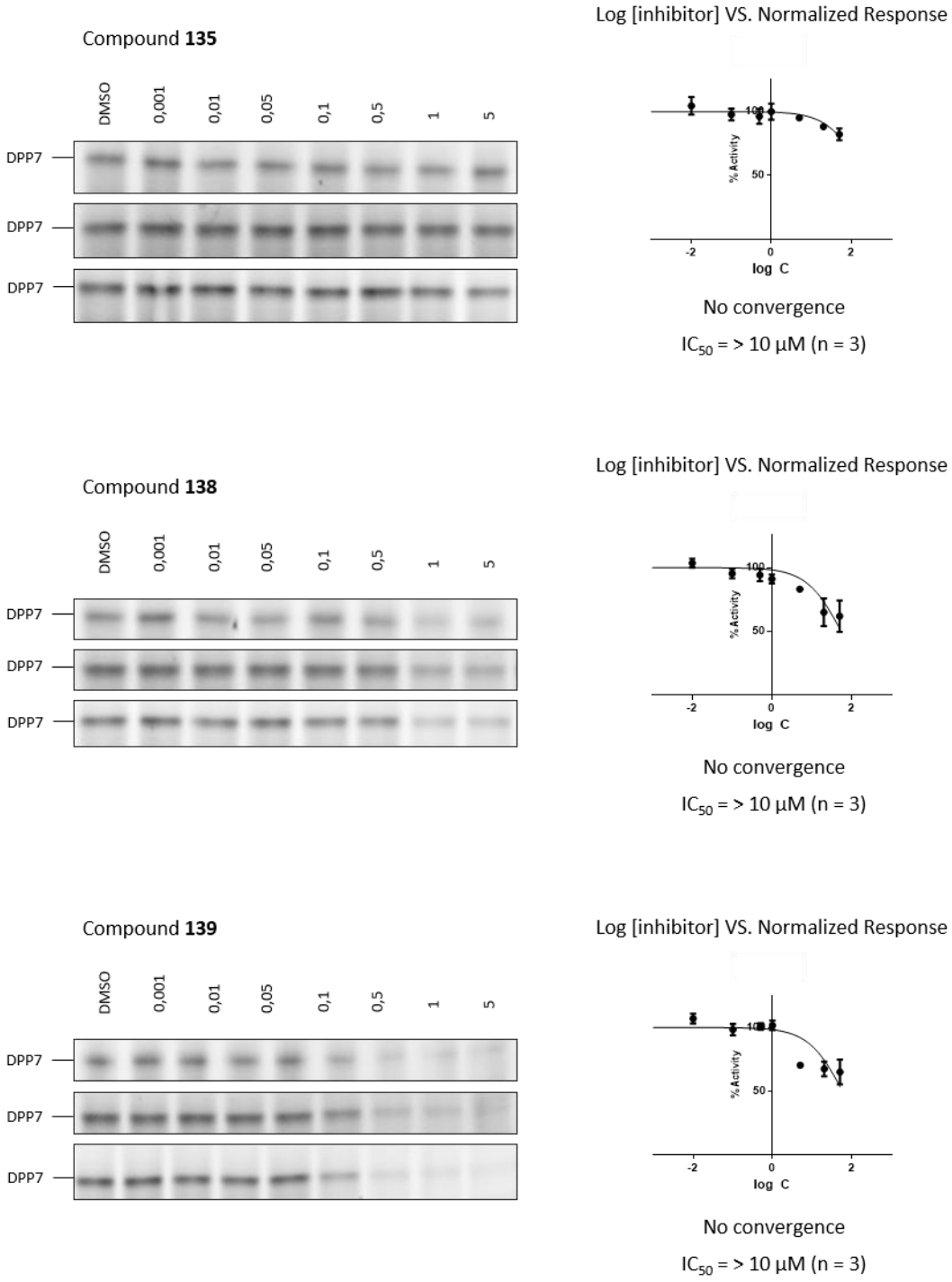

Fig. SX – DPP7 IC_{50} determination by competitive ABPP for compounds **135**, **138** and **139**.

S7.7. ABHD6

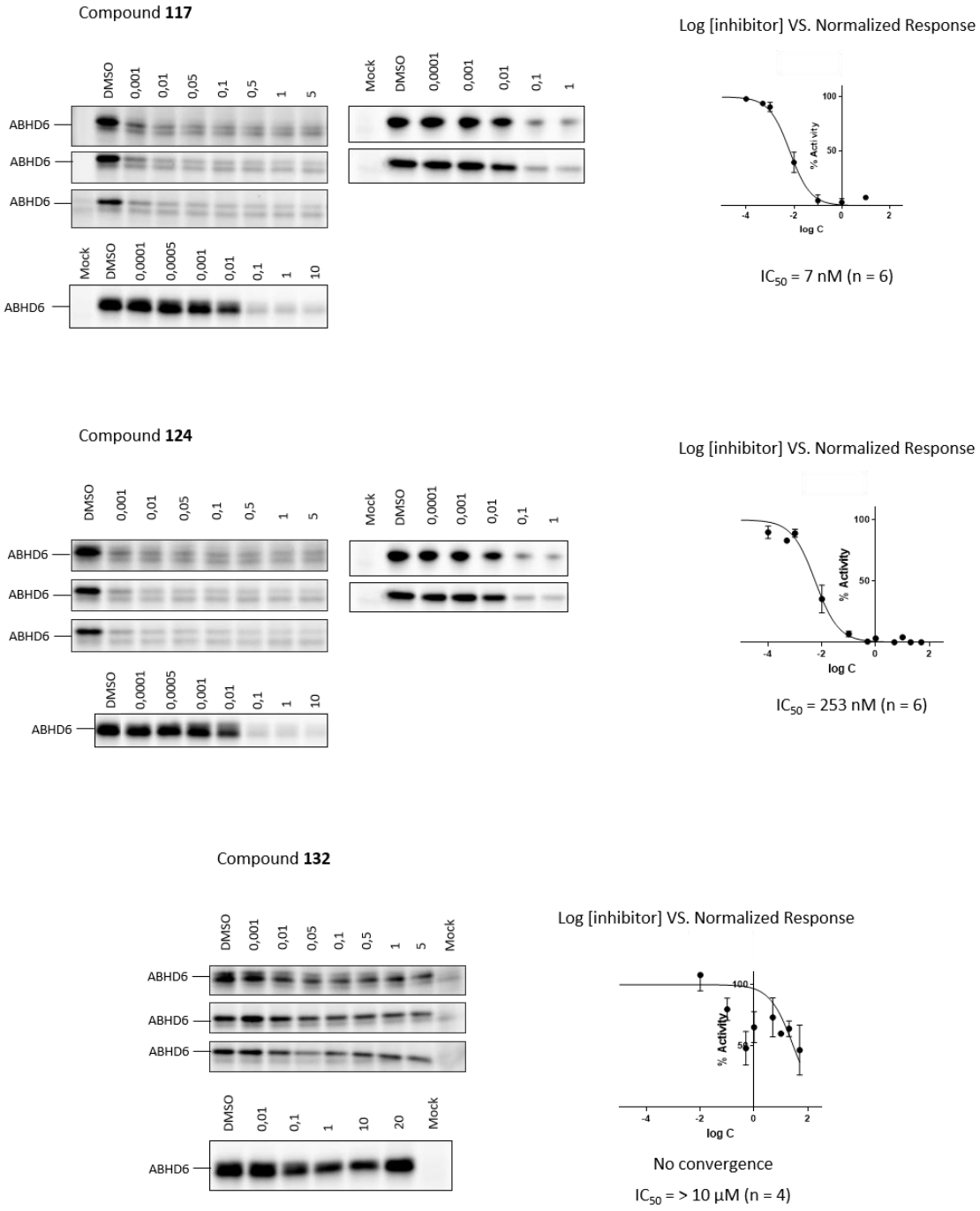

Fig. SX – ABHD6 IC_{50} determination by competitive ABPP for compounds **117**, **124** and **132**.

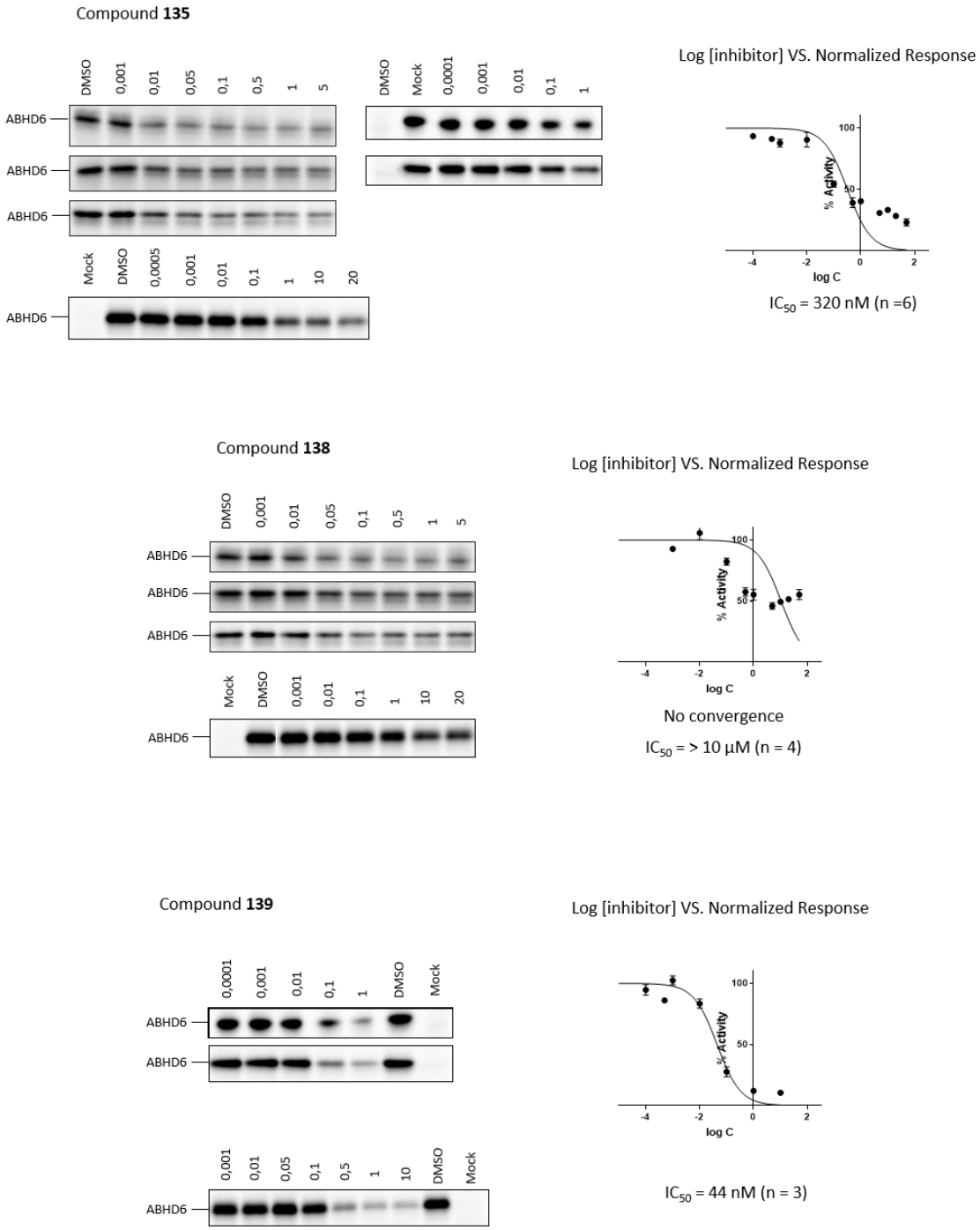

Fig. SX – ABHD6 IC_{50} determination by competitive ABPP for compounds **135**, **138** and **139**.

S7.8. ABHD2

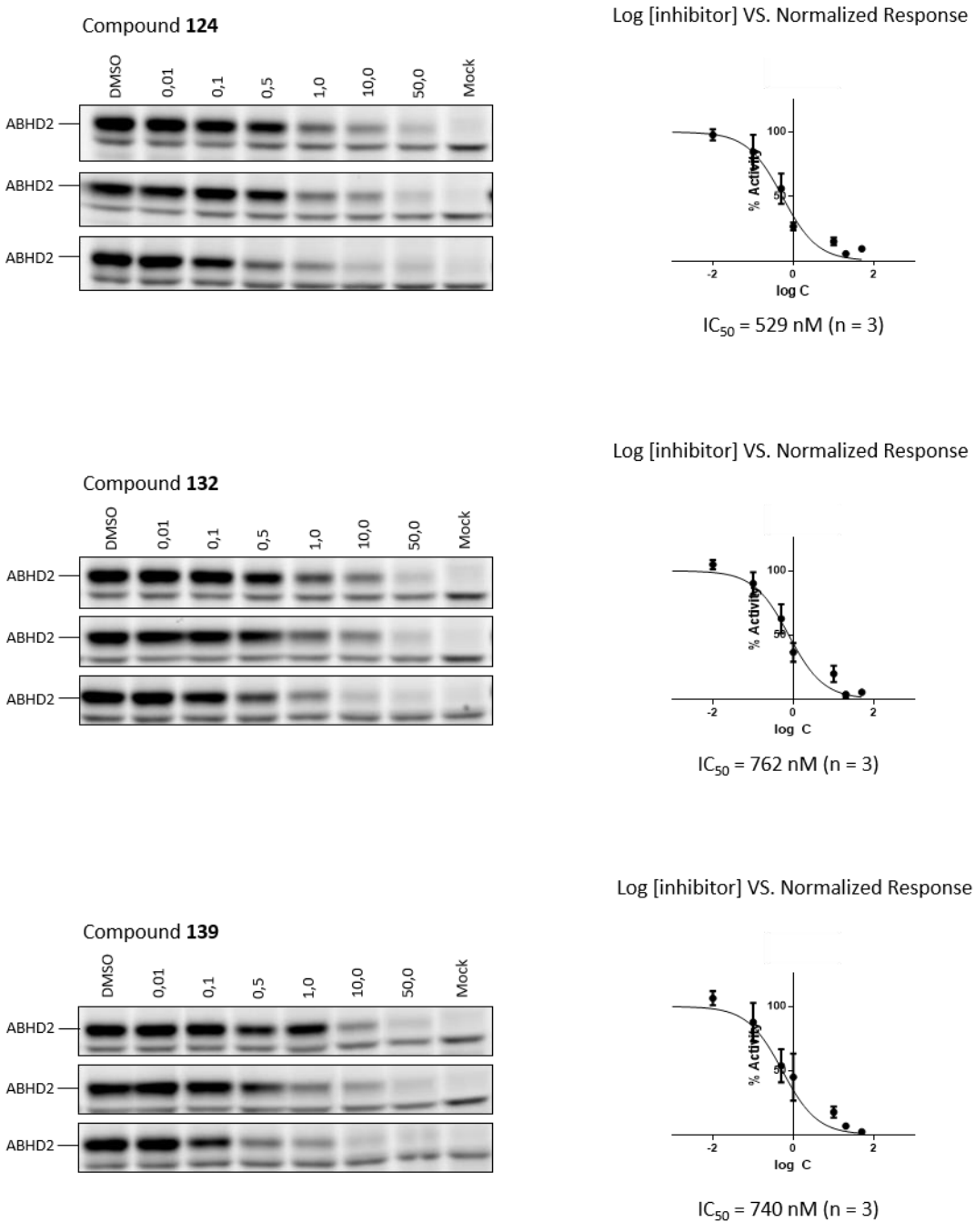

Fig. SX – ABHD2 IC_{50} determination by competitive ABPP for compounds **124**, **132** and **139**.